PROBABILISTIC SEISMIC DEMAND ANALYSIS:
SPECTRUM MATCHING AND DESIGN.

Jorge Eduardo Carballo

C. Allin Cornell

Department of Civil and Environmental Engineering, Stanford University

Report No. RMS-41

July 2000

PROBABILISTIC SEISMIC DEMAND ANALYSIS: SPECTRUM MATCHING AND DESIGN.

Jorge Eduardo Carballo

C. Allin Cornell

Department of Civil and Environmental Engineering, Stanford University

Report No. RMS-41

July 2000

Abstract

The current state and trend of Earthquake Engineering practice calls for better understanding of structural nonlinear response due to strong ground motion excitation. The present study deals with issues on such structural-systems understanding, in light of recent developments in Probabilistic Seismic Demand Analysis (PSDA), which is a practical interface between the elastic and inelastic representations of structural behavior and ground motion hazard, in a probabilistic framework.

One part of this study deals with requirements of PSDA in terms of structural response representation: efficient and accurate estimations of response. Ground motion response spectral shape is studied and is recognized as having an important contribution to structural displacement demands, especially for structures that are forced into large nonlinear displacements. Methods based on the use of particular spectral shapes for providing accurate and efficient estimates of response are studied.

In particular, the use of *Spectrum Matched* Records (also known as *Spectrum Compatible* Records) for the prediction of M-R (magnitude-distance) scenario-based displacement demands is discussed. It was found that the use of Spectrum Matched accelerograms, for the estimation of these nonlinear demands associated to a scenario event, can lead (albeit very efficiently) to obtaining unconservative results. An important cause of this bias is identified.

The second part of this study "dis-assembles" the components of PSDA for structural design purposes. The final product of PSDA is a probabilistic representation of a structure's response given its seismic environment. A methodology is proposed by assigning a desired exceedence probability to a particular response level of interest (e.g., collapse) in order to try to estimate the design-level ground motion to consider for design. The proposed method is tested and presented with an example, for which a 3-D model of a steel offshore platform is considered. Some issues that arise from considering the traditionally uni-dimensional PSDA and spectrum matching (*one* horizontal component of ground motion) on a three-dimensional system (*two* horizontal components of response) are discussed as well.

Acknowledgments

Contents

Chapter 1

Introduction

1.1 Background.

Modern seismic design philosophy recognizes the need to target a broader set of *design objectives* than have been historically considered for different structural systems. Examples for offshore, nuclear, and conventional buildings include: ISO-WG3, 1995; DOE-1020, 1994; and FEMA-273, 1996, respectively. For example, *Performance Based Seismic Design* (PBSD) (SEAOC, 1996) not only introduces a framework by which the owner of a structure may select from a range of behavior levels and objectives but also calls for the means to confirm accurately that a proposed structural design meets those objectives.

Conceptually, as considered for example in SEAOC, 1996, PBSD encompasses the issues that need to be addressed in order to design civil structures "for *predictable* and definable seismic performance, within established levels of risk". The *Earthquake Performance Levels* (or damage states) that PBSD considers range from "Fully Operational" to "Near Collapse"; the levels of risk it considers by means of *Earthquake Design Levels* range from "Frequent" to "Very Rare". By defining such performances and levels of risk, it recognizes the need to "more directly address the inelastic response of structures and provide alternative procedures to better achieve defined seismic performance objectives".

A tool that can aid the engineer in such schemes is *Probabilistic Seismic Demand Analysis* (PSDA). It provides a means for establishing the annual likelihoods of different *Performance Levels* (e.g., by defining performance in terms of structural response), given the seismic exposure of the structure.

Probabilistic Seismic Demand Analysis is built upon the more traditional *Probabilistic Seismic Hazard Analysis* (PSHA). PSDA couples the stochastic description of future ground motions from PSHA with their random dynamic effects on the structure. In brief, the demand hazard can be computed by the following equation:

$$P[Z > z] = \sum_{\forall i} P[Z > z \,|\, y_i] P[Y = y_i]$$

1.1

where Z is some structural response (e.g., maximum interstory ductility), and Y is a relevant seismic intensity (e.g., spectral acceleration). PSHA takes care of computing $P[\, Y = y_i \,]$, the probability distribution of the intensity (Cornell, 1968)

A closed form solution to the above probabilistic description of response, can be given by the following equation, under some mild assumptions of the variables involved (See for example Luco and Cornell, 1996; also see Appendix A for a derivation):

$$P[Z > z] = H[y_z] e^{[\frac{1}{2}(\frac{\sigma_{\ln(Z|Y)} K}{b})^2]},$$

1.2

where H[.] is the site-specific seismic hazard curve (in terms of the intensity *Y)*, y_z is the "expected value"[1] of the intensity that will cause the response *z*, *K* is the (log-log) slope of the site-specific hazard curve, *b* represents the slope of the (log-log) relationship

---

[1] It is not precisely the *expected* value; y_z is the value of the intensity whose *median* response is found to be *z*; this distinction arises from the fact that intensity is the independent variable considered to describe the response-intensity relationship. This relationship is considered to be linear in logarithmic terms of both variables, with a Gaussian distribution about the prediction. See Chapter 4 for a more detailed discussion.

between Z and the observed intensity, and $\sigma_{ln(Z|Y)}$ represents the dispersion of the response given the seismic intensity.

Needless to say, both PBSD and PSDA require the understanding of structural behavior. Such understanding is necessary to produce *accurate* predictions of structural response to given levels of ground motion, ranging from the elastic behavior through the non-linear regime. PBSD and PSDA also rely on *efficient* means of obtaining such predictions. As can be seen in equation 1.1, the conditional probability distribution of exceeding a structural response z needs to be established. *Accurate* will mean, for example, that given that a particular probability distribution can be assumed for Z we can confidently find representative (i.e. unbiased) estimates of the corresponding parameters for it (e.g., mean and variance). *Efficient* will mean that for the same previous assumption, we can statistically estimate such parameters from as small a sample size as possible.

It is not uncommon to observe variability of nonlinear response to ground motion of a particular *scenario* (i.e., of a given magnitude and distance) having a coefficient of variation (COV) close to unity (see for example Shome and Cornell, 1999). For the usual lognormal description of response, such unitary COV translates into a standard deviation of the logarithm (σ_{lnZ}) of response of around 0.8 (for smaller values of COV, it is approximately equal to σ_{lnZ}). Such a large dispersion value implies the need of a large number of observations in order to predict with reasonable accuracy the estimates of the parameters of the distribution of response. For example, for a one-sigma confidence (i.e., approximately 64% confidence) of estimating the median response within a bandwith of ±10% of its real value, the above variability translates into $(0.8/0.1)^2 = 64$ required observations[2].

---

[2]For a N-sigma confidence (roughly: for N = 1, confidence = 64%; for N = 2, confidence = 95%), and a w-percent confidence band width (precision on the estimate of the median response), the required number satisfies: $(w/100) = N \sigma / n^{1/2}$, or $n = (N \sigma / (w/100))^2$. This means we are fixing the (N-times) standard error of estimation ($SEE = \sigma / n^{1/2}$) of the (log-average) response to a desired precision (w-percent).

Shome, et al, 1998, show that by simply *normalizing* (i.e., scaling to a common value of spectral acceleration for an "appropriate" frequency) the records to be used in the structural analysis, one can reduce the value of σ_{lnZ} by roughly a half, implying that one will be able to reduce the required number of observations by a factor of four. For the previous example, it means running only $((0.8/2)/0.1)^2 = 16$ records. In other words one gains *efficiency* by normalizing. Fortunately, this method does not lose accuracy while gaining such efficiency.

As will be seen in Chapter 3, *Spectrum Matching*, another record manipulation scheme currently used in engineering practice, further reduces the dispersion of the results. Roughly, a reduction of four in the required number of records with respect to the original data set can be expected. One can see that this means now, for the same confidence, a required sample size of only $((0.8/4)/0.1)^2 = 4$ records. Caveat: such an increase in efficiency does not come, however, without loss in accuracy. In other words, the estimation of the parameters is biased. As will be seen, it is biased unconservatively.

Traditional structural element sizing schemes have considered the seismic forces that could be related to a single earthquake design level (e.g., associated to a probability of exceedence of 10% in 50 years, SEAOC, 1996), albeit reduced to allow for the consideration of nonlinear structural behavior. Other than for such a reduction, postelastic behavior is not explicitly considered in the sizing. It is seldom even tested or verified by nonlinear structural analyses. Typically, any assumption on the force reduction given a ductile behavior (provided by appropriate detailing, for example) will be considered valid. Some codes (e.g., API, 1993) will, however, require that such ductility and nonlinear response assumptions do indeed hold for the "rare, intense earthquake without collapsing", and that they be verified.

The transition between elastic-force-based design and an actual nonlinear-response-based design is not a straightforward one. Traditionally, the definition of the seismic environment was considered virtually completely defined by means of an elastic design spectrum. Typical spectral shapes considered for design are, for example, Newmark-and-

Hall-spectrum based (FEMA-274, 1997), Uniform Hazard Spectra (UHS) or scenario or site-specific spectral shapes (by means of an attenuation law and a particular scenario seismic event; i.e., M, R, and soil type), etc. Even if all of the above shapes can be somehow related to the same earthquake design level, upon considering the need to describe more thoroughly the nonlinear response of structural systems, one begins to question such elastic representations of the ground motion. One may wonder, for example, what the relevance of the ground motions' different relative spectral shapes is, and how these differences should be taken into account.

Certain codes do recognize that there might be cases where dynamic analyses should be carried out in order to determine adequate seismic responses. Even in those cases, the requirements for the time-history analyses may be seen as vague. For example, one of SEAOC's Blue Book (SEAOC, 1996) recommendations for some seismic-isolated structures is to consider the seismic response obtained by *averaging* those obtained from *seven* different time-histories. Implicit in such a recommendation is the expected variability in the nonlinear response, for which *seven* analyses should be an adequate number. Another recommendation is that if only *three* records are considered for analyses (the minimum allowed number) the response to consider for design should be that of the *maximum* of the three; this is an attempt to be at least conservative. Again, some unspecified level of variability is implicit in such recommendation, such that *three* was deemed a reasonable number. Although not explicitly quantified in many codes it may be recognized that non-linear analyses yield results with a certain level of variability (FEMA-273, 1997): "A greater number of acceleration time histories is required for nonlinear procedures than for linear procedures because nonlinear structural response is much more sensitive than linear response to characteristics of the ground motions, in addition to the characteristics of response spectral content".

For dynamic structural analyses, general provisions may be made in terms of particular "matching" schemes for the response spectra of the selected accelerograms, be they recorded or simulated (e.g., UBC, 1997). The scaling of the former and the scaling or construction of the latter should be "appropriately" carried out: the whole set of

accelerograms should be scaled such that the *average* value of the SRSS spectra doesn't fall below a prescribed value of the design-basis earthquake (DBE) in a somewhat ad-hoc "region of interest" between 0.2T second to 1.5T seconds. T is the fundamental period of the structure considered. As mentioned above this is an important issue to consider. Is the design-basis spectrum really a good basis for selection of "appropriate" ground-motion accelerograms? We may be able to answer this question by analyzing what "information" is contained in the design-basis earthquake spectrum. For example, a UHS can be "dissaggregated" into the events that contribute the most to the hazard of a particular oscillator frequency. Ground motions can directly be associated to such events, and will not, in general, have spectral shapes that resemble the whole UHS.

Elements implicit in the aforementioned recommendations will be addressed here. For example, regarding *accuracy*, to be discussed are issues on design spectral shape, and the records' spectral shapes relative to the design spectrum and to each other . On addressing *efficiency* issues on the number of records to consider adequate will also be discussed. It will be discussed that the elastic spectral shape linked to nonlinear time history analysis is important, especially if recorded acceleration time histories are to be artificially modified. Finally, an attempt will be made to bridge the gap between nonlinear structural understanding, and its use to guide the traditional elastic-based member sizing design schemes.

1.2 Organization and Scope.

It is intended in this study to address some of the issues discussed above, and to improve PSDA as an engineering tool. The main focus is on nonlinear structural behavior; how to benefit from currently used methods (e.g., *Spectrum Matched Records*) to estimate it accurately and efficiently, and how to profit from the understanding of nonlinear behavior for design.

Even if one is willing to perform as many nonlinear analyses as necessary, it is easy to realize that ground motions may not be available. The engineer's preferred option is to employ recorded ground motion before having to make use of artificially generated accelerograms. Chapter 2 addresses this problem briefly, and proposes one intermediate solution, by using recorded ground motions as *seeds*, and subjecting them to mild modifications, unlike the comparatively "harsh" manipulation that some methods utilize.

It discusses the importance of spectral shape and the way to take advantage of available ground motions from different characteristics than those desired, by modifying them accordingly. It allows the engineer to use artificially generated ground motions, with more natural "jagged" spectral shapes and phase spectra than some artificial ground motion schemes can offer. It introduces the concept of *Spectrum Matching* or *Compatibilizing*, but unlike traditional uses of these methods, makes use of non-smooth *target* spectral shapes, which are more closely related to the input seed.

The more traditional consideration of using a smooth target spectral shape for response spectrum matching is addressed in Chapter 3. The actual efficiency that the method can allow, briefly mentioned in the previous section above, is presented and discussed. Also discussed is the far-from-obvious presence of bias in the estimation of displacement-based response. Upon such demonstrations, an attempt to explain this bias is carried out, as is a procedure for bias correction.

Chapter 4 makes use of the PSDA format in order to provide for information relevant for structural design. By disassembling the analytic formulation of the probability of failure (Eq. 1.1) , and by making engineering judgement on the expected postelastic behavior of the structure-to-be, it presents a scheme for computing a design-basis earthquake representation (e.g., in terms of spectral acceleration) for sizing. This resulting DBE is not tied to a fixed probability of exceedence itself, but to a level that will cause the expected (post-elastic) failure to occur with a prescribed probability. The proposed design scheme also allows for *local* sizing for direct reliability improvement. A case study is presented for the design of a 3-dimensional fixed steel offshore platform. Some of the bi-

products of considering a 3-dimensional structure in a traditional uni-dimensional PSDA (one horizontal component of ground motion and response) framework are presented in Appendices 4.A. The design scheme proposed in Chapter 4 is tied to a *failure* performance level. Interesting issues arose in the design procedure, such as the need for identification of a scalar representation of seismic intensity, as well as of failure; the probabilistic description of seismic demands and threats, as proposed by equation 1.2, consider scalar representations. Chapter 5 also addresses some of the problems of considering such uni-dimensional PSDA with a 3-dimensional system, from the point of view of using spectrum-matched records.

Finally, Chapter 6 presents a summary and conclusions of the findings of all Chapters. It presents an overview of the Chapters and lays out the relationship between one another, laying out the foundations for future work.

It is worthwhile mentioning what was deemed to be important but was not considered, due to either need of focus, lack of time, or a combination of these. The study of "representative" accelerograms, and their spectral shape is limited to scenario-based records, i.e. a M-R *bin* of records. One potentially important special case scenario, i.e., the explicit identification of the issues that arise from considering records from *near-source* events records, was not considered. Records considered are mainly stiff-soil California ground motion records.

In terms of spectral shapes, also only scenario-based shapes are considered. The use of other shapes to be used as targets for spectrum compatibilizing is not addressed, limiting the practical use of the results presented. The description of a more rational spectral shape to be explicitly linked to nonlinear dynamic analysis in a PSDA framework is left for future work.

The systems analyzed in Chapter 3 did not consider strength-degrading behavior, including P-Δ effects. Also not studied were issues related to the presence of important higher-mode effects. Torsional effects, very likely to be an important issue on the study

of realistic 3-dimensional systems, were kept at a minimum by considering a near-symmetric system.

The need for improving the definition of the seismic capacity of a structural system is a complex problem, the solution to which is not addressed here. Also, the capacity description considered in Chapter 4 was limited to a prescribed (but not uncommon) definition. The performance level considered for providing member-sizing was unique (i.e., collapse); it did not consider lower or multiple performance objectives, as a more complete Performance Based Design would require.

The required input for failure-level based design or PSDA includes both capacity and demand random variables. Typically one can model these by simple two-parameter descriptions. Although sensible numbers were used for the dispersion quantification, the estimation of this parameter was not addressed directly. A more in-depth study of the sources of this dispersion, and an efficient means for its estimation is needed.

Chapter 2

Spectral Shape Modification of Recorded Ground Motion

2.1 Background.

For many parts of the world, including Eastern North America (ENA), there exists a severe lack of available strong motion earthquake records, especially for moderate to high magnitudes at a wide range of distances and for different local soil conditions. Even in data-rich regions such as coastal California (CC), the need to have suites of records representative of specific source-site characteristics often arises, e.g., for linear or non-linear dynamic soil and structural analyses (e.g., Han and Wen, 1997; Yeh and Wen, 1989). Therefore, records need to be "constructed". In ENA practice, theoretical synthetic time histories are most commonly used today. This chapter considers, in contrast, a procedure to modify existing instrumental recordings with their often broader inherent variability and ``rougher'' response spectra. The source-site characteristics that have been considered here are magnitude-distance, and a given soil representation of the site.

The focus of both Chapters 2 and 3, with respect to the use of artificially generated time histories, is not to represent ground motion with geophysically "correct" entities, but rather to provide the engineer with a valid pragmatic tool for estimating the effects of ground motion on the structure.

With this in mind it can be said that any scheme for creating artificial accelerograms, such as colored gaussian processes, spectrum compatibilized records, etc., for this purpose, must be verified with respect to the responses they produce in structural models beyond the simple linear SDoF oscillators associated with elastic response spectra. The effectiveness of the method presented here is evaluated by a control case that uses samples of real Coastal California records representative of a particular magnitude-distance scenario, as representative of "reality". Records from other magnitude-distance and site soil characteristics are used as *seeds* and then modified by the proposed method to represent the scenario. Certain inherent characteristics of these original records, such as the realistic non-smooth character of their response spectra, are to be maintained in the artificial records generated. The comparison between the "artificial" (modified) records and the real records is made through linear and nonlinear SDoF and MDoF structural responses. We conclude that the method works well for predicting the median ductility demands of the scenario.

As discussed in Chapter 1, current engineering practice and code recommendations for the investigation of nonlinear structural demands are based on two elements: the use of a design-basis response spectrum, and the selection of appropriate accelerograms that can somehow represent the design spectrum. One method, for example, for finding adequate accelerograms associated with a UHS consists of *disaggregating* the hazard into the contribution of different scenario events (M,R) (e.g., McGuire, 1995; Bazzurro and Cornell, 1999). In terms of appropriate record selection, throughout this work only the selection of scenario records will be considered.

The scarce character of earthquake records in many regions of the world can impose the need to generate artificial earthquake records for scenarios considered. This problem arises frequently. What is attempted here is to provide a means for even employing regional records that fall well outside the scenario event.

The use of existing records is considered here, keeping from these some characteristics that are of interest to non-linear dynamic analyses, such as the Fourier phase spectra, and the non-smooth character of their elastic response spectra. Other more traditional methods for generating earthquake records consider using smooth power spectra and random phases (e.g., Boore, 1983), and/or smoothed response spectral shapes (e.g., Silva, 1987). Many engineers prefer, however, the use of real records, with their rough response spectra, when conducting non-linear spectral analyses.

2.2 Methodology.

The starting point for correcting records is to define an objective to which the resulting artificial record or records will correspond.   The objective can be defined by a magnitude-distance pair (M-R) and a soil type. Such objective is related to the *scenario event* for which the analyst is interested in computing nonlinear structural responses.

A given real record, e.g., a *seed*, (in general) of different M-R and soil characteristics than that of the objective will be modified to meet the objective's features by means of a (rough) *target* spectral shape associated to both the objective and the original record's characteristics, by matching the response spectrum of the seed to it.

The target response spectrum is generated by *factor functions* that correspond to two levels of correction, the M-R correction, and the soil correction. These factor functions, when multiplied by the seed's response spectrum, generate the target response spectrum. Note that for each candidate record to be modified there will be a different target response spectrum to which it needs to be matched.

2.2.1 Factor Functions.

Assume for the moment that there is no need for a soil correction. Magnitude-distance factor functions can be obtained by means of available attenuation laws. Two median response spectra are computed, associated with the M-R pairs of the objective and of the seed. The ratio of these is defined as the "factor function" for M-R correction (see Figs. 2.1 and 2.3). The response spectrum of the seed (jagged) will not equal the attenuation law's calculated median spectrum (smooth), which is in accordance with the observed record-to-record variability of spectral ordinates.

The M-R factor function represents the systematic increase or decrease in the (predicted) frequency content that the seed's response spectrum should have, had it had the objective's M-R pair. Typically, for example, for a given distance, a higher magnitude for the objective will generate a function than is higher than 1.0 in the lower frequencies, which reflects the fact that high-magnitude events are richer in low frequency content than are low-magnitude events. The opposite is true for a lower objective magnitude (e.g., see Fig. 2.1b). Also, for a given magnitude, a higher distance in the objective causes a factor function to be lower than 1.0, more or less homogeneously throughout the whole frequency range, reflecting the loss of energy with distance in all frequencies of the earthquake signal. The following example considers a seed lower in magnitude than the objective, but a shorter distance, such that the overall required factor function is mixed: low frequencies will require amplification, while higher frequencies will need to be reduced.

When the objective's soil type is the same as that of the seed's soil type the M-R factor function obtained, when multiplied to the seeds' response spectrum, generates the target response spectrum (see Fig. 2.1c).

The soil factor function can be obtained also by means of appropriate attenuation laws that include soil types. If the objective soil type is "deep broad soil", for example, then the corresponding factor function is computed from the ratio of the median response

spectrum obtained by using the seed's M-R pair into the "deep broad soil" attenuation law, to the median response spectrum obtained by using the same M-R pair, but using the law corresponding to the seed's soil type, e.g. "rock".

Alternatively, site-specific soil factor functions can be used. The response spectrum of a seismic signal that has traveled through a soil model can be computed from the time history obtained by an analysis like that of SHAKE (Schnabel et al, 1972). Such analyses can be carried out on several records, for the same soil conditions (typically for a single magnitude due to the systematical amplitude dependence), to obtain an average factor function describing the amplification or de-amplification of spectral ordinates, caused by the soil layer(s). If the objective's M-R pair is precisely the same as the seed's M-R pair, the target response spectrum is the soil factor function alone multiplied by the seed's response spectrum.

In the case of using solely attenuation laws to generate the factor functions, one needs not to generate separately both M-R and soil factor functions, but directly the one that corresponds to both corrections simultaneously.

The use of such factor functions (obtained by attenuation laws, or average amplification-de-amplification functions) will generate "rough" target spectra, since while the factors themselves tend to be smooth (especially if attenuation-law-based), they will be multiplied by the original (seed) record's "rough" response spectrum (see Figs. 2.1c, 2.3 and 2.5). These "rough" target spectra present close resemblance to their corresponding seeds' response spectra. In other words, the seeds' spectra will only change in shape to the extent that the predicted response (from the attenuation laws) spectra differ from one another.

2.2.2 Target Spectrum Matching.

The goal is to generate a time history that will have a response spectrum as close as desired to the target spectrum. Traditionally, the problem of forcing a record to have its SDoF response spectrum equal another, usually smooth, response spectrum is called spectrum *compatibilizing* or spectrum *matching*. There are available different algorithms that modify the seed record either in the time domain (e.g., RSPMATCH, Abrahamson, 93), or in the frequency domain (e.g., SYNTH, Naumoski, 85; RASCAL, Silva, 1987). A more in-depth description of these methods will be presented in Chapter 3.

It is important to realize the role that the use to be made of the artificial time histories plays in their generation. This is in accordance with the earlier mentioned statement that what are sought are representative ground motion for non-linear *structural* response prediction. One of these roles is the definition of the region of interest where the created records' spectra will need to be more accurate. For the very basic case of the analysis of lightly damped elastic SDoF systems such a region need not be more than only the close vicinity of the structural frequency. Only a mere scaling of the seed records (e.g., to the target level of spectral acceleration) will generate the same SDoF response. For a linear MDoF system one must consider the higher modes of the structure (i.e., match also higher frequencies), to the extent that these participate in the total response. For more general non-linear MDoF systems, one needs to have a certain appreciation for where the region of interest might be; the response of the structure might be mostly influenced by the frequency of the softened first mode, so the region of interest is in the range of frequencies lower than the fundamental frequency of the elastic structural counterpart. The width of the range will be determined by the degree of "softening", that can empirically be related to the level of non-linear displacement (in terms of ductility, μ) caused by the record (Kennedy et al, 1984). The lower frequency, f_μ, should be about $1/(\mu)^{1/2}$ times the first-mode frequency, f_0. Also, one might need to judge the level to which higher modes contribute to the response, and also the effect of softening on these. Current code recommendation for such a region of interest for time history analysis (e.g.,

UBC, 1997) is a range of frequencies ranging from $3/2\ f_0$ to $5\ f_0$, where f_0 is the fundamental frequency of the structure to analyze.

The matching approach considered for this chapter was a frequency-domain one. It modified the Fourier spectral amplitudes of an input seed record, while keeping its phases. This approach generally creates artificial time histories that resemble the seed. See Fig. 2.4 for example. In order to keep the phases one applies to the signal a real-only "transfer function" (i.e., with a zero-imaginary component), to rescale the fourier amplitudes (without altering the phases).

In the examples presented below, the modification of earthquake accelerograms will be done for the nonlinear dynamic analysis of structural systems with known elastic properties (e.g., their elastic mode shapes and frequencies). For these cases one did not need to have the spectra match perfectly the entire expected response spectra but rather only sufficiently match the target in the region of interest, as discussed above.

Before the records can be used for non-linear dynamic analyses it is recommended that they be baseline corrected, as one would expect a real record to be. It can be the case that while correcting the original record one introduces low frequencies that cause the displacement time history of the record to drift away from the origin, which is not generally expected from a real (corrected) accelerogram.

Summarizing, the steps to follow for each record are:

- Given the objective's M-R pair, and also the M-R pair of the record to correct, generate their median predicted response spectra, by means of an attenuation law, and from their ratio find a factor function for M-R correcting (Fig. 2.1);

- Find a factor function for soil correcting, if necessary (Fig. 2.2);

- From the product of the factor functions and the spectrum of the seed record, determine the target response spectrum sought (see Figs. 2.1c , 2.3 and 2.5 for examples);

- Define the region of interest, and spectrum-compatibilize the seed to have its response spectrum match the target, in this region (see Figs. 2.4 and 2.5 for examples).

2.3 Method Testing: Coastal California records.

The objective of this section is to verify that the method proposed works and to justify the need for record modification in some cases, as well as to clarify the procedure.

Due to the abundance of records for different M-R scenarios it was convenient to make use of Coastal California records. Several examples that modify such records are presented.

By making use of a "control" set, the results that modified records produce were able to be verified. As a first example an extreme case was considered. Records from large magnitude earthquakes were modified to "represent" a particular scenario of a lower magnitude. Real accelerographic records were available for the low magnitude scenario. Non-linear runs were made on several SDoF and MDoF systems in order to verify the results generated from the artificial records. Their results were compared to those produced by the actual records, in order to establish the justification of the need to modify the spectral shape.

A second example considered the correction of records from different M-R and soil characteristics, which is usually the case the engineer will run into in practice.

2.3.1 Extreme Record Modification.

All results were generated in a framework such that comparisons can be made to show the effectiveness of the method. The non-linear runs were made after all the records were normalized (scaled) setting their response spectra to have the same ordinate at an appropriate reference frequency, which was taken here to be the fundamental frequency of the considered structure (the records were re-normalized for each structure considered). This normalization procedure allows us to separate more easily systematic differences in the non-linear response values due to the differences in response spectral shapes and other characteristics of the records, as distinct from the large differences in responses that arise from the "intensity" of the records. Intensity was defined by the response spectral ordinate at the reference frequency (Shome, et al, 1998; Shome and Cornell, 1999).

To briefly illustrate this scaling we can look at the results from running a small suite of six magnitude 7.0^+ records before and after scaling to the median spectral acceleration at the corresponding structural frequency. The runs were done on two SDoF non-linear systems and Table 2.1 shows the median ductility demands (μ_m) and dispersion for the systems.

The median (here, and throughout the work) is computed as the exponential of the average of the natural logarithms, and $\sigma_{ln\mu}$ represents the standard deviation of the natural logarithms of the results. Notice the obvious reduction in $\sigma_{ln\mu}$ in Table 2.1. The medians are, however, not statistically different, implying that this normalization does not introduce any bias. The smaller variability permits the use of fewer records to estimate the median with a specified confidence, as pointed out in Chapter 1.

The control study involves choosing a target M-R scenario and, associated with this scenario, a "bin" from which to take existing records. Ideally the bin will have a narrow range of magnitudes and distances centered on the scenario magnitude and distance.

Higher magnitude records are generally richer in lower frequencies. See Figure 2.6a for the response spectra of the six magnitude 7^+ records, scaled to 1g at 4Hz. The stronger low-frequency content of the selected records are expected to cause more damage to the structure than the target bin records, because the structure behaves in an inelastic fashion, thus reducing its effective fundamental frequency. This means that, in general, records from the unmodified high magnitude bin will be more damaging than those of the target bin (Fig. 2.6 b). In other words, the median ductility response is expected to be higher (after the records have all been normalized to the same intensity), which justifies the need for the correction (Fig. 2.6 c).

For the first Coastal California cases there will be a low magnitude (Mw = 5.3) scenario as a target, and a high magnitude range (7.0^+) is selected for records to be corrected. The reason for this selection is to show that characteristics of records from different M-R pairs can indeed cause different nonlinear demands in the system and that this distinction, if significant, should be corrected. A large difference[1] (almost two units) was selected to maximize this difference and hence challenge the method to the extreme.

The systems that were analyzed correspond to a set of SDoF models of different natural frequencies (1.0, 2.5, 4.0 and 10hz), and two different MDoF structures (low and high fundamental frequency). The low frequency MDoF model corresponds to a 5-DoF model of a 1hz 5-story steel special moment resisting frame. The high frequency MDoF model corresponds to a 5 DoF model of a 4hz nuclear power plant. See Appendix 2.A.1 for more information on structural details.

The target was chosen to be Mw = 5.3, at 20km, on deep soil. The spectral amplitude (i.e., at the reference frequency, f_0) for the analysis of the 5-DoF, f_0 = 4Hz, system was deliberately chosen to be relatively high (4.35 g) relative to the strength of the structure to show the possible high reduction in non-linear demands caused by the correction. A set

---

[1] Shome and Cornell (1999) have shown that the difference in displacement may not be great unless the magnitude difference is large. He suggests about 10% difference per unit magnitude.

of records that were considered to generate the control statistics was selected from a narrow bin associated with the target (see Table 2.2).

For the high magnitude records three earthquakes (average magnitude 7.3) were chosen from the database, also for deep soil. Both components were considered, which do not have the exact same spectral shapes but are corrected by the same factor functions since they come from the same (M, R) pair (see Table 2.3).

Remember that the difference in the average magnitudes was high; the difference was intentionally chosen to be large in order to test the method as severely as possible.

Note that since the soil types of the objective and the original records are the same, there is no need in this case for a soil factor function to be used. The factor functions were generated using Coastal California attenuation laws (Abrahamson and Silva, 1997).

The overall suppression of the relatively strong low-frequency upon modification is apparent by comparing Figs. 2.6a and 2.6b. The effect in time-domain can be seen for one record in Fig. 2.4. Notice, however, that the method can not provide alteration for typical time-length differences of the different scenarios (corresponding to that of the seed and objective).

2.3.1.1 Nonlinear Demand Statistics.

The large magnitude (seed) records were first run through the structures (after normalizing) without modification, and then run in their modified versions. Structural response was measured in terms of ductilities (interstory and roof) and normalized hysteretic energy (interstory and global). See Appendix 2.B for the definition of these measures. It will be seen that, as desired, the modified version set was able to predict the displacement-based results of the target bin records. Also, the modified records showed a lower response compared to the unmodified set, due to the suppression

of the richer low frequencies. Results were not, however, satisfactory for the energy-based response prediction.

First let us look at the displacement-based response results for the single degree of freedom systems (all systems have 5% damping) (Table 2.4, (a) through (c)). For all cases, statistics corresponding to the scenario (b) were satisfactorily obtained from the runs for the modified versions of the records (c), showing the spectral-shape-induced reduction from the unmodified versions (a).

For the different systems (e.g., 1Hz through 10Hz), different spectral ordinates were considered to which the records were normalized, as well as different structural designs (i.e., yield displacements). The higher frequency systems were designed with lower resistances such that the lower portion of their frequency region of interest overlapped more or less with the lower portion of the frequency region of interest for lower frequency structures. Due to the frequency range of interest, spanning from f_0 to the nonlinear-demand-related "softened" frequency (i.e., $f_\mu = f_0 / \mu^{1/2}$), the higher frequency systems' ductility demands were more noticeably reduced. This was achieved by scaling the records to higher intensities for higher frequency systems. Table 2.4 shows the demand statistics obtained for the various systems.

The same observations can be made for the results from the two MDoF cases studied (1Hz and 4Hz), for the global ductility measure, as well as the maximum interstory ductility (Table 2.5):

In table 2.5 we can see that the median ductilities are reduced by the use of the modification procedure and that they match within the error of estimation that the real records present. The reductions (fluctuating around 20%) are consistent with the typical magnitude-dependent differences of about 10% per unit magnitude, as reported by Shome (1999).

In terms of normalized hysteretic energy (*NHE*), tables 2.6 and 2.7 compare the responses obtained from the large magnitude unmodified records, the objective records' results, and the modified version of the large magnitude records. As can be seen, the reduction is small, relative to the results shown by the target bin records. The much reduced values that the objective records yield indicate that spectral shape modification does not allow to correct for energy related measures. The difference in magnitude also induces a difference in average record durations (on the order of 35 seconds for our selection of high magnitude records and 15 seconds for the low magnitude records; again, the large 2 unit magnitude difference was selected to maximize this difference). Presumably, the *number* of nonlinear excursions is not adequately reduced by the correction, but perhaps only the *amount* of (high) energy dissipation of just a few large response cycles is reduced, causing only an overall insufficient decrease in *NHE* response.

2.3.2 Mixed-Characteristic Available Records.

More generally, only records from a variety of M-R pairs and soil characteristics different from the objective ones will be available. To illustrate this case six records were selected from a wide range of magnitudes and distances, as well as for different soil conditions (deep soil, and rock). The objective was selected for a M-R scenario of Mw=5.55, and R = 12.5km, on deep soil, represented by five real records from a narrow bin with ranges Mw [5.3, 5.7] and R [12.6, 16.9]kms. This M-R scenario was run for both MDoF structures using both the 6 modified records and the 5 actual recordings in order to compare the results. Attenuation laws for both soil and rock were available (Abrahamson and Silva, 1997) from which the factor functions were generated. The records to correct are listed in Table 2.8.

The difference in characteristics of the records with respect to the target can be revealed by close inspection of the factor functions generated. Some are flatter than others, some suppress frequencies in the lower ranges, and some amplify them, as expected for a

comparison made for records of various properties. Figure 2.7 shows different factor functions for the two extreme magnitudes in the set (M = 5.2 and M = 6.9).

Once the records were modified, the non-linear structures were subjected to them and the following statistics were obtained. Comparisons for global (top story) ductility and maximum interstory ductility statistics are made.

As can be seen in the numbers presented in Table 2.9 there is no statistically significant difference between the median response estimates using the real bin records and the modified records.

It is worth mentioning that for the particular set of available records for correction, the results for the unmodified records and the modified records produced very similar results. One possible reason for this is the relatively small softening region, which renders both normalized sets to be very similar. It can be mentioned that the values obtained for the Normalized Hysteretic Energies were virtually identical, for the both systems considered.

2.4 Recommendations and Observations.

The method of "correcting" a record proposed here has proven to be effective for the creation of an "artificial" earthquake time history which can be associated to a ("objective") M-R pair and soil type different from its own. The usefulness of the method lies in the fact that the generated time history can produce ductility demands in non-linear SDoF and MDoF systems similar to those real records of the objective M-R pair and soil type produce. The correction of the record is done to match a (rough) target spectrum which is constructed with a (smooth) *factor function*, which represents the expected change in spectral shape as indicated by the difference in M-R pairs and soil types. The factor function is multiplied by the original record's (rough) response spectrum to obtain the sought-after target.

In general one might use conventional, iterative spectrum-matching algorithms for this purpose. The spectrum-matching that was performed for this chapter was simpler. It used the factor functions as "transfer functions" applied to the Fourier amplitudes of the seed's record, not touching the phases. The modified records' spectra were satisfactorily close to the targets. One might consider this simply as the first step in a conventional iterative procedure. As suggested by Silva, 1987, the fast convergence noted here might be related to the fact that the compatibilization was made to an atypical "rough" spectrum by means of a "smooth" factor function. Such spectrum was not strongly different in shape from the seed's own response spectrum, as opposed to the usual practice of trying to compatibilize to a smooth spectrum (e.g., a design spectrum from a building code).

Unfortunately, for some cases, not presented here, results of compatibilizing to the correction targets can be unsatisfactory. This can true, for example, for the important case of low magnitude seeds with weak low frequency content and/or small duration that are to be used for modification to high magnitude scenarios with rich low-frequency content. The results may be very unusual in their (time domain) appearance and potentially also in their effect on structures; such effect was not tested here. In the Eastern U.S. one may be forced to use as seeds low magnitude records which may have these characteristics. However, this is especially true when compatibilizing to a smooth target shape that has very marked different spectral characteristics.

It is important to consider the high-pass filter frequency used in processing the records to be used as seeds. Typical lower cut-off frequencies can be as low as 0.2Hz, but higher frequencies, as high as 1Hz, should not be surprising to find in published accelerographic catalogues (e.g., Silva, 1999). Any actual frequency content below or even close to these filter-related frequencies (depending on the "windowing" scheme), usually presents a large noise-to-signal ratio. For these cases, perhaps hybrid correction schemes can be proposed, where the low-frequency portion of the to-be-modified record is simulated and not taken directly from the seed.

A possible improvement to the method, which was not tested, includes considering the deviation (e.g., in terms of number of standard deviations) of each ordinate of the original record's response spectrum with respect to the median response spectrum predicted by the attenuation law. As will be seen in Chapter 3, these deviations from the median spectral ordinates define the *global shape* of the record. It will also be seen that the scatter of such global shape in a collection of records has an effect on the median ductility that they produce on a nonlinear system. The scatter of global shape in the available set of records can then be altered (or preserved, if needed) by use of appropriate target response spectra, based on corresponding M-R factor functions.. This may be useful for correcting a suite of records that do not particularly meet required statistical properties (for example, if all to-be-modified records from a bin, are lower than the predicted attenuation shape). As will be discussed in Chapter 3, such anomalies in the modified set may produce biased estimates of median response. For example, if we have a set of records that are particularly low with respect to their predictions, we would want to consider a higher version of the factor function correction, than the one that the simple objective-to-seed prediction spectra can produce.

A limiting characteristic of the procedure is that the duration may not be modified; the duration can be associated with magnitude (rupture size) and distance (wave dispersion). This might limit the applicability of the results to those response measures that are not sensitive to the duration of the record, e.g., ductility demands and Park-Ang-type damage indices (e.g., Park, et al, 1985) with heavily-weighted ductility participation. In particular, normalized hysteretic energy measures were not successfully predicted for the cases studied here.

The principal goal of the procedure was to obtain a means for the prediction of median displacement-based nonlinear responses. The "rough" character of the spectral shapes of the records involved may also play an important role in the prediction of response variability statistics. How well these were reproduced here is not clear due to the very limited sample sizes; the statistical uncertainty in standard deviation estimates is large relative to that in the median. Future work should consider the application of record

correcting or ground motion simulation schemes that will allow the reliable prediction of this important statistic.
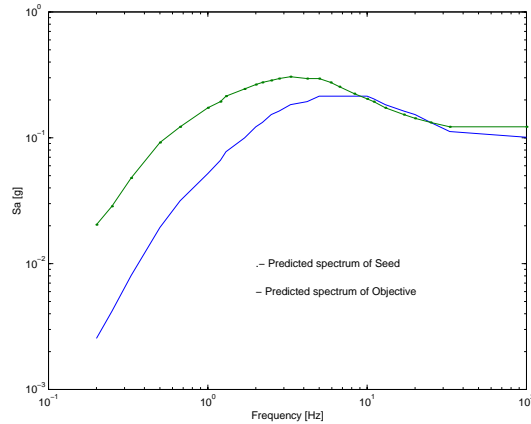
Chapter 2 Figures.

Figure 2.1a The "seed" record will be modified to a particular "objective". The amount of modification will be established by means of appropriate attenuation laws. In this figure, the relative shapes of the seed (e.g., an "earthquake" of M=7.3 at R = 88.5km) and objective (e.g., an "earthquake" of M = 5.3 at R = 20km) response spectra are computed by predictive spectral shapes as per Abrahamson and Silva (1997) (both seed and objective correspond to Western North America events, rock sites)
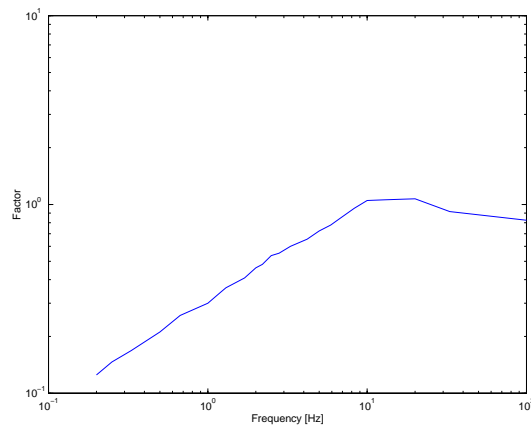
Figure 2.1b. The ratio of the predicted objective response spectral shape to the predicted seed response spectral shape yields the "Factor Function". This function, when multiplied by the actual response spectrum of the seed record, generates the "target" response spectrum to which the seed needs to be matched. It represents the modification that the seed-record's response spectrum will be subjected to. This example corresponds to the ratio of the predicted spectra shown in Figure 2.1a (Western North America seed and objective, rock sites).
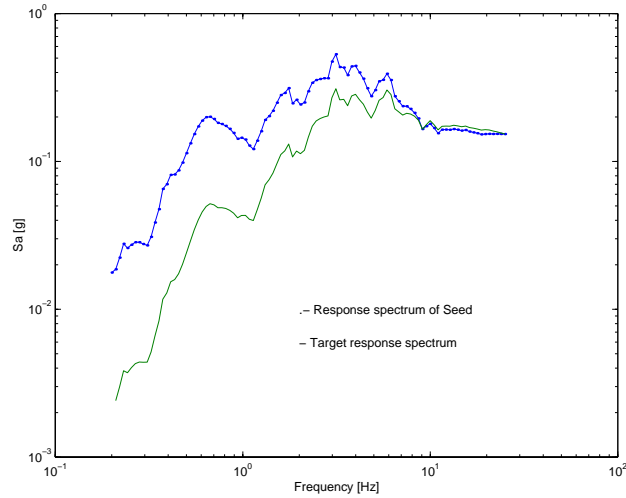
Figure 2.1c. The multiplication of the factor function by the seed's response spectrum yields the "target" response spectrum to which the seed record need to be modified. The seed corresponds to a seismic event with M=7.3, R = 88.5km. The modified shape corresponds to an "objective" of M = 5.3 and R = 20km.
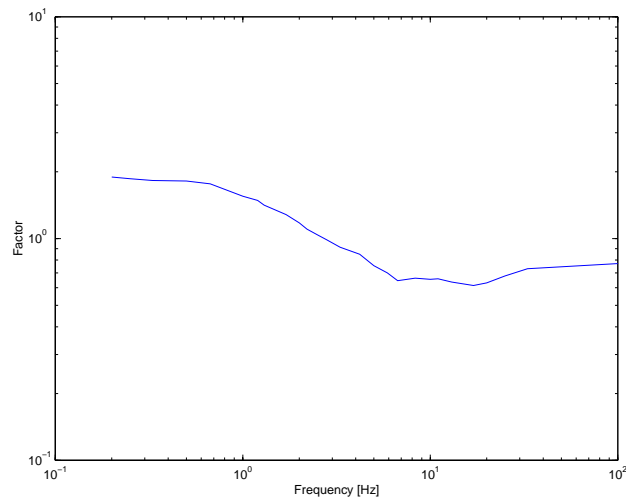

Figure 2.2a. Factor function for soil-only modification. This example corresponds to a Western North America site, for a fixed M = 7.0 and R=20Km, where the objective is "deep soil" and the seed corresponds to "rock". Attenuation law by Abrahamson and Silva (1997).
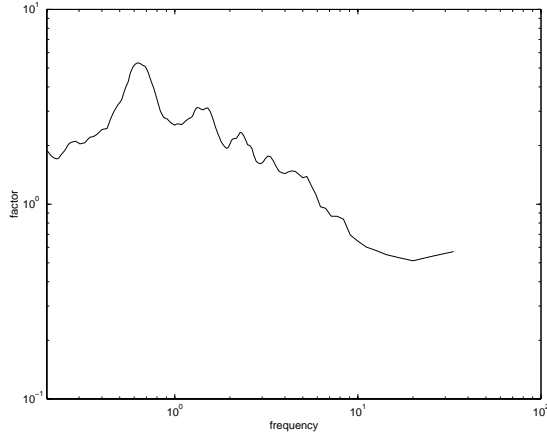
Figure 2.2b Factor function for soil-only modification. This example corresponds to an Eastern North America site (Savannah River) for which a site-specific amplification study was carried out (for near high-6 magnitudes) (Lee, 1996).
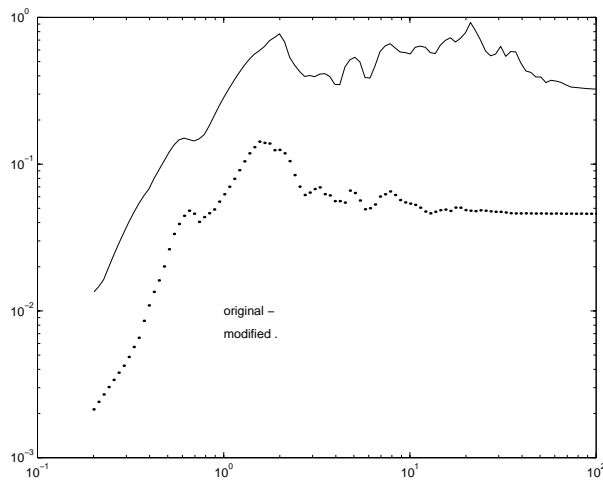

Figure 2.3. Response spectrum of the original (seed) record and the ("rough") target spectrum resulting from multiplying by the net factor function. For this example, the soil factor function was taken as that of Figure 2.2b, and the M-R factor function considered a seed of M = 6.8 at 8kms, and an objective of M = 5.85 at 27.5kms (note that such an objective for this case should overall reduce the frequency content).
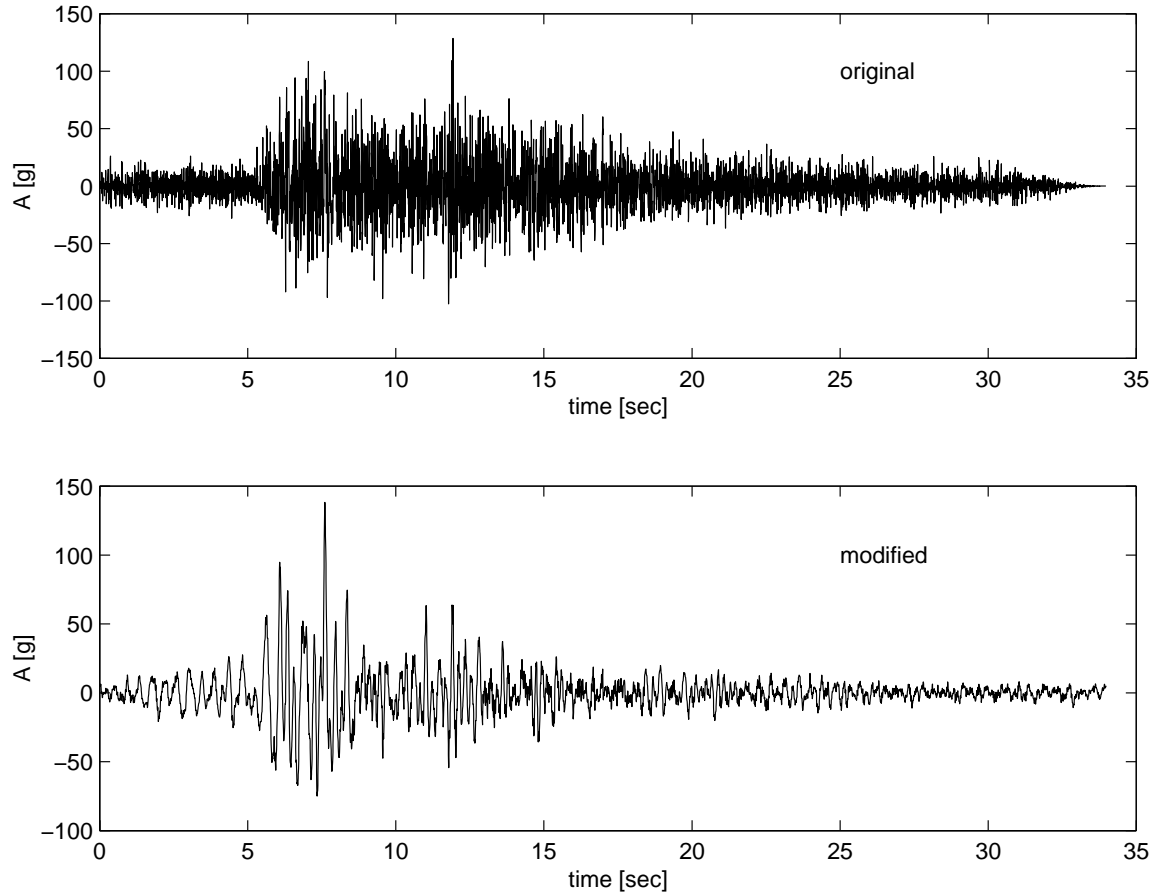
Figure 2.4: Keeping the phases of the seeds causes the modified records to "look like" their parents, at least with respect to the time-variation of intensity. This example shows a Mw 6.0 at 43.1 km record, modified to a Mw 5.85 at 27.5 km target. The site-specific soil factor function depicted on Figure 2.2b is also applied. Clearly, high-frequency content has been reduced, due to the change in magnitude.
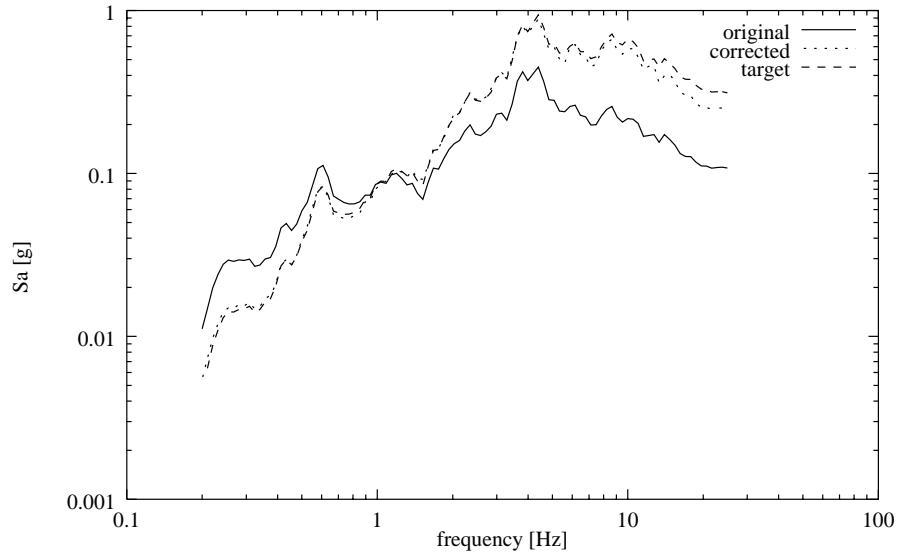
Figure 2.5: The response spectrum of a corrected record corresponding to a seed of Mw = 7.3 at 88.5 km modified to an objective: Mw = 5.3 at 20km, shows a good resemblance to the expected ("rough") spectral target shape.
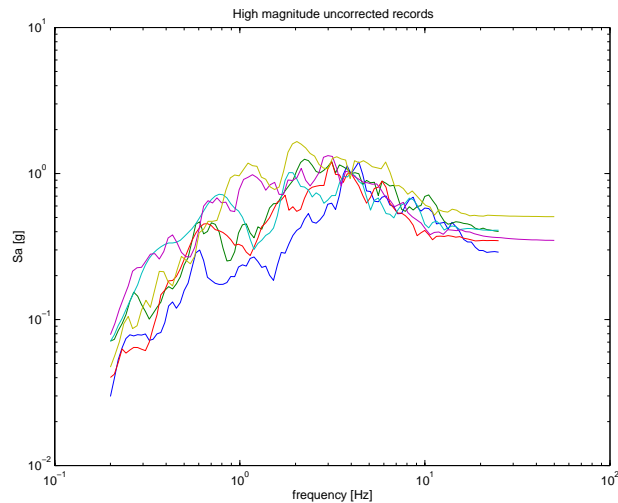

Figure 2.6a. Unmodified M7[+] Coastal California records, normalized to 1g at 4Hz. The damping corresponds to 5%. The high magnitude shows stronger low-frequency content than low magnitude records; compare to Figure 2.6b.
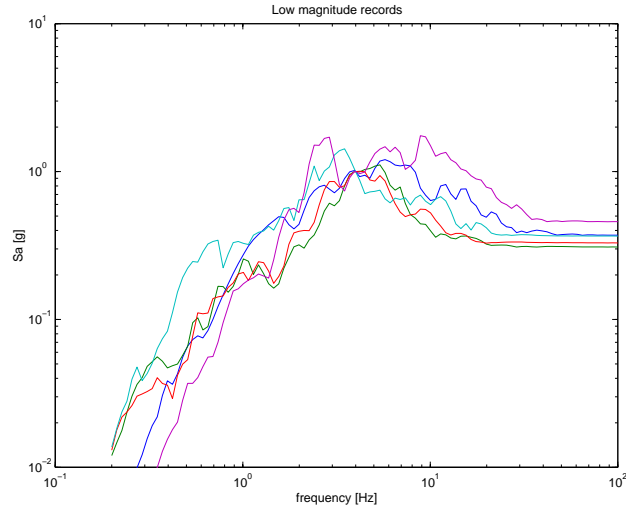
Fig 2.6b. Control low magnitude bin records (representative of the M = 5.3 objective), ranging from M = 5.2 to M = 5.4, from Coastal California. The damping corresponds to 5%. Records are normalized to 1g at 4Hz. Notice the weaker low-frequency content, with respect to the larger M = 7[+] magnitude records in Fig. 2.6 1.
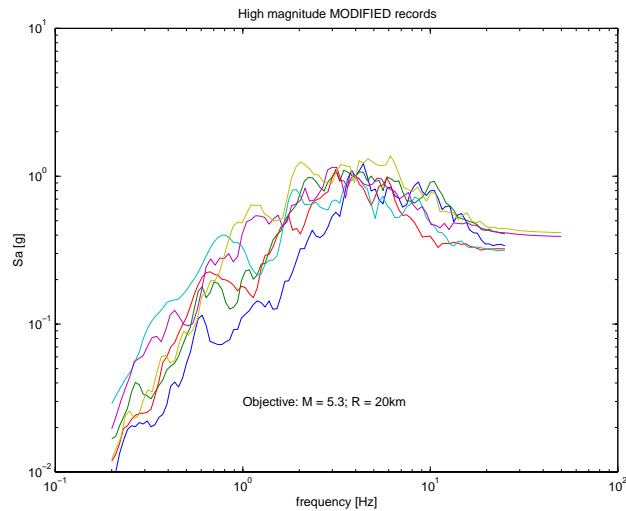

Fig. 2.6c. Seed records (M = 7+ records) modified to objective characteristics (M=5.3 R = 20 km). Records are normalized to 1g at 4Hz. (The damping corresponds to 5%). Compare to the real low magnitude records in Fig. 2.6.b.
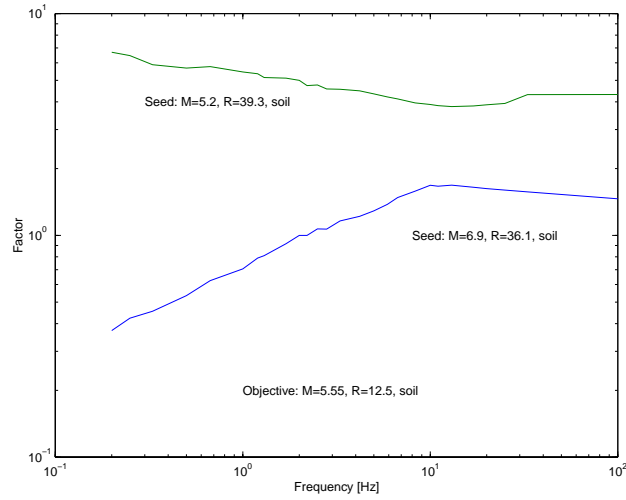
Figure 2.7. Factor functions for the highest magnitude record in the set (M = 6.9) as well as for the lowest magnitude (M = 5.2). Notice the suppression of the low frequencies for the former, as well as the increase in content of low frequencies for the latter.

Chapter 2 Tables.

	Un-normalized		Normalized	
	4Hz	1Hz	4Hz	1Hz
μ_m	7.65	3.27	7.95	3.44
$\sigma_{ln\mu}$	0.64	0.80	0.37	0.44

Table 2.1 Nonlinear demands for normalized and un-normalized bin records. Note the reduction in dispersion for the normalized case, while the median ductility is virtually the same.

Event	Date	Mw	R [Km]
Imperial Valley	10/15/79	5.2	15.0
Coalinga	6/11/83	5.3	10.5
Hollister	1/26/86	5.4	16.9
North California	6/7/75	5.2	29.9
Whittier Narrows	10/4/87	5.3	12.6

Table 2.2. Coastal California target bin records for control statistics (low magnitude records).

Event	Date	Mw	R [Km]
Landers	6/28/92	7.3	88.5
Cape Mendocino	4/25/92	7.1	44.6
Kern County	7/21/52	7.4	120.5

Table 2.3. High Magnitude records for Coastal California.

a)	Unmodified Records (average Mw ~ 7.3)			
Statistic	1Hz	2.5Hz	4Hz	10Hz
μ_m	3.33	6.70	8.63	17.90
$\sigma_{ln\mu}$	0.45	0.24	0.48	0.37

b)	Real Records from Target Bin			
Statistic	1Hz	2.5Hz	4Hz	10Hz
μ_m	2.49	4.40	5.43	10.50
$\sigma_{ln\mu}$	0.31	0.43	0.55	0.64

c)	Modified to Objective: Mw = 5.3, R = 20Km			
Statistic	1Hz	2.5Hz	4Hz	10Hz
μ_m	2.72	4.78	5.67	11.13
$\sigma_{ln\mu}$	0.42	0.15	0.32	0.65

Table 2.4 Nonlinear ductility demand statistics from SDoF systems. (a) High magnitude bin (seeds), (b) target bin records, and (c) seeds modified to objective. For all different systems we can see the clear reduction in ductility demands caused by the correction ((a) vs. (c)), and a reasonable prediction of the median ductility demand as indicated by the results of the real records (b). Indeed, the medians of the two last sets are not statistically significantly different ((b) and (c)). It can also be pointed out that even though there appears to be a big difference in the observed standard deviations (across frequencies, and across record set results), the variability of this statistic can in fact be large (e.g., differences of 100%), for the small sample sizes considered here.

a)	Unmodified Records (average ~ 7.3)			
Statistic	1Hz		4 Hz	
	Global	Max. interstory	Global	Max. interstory
μ_m	3.18	6.03	7.55	14.85
$\sigma_{ln\mu}$	0.39	0.50	0.43	0.34

b)	Real Records from Target Bin			
Statistic	1Hz		4 Hz	
	Global	Max. interstory	Global	Max. interstory
μ_m	2.39	4.12	5.54	12.84
$\sigma_{ln\mu}$	0.18	0.20	0.37	0.21

c)	Modified to Objective: Mw = 5.3, R = 20Km			
Statistic	1Hz		4 Hz	
	Global	Max. interstory	Global	Max. interstory
μ_m	2.65	4.84	5.69	12.68
$\sigma_{ln\mu}$	0.27	0.43	0.41	0.25

Table 2.5 Nonlinear ductility demand statistics (global and maximum interstory) for two MDoF systems (4Hz and 1Hz). (a) High magnitude bin, (b) target bin records, and (c) modified records.

a)	Unmodified Records (average Mw ~ 7.3)			
Statistic	1Hz	2.5Hz	4Hz	10Hz
NHE_m	9.89	38.20	72.75	253.03
σ_{lnNHE}	0.43	0.56	0.81	0.72

b)	Real Records from Target Bin			
Statistic	1Hz	2.5Hz	4Hz	10Hz
NHE_m	3.66	13.08	17.14	57.10
σ_{lnNHE}	0.73	0.76	1.04	0.89

c)	Modified to Objective: Mw = 5.3, R = 20Km			
	1Hz	2.5Hz	4Hz	10Hz
NHE_m	7.21	23.32	42.96	156.98
σ_{lnNHE}	0.41	0.40	0.65	0.89

Table 2.6 Normalized Hysteretic Energy (*NHE*) response statistics from SDoF systems. *NHE$_m$* represents the median value, and σ$_{lnNHE}$ the standard deviation of the logarithm. The required reduction is not obtained by the proposed correction scheme.

a)	Unmodified Records (average ~ 7.3)			
Statistic	1Hz		4 Hz	
	Global	Max. interstory	Global	Max. interstory
NHE_m	20.01	52.24	29.04	222.90
σ_{lnNHE}	0.53	0.67	0.71	0.61

b)	Real Records from Target Bin			
Statistic	1Hz		4 Hz	
	Global	Max. interstory	Global	Max. interstory
NHE_m	8.92	19.60	15.89	101.72
σ_{lnNHE}	0.37	0.41	0.59	0.64

c)	Modified to Objective: Mw = 5.3, R = 20Km			
Statistic	1Hz		4 Hz	
	Global	Max. interstory	Global	Max. interstory
NHE_m	19.04	43.69	25.44	184.88
σ_{lnNHE}	0.48	0.60	0.62	0.49

Table 2.7 Normalized Hysteretic Energy (*NHE*) response statistics for two MDoF systems (1Hz and 4Hz). NHE_m represents the median value, and σ_{lnNHE} the standard deviation of the logarithm. The required reduction is not obtained by the proposed correction scheme.

Event	date	Mw	R [Km]	site
Coalinga	6/11/83	5.3	9.7	rock
San Fernando	2/9/71	6.6	29.1	rock
Loma Prieta	10/18/89	6.9	36.1	soil
Coalinga	5/2/83	6.4	27.7	rock
Hollister	1/26/86	5.4	16.9	soil
North California	9/22/52	5.2	39.3	soil

Table 2.8. Western U.S. selected records, from mixed M-R characteristics.

Mixed-characteristic records modified to objective				
Statistic	1hz		4hz	
	Global	Max. interstory	Global	Max. interstory
μ_m	2.76	4.65	2.18	4.45
$\sigma_{ln\mu}$	0.54	0.57	0.3	0.27

Real records from target bin (M = 5.55, R = 12.5)				
Statistic	1hz		4hz	
	Global	Max. interstory	Global	Max. interstory
μ_m	2.66	4.68	2.05	4.33
$\sigma_{ln\mu}$	0.4	0.5	0.33	0.25

Table 2.9. Nonlinear ductility demand statistics for two MDoF systems (1Hz and 4Hz) from modified and real records.

Appendix 2.A: Structural details

The structural properties for the MDoF systems considered in Chapter 2, corresponding to the 4Hz and the 1Hz structures are shown below.
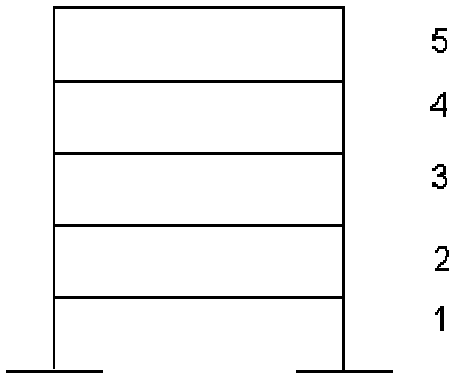
Figure 2.A.1 Structural model of the (stick) MDoF systems considered. The model represented either a 5DoF, 4Hz nuclear power plant (concrete shear walls) or a 5DoF, 1Hz SMRF. See Tables 2.A.1 and 2.A.2 for the properties assigned.

System	floor	M [kips s^2/in]	K [kips/in]	de [in]
4Hz	5	17.10	1.85E+04	0.18
	4	40.20	1.13E+05	0.07
	3	48.80	1.83E+05	0.07
	2	47.90	4.14E+05	0.04
	1	61.00	6.47E+05	0.02

Table 2.A.1a. Structural properties for the 4hz system. It represents a reinforced concrete nuclear power plant. Inoue (1990). The hysteretic model considered a pinching loop, with a post-yield slope of 3% that of the elastic slope (elastic stiffness).

System	floor	M [kips s^2/in]	K [kips/in]	d_y [in]
1Hz	5	0.24	5.88E+01	0.68
	4	0.58	3.10E+01	0.68
	3	0.58	8.10E+01	0.83
	2	0.58	7.20E+01	0.91
	1	0.58	1.86E+02	0.6

Table 2.A.2 Properties for the 1Hz system. It represents a SMRF. The hysteretic model considered a bilinear elasto-plastic system, with a yield slope of 3% that of the elastic slope (elastic stiffness).

Appendix 2.B: Structural Response Definitions.

The seismic demands of the systems mentioned above are both displacement and energy-related ones. The emphasis, however, is on the former, in the normalized version, for both top story (roof) ductility and maximum interstory ductility (for the MDoF systems). The definition of the measures used are as follows:

2.B.1. Interstory (Displacement) Ductility, μ_i.

It is defined as the maximum interstory displacement of a MDoF system divided by the yield displacement of the corresponding interstory:

$$\mu_i = \frac{|u|_{max}}{u_y}$$

where $|u|_{max}$ is the maximum interstory displacement, and u_y is the corresponding interstory's yield displacement. The subindex i denotes *interstory*.

2.B.2. Global Ductility, μ_g.

This parameter corresponds to the ductility of the top story's total displacement, normalized by the yield displacement obtained by means of a static nonlinear analysis (pushover analysis):

$$\mu_g = \frac{|u|_{roof}}{u_{gy}}$$

where $|u|_{roof}$ is the maximum roof displacement (relative to the base), and u_{gy} is some representative *global* yield displacement, obtained from the tangential intersection of the elastic branch and the strain-hardening branch of a force-deformation curve from the pushover analysis. The subindex g denotes *global*.

2.B.3. Normalized Hysteretic Energy, *NHE$_I$*.

This parameter is defined as the cumulative energy absorbed per interstory, normalized by some measure of the elastic strain energy in the interstory:

$$NHE_i = \frac{\sum_{j=1}^{N} (\oint_{cycle\,j} F\,du)}{F_y u_y} = \frac{HE_i}{F_y u_y}$$

where N is the number of response cycles, F is the varying interstory shear force (as a function of the corresponding interstory displacement u), and F_y is the interstory yield shear force corresponding to the interstory yield displacement u_y. The hysteretic energy dissipated per interstory is denoted by $HE_{i.}$ The subindex i denotes *interstory*.

2.B.4. Global Hysteretic Energy, *NHE$_g$* .

The global hysteretic energy was defined in terms of all interstory hysteretic energies (HE_i) , by considering their addition normalized by the *global* yield displacement, u_{gy} (as defined in the global ductility, above):

$$NHE_g = \frac{\sum_{all\,floors} HE_i}{F_{gy} u_{gy}}$$

where F_{gy} is the global shear force present at the value of u_{gy}. The subindex g denotes *global*.

Chapter 3

Spectrum Matching

3.1 Introduction.

This chapter investigates the validity of using spectrum-matched accelerograms for the estimation of seismic nonlinear structural demands. Their use should be tested in terms of the efficiency and the accuracy of the demand estimates they produce. This investigation assumes a given seismic scenario (i.e., given a magnitude and a distance, by means of a representative spectral target shape). Unlike Chapter 2, this chapter focuses on the use of a single (smooth) target spectrum, and will not address different contexts for the use of spectrum compatible records, such as spectral shapes defined by uniform hazard spectra (UHS).

The use of spectrum matched records for the estimation of nonlinear structural response has become increasingly widespread in the past 15 years. Its origins arise from the inability of traditional response spectral analyses to be used to estimate maximum responses of linear systems, for which a time-integration scheme was deemed more appropriate (Preumont, 1983). The use of spectrum matched accelerograms as surrogates for actual recorded ground motion is attractive for multiple reasons. It is generally accepted that they are able to produce results that present relatively lower dispersion, such that they can more efficiently allow the estimation of seismic demands. This is an important benefit, especially for nonlinear analyses that can be highly computer intensive. Modern codes recognize this fact and allow for their use (e.g., UBC, 1997).

Another good reason for their use is simply the scarcity of recorded ground motion for many regions in the world (Léger, 1994).

The use of spectrum compatible records has been common for different nonlinear systems. Examples can be found in Barenberg (1998) and in Mayes (1990) for bridge structures; Naeim (1995) presents results for a base-isolated building; results for a soil column can be found in Ostadan (1996). It should be mentioned that the level of satisfaction of the results obtained by different authors has not been constant. Different warnings have been published in terms of the accuracy of the results and the efficiency that the use of spectrum compatible accelerograms can offer. In terms of efficiency, for example, Preumont (1984) recognizes the variation on demands that accelerograms matched to the same target may produce.

Naeim (1995) indicates the possibility that spectrum matched records may yield highly conservative results. It compares results from spectrum matched accelerograms to a small suite (6 seeds and 2 components) of real records scaled to represent a particular code-based smooth design spectrum, for a base isolated building. Barenberg (1989) presents results for SDoF oscillators of frequencies ranging from 1 to 10Hz, and concludes that results may be unconservative for high frequency systems ($f_0 > 5Hz$). He also compares a single spectrum-matched record to results generated from actual recorded ground motion (a small suite of 8 records), appropriately scaled to envelop a code-based design spectrum.

It is important, however, to put the results obtained by these different authors in the context in which they were generated. As mentioned above, in contrast to other studies, this chapter considers the use of spectrum matched records for obtaining representative demands corresponding to a particular M-R seismic event. We found that for this particular case the use of spectrum matched accelerograms may yield unconservatively biased estimates of nonlinear ductility demands. It was also found here that a possible underlying reason for such bias can not be effectively used in generating accelerograms that produce unbiased estimates of median response, but that the observed systematic bias

can be used to correct, or *de*-bias such observed estimates. Another important finding is the fact that the nonlinear demands obtained do indeed present a significant reduction in dispersion, which allows the use of a substantially smaller suite of accelerograms (of the order of 1/4 the size of an actual recorded ground motion suite) for estimating the median response.

This chapter does not discuss the validity of artificial ground motions as geophysical representative entities. Their inspection is from an engineering point of view in terms of their ability to predict observable effects of interest on civil structures, as would actual recorded ground motions. In other words, the use of spectrum compatible records is only a simulation tool, with the purpose of determining expected seismic induced responses to actual situations.

As mentioned above, also not considered is the use of spectral targets that are not scenario specific (e.g., a code design spectrum, or a uniform hazard spectrum). It is important to mention that the near-source phenomenon was not considered here. The systems studied here do not consider degradation in resistance, including degradation arising from considering P-Δ effects.

The organization of the chapter is in two main parts. The first part, sections 3.2 through 3.5, discusses spectrum compatibilization in general, and presents empirical results for SDoF systems as well as for MDoF systems. The second part, sections 3.6 through 3.8, deals with the understanding of the aforementioned unconservatism present in the estimation of ductility demands by the use of the spectrum matched accelerograms.

3.2 Spectrum Compatibilization.

Spectrum Compatible Records (SCR), also known as Spectrum Matched Records, are artificially generated time histories of ground motion acceleration (or other relevant

parameter, e.g., velocity) whose response spectral shapes are equal within a prescribed tolerance (i.e., "compatible with" or "matched to") to a predetermined "target" spectrum.

The iterative generation of such an artificial accelerogram can be done in many ways, but the different schemes can be separated into two major groups: Frequency-Domain- based (FD), and Time-Domain-based (TD) compatibilization or matching. These characterizations are related to the domain in which the modification or alteration of a record (including all iterations) is conducted. The first-step iteration will use an accelerogram, itself being from an actual recording or artificially generated as well. The initial record to use is typically designated as a *seed* record.

3.2.1 Frequency Domain Compatibilization.

Available Frequency-Domain techniques for the generation of artificial accelerograms associated to earthquake response spectra have existed for many years. An early proposition, which is still somewhat popular today, is utilized by the computer code SIMQKE (Gasparini, *et al*, 1976); it is based on the relationship between expected response spectral values and the spectral-density function of a random process representation of ground motions. This relationship is derived from analytic random vibration theory (RVT) techniques (Vanmarcke, 1976). A seed record is generated as a simulated realization of this random process, and subsequent iterations are conducted in the frequency domain.

In Chapter 2, the modification of existing earthquake records was discussed. In that case, the target spectrum depended on the response spectrum of the record itself (i.e., all records were matched to different seed-specific targets). There, the described modification technique is a simple one, based on scaling the record's Fourier amplitude spectrum by a smooth "factor function" which is computed by finding the ratio of the predicted response spectrum of the target scenario event to the predicted target of the seed event. The main difference between this method and the one used in that chapter is

the fact that there (Chapter 2) the target spectrum (unique for each record to be modified) is a "rough" spectrum, whose shape is not strongly different to the seed's rough spectrum, and hence the convergence was fast. Compatibilization, as done in practice in general, involves a smooth target, which differs in shape strongly from the rough spectra of the seeds.

The Frequency-Domain method utilized in this chapter is coded in the computer program RASCAL (Response Spectra and Acceleration Scaling) (Silva, 1987). It is a semi-empirical procedure, which evolved from RVT-based techniques, with the additional (empirical) utilization of the observed Fourier phase spectrum of a real ground motion recording (as done in the simplistic approach of Chapter 2). The RASCAL procedure modifies the Fourier amplitude spectrum of a seed record in two stages, and the convergence is very quick, requiring typically two to four iterations.

In the first stage, the factor function applied to the Fourier amplitude spectrum is a smooth one, generated by the ratio of the RVT-predicted expected smooth response spectrum associated to a Brune-based source spectrum (Boore, 1983) to the target response spectrum. Such generated factor function is then used to modify the Brune Fourier amplitude spectrum. This product is taken as the Fourier amplitude spectrum of the first iteration for a number of predefined iterations. The use of this smooth factor function provides for a more stable convergence, especially during the stage where the amplitude spectra are iteratively modified the most.

The Brune source spectrum considered is that of the so-called ω-squared model:

$$S(\omega) = \frac{\omega^2}{1 + (\omega/\omega_c)^2}$$

(3.1)

where ω_c is the corner frequency (related to the seismic moment and the stress drop). This basic form is then modified to include the radiation pattern, the amplification due to the free surface, high frequency filtering, and the path attenuation (Boore, 1983).

In the second stage, the factor function is based on the observed (jagged) response spectrum (computed in the time domain) of the current iteration's time history (which is generated from the current amplitude spectrum and the seed's phase spectrum). A different prescribed number may also be assigned for the iterations in the second stage.

3.2.2 Time Domain Compatibilization.

Even though the target used as the criterion for generating the artificial accelerogram is based on what looks like a frequency representation (i.e., the target response spectrum), such a representation indicates a (maximum) response that occurred in time.

Time-Domain schemes, such as the one utilized in this study, take advantage of the previous fact, working in a backward approach to modify the time-specific event of maximum response (e.g., the maximum observed acceleration of an oscillator). The basic idea of such time-domain modification of earthquake records assumes that the time of the peak response will not be perturbed by adding a small adjustment to the original time history. This way, the observed response is modified to that of the indicated value given by the response spectrum, taking care of the observed difference between it and the accelerogram's actual observed maximum response.

Sets of "adjustment functions" are then found iteratively, correcting the accelerogram at all the corresponding frequencies of the target, requiring the solution of simultaneous equations to find the amplitudes of the adjustment functions. Two good properties of the procedure are its fast convergence and the ability to conserve for most cases the non-stationary character of the seed time history, provided that the adjustment functions are appropriately selected.

A good choice for the adjustment functions that allows the method to be more efficient (i.e., introducing the minimum change to achieve the maximum possible required change) than the frequency domain schemes (since the added adjustment is not constant in time) includes the (reversed) impulse response function of the SDoF oscillator, associated to the period and damping needed to be modified (see Preumont, 1984, for a discussion of this method and for more references on compatibilization). The method used in this study (based on Lilhanand and Tseng (1987)), coded in the computer program RSPMATCH (Abrahamson, 1993), uses a different adjustment function type, that of a tapered cosine, to improve the correction for high periods:

$$f_j(t) = \cos(\omega_j \, (t - t_j + \Delta t)) \, e^{(-|t - t_j + \Delta t | \alpha_j)} \tag{3.2}$$

where t_j is the time at which the maximum response occurs for the jth spectral mismatch; Δt is the time delay between the maximum of $f_j(t)$ and a peak in the response of $f_j(t)$, and α_j is a frequency-dependent term that controls the effective time duration of $f_j(t)$, that helps preserve the non-stationary character of the reference time history.

As with frequency domain based methods, adjustment factors are applied iteratively until the desired matching criteria are met.

3.3 Systems Studied.

Based on the results of Foutch and Shi (1998), considering many different hysteretic types was not deemed important in this study. In their study it was concluded that the effects on seismic displacement demands in 2-D building frames, are not importantly affected even if the hysteretic models for the nonlinear point hinges introduced to capture member behavior are varied widely. For this study we considered two almost extreme types of basic hysteretic energy absorbed per loop: a bilinear type (large hysteretic loops),

and a pinching type (small hysteretic loops). Figure 3.1 shows a schematic of the types considered.

The range of fundamental frequencies studied spans from 0.2 Hz to 5 Hz, in more or less equally spaced intervals in logarithmic scale. The first set of structures to be analyzed is represented by single degree of freedom (SDoF) systems, for both the bilinear and for the pinching hysteretic types. For each structural frequency three basic designs were generated: high, medium and low ductility, approximately, μ_D = 8, 4, and 2, respectively. The designs were made by modifying the yield displacement of the corresponding system (e.g., 1Hz), such that the median ductility observed was of the level desired (e.g., μ_D = 4).

Also considered are simple models of base-isolated structures. The equivalent representation for a base isolated SDoF system is done by means of the nonlinear SDoF oscillator mounted on an additional degree of freedom representing the isolation-system. For this case, the superstructure considered is of a unique (fixed-base) dynamic frequency, and the isolator is designed to cause a period shift of around 2.5 seconds. This simple model corresponds to a typical elastomeric bearing. The isolator is modeled by a bilinear spring.

Simple multi-degree of freedom (MDoF) systems are also analyzed, represented by several five-lumped-mass stick models, for frequencies ranging from 0.25 Hz to 4Hz. Interstory springs of both hysteretic types described above are used to approximate the building behavior, only for the 1Hz system.

Finally, two 2-dimensional frames are analyzed, representing a 1Hz 3-story fixed base steel moment resisting frame (SMRF), and the same system base isolated, on a friction pendulum.

See Appendix 3.B for structural details of the systems considered.

3.4 Target Spectrum.

All systems were analyzed firstly with a set of 63 real records, with characteristics in the vicinity of a hypothetical scenario of M = 7.0 and R = 20km. The suite of records selected were primarily (44 records) in the range of magnitudes from M = 6.7 to 7.3 (moment magnitude), and distance from R = 10 to 30kms (closest distance to the rupture zone). These correspond to California soil sites with Geomatrix soil classification B, C or D (which correspond generally to class C or D as per FEMA-273, 1996).

An additional 19 records, somewhat outside the aforementioned bin range, were also included, for enhanced statistical robustness. As discussed in Appendix B, the inclusion of these additional records has minimal impact on results, and does not affect the results presented in this chapter. See Appendix 3.A for the description of the recorded ground motion used.

The structural analysis runs corresponding to the unmodified original records generated what is considered to be the answer to the question: "What are the observed statistics (e.g., median and coefficient of variation) of seismic structural response (e.g. maximum interstory ductility), corresponding to a nonlinear system at a stiff soil site, excited with accelerograms from a given event (of magnitude $7.0^{\pm}$ and distance $20^{\pm}$ kms)?"

The justification of working with a bin of records is that one may want to measure the response of a structure to a "scenario" event, of a particular magnitude and distance. Such an event might be, for example, the characteristic event on the main nearby fault. Also, these bin records represent samples of a specific event, and it makes sense to consider the median responses, which include the elastic ones (i.e., the median response spectrum) for such an event. The use of exactly 63 records does not come from a specific necessity, but because it is the number that was available for use.

The object of using spectrum compatibilized records is to reduce the variability of the results, and hence permit the estimation of the demands in a more efficient way, by allowing a reduced number of runs in order to obtain the same confidence. Traditional use of spectrum matched records employs a target spectral shape not always directly linked to a particular set of real recordings (e.g., a UHS) (or, more precisely to their response spectra).

The natural choice for the target spectrum to which to match the set of original records is the *median*[1] spectral shape. Such shape is defined by the locus of median spectral accelerations at each frequency, for a particular damping level of interest. Justifications for this selection are multiple:

- The response statistics sought include a central tendency measure (e.g., the median), hence a representative "centralized" shape is searched for. This is in contrast to a shape that would seek to cause the compatibilized records to directly estimate a different statistic, e.g., an 84th percentile. In particular, our objective is to estimate the median response of the systems studied. Such a statistic is the required input to Probabilistic Demand Analysis (see, for example, Chapter 4). The median spectral shape corresponds as well to the median responses of SDoF elastic systems, so this measure is consistent.

- The natural choice of a spectral shape associated to an event comes from the use of an appropriate attenuation law, which would give us the expected *median* (as described

---

[1] Strictly, what is called *median* throughout this work corresponds to the *geometric mean*, which is computed as the exponential of the mean natural logarithms of the values of interest (e.g., spectral accelerations, displacements, etc.). If we denote *n*-observed values by x_i the we can write the median, x_{med}, as:

$$x_{med} = \exp[\frac{\sum_{i=1}^{n} \ln(x_i)}{n}] .$$

The geometric mean is a logical estimator of the median for data that are at least approximately lognormally distributed, an assumption to be verified.

above) spectral accelerations for all frequencies. This shape should theoretically coincide to the median shape of an extremely narrow bin, with a very large number of records.

- The traditional treatment of the distribution of the value of spectral acceleration is to treat its logarithm as Gaussian, as can be seen in numerous published attenuation laws (e.g., Abrahamson and Silva, 1997) (also, different authors have confirmed the validity of modeling the nonlinear response as lognormal, for example, Song (1999)). That makes the natural choice for a single frequency's representative value that of the median. An alternative possible selection for a representative shape could be that of the *average* (i.e., the arithmetic mean at each frequency). The disadvantage of this shape would be that it is "frequency-dependent" in that the shape would change for each different structural frequency selected. An ideal shape should not depend on the structure, allowing the use of a single set of compatibilized records to be used to study all systems. The advantage then of using the *median* shape is obvious, rendering it structure-independent.

- In this work, as done in the work of other authors (e.g., Shome, 1999) a typical representation of the median *response* (e.g., maximum interstory ductility) as a function of spectral acceleration is a *linear* one in logarithmic terms (of both Sa and response). This treatment also causes the set of records that will cause a higher-than-median response to be approximately equal in number to the set that will cause a lower than median response.

- In practice, the design spectrum considered for a scenario event is the median shape (NUREG (1997), U.S. DOE (1994), etc.).

Notice that the intention is to be able to generate more efficiently the response statistics by means only of considering a particular spectral *shape* as a target to compatibilize to. One may find reasons to believe that the *matching* of any seed should be done not only in a spectral-shape sense, but could also be done with respect to other parameters that can be

linked to the earthquake time history (e.g., the time-distribution of energy, etc.). Matching objectives of strong ground motions other than spectral shape are considered to be beyond the scope of this work.

Following the previous bulleted discussion it is then considered that the best spectral shape to choose, as a target spectral shape, is that of the median shape of all records. As will be discussed in subsequent subsections, this shape can be improved, but was taken as the shape to which all records were compatibilized to (i.e., all records were taken as seeds for compatibilization to this target).

Once the different systems were analyzed to the set of the original records, the results are compared to those generated by the artificial ground motions in order to establish the implications of using the latter as appropriate surrogates for determining the desired estimations. As will be seen in the following section, the results that spectrum matching (to the proposed target) yields are unconservatively biased for the prediction of displacement-based responses, yet present a very useful reduction in their dispersion with respect to the results that unmodified records produce.

3.5 Nonlinear Seismic Demands.

The seismic demands of interest are both displacement and energy-related ones. The emphasis, however, is on the former. Specifically in the normalized versions, for both top story (roof) ductility, and maximum interstory ductility (for the MDoF systems). We believe that the systems considered are representative of those used in practice, and that they are sufficiently broad in characteristics to draw some general conclusions. One may need, however, further research in order to extend any conclusion drawn here to consider other cases not considered here, such as P-Δ driven systems, near-source phenomena, etc.

 The definition of the measures used, repeated from Appendix 2.B, are as follows:

1) *Interstory ductility,* μ_I

$$\mu_i = \frac{|u|_{max}}{u_y} \tag{3.3}$$

where $|u|_{max}$ is the maximum interstory displacement, and u_y is the corresponding displacement at first yield. The subindex i indicates *interstory*.

2) *Global ductility,* μ_g

$$\mu_g = \frac{|u|_{roof}}{u_{gy}} \tag{3.4}$$

where $|u|_{roof}$ is the roof displacement (relative to the base), and u_{gy} is some representative global yield displacement, obtained from the tangential intersection of the elastic branch and the strain-hardening branch of a force-deformation curve obtained by means of a static nonlinear analysis (pushover).

3) *Normalized hysteretic energy[2], NHE$_i$*

$$NHE_i = \frac{\sum_{j=1}^{N} (\oint_{cycle\,j} F\,du)}{F_y u_y} = \frac{HE_i}{F_y u_y} \tag{3.5}$$

where N is the number of response cycles, F is the varying interstory shear force (as a function of the corresponding interstory displacement u), and F_y is the interstory yield

---

[2] The precise definition of this measure is not critical for the purposes of this study, and any variation should not affect our conclusions. This normalized measure permits the comparison across different systems (e.g., SDoF vs. MDoF, etc.).

 shear force corresponding to the interstory yield displacement u_y. The hysteretic energy dissipated per interstory is denoted by $HE_{i.}$. The subindex i denotes *interstory*.

4) *Global hysteretic energy, NHE$_g$*

$$NHE_g = \frac{\sum_{all\ floors} HE_i}{F_{gy}u_{gy}}$$ (3.6)

where F_{gy} is the shear force present at the value of u_{gy}.

The different cases studied intend to represent different possible situations for typical structures, in terms of hysteretic type, and design level (level of ductility). Since the real records' results are to be considered the "control" set, the level of yield displacement for each structural model was varied, such that the median responses for the different systems corresponded to *nominal* ductility values of approximately 2, 4 and 8. The designs were made first for the bilinear systems, and the yield displacement for each of these designs was taken intact to be considered for the corresponding (same nominal design level) model of the pinching hysteretic system. This is reflected in median responses that are not exactly at the same levels of ductility for both hysteretic types, at the same *nominal* design level (compare the observed median ductilities for the same nominal design levels, of tables 3.1a and 3.1b.).

3.5.1 SDoF Results.

The response results for the SDoF systems subjected to the 63 original records from this magnitude 7^+ and 20^+ km distance bin are shown in Tables 3.1a and 3.1.b, for the different structural frequencies. The response statistics presented correspond to the estimate of the median ($\mu_m = \exp(\sum(\ln(\mu)) / n)$), and the standard deviation of the natural

logarithms (defined as $[\sum(\ln\mu - \ln\mu_m)^2 / (n-1)]^{1/2}$). Tabulated results are presented in three pairs of columns, one pair for each different design (as described previously).

We can make some observations on Tables 3.1a and 3.1b. Notice that a representative standard deviation of the natural logarithm of ductility demands, for the original bin-records, is around 0.8. This means that the standard error of the logarithm of the median estimates of ductility (for both hysteresis types) is roughly $0.8 / (63)^{1/2} \approx 0.1$ (approximately equal to the coefficient of variation of the ductility). In the case of the normalized hysteretic energy, NHE, the standard error of the estimate of the median is a little higher at around $1.2 / (63)^{1/2} \approx 0.15$ for the bilinear hysteresis, and a little lower ($\approx$ 0.12) for the pinching systems. Although these were "representative" values (for the entire set) one can notice a small frequency dependence, especially at high deformation levels, of the scatter of ductility demand. The dissipated NHE for the pinching-type systems is roughly half that of the bilinear systems.

Tables 3.2 through 3.3 Figures 3.2 through 3.9 show the results of using the compatibilized version of the same 63 records compared to those that the unmodified version produced. We define here *bias* as the ratio of the original records' median (ductility or *NHE*) to the modified records' median. Therefore, a larger than unit bias implies that the spectrum compatibilized version of the records produce an unconservatively biased estimate of the median. Next to the biases, the reduction of dispersion is presented, defined by the ratio of the standard deviation of the natural logarithm of the original records' results and those of the compatibilized records.

A graphical representation of the above results can be made in the form of contour plots, representing the bias and dispersion ratios as a function of nominal-design ductility and frequency. Figures 3.2 and 3.3 show the corresponding plots related to ductilities in tables 3.2 and 3.3. These plots show in a compact way the effect of using spectrum matched records vis-à-vis the use of the set of original records, for the various systems analyzed and for the several designs (low to high resistance) considered. The plot on Figure 3.2a-ii

is a "slice" of the contour plot shown in Figure 3.2a-i, which corresponds to the variation of bias across structural frequencies for the bilinear-hysteresis model.

A result of presenting the results in such a way is the consistent unconservative ductility bias of the compatibilized records' results vis-à-vis those of the original records. One can argue that for an individual set of results (e.g., 1Hz, bilinear, frequency-domain matching), the difference between the median value caused by the compatibilized records and that of the original records is *not* statistically significant, due to the large standard error of this difference (which can reasonably be approximated by the dominant standard error of the original records' results alone). However, the direction of the bias is consistent throughout the frequency domain and the design domain. As can be seen, although the bias may not be too high (e.g., typically ranging from 1.1 to 1.2), it is *unconservative* and should be accounted for, for all cases, especially for ductility levels higher than 4. Notice that the tendency is for the bias to increase as the ductility in the system increases.

These observations are not applicable to the estimation of the median NHE's, where consistent bias is not apparent, and may be neglected. The larger values of their standard deviations as well as the oscillating-about-unit bias (i.e., sometimes conservative and sometimes unconservative) make them really be not significantly statistically different. Figures 3.4 through 3.5 show the corresponding contours.

As mentioned earlier, a great benefit of the use of spectrum matched records is the large reduction in scatter. Such a reduction (typically of 3 to 4 for bilinear system ductilities and NHE for both hysteretic types, and even higher, 5 to 6 for the pinching system ductilities) in the values of the standard deviation of the logarithms signifies the possibility of a more efficient estimation of the median. By equating the SEE for both cases, considering that we are interested in estimating the median with the same confidence, the reduction in the sample size caused by the reduced dispersion is equal to the *square* of the reduction in dispersion. Similar to the bias contour plots, the following

plots represent the variation of the reduction of the standard deviation of the logarithms of the original records' results with respect to those of the compatibilized records.

There seems to be no clear relationship between the dispersion reduction and the oscillator frequency or level of design (μ_D). In general terms the observed reduction can be summarized by values approximately ranging from three to four for ductility, for the bilinear systems, and ranging from five to six for the pinching systems.   Also, representative values for the reduction of dispersion in normalized hysteretic energy (*NHE*) for all systems approximately ranges from three to four.

3.5.2 MDoF Results.

The MDoF systems considered in this section are divided into fixed-base and base-isolated systems. For both cases, examples for simple stick models as well as more complex 2-D frame models are presented.

3.5.2.1 Fixed Base Systems.

The simplistic SDoF cases presented in the previous section are not unique in presenting a biased estimate of the median displacement demands. The MDoF systems studied here present the same order of bias measure as well as the same order of dispersion reduction. In other words, the "bad" news and the "good" news are consistent as the modeling of the systems become more detailed. In particular one would like to identify the role that the presence of important higher modes has in the estimation of demands via the use of compatibilized artificial records.

The 5 degree-of-freedom stick models represent an original 1Hz planar ductile SMRF designed for UBC Zone 4 at a Los Angeles site. The representative parameters for the simplified 1Hz model are taken from Shome, et al., 1998. In order to analyze the influence of varying the structural fundamental frequency, without necessarily modifying

the relative higher mode frequencies, the bilinear system's masses were scaled such that 3 different systems were considered: 0.25Hz, 1Hz, 4Hz. The original 1Hz system was also modified to represent the other hysteresis type considered for the SDoF systems , i.e., the pinching model, keeping the same force-deflection backbone.

The MDoF designs were kept fixed; the multiple ductility levels were obtained by scaling the records used for the SDoF cases, with pre-fixed factors (e.g., 1, 2, 5 and 8) in order to cover ductility ranges similar to those of the SDoF cases (at least for maximum interstory ductility in the 1Hz case). Tables 3.4 through 3.7 show the corresponding relationships between the original sets' results and the compatibilized sets' results.

Notice the similarity of results with respect to bias and dispersion reduction with those generated by analyzing the SDoF systems, although a little larger biases for interstory ductilities. Typical biases, at least for ductilities larger than 4, are greater than 1.2 for the bilinear systems, and just slightly lower (1.1 to 1.15) for the pinching systems. The level of bias seems to increase with the ductility level for the interstory ductilities of the bilinear systems, and for both interstory and global ductilities for the pinching systems. The results for the 1Hz pinching system show very large reductions in ductility dispersions, even higher than 6, for global ductilities above 3.

One might argue that the simplicity of the MDoF model may hide effects that more detailed models may present. At a third level of detail, a 1-Hz two-dimensional frame was analyzed. The system corresponds to a SAC structure, a 3-story SMRF ductile 1Hz system. It was taken from Barroso, 1999 (the computer runs were also made by L. Barroso, on a Matlab-platform nonlinear dynamic analysis code, whose results were demonstrated to be compatible with DRAIN-2D analyses). Table 3.8 summarizes the results for the different 1Hz- first mode dominated systems, and as can be seen, results are consistent for all cases. (Note: the results of ductility levels are not to be compared directly, only the presence of unconservative bias and dispersion reduction. The designs

of the SDoF and stick MDoF 1Hz models—which do not represent each other— do not represent that of the two-dimensional frame either)[3].

3.5.2.2 Base Isolated Systems.

As mentioned earlier, also of interest are other kinds of non-linear systems considered in practice: those representing base isolated-structures. Firstly, we analyze a base-isolated 1Hz super-structure (i.e., would be 1Hz if its base were fixed) modeled by considering a 2DoF representation. The simple model represents a 1Hz ductile (bilinear) system on an elastomeric bearing base isolation system. The design is typical of what is done in practice (Mayes, 1998). The lateral resistance of the superstructure was set to 12% of its weight (a representative criterion for non-near fault designs). The design of the isolation system was such that there was a period shift of the response (i.e. of the superstructure responding in conjunction with the isolator) of around 1.5 seconds. (for this case, this corresponds to an isolated period of $T_b = 2.5\ T_0$, or $T_b/T_0 = 2.5$)

The simplistic design assumed an additional mass at the base of the (SDoF) superstructure equal to a fraction α of its own. Combining both masses, the stiffness of the bottom spring can be solved for (assuming only for design purposes a rigid superstructure and base), yielding an isolation stiffness of:

$$K_b = \alpha/(T_b/T_0)^2 . \tag{3.7}$$

---

[3] For comparison purposes, since the design was taken intact from Barroso, 1999, the bin original records considered were scaled such that they presented the same median spectral acceleration at the fundamental frequency of vibration of the structure (1Hz). This scaling does, however, maintain the relative dispersions of all spectral accelerations. The results from Barroso, 1999, for the structure, subject to the record set constructed by Sommerville (1997) are as follows:

Ductilities and Standard deviations of the log.				
record set	μ_i	$\sigma_{\ln(\mu)}$	μ_g	$\sigma_{\ln(\mu)}$
scenario (Ch. 3)	4.6	0.6	2.9	0.83
SAC 2% in 50	4.6	0.45	2.9	0.61

This corresponds to the required stiffness of the isolator *once* it has yielded (i.e. the post yield slope of a bilinear force-deformation curve). A typical value of the initial elastic slope of the isolator system (corresponding to the stiffness of the lead core) of 8 times the above computed isolation stiffness was considered. For our example, this corresponded roughly to 1.7 times the superstructure's stiffness. The yield force of the isolation system was set to 5% of the total weight, also typical for non-near source conditions. In order to have some point of comparison with known SDoF results, it can be said that the initial (un-yielded) system vibrates at a fundamental frequency of 0.78Hz. Table 3.9 summarizes the results of having run the 2DoF system with the original 63 records and to the corresponding frequency-domain-based compatibilized records.

It is to be noted that the particular design of the isolation considered above rendered the superstructure undamaged (in terms of displacement ductility) as normally desired (the superstructure corresponded to that of the SDoF's $\mu_D= 2$ design). There may be cases where different combinations of isolated and superstructure period as well as relative yield levels, might cause nonlinearity (even high levels) in the superstructure, where bias may be observed too. The point to be made in this experiment is the presence of bias in the results generated by the use of spectrum matched records of the isolation's nonlinearity. These findings are consistent with the results observed for fixed-based nonlinearly behaving systems, i.e., bias around 1.2 for ductilities higher than 4, and dispersion reductions of 3 to 4. However, the reduction of dispersion is also present, consistent too with previous reductions observed, permitting a more efficient study of the response statistics for this kind of structural systems.

A more detailed base isolated structural model was also considered. It corresponds to the same two-dimensional detailed SMRF considered above, isolated in this case with a friction-based pendulum system (FPS), itself more complex in behavior (e.g., it has a velocity dependent dynamic coefficient of friction) than the previously considered

isolation system. The system was taken from Barroso[4], 1999 (and run by her as well, with the same Matlab-based program). The isolated system's period corresponds to a period of 3.1 seconds (a FPS based isolation system's period depends on the radius of curvature of the concave interface —the curvature provides the restoring force). See Barroso, 1999 for details on the bearing's parameters. It is worth mentioning that the elastic (pre-nonlinear) vibration frequency of the system is exactly the same as that of the elastic superstructure's fundamental frequency, because there is no relative displacement in the interface before sliding occurs. This fact forces the results of the demands on the isolator to be presented in terms of (un-normalized) displacements, for cross-comparison of original to compatibilized records' results. Table 3.10 shows the results obtained for this system, which are compatible with all results shown.

Once again it can be said that the presence of unconservative bias of the predicted nonlinear structural demands can be noted, as was for all systems previously considered, and that there is as well a similar reduction in dispersion.

3.6 Understanding the Effect of Spectral Matching on Bias.

The results shown in the previous section seem to be very consistent with each other, regardless of the degree of modeling detail, hysteretic type, or matching technique. This calls for decomposing the effect of spectral compatibilization, or to identify the constituents of the differences between the two sets of records (original and

---

[4] As done for the fixed base MDoF two-dimensional model of the SMRF, the results of scaling the bin records to the same median spectral acceleration than the 2% in 50 year level SAC records are presented in comparison in the following table:

Ductilities and Standard Deviations of the log.						
record set	d [in]	σ_d	μ_i	$\sigma_{\mu i}$	μ_g	$\sigma_{\mu g}$
scenario (Ch. 3)	10.1	0.92	1.8	0.58	1.15	0.61
SAC 2% in 50	15.2	0.54	1.8	0.44	1.2	0.57

compatibilized) and their effects on seismic demands. The focus in this section is on displacement demands. We shall look both at the "intensity" of the record and at the "shape" of its spectrum, locally and globally.

It is known (Shome, et al, 1998) that a prime contributor to the prediction of the level of nonlinear displacement demand is a record's level of a relevant spectral acceleration, e.g., that at the fundamental frequency of the linear structure. In a statistical sense, the better the relationship (e.g., the higher the coefficient of correlation, for a linear relationship) between the dependent variable (e.g., logarithm of the spectral acceleration) and the independent variable (e.g., logarithm of ductility) the lower dispersion there will be in the observed response given a particular ground motion intensity level. (See Shome et al, 1998, for a discussion on the selection of a good dependent variable). In the following section, the spectral acceleration at the fundamental frequency of the structure to study (at the first mode damping, 2%) will be used (it is a better selection than, for example, the peak ground acceleration).

Shome, et al, 1999, discusses the validity of *normalizing* a set of ground motion records for the purpose of estimating the median nonlinear response of a structure to such a set of records with the advantage of observing a reduced dispersion. *Normalization* refers to scaling each record in the set to a particular intensity level (e.g., $Sa(f_0)$, where f_0 is the elastic fundamental frequency), the same for all records. Typical reductions in response dispersions are 40% to 50%. The previous scheme translates into the ability of using a smaller number of records to estimate with the same degree of accuracy such a centralized tendency measure (i.e., the median). Shome (1999) also found that knowledge of an additional spectral ordinate away from f_0 permitted further dispersion reduction.

For the experiments with spectrum-matched records that were shown in the previous sections, it was seen that there was a much higher dispersion reduction than the one that could be obtained by this normalizing of the records. By definition, spectrum matching involves normalization not only to a particular $Sa(f_0)$ value (the median), but also to all Sa values within the domain of frequencies in the target response spectrum. In other words,

one can think of spectral matching as, first, a normalization at the fundamental frequency's spectral acceleration, and second, the adjusting of the remaining spectral accelerations to the target, i.e., matching the spectral shapes of all the records. Following the previous paragraphs' discussion, the additional dispersion reduction must come from considering in the records' modification the inclusion of spectral *shape*.

It is important then to quantify spectral *shape*, the effect of it on observed seismic demands, and its content in each of the records. The following sections will address this subject. Section 3.6.1 will dissect the elements that compose *shape* in real records, and a statistical relationship will be studied in order to link these elements with response. Then, section 3.6.2 will isolate and study such elements with the use of spectrum matched accelerograms. This will lead to an attempt to correct the bias (section 3.7) and to offer an explanation of the introduction of bias that these accelerograms show, in section 3.8.

3.6.1 Spectral Shape and Intensity Effects in Nonlinear Seismic Displacement Demands (Using M-R Bin Records).

By analyzing the results that were generated from the unmodified bin records (see section 3.5), this section will associate the inherent elements of the records' different spectral shapes with the demands that they produced.

A notion that will be very helpful in understanding the effect of spectral shape in seismic displacement demands is that of *nonlinear effective period*. It helps to define the lower-end of frequencies of interest on the spectral shape one should focus on.

Design procedures for isolation systems consider a target design displacement that the system should withstand, associated to a period computed with an *effective stiffness*, K_e, *defined* as the ratio of the maximum force (F_u) in the system to the maximum (nonlinear) displacement, d_u, (Mayes, 1989; FEMA-273, 1996). The *effective period* is then computed with the total mass, m, of the system and the corresponding effective stiffness:

$T_e = (m / K_e)^{1/2}$. The intention of utilizing such measures is to recognize the change in dynamic response once the linear limit has been exceeded. In other words, the purpose is to understand the limits of the range of frequencies to which the nonlinear oscillator becomes sensitive. In terms of considering SDoF elastic representations, the adjusted expected demand for a given design spectral shape, is computed with the spectral value (*Sa*, *Sv*, or *Sd*) corresponding to the effective period (see Fig. 3.10).

Following the same reasoning, we have assigned the following definition of expected effective period of a nonlinear system (where the nonlinearity is not necessarily associated to isolation, but to the inelastic properties of all elements in the system), associated to an observed ductility demand. For an elasto-perfectly-plastic system (i.e., $F_u = F_y$, for all $d_u \geq d_y$, see Fig. 3.10), the maximum displacement can be defined by the ductility demand as $d_u = \mu\, d_y$. We compute the elastic period as:

$$T_0 = (m/K_0)^{1/2}$$
(3.8)

Thus, considering the less rigid effective stiffness, we can compute the effective period as:

$$T_\mu = T_e = (m/K_e)^{1/2} = (m/(F_y/\mu\, d_y))^{1/2} = (\mu\, m/K_0)^{1/2} = T_0 * \mu^{1/2}$$
(3.9)

where $K_e = F_u / d_u = F_y / d_u = F_y / (d_y\, \mu)$. The notation of the subindex of T_μ indicates that the effective period of interest is directly related to the level of ductility μ.

Having established the effective period of the nonlinear maximum response, our focus is on the value of a record's spectral acceleration associated with such a period (which is longer than the elastic fundamental period). For example, the spectral acceleration of interest corresponding to an elastic period of 1sec (T_0 = 1.0sec or f_0 = 1.0Hz), which observes a ductility demand of 4.0, should be related to a period of 1.0sec*$4.0^{1/2}$ = 2.0 sec. In terms of the completely analogous effective frequency, f_μ, the previous spectral

acceleration of interest is associated to $f_\mu = f_0 / \mu^{1/2} = 1.0\text{Hz}/2 = 0.5\text{Hz}$. For the sake of consistency and clarity, the following discussions will be in terms of frequencies alone, and no longer in terms of period. (See Kennedy, et al, 1985, for another discussion on the concept of effective frequency).

It is not solely the fundamental frequency and the lower nonlinear effective frequency (associated to the maximum demand) we should be interested in, but the range of frequencies the system responds to as it "softens" (i.e. as its effective frequency decreases) while undergoing higher nonlinear displacements. However, only these two extreme values (f_0 and f_μ) will be used here in the representation of spectral shape.

Overall, the effects of spectral shape are considered in two parts, *global shape* effects and *local shape* effects, as described as follows:

- "*Global Shape*" effects (GS): such spectral shape effects come from considering the relative values of the range of spectral ordinates between the effective frequency, f_μ, associated with the maximum expected nonlinear displacement in the system, and the initial elastic frequency, f_0. In particular, for a given ground motion record, such an effect will be predicted here by the ratio of the difference in spectral accelerations at those two frequencies. (The spectral shape considered here is only in the lower-than-elastic frequency range (i.e., $f_0 \Rightarrow f_\mu$)). The global-shape can be thought of as the intensity that the record presents at f_μ (e.g., the spectral acceleration at f_μ, or Sa_μ) relative to the intensity at the elastic frequency, f_0, (e.g., the spectral acceleration at the elastic fundamental period, Sa_0), i.e., the ratio Sa_μ / Sa_0. This simple notion will be refined below, however.

- "*Local-Shape*" effects (LS): These consider the variation of spectral shape immediately adjacent to the spectral acceleration at the fundamental elastic frequency, f_0. In contrast to the *global shape* effect, this is the effect of the variation or "jaggedness" of the spectral shape locally. For example, one might define an indication of a local "peak" when the value of the response spectral acceleration (at

the fundamental frequency) decreases for immediate lower values of frequency (if the spectral acceleration also decreases also for higher frequencies, then locally the spectral shape is indeed at a maximum).

In addition to the *intensity* of a record (e.g., the spectral acceleration at f_0, or Sa_0), one can consider two ground motion record characteristics associated with the previous effects as parameters that help to predict observed seismic displacements. We will study their effects independently in the following sections.

In a first attempt to quantify the characteristics that predict *global-shape* and *local-shape* effects (relative to the intensity effects), the following parameters were defined, to characterize each record belonging to the set of original (unmodified) M-R bin ground motions.

1) *Normalized shape ratio, $R_{GS\mu}$, to be considered for the global shape (GS) effect.* For each record, this parameter was defined as the ratio of (a) the quotient of the record's moving average spectral acceleration at f_μ (called here $Sa_{MA\mu}$) divided by its moving average spectral acceleration at f_0 (or Sa_{MA0}) to (b) the quotient of the target's (i.e. the bin median value) spectral accelerations at these two frequencies ($Sa_{\mu m}$, and Sa_{0m} respectively):

$$R_{GS_\mu} = \frac{Sa_{MA\mu} / Sa_{MA0}}{Sa_{\mu\, m} / Sa_{0\, m}} \tag{3.10}$$

The subindex μ in $R_{GS\mu}$ denotes the implied level of softening, in other words, the range of frequencies considered (i.e., from f_0 to f_μ). The introduction of the moving average is to smooth the jagged response spectrum of the record, to remove the possibility of having a pronounced value at either f_0 or, and to capture the general trend of the record's shape. Notice that the division by ($Sa_{\mu m}/Sa_{0m}$) makes this parameter normalized with respect to a particular global spectral shape, in this case that of the median shape (used as the target to

which the records were compatibilized). Therefore, records with $R_{GS\mu} > 1$ have global shapes that are "stronger" in this frequency range than a "typical" record. The selection of the window size to produce the moving average is subjective. The response spectra of the records were computed at 100 equally spaced frequencies in logarithmic space, ranging from 0.2Hz to 25.0Hz (i.e., corresponding to increasing frequencies around 5% higher than the previous one); and the windowing considered 4 of these points (or roughly frequencies at 20% higher values from the previous one), in order not to smooth the response spectrum too much, nor to leave it too jagged. See Figure 3.11 for a description of the quantities involved in this ratio and the ones to follow.

2) *Local-Shape ratio, R_{LS}, to be considered for the local shape (LS) effect.* With respect to the same moving average described above, this parameter was defined here as the ratio of the actual spectral acceleration Sa_0 to the moving average spectral acceleration at f_0.

$$R_{LS} = Sa_0 / Sa_{MA0} \qquad (3.11)$$

The purpose of this parameter is to try to identify the effects of the spectral shape being locally above or below the smoother moving average spectrum. Notice that a value of R_{LS} considerably higher than unity most likely determines the presence of a local "peak" (i.e., the spectral shape tends to locally decrease with lower frequencies) and a value lower than unity is likely related to the presence of a local "valley" (i.e., the spectral shape tends to locally increase with lower frequencies). Of course, the window size will affect the relative size of the local-shape ratio.

3) *Intensity ratio, R_{SaMA0}.* In order to distinguish the above *shape* parameters from each record's general *intensity*, a record intensity parameter was defined here as:

$$R_{SaMA0} = Sa_{MA0} / Sa_{0m} \qquad (3.12)$$

Recall that Sa_0 itself was considered separately (i.e., within R_{LS}, Eq. 3.11). This parameter reflects the intensity of the smoothed moving average relative to the median intensity of all records in a M-R bin.

The overall effect that the previous ratios have on the ductility can be expressed by a normalized parameter, the *normalized ductility*, R_μ, defined as:

$$R_\mu = \mu / \mu_m ,$$
(3.13)

where μ is the ductility demand for a particular record and μ_m is the median ductility of all records. In order to try to quantify the effect of the different shape and intensity parameters, their relationship to the *normalized ductility* demanded was tested.

The total effect was tested by assuming the following model for the contribution of all three effects, $R_{SaMA0,}$ $R_{GS\mu}$, and R_{LS}:

$$R_\mu = R_{SaMA0}{}^{a_1} \; R_{GS\mu}{}^{a_2} \; R_{LS}{}^{a_3}$$
(3.14)

Departing from Equation 3.14, the logarithmic linear relationship was used to perform a linear regression analysis, which yields the exponents of the ratios, a_1 through a_3:

$$\ln(R_\mu) = a_1 \ln(R_{SaMA0}) + a_2 \ln(R_{GS\mu}) + a_3 \ln(R_{LS})$$
(3.15)

Equations 3.14 and 3.15 can be thought of as an extension to a previously used functional description of median displacement seismic demands with spectral acceleration (Bazzurro, et al, 1998; Luco and Cornell, 1998; Shome, 1999). In ductility terms it is:

$$\mu_m = a \; Sa^b$$
(3.16)

The new form considers the additional contribution of the shape quantities; the more refined model is:

$$\mu = \mu_m \ R_{SaMA0}{}^{a_1} \ R_{GS\mu}{}^{a_2} \ R_{LS}{}^{a_3} \tag{3.17}$$

where μ_m (from Eq. 3.16) equals $a \ Sa_{0m}{}^{b}$, and Sa_{0m} is the median spectral acceleration of the bin records (i.e., the target elastic frequency spectral acceleration).

A first attempt to explain the cause of the observed bias that the use of spectrum matched records produces is to try to identify an *asymmetry* in the coefficients a_1 through a_3, by using subsets of sample records. What is meant by *asymmetry* is simply the obtaining of a different value of the coefficients by performing the regression on the appropriately defined subsets (see below). The effect of the asymmetry on the value of the coefficients would be reflected in different deviations (e.g., a different increment) from the median ductility, depending on the value of the corresponding shape or intensity ratio relative to unity (or, equivalently, the value of the logarithm of the ratio with respect to zero). Consider the following example, in logarithmic terms (as expressed by Eq. 3.15). For example, an asymmetric coefficient a_1 would mean that if for a record its $\ln(R_{SaMA0})$ = +0.2, then it would imply that the logarithm of the ductility ratio, in absolute value, would be different from that of a record with $\ln(R_{SaMA0})$ = -0.2, all other values (i.e., $R_{GS\mu}$ and R_{LS}) being fixed. This is not expected to be the case for a_1, since, as seen in Shome, 1999, normalization does not introduce apparent bias.

It was considered that such subsets could be generated by separating those samples that yielded lower-than-unity values of R_μ from those that presented values above one. In other words, the values of the coefficients were obtained from performing linear regressions on the logarithms of the normalized shape and intensity effects (i.e., $R_{GS\mu}$, R_{LS} and R $_{SaMA0}$) for these two subsets independently.

The data set of 63 observations corresponding to the 1hz bilinear, SDoF, low resistance (μ_D = 8.0) was used. It was manipulated in order to have the data in terms of the previously described ratios.

Before looking at the two subsets, first a regression was performed on the entire data set. Table 3.11 shows the correlation matrix for the variables considered in the regression (i.e., $R_{GS\mu}$, R_{LS} and R_{SaMA0}). As expected, they can be considered uncorrelated.

The coefficients for equation 3.15 were found, and can be seen in table 3.12. To confirm the form of the model, the regression was run with an intercept coefficient (a_0). As expected, the regression showed that a zero-intercept model can be considered valid. Also, it seems that the coefficient for the variable R_{LS} is not significant (at the 95% confidence level). The near-unit value of a_1 confirms the findings of Shome, 1999, that nonlinear displacement is approximately proportional to intensity (as measured by first-mode *Sa*). The statistical significance of a_2 confirms that records with comparatively higher $Sa_{MA\mu}$ values (i.e., at f_μ) cause larger nonlinear displacements. Table 3.13 shows the coefficient of multiple determination, R^2, corresponding to regressions with different variables. Clearly there is no benefit to using R_{LS}, in contrast to $R_{GS\mu}$; it provides no additional explanatory power.

The regressions on the subsets of data (corresponding to $R_\mu < 1$ and $R_\mu > 1$) were forced through the origin. The results are summarized in table 3.14. As done above, a table for regressions with incremental addition of variables is shown in table 3.15. It is worth noting that, because the regressions are forced through the origin, the coefficient of multiple determination, R^2, has no clear meaning and is not shown. However, closely related to the R^2, is the error sum of squares (SSE), presented alongside the coefficients obtained (not to be confused with S<u>EE</u>, the standard error of estimation, related to each coefficient).

There are several things that can be noticed:

- The relatively small standard errors on the coefficient a_2^+ and a_2^- (affecting $R_{GS\mu}$, the *global shape* parameter) seem to indicate a statistically significant difference. This would imply that the *global shape* effect is stronger for those data points corresponding to the above-unit R_μ data set than those with $R_\mu < 1$. If this is the case, this is the *asymmetrical* effect we have been looking for.

- The data seems in general to indicate the lack of significance for the coefficient a_3, reflecting the *local shape* effect. The relatively small increase in the value of R^2, the coefficient of multiple determination, for the entire data set, as well as the small decrease in the value of SSE, the square sum of the errors, for the partial-data-set regressions, once the additional variable (R_{LS}) was introduced, seemed to indicate the lack of benefit of adding such a value. Only for the above-unit R_μ subset regressions, did there seem to be some significance (yet low) in the value of the coefficient a_3 (Table 3.16).

- The value of the coefficients a_1 and a_2 present small standard errors. The value of a_1 seems to be symmetric, i.e., the values obtained by both sets are not statistically significantly different. The values obtained for this coefficient agree with typical values (around unity).

- In general, the standard errors for the coefficients obtained from the negative below-unit R_μ subset regression are higher than those for the positive set. This fact is only marginally due to the lower number of observations.

The fact that there appears to be an asymmetry in coefficients a_2^+ and a_2^- is a reason for spectrum-matched records to show an unconservative bias. Real records will present high and low values of $R_{GS\mu}$; the records with high-valued $R_{GS\mu}$ have a relatively larger effect on the median ductility than do the records with low-valued $R_{GS\mu}$, and also relative to a hypothetical "typical" record with a median shape (i.e., with $R_{GS\mu} = 1$). The median ductility is larger than the one caused by such "typical" record. All records, having been spectrum compatibilized, will be forced to have the "typical" shape, hence generate responses with a biased median with respect to the one estimated with all unmodified records.

Consider the following hypothetical example. If 1/3 of all real bin records would have an above unit value of $R_{GS\mu}$ = 1.8, 1/3 an exactly unit value, and 1/3 a below-unit value of $R_{GS\mu}$ = 1/1.8, by considering the above coefficients a_2^+ = 0.66, and a_2^- = 0.41, the average logarithm of the ductility ratio could be computed as:

$$\text{avg}(\ln(R_{\mu t})) = (1/3)\ln(R_{GS\mu} > 1)\, a_2^+ + (1/3)\ln(R_{GS\mu} = 1)\, a_2^\pm + (1/3)\ln(R_{GS\mu} < 1)\, a_2^-$$
$$= (1/3)(0.59)(0.66) + 0 + (1/3)(-0.59)(0.41) = 0.05.$$

In contrast, these records once spectrum-matched to the median spectral shape (i.e., in order to have all records with $R_{GS\mu}$ = 1) would clearly have a zero average logarithm of the ductility ratio, and hence be biased low with respect to the previous result.

3.6.2 Isolated Spectral Shape and Intensity Effects in Nonlinear Seismic Displacement Demands (Using Spectrum-Matched Accelerograms).

The previous statistical analysis provided useful insight into the potential source of bias. In addition, a modified experiment was carried out in order to isolate each of the effects (i.e., intensity, global and local shape effects).

Completely new data sets were generated in an attempt to isolate the different effects. In order to isolate the aforementioned characteristics, spectrum compatibilized accelerograms were used (the compatibilization scheme used was that of the frequency domain, with use of the program RASCAL described earlier). The different sets allowed us to focus on varied values of the intensity (Sa_0) and shape ratios ($R_{GS\mu}$ and R_{LS}), one at a time, while keeping all other parameters constant. The control set for all cases to be considered was the suite of 63 compatibilized accelerograms matched to the original target (i.e., the median spectral shape of the original records), for which results were already available.

The definitions of equations 3.10 through 3.13 were slightly modified because the comparison criteria (the normalization parameters) were not taken from the new records, but were set to the existing-data control case. In other words, the normalizing parameters were not taken from the modified sets themselves, but from the control set. In terms of the normalization for observed ductility, its new definition was:

$$R_{\mu c} = \mu / \mu c ;$$

(3.18)

where μ corresponds to the observed demand of each accelerogram in the new set generated, and $\mu_{mc} = 7.01$ (which is the control set's median ductility, for the 1Hz, SDoF, bilinear system, computed from tables 3.1a and 3.2a). The subindex c applied to the ratio denotes "with respect to the *control* set".

3.6.2.1 Isolated Intensity Effects.

The modified version of the intensity ratio involves normalizing the record's spectral acceleration not by the set's median spectral acceleration at f_0 but by the control set's median spectral acceleration. For this case, the re-defined parameter is:

$$R_{Sa0c} = Sa_0 / Sa_{0mc}$$

(3.19)

Other than the difference in the normalizing parameter (i.e., now with respect to the control set), this re-definition differs from Eq. 3.12 in that the consideration of the *moving average* spectral shape was not necessary because of the smooth nature of the target spectrum to which the control set records were compatibilized. In order to generate record sets of different intensity levels the control set was directly scaled by different factors, i.e., 1.6 and 1/1.6. For all practical purposes[5], the value of R_{Sa0c} for all scaled records can be taken as that of the factor that all control records were scaled by. In order

to test the isolated intensity effects, given that no shape parameters are considered, the model used was $R_{\mu c} = R_{Sa0c}{}^{a_1}$. The results generated are shown in table 3.17.

We can see that the estimated value of the coefficient a_1 is very stable and symmetric: the values obtained for the two data sets are not statistically significantly different. These findings are congruent with those concluded in Shome (1999) where the validity of "scaling" (i.e., *normalizing*) records was discussed. In other words, scaling "up" or "down" (for a particular value of $\ln(|R_{Sac}|)$) the records had the same relative effects (that of an increase/decrease of around 0.5 in terms of $\ln(R_{\mu c})$).

Figure 3.12 shows the sets of data points for both new sets, as well as the control case. One can draw a straight imaginary line that will connect the mean of the logarithms, with a slope ≈ 1.0. This means that the relative effects were the same for both new sets: both new data-"clouds" are equally far from the median control-set ductility.

A bi-product of this isolated-effect experiment was the obtaining of an additional parameter. By using the three sets altogether, the value of a from Equation 3.16 was able to be obtained. In conjunction with the regression estimate of the value of b, now representing simultaneously both new data sets, these parameters should allow us to estimate the median value of ductility given spectral acceleration, if no *global-* or *local-shape* effects are to be present.

From the regression using all data sets together we obtained:

$a = 0.0709$ (for *Sa* in units of $[\text{in/s}^2]$); $\quad b = 0.9995; \quad \sigma_{ln\mu|lnSa} = 0.22$

Notice that the value of b lies between the two values obtained for the coefficient a_1 (table 3.17), corresponding to both scaled-records data sets. Also notice that the low dispersion is valid only for compatibilized records.

3.6.2.2 Isolated *Local-Shape* Effects.

Although the regression analyses performed in the previous section tend to agree on the lack of importance of the *local-shape* parameter, an additional attempt to study its effect was performed.

In order to construct data sets that will allow the study of *local-shape* effects, the following "factor functions" (as defined in Chapter 2) were chosen to be applied on the original target spectral shape of the control set (Fig. 3.13). The geometry of the *local-shape* was an ad-hoc one (as was the definition of R_{LS} in the previous section); the base and the height of the triangle were taken from slightly larger than "typical" half cycles of jagged response spectra. Note that for both cases only the values of the spectral accelerations in the "softening" direction (i.e., in the direction of decreasing frequencies) were modified. The importance of different geometries (e.g., different heights, bases, and locations of the maxima/minima) on the response can be argued, but it was not believed of great importance that it be studied here.

A new definition of R_{LS} was not attempted, due to the degree of arbitrariness already involved[5]. Instead, the effect was quantified by directly observing the values of $R_{\mu c}$ caused by the different sets. The results are recorded in Table 3.18.

Given the observed variability on the normalized demands, in terms of $\ln(R_{\mu c})$, it can be said that the effects are virtually symmetrical for the two cases, i.e., $|0.13| \approx |-0.10|$. Notice that the average value of $|\ln(R_{\mu c})|$ is very low for both cases even though the peak/valley considered was selected to be of "representative" dimensions. The spectral ordinates are changed by as much as 60%. This would imply that the *local-shape* effect is not important, relatively speaking, even if the presence of asymmetry actually did exist

---

[5] A real jagged response spectrum will not necessarily have Sa_0 be at the base of a peak or valley. Also, the case considered here should really consider a higher value for R_{LS} than the one that the previous definition could provide, due to the possible effect of considering a moving average (provided that the numerator of Eq. 3.11 were at the maximum/minimum of the triangles considered in the factor functions). Also notice that the imposed shape does not consider any consideration of the higher-than-fundamental frequencies, as is the case for the local shape variations that real records show.

for it. One possible explanation is the fact that we were looking at a control case of a high median ductility ($\mu_D = 7$), and that the effective frequency is such that the structure has "softened" well past the influence of the peak/valley. In order to test this idea, higher resistance designs were also analyzed with the same sets of accelerograms (Table 3.19). The "higher resistant" designs correspond to systems that show lower values of median ductilities, when subjected to the same set of records. There seemed to be no trend in the *local-shape* effect, however, as described by $\ln(R_{\mu c})$. A trend (either increasing or decreasing) in the asymmetry (if any) in the coefficients can not really be established.

3.6.2.3 Isolated *Global-Shape* Effects.

In order to test the global-shape effects, factor functions (FF) were also constructed for modifying the original target shape (i.e., the control shape). The experiments were also done based on the $\mu_D = 8$ design (i.e., the system that showed a ductility of 8 to the unmodified set of 63 original records) of the 1hz bilinear SDoF system. The median value of ductility observed by running the control record set (i.e., the records compatibilized to the median shape) through the system was $\mu_m = 7.02$. However, the softened effective frequency was considered for simplicity to be $f_\mu = f_0 / \mu^{1/2} = 1\text{Hz} / 8^{1/2} = 0.35\text{Hz}$. The value of the normalized shape ratio was directly related to the factor, FF(.); it increases (or decreases) the value of Sa_μ with respect to that of the control shape (at such frequency). For this case, Fig. 3.14 shows the factor functions used. Here, the factor is $FF(f_\mu) = FF(0.35) = 1.8$ and $1/1.8$.

For both cases the factor functions that were considered extend linearly to lower-than f_μ frequencies. The value of the factor function at the softened effective frequency (considered to be at $f_\mu = 0.35\text{Hz}$) was such that the logarithm of the global shape ratio had the same absolute value of $\ln(R_{GS\mu c}) = |\ln(1.8)| = |\ln(1/1.8)|$ (see Figure 3.14).

The re-definition of the corresponding shape parameter describes the change in spectral shape, from f_0 to f_μ, with respect to the corresponding description of shape for the control spectrum:

$$R_{GS\mu c} = \frac{Sa_\mu / Sa_0}{Sa_{\mu mc} / Sa_{0mc}} \tag{3.20}$$

Note that the subindices corresponding to the description of "moving average" as they appear in Eq. 3.10, have been removed for simplicity; the spectral jaggedness was considered to have been removed by the compatibilization applied (i.e., it was considered that $Sa_{MA\mu} = Sa_\mu$ and $Sa_{MA0} = Sa_0$ for all records of each new set). Again, the c subindices in the denominator values indicate that the normalization was done with respect to values of the control spectral shape (the original target). The value of the shape ratio selected here ($R_{GS\mu c} = FF(f_\mu) = 1.8$) was somewhat ad-hoc, slightly larger than typical values (the exact "typical" value will be discussed in the next section). Other values will be considered below. Because the regression considers only the global-shape effects, we can write $R_{\mu c} = R_{GS\mu c}{}^{a2}$. For this case, the results obtained from the regressions are shown in Table 3.20.

The sought-after asymmetry is evident from the absolute values obtained for the a_2 coefficient for both sets; let them be called a_2^+ and a_2^-, as previously done. There is a statistically significant difference between the estimated absolute values of the two exponents. The relative difference in the values obtained for these coefficients can be seen in Figure 3.15, where runs for all three sets are shown (plotted μ vs. $FF(f_\mu) = R_{GS\mu c}$).

As done for the isolated *local-shape* case, the newly generated spectrum-matched sets were also tested on the lower resistance designs. In this case, the asymmetry seems to be "constant", in terms of the ratios of the estimated coefficients (i.e., about 2:1) regardless of the systems' resistance (Table 3.21).

Notice that since the same set of compatibilized records was used for all three systems (i.e., $\mu_D = 8$, 4 and 2), the value of FF(f_μ) was different for each case. The corresponding values of FF(f_μ) can be obtained from Fig. 3.14, where f_μ is to be computed from considering $\mu = 4$ and $\mu = 2$, i.e., they correspond to the values of FF(f_μ) at $f_\mu = f_0/4^{1/2}$ (i.e., FF(0.5)) and $f_\mu = f_0/2^{1/2}$ (i.e., FF(0.71)), respectively, (where $f_0 = 1$Hz).

The following sections will explain in detail the reason for the presence of bias observed in section 3.5, and how it can be predicted, and corrected. As done earlier, a brief and simplistic first-cut attempt to explain it, consider the following hypothetical situation: assume that all 63*3 records (corresponding to the control and both modified sets of compatibilized records above) belonged to a particular (hypothetical) M-R bin (i.e., 1/3 of the records having $R_{GS\mu c} \approx 1$, 1/3 greater than one ($R_{GS\mu c} = 1.8$), and 1/3 of them lower than one ($R_{GS\mu c} = 1/1.8$). The value of the median ductility that would be observed from all those records could be computed from the median normalized ductilities ($R_{\mu c} = \mu / \mu_c = \mu / 7.02$) (from values in Table 3.20):

$$\mu = \mu_c \exp((0.37 + 0 - 0.19)/3) = 7.44 \tag{3.21}$$

If all 63*3 records were then compatibilized to the median target (i.e., the control set shape), we would expect the median ductility to be equal to the control set's median ductility (i.e., $\mu_c = 7.02$) which would be unconservatively biased with respect to the hypothetical set. In short, this asymmetry may well be the cause of the bias observed in spectrum matched records.

3.7 Effects of the Variation of the *Global-Shape* Ratio: Bias Correction.

By using the information generated in the previous section, we can attempt to provide a means for producing a *corrected* spectral target for spectrum compatible records, such that it would allow for the unbiased estimate of the median ductility that unmodified records would show. For example, suppose that we know *a priori* that the bias in median ductilities that spectrum compatible records produce (using the median spectral shape of a bin as a target) is 1/1.14 ,e.g., as indicated in table 3.2a, for a 1Hz SDoF bilinear system. For this system the value obtained from regression was $a_2^+ = 0.623$ (the coefficient affecting the above-unity $R_{GS\mu c}$); one would hope that this would allow us to estimate the *required* global-shape ratio, $R_{GS\mu c}$, that should be forced on a (corrected) set of spectrum compatibilized records in order to offset such bias. In other words, setting $R_{\mu c} = 1.14$, the required global shape ratio might be:

$$\ln(R_{GS\mu c}) = \ln(R_{\mu c}) / a_2^+ = 0.21, \text{ or}$$
$$R_{GS\mu c} = 1.24. \hspace{6cm} (3.22)$$

With this, we could construct a factor function that enforces a $R_{GS\mu c} = 1.24$, i.e., one with $FF(f_\mu) = 1.24$. We will see below, however, that such a correction is not sufficient for this system, due to the variation of a_2^+ with different values of the *global-shape* ratio. Notice that for correction we need only the corresponding above-unity $R_{GS\mu c}$, because the *de*-biasing of the median estimate requires that the demands be higher than were observed for the original set of compatibilized records.

The following section, 3.7.1, studies the variation of the global-shape ratio effect on the normalized ductilities for different systems. Section 3.7.2 presents options for obtaining un-biased estimates of the median ductilities that a set of bin-records would produce.

3.7.1. Study of the *Global-Shape* Ratio on Different Systems.

Given that the potential source of bias was identified, one can ask the following questions:

- Do the values of a_2^+ and a_2^- (corresponding to above- and below-unity values of the *global-shape* ratio, $R_{GS\mu c}$) hold for different levels of the global-shape ratio, $R_{GS\mu c}$? Does the asymmetry still exist?
- Can we artificially control and ultimately eliminate the bias by setting an appropriate value of $R_{GS\mu c}$, to the target shape? If so, What is such an "appropriate" value?

For the same low resistance system considered above ($\mu_D = 8$), a set of different values for FF(f_μ) (and hence, new factor functions altogether, Figure 3.16) were considered for constructing new sets of compatibilized records, in order to vary the value of the *global-shape* ratio, $R_{Sa\mu}$. We can plot the mean values of $\ln(R_{\mu c})$ obtained with these new sets of records, against the values of $\ln(R_{GS\mu c})$. The new sets correspond to values of $R_{GS\mu c}$ of 1.24, 1/1.24 ,1.4 and 1/1.4 in addition to the previous sets of $R_{GS\mu c} = 1.8$ and 1/1.8. For each new set of records, the corresponding estimate of a_2^+ and a_2^- was obtained by regression as was done in the previous section, i.e., by equating them to the ratio of the mean natural logarithms of R_μ to $R_{GS\mu c}$.

Note that the ratio of normalized ductility $R_{\mu c}$ to the shape ratio, $R_{GS\mu c}$, increases as the value of $R_{GS\mu c}$ grows; in particular the relationship is not linear. Assumed in the regression model (i.e., $\ln(R_{\mu c}) = a_2 \ln(R_{GS\mu c})$) was a logarithmic *linear* relationship between $R_{\mu c}$ and $R_{GS\mu c}$. The plot shows a non-constant value of the estimate a_2^+, because it depends on the value of $R_{GS\mu c}$. It appears that these nonlinear softening systems are non-proportionately sensitive to increased global shape ratios, i.e., increase in the strength of the spectrum at lower frequencies than f_0. This is in contrast to the simple "intensity changes", i.e., scaling records up and down, where the effect is roughly proportional over a broad ductility range. We can notice that for the value of $R_{GS\mu c} =$

1.24, which corresponds to $\ln(R_{GS\mu c}) = 0.21$, the corresponding normalized ductility ratio, $R_{\mu c}$, is lower than the value of 1.14 we would require to correct for (i.e., $\ln(R_{\mu c}) = 0.068$, or $R_{\mu} = 1.07$), for a 1hz, $\mu_D = 8$, bilinear SDoF system.

Figure 3.17 now allows us to generate a set of compatibilized records that will produce the desired un-biased estimates. For example, as mentioned above for the low resistance 1hz bilinear system ($\mu_D = 8$), we know that the median bias was $8.0/7.02 = 1.14$ (table 3.2a). Hence, for the required level of modification, i.e., $R_{\mu} = 1.14$ (or $\ln(R_{\mu}) = 0.13$), Figure 3.17 shows that the corresponding value of $\ln(R_{GS\mu c})$ *required* is 0.34. Hence, the value of FF(f_{μ}) that will cause such value is exp(0.34) = 1.4 (which coincidentally corresponds to one of the values selected for the experiment). We shall confirm that this scheme works below.

But first, it is of interest to know whether knowing the variation of the normalized ductility with different values of the *global-shape* ratio of an SDoF system permits one to predict as well the impact on responses of other SDoF or even MDoF systems. If so, are such predictions valid for both interstory and global ductility measures? Remember that Figure 3.17 corresponds to the low-resistance SDoF 1Hz system, which allows us to construct *corrected* compatibilized records, strictly only for that system.

Table 3.22 compares the median displacement values obtained by using a set of 63 "corrected" compatibilized records, using a target spectra equal to the bin-median spectrum multiplied by a factor function with FF(0.35Hz) = 1.4 (based on Fig. 3.14). The results are for the different 1Hz systems studied in section 3.5 (including the 2-D friction-pendulum based isolated system).

As expected, the estimate of the median ductility for the low resistance SDoF system is now unbiased (compare 8.00 and 8.10 versus 7.02). Not expected, but welcome however, the higher-resistance SDoF systems also yielded reasonably unbiased estimates of the median ductilities. Notice that the modified-shape spectrum compatible records continue

to produce very low dispersions ($\sigma_{ln\mu} \approx 0.2$) and hence would still permit the use of smaller sample sizes.

The use of this particular corrected set of compatibilized records was, however, not too good for the MDoF systems, although some improvement in the estimates (i.e., a little lower bias) was attained for the stick models. For the fixed-base 2-D frame the correction was apparently only half of what it needed to be (i.e., $\mu_i = 4.20$ to estimate a median interstory value of $\mu_i = 4.6$). For the base isolated 2-D frame, for which interest is mainly in the nonlinear isolator displacement, the displacement estimated was apparently "over-corrected", but given the large standard error $(0.92 /(63)^{1/2} \approx 0.12)$ on the original-data set median value (10.1 in) the two estimates are not significantly different. Both sets of compatibilized records predicted poorly (i.e., showed a biased prediction for) estimates of both median interstory and global ductilities in the superstructure. Curiously there was no increase in these values for the second set of spectrum matched records; this is perhaps because they repeat virtually linear behavior.

In order to provide an appropriate system-specific correction of the above systems, compatibilized record sets with different levels of global shape correction on the original target were also tested on them. Also, for the high frequency 4Hz systems, new compatibilized records were generated for the same purpose. The corresponding modified spectral shapes considered factor functions similar to those shown in Figure 3.14, now with constant unit values above 4hz. Figures 3.18 through 3.24 show the plots corresponding to the effect that different levels of the global-shape parameter have on the normalized ductility. In order to show comparable plots for systems of the same elastic frequency but different resistances, a new characterization of the factor functions was made, in terms not of the values of the factors at different frequencies (e.g., $FF(f_\mu) = x$), but of the angle θ that the line corresponding to the variation of the factor with frequency (below f_0) has with respect to the horizontal. For example, Figure 3.14a (which, for $f_0 = $ 1hz, and $FF(f_\mu) = FF(0.35) = 1.8$) corresponds to an angle of $\theta = 0.89$rad (i.e., 51°). The correction angle that was used to modify the records for the generation of Table 3.22 (i.e., 1Hz systems) , was $\theta = 0.55$rad ($FF(f_\mu) = 1.4$; $f_0 = 1$Hz, $f_\mu = 0.35$Hz).

Figures 3.18 through 3.24 show only the variation of the normalized ductility with a positive θ-angle; the required correction corresponds only to positive values for $R_{GS\mu c}$ (and hence for FF(f_μ), which can directly be mapped into the value of the required angle). The first graph, Figure 3.18, is derived from the values in Fig. 3.17 (for $R_{GS\mu c} >$ 1); also presented in Fig. 3.18 are the plots corresponding to the higher resistance, SDoF, 1Hz systems ($\mu_D = 4$ and 2).

3.7.2. Un-Biased Estimate of Bin-Records Median Ductilities.

For a known (a priori) level of required *de*-biasing, the previous plots allow us to construct system-specific corrected (with respect to the bin-median shape) compatibilized records, using the appropriate θ-angled factor function.

Based on Table 3.22 and on Figures 3.18 through 3.24, one can make the following observations:

- Plots corresponding to SDoF systems, which are relatively "cheap" to obtain, are unfortunately not necessarily sufficient for obtaining correcting-factor-functions in order to generate spectrum compatibilized records that will produce un-biased estimates of median ductilities for MDoF systems. For example, for both 1Hz stick models, the corrected records (having corrected by using the $\theta = 0.55$rad correction angle) still under-predicted the median ductility, for both interstory and global measures (the best they could do was for the low-resistance interstory ductility estimate, 7.12 vs. 7.21).
- Not always can the same corrected target shape correct both interstory and global estimates of ductilities by the same amount. See for example Figs. 3.19 and 3.20. For such a case, in order for a single corrected curve to be useful, the amount of required bias correction for both responses would need to be different. Alternatively, both

interstory and global ductility angle-correction curves need to be close to each other, such that the same amount of bias correction is attained, and the amount of bias to correct must be the same. For example, for the 2-D fixed frame both ductilities needed corrections of about 20% and, although the angle used for the correction of the records ($\theta = 0.54$) was insufficient, both measures were corrected by comparable amounts, which is consistent with the proximity of the 2-D fixed frame μ_i and μ_g correction-angle curves (Fig. 3.21). For levels of bias up to around 1.4, the 4Hz MDoF stick-model curves (Fig. 3.23) indicate that both measures should be corrected equally; however, as indicated by table 3.6*a*, the required correction is different (i.e., 1.32 for global, and 1.13 for interstory), such that a single curve would not work for correcting these measures simultaneously.

- In terms of the correcting factor function angles, it seems that as the system's fundamental frequency increases, the angle required is smaller, as can be seen, for example, by comparing figures 3.19 and 3.23.

The major implications of the above observations are that not only are the different biases to be corrected not necessarily consistent within a system, but also the correction curves are highly system-dependent. More systems need to be analyzed in order to try to identify some consistent pattern, or to make useful generalizations.

For the systems that were analyzed for the construction of Figures 3.18 through 3.24, Table 3.23 shows the "correct" required angle, given the system and response-specific (i.e., μ_i or μ_g) observed bin-median-shape-matched records' biased estimate of the median responses.

Observing the limited data, the following conclusions can be drawn. In general, SDoF-based angles tended to be insufficient for "correcting" for MDoF results (except for the low resistance interstory ductility of the 4Hz-MdoF-stick model — because of the bias it showed, Table 3.6 — and those of the displacement of the friction pendulum-isolated 1Hz system). As mentioned earlier, the required angles seem to decrease as the frequency

of the system increases. In general, for stronger systems, the angle required seems to be higher.

One would like, of course, the efficiency (implied by the ductility dispersion of spectrum-matched records) while avoiding their potential inaccuracy. At this point we have the following three options for obtaining an unbiased estimate of the corresponding M-R bin median ductilities by means spectrum compatibilized records:

1) The simplest scheme is to run the bin-median-shape matched spectrum compatible records through the system and obtain the biased estimate of the median. The typical values of "bias" for the various systems in Tables 3.2 through 3.10 can be used as factors on the spectrum matched estimated median values in order to *de*-bias the estimate.

2) The second option is to consider "scaled" compatibilized records (i.e., no shape alteration), in order to adjust their intensity. The bin-median-shape-matched accelerograms are to be scaled by a factor proportional to the "bias" values estimated as above from Tables 3.2 through 3.10. This assumes a $b \approx 1.0$ model (as given by Eq. 3.16) (The factor can be appropriately modified for non-unit b values). The difficulty here is that one does not know the level of ductility involved before matching the bias estimate. And it may be different for different responses of interest (e.g., global vs. interstory drift), implying that no single factor is sufficient.

3) If an appropriate correction-angle curve is available, the last option is to shape-modify the target for spectral matching. Provided that we know the level of required *de*-biasing one obtains the corresponding correcting angle, modifies the bin-median-spectral shape, generates the corresponding compatibilized accelerograms, and runs them through the system.

Consider the simple following example: If the system we are interested is, a 1Hz MDoF high-interstory ductility system, we can make use of the top curve in Figure 3.19. Assuming we know the expected uncorrected-shape bias is 1.19 (e.g., from Table 3.5*a*),

we find from interpolation that the angle required for correcting the spectral target is $\theta =$ 0.57rad; this angle is the inclined line parting from 1Hz to lower frequencies, such that we use the factor function shown on Fig. 3.25 on the original target.

Such a factor function is then applied to the original target, i.e., the M-R bin median spectral shape. Figure 3.26 shows the original target, and the corresponding "corrected" shape that would yield corrected accelerograms for estimating unbiased estimates of the bin median ductilities.

It is necessary to point out that the use of this exemplified scheme will depend on the (unlikely) existence of these curves. For the particular case of interest (be it interstory or global ductility) we are interested in a SDoF system or a MDoF system, a high frequency one or low frequency one. The applicability of this scheme is very restricted, due to the highly system-dependent nature of the angle correction curves.

3.8 Simple Analytic Prediction of Spectrum Matched Records' Bias.

The previous example made use of modified target shapes that would remove the apparent bias of the estimate that median-bin-shape spectrum matched records would produce (given the unlikely event that it was actually available). However, it required knowing beforehand the amount of bias that the set of compatibilized records would introduce. One identifies the amount of bias expected (e.g., by means of tables 3.2 through 3.10), and from the corresponding correction-angle plot (if available) one then estimates the required value of the angle for constructing the factor function that will "correct" the spectral target shape. The first two more accessible methods proposed (scaling the records or directly correcting the bias) also required knowledge of the bias.

The following sections incorporate what was learned with the controlled-isolated effect studies in section 3.7, with what can be known about a set of bin-records, in order to try to predict the bias that median-shape-compatibilization records might introduce in estimating the median ductility demands. Section 3.8.1 proposes, for this purpose, an analytical description of such bias introduction. Following that, section 3.8.2 applies the model for the different systems considered in the previous section, and describes the ability to use it, and provides the required information.

3.8.1. Analytic Description of Observed Bias.

In an attempt to explain the inherent amount of nonlinear displacement bias in the estimate of the median introduced by compatibilizing a particular set of records (e.g., from a narrow M-R bin) to the bin median spectral shape, consider the following observations:

- A refinement in the model for describing nonlinear response vs. seismic input considers knowing the distribution of the *global-shape* parameter, $R_{GS\mu}$ (as described by Eq. 3.10), for a set of a M-R bin (unmodified) records. Given the median spectral shape, some records will show above-unit values of $R_{GS\mu}$, and some will show below-unit values.

- The value of the *global-shape* ratio, $R_{GS\mu}$, is related to the softened effective frequency, f_μ. The latter can be estimated by considering an estimated median ductility (based on, for example the *equal-displacement* rule, where $\mu \approx Sa_{0m} / Sa_{0y}$, Sa_{0y} being the yield level spectral acceleration) and applying the effective frequency concept, i.e., $f_\mu = f_0 / \mu^{1/2}$. The *global-shape* ratio is also related to the median-bin-spectral shape, in terms of its values at f_0 and f_μ (i.e., Sa_{0m} and $Sa_{\mu m}$), values that, for a narrow bin, can be obtained from appropriate attenuation laws at f_0 and f_μ.

- For a narrow bin, the probability distribution of Sa_0, for any particular frequency f_0, can be considered to be known from the corresponding attenuation law and its dispersion (σ_{lnSa0}) (typically modeled as lognormal, Abrahamson, 1997).

By taking the previous observations into account, the following is an analytical prediction of the bias, based on assuming valid for the bin-records the functional relationship between the isolated-effect *global-shape* ratio, $R_{GS\mu c}$ and the normalized ductility, R_μ, as depicted in Figure 3.17. As will be seen, such a description of the bias is put in terms of the asymmetry that such functional relationship for above-unit values of $R_{GS\mu c}$ have with respect to the below-unit values' relationship, i.e., a_2^+ vs. a_2^-. The existence of an underlying biased estimate lies on the fact that real bin-records present a dispersion of values of the *global-shape* ratio (dispersion which is linked to the median level of non-linearity in the system). Spectrum compatibilized records, by definition, lack such dispersion, which keeps the asymmetry in the *global-shape* ratio effect from "operating", leading them to being biased low, relative to the unmodified bin records' estimate.

What is about to be computed in this section is the expected value of the ratio of the estimated median ductility that bin-records yield, *with respect to* the estimated median ductility that a set of compatibilized-to-the-median-shape accelerograms would produce. Such value, is analogous to the "bias" values presented in tables 3.2 through 3.10. We will part from the assumption that all records have been normalized to the spectral acceleration at the fundamental frequency, such that we need not worry about intensity effects. This, of course, makes use of the belief that normalized records yield the same estimated median ductility. Also, noticing that by normalizing, the distribution of *global-shape* ratios of the bin records is maintained.

In logarithmic terms, the expected value of the sought-after ratio is:

$$E[\ln(\mu/\mu_m)] = E[\ln(R_\mu)] = E[g(\ln(R_{GS\mu}))] \tag{3.23}$$

where $g(.)$ is the functional relationship between the global shape ratio, $R_{GS\mu}$, and the normalized ductility, R_{μ} (an example of such function, although not called $g(.)$ there, is illustrated in Fig. 3.17). $E[.]$, is the expectation of the bracketed function of the random variable.

As mentioned above, the normalization ductility, μ_m, is the value of the median ductility that the median-shape-matched records would produce. Unlike the definition of R_{μ} given by equation 3.18 (section 3.6.2), the ductilities that are being normalized here (i.e., μ) do not come from compatibilized records with a predefined value of $R_{GS\mu}$, but from the normalized bin records. Also, the definition used here of $R_{GS\mu}$ (analogous to that of Eq. 3.20) was not made in terms of the moving average, as was done in Eq. 3.10. As will be seen, we have estimated intensities (spectral accelerations) by means of appropriate attenuation laws that are not related to the corresponding *moving average* value, but Sa_0 itself.

Let us consider separately the contributions of the negative and positive subsets of $\ln(R_{GS\mu c})$ to the normalized ductility, because the asymmetry in figure 3.17 (i.e., $\ln(R_{\mu c})$ vs. $\ln(R_{GS\mu c})$) suggested the possibility of defining the function $g(.)$ differently for these sets. Let us call these $g^+(.)$ and $g^-(.)$:

$$E[\ln(R_{\mu})] = E[g^+(\ln(R_{GS\mu})) \mid \ln(R_{GS\mu}) > 0] \, P[\ln(R_{GS\mu}) > 0]$$
$$+ E[g^-(\ln(R_{GS\mu})) \mid \ln(R_{GS\mu}) < 0] \, P[\ln(R_{GS\mu}) < 0] \tag{3.24}$$

where $P[.]$ is the probability of the bracketed event.

It is important then to establish the distribution of $\ln(R_{GS\mu})$. Based on the definition used here : $R_{GS\mu} = (Sa_{\mu} / Sa_0) / (Sa_{\mu m} / Sa_{0m})$, for a particular record from a narrow bin, we can establish such distribution by considering the logarithmic representation:

$$\ln(R_{GS\mu}) = (\ln(Sa_\mu) - \ln(Sa_0)) - (\ln(Sa_{\mu m}) - \ln(Sa_{0m}))$$
$$= (\ln(Sa_\mu) - \ln(Sa_0)) - (E[\ln(Sa_\mu)] - E[\ln(Sa_0)]) \tag{3.25}$$

Let us assume that this is the difference of two normal variables , which is consistent with what is observed when constructing attenuation laws, minus their means. Assume further that $\ln(Sa_\mu)$ and $\ln(Sa_0)$ are *jointly* normally distributed, with correlation coefficient $\rho_{lnSa0,lnSa\mu}$ (given M and R of the bin), implying that $\ln(R_{GS\mu})$ is a gaussian variate: $N(0, \text{Var}[\ln(R_{GS\mu})]$, with

$$Var[\ln(R_{GS\mu})] = \sigma^2_{\ln Sa_0} + \sigma^2_{\ln Sa_\mu} - 2\rho_{\ln Sa0,\ln Sa\mu}\sigma_{\ln Sa_0}\sigma_{\ln Sa_\mu} \tag{3.26}$$

Also,

$$P[\ln(R_{GS\mu}) > 0] = P[\ln(R_{GS\mu}) < 0] = 0.5 \tag{3.27}$$

It is expected that as the softened effective frequency, f_μ, is further away from f_0, the value of $\rho_{lnSa0,lnSa\mu}$ will decrease, such that the variance of $\ln(R_{GS\mu})$ will be higher as the value of the expected ductility demand increases. Recall that $f_\mu = f_0 / \mu^{1/2}$, implying $f_\mu / f_0 = 1/\mu^{1/2}$. Inoue, 1990, found an empirical relationship that defines such a correlation, given in terms of the ratio of frequencies.

$$\rho_{\ln Sa0,\ln Sa\mu} = 1 - 0.33|\ln(f_\mu / f_0)| \tag{3.28}$$

which here becomes $(1 - 0.33|\ln(\mu)^{1/2}|)$. Let us consider, based on Fig. 3.16, a quadratic model for $g^+(.)$ of the form:

$$g^+(\ln(R_{GS\mu})) = \alpha^+ \ln(R_{GS\mu}) + \beta^+ (\ln(R_{GS\mu}))^2 \tag{3.29}$$

Also, let us consider a linear model for $g^-(.)$:

$$g^-(\ln(R_{GS\mu})) = \alpha^- \ln(R_{GS\mu}) \tag{3.30}$$

i.e., $\alpha^- = a_2^-$ (the coefficient obtained for the below-unit values of $R_{GS\mu}$). We are now in condition to expand Equation 3.24 by means of the following two equations:

$$
\begin{aligned}
E[g^+(\ln(R_{GS\mu})) \mid (\ln(R_{GS\mu}) > 0] &= E[\alpha^+ \ln(R_{GS\mu}) + \beta^+(\ln(R_{GS\mu}))^2 \mid \ln(R_{GS\mu}) > 0] \\
&= \alpha^+ E[\ln(R_{GS\mu}) \mid \ln(R_{GS\mu}) > 0] \\
&+ \beta^+ \Big[E^2[\ln(R_{GS\mu}) \mid \ln(R_{GS\mu}) > 0] + Var[\ln(R_{GS\mu}) \mid \ln(R_{GS\mu}) > 0] \Big]
\end{aligned} \tag{3.31}
$$

and

$$
\begin{aligned}
E[g^-(\ln(R_{GS\mu})) \mid (\ln(R_{GS\mu}) < 0] &= E[\alpha^- \ln(R_{GS\mu}) \mid \ln(R_{GS\mu}) < 0] \\
&= \alpha^- E[\ln(R_{GS\mu}) \mid \ln(R_{GS\mu}) < 0]
\end{aligned} \tag{3.32}
$$

The required conditional distributions, i.e., $f_{ln(RGS\mu)) \mid ln(RGS\mu) < 0}$ and $f_{ln(RGS\mu)) \mid ln(RGS\mu) > 0}$, are mirror images of one another; they correspond to truncated-at-zero normal distributions (in which the underlying normal distribution has parameters mean = 0, variance = $\sigma^2_{lnRGS\mu}$). One is truncated above zero, and one below zero. There is a normalization by the corresponding half area, i.e., by 0.5. The mean and variance of such conditional distributions can be found in terms of the parameters of the unconditional gaussian distribution of $\ln(R_{GS\mu})$. For example,

$$E[\ln(R_{GS\mu}) \mid \ln(R_{GS\mu}) > 0] = \frac{2}{\sigma_{\ln R_{GS\mu}} \sqrt{2\pi}} \int_0^\infty x e^{\left(\frac{-1}{2}\right)\left(\frac{x}{\sigma_{\ln R_{GS\mu}}}\right)^2} dx$$

$$= \frac{2}{\sqrt{2\pi}} \sigma_{\ln R_{GS\mu}} \approx 0.8 \sigma_{\ln R_{GS\mu}}$$

(3.33)

The conditional mean given $\ln(R_{GS\mu}) < 0$ is of course negative, with the same absolute value. Also,

$$Var[\ln(R_{GS\mu}) \mid \ln(R_{GS\mu}) > 0] = \frac{2}{\sigma_{\ln R_{GS\mu}} \sqrt{2\pi}} \int_0^\infty \left(x - \frac{2}{\sqrt{2\pi}} \sigma_{\ln R_{GS\mu}}\right)^2 e^{\left(\frac{-1}{2}\right)\left(\frac{x}{\sigma_{\ln R_{GS\mu}}}\right)^2} dx$$

$$= 2\sigma^2_{\ln R_{GS\mu}} \left(\frac{1}{2} - \frac{1}{\pi}\right) \approx 0.36 \sigma^2_{\ln R_{GS\mu}}$$

(3.34)

Finally, using Eqs. 3.31, 3.32, 3.33, 3.34 and after a little algebra, the expected amount of bias can be written as:

$$E[\ln(R_\mu)] = \sigma_{\ln R_{GS\mu}} [(\alpha^+ - \alpha^-)(2\pi)^{1/2} + (\beta^+/2)\sigma_{\ln R_{GS\mu}}]$$

(3.35)

with $\sigma_{\ln R_{GS\mu}}$ given by Eq. 3.26.

In summary, Eq. 3.35 indirectly quantifies the bias that spectrum compatibilizing to the median shape of a set of bin records would have. In fact, compatibilization eliminates the dispersion of the *global-shape* ratios that a set of bin records naturally has, thus not permitting the *asymmetry* of the effect of above- or below-unit values of $R_{GS\mu}$ to contribute to the overall median estimate of response, therefore we believe that $E[\ln(R_\mu)]$ (Eq. 3.35) is the amount of this effect in the real records and hence the amount by which the median of the spectrum matched records must be multiplied to correct for its bias. Eq. 3.35 makes explicit such *asymmetry* "effect": the difference in the parameters α^+ and α^-

plus the contribution of the square of $R_{GS\mu}$ given by β^+. Also, it can bee seen that the level of the *asymmetry* effect depends on the level of ductility expected, implicit in $\sigma_{lnRGS\mu}$.

Notice that if the relationship between $R_{GS\mu}$ and its effect on the normalized ductility had been modeled as linear, i.e., by assuming in the model $\beta^+ = 0$, then the *asymmetry* "effect" is totally described by $(\alpha^+ - \bar{\alpha})$. This particular case is equivalent to requiring only the coefficients a_2^+ and a_2^- as obtained in Table 3.20, where α^+ would correspond to the coefficient obtained for the above-unit $R_{GS\mu}$, i.e., a_2^+, and $\bar{\alpha}$ would correspond to the coefficient obtained for the below-unit $R_{GS\mu}$, i.e., a_2^-.

3.8.2. System-specific Parameters for Bias Estimation.

Only for the (rare) particular case where the angle correction curves were available, knowing the expected ratio of the bin-records' estimate of median ductility to that obtained from compatibilized records, the required level of modification of the target shape, at f_μ (as described in section 3.7), can then be found by solving for the value of $\ln(R_{GS\mu c})$ required to cause the expected (positive) value of $\ln(R_{\mu c})$ by using Eq. 3.29, i.e., by making use of the function $g^+(.)$. This is done by finding the value of the global-shape ratio required, and using it to construct the correcting factor function (like that in Fig.3.14, section 3.7) (i.e., $FF(f_\mu) = R_{GS\mu c}$). The required correction then, in terms of $\ln(R_{GS\mu c})$ is:

$$\ln(R_{\mu c}) = g^+(\ln(R_{GS\mu})) = \alpha^+ \ln(R_{GS\mu}) + \beta^+ (\ln(R_{GS\mu}))^2 \tag{3.36}$$

Solving for (the positive solution of) $R_{GS\mu c}$ from Eq. 3.36 we obtain:

$$R_{GS\mu c} = FF(f_\mu) = \exp\left[-\alpha^+ + \sqrt{(\alpha^+)^2 + 4\beta^+ \ln(R_{GS\mu c})} \right]/(2\beta^+) \tag{3.37}$$

Of course the parameters α^+ and β^+ are required in order to find such a correction. For computing the amount of bias, the value of $\bar{\alpha}$ is also required. The systems for which the value of $\ln(R_\mu)$ as a function of θ-angles were given in section 3.7 (e.g., Figs. 3.18 through 3.24) present the g^+ and g^- functions (in terms of $\ln(R_{GS\mu c})$) depicted in Figures 3.27 through 3.32.

The previous graphs permit us to get an idea of the degree of asymmetry, and hence the level of potential bias that spectrum compatibilization might introduce. The apparent level of asymmetry varies from system to system, but for the most part, it can be identified. Except for the global ductility case of the medium resistance 1Hz MDoF stick model (Fig. 3.29), the asymmetry in global-shape ratios with respect to the origin is apparent for all cases and will lead to an above-unit estimation of the expected bias (see Table 3.24). However, other variables are involved in the computation of such estimate (e.g., the level of dispersion in the bin-records' spectral acceleration at f_0, which can not be seen in the graphs, Eq. 3.35).

Notice the difference in vertical scale (associated to the ductility ratio) of the 4Hz systems with respect to the 1Hz systems. The "stretching" of the axis for the higher frequency systems is tied to the fact that these require smaller correction angles of the factor functions in order to introduce the same level of *de*-biasing.

The parameters for the g^+ and g^- functions, obtained from the previous graphs are presented in Table 3.24. Also presented are the α_l^+, i.e., the α^+ values for a linear model of g^+, such that Eq. 3.35 can be used setting $\beta^+ = 0$. For such a case, the *asymmetry* effect, as described earlier, can be expressed in terms of simply $\Delta\alpha = \alpha^+ - \bar{\alpha}$ alone (see the second "bias computed" column in Table 3.24). For these systems, the expected effect, in terms of $R_{\mu c}$, is also shown (first "bias computed" column in Table 3.24), and compared to the actual ratio of compatibilized median ductilities to the bin-records' median ductilities ("bias observed" column, Table 3.24) which were directly taken from Tables 3.1 through 3.9)

As an example of how the values for the estimated *asymmetry* effect, in terms of $R_{\mu c}$, were computed in Table 3.24 (see below), consider the 1hz, bilinear system, low resistance system ($\mu_D = 8$). Equation 3.26 requires the values of the standard deviations of the logarithms of the spectral accelerations involved ($Sa_0(1\text{Hz})$, $Sa_\mu = Sa(1\text{Hz}/8^{1/2})) = Sa(0.35\text{Hz}))$. From Abrahamson (1997), we find:

$\sigma_{lnSa0} = 0.59$, so $\sigma^2_{lnSa0} = 0.35$; and,

$\sigma_{lnSa\mu} = 0.66$, so $\sigma^2_{lnSa\mu} = 0.44$.

From Inoue(1990), we can estimate:

$\rho_{lnSa0, lnSa\mu} = 1 - 0.33 \, |\ln(f_\mu/f_0)| = 0.66$.

Hence, from Eq. 3.26

$\text{Var}[\ln(R_{GS\mu c})] = \sigma^2_{lnSa0} + \sigma^2_{lnSa\mu} - 2\rho_{lnSa0,lnSa\mu} \, \sigma_{lnSa0} \, \sigma_{lnSa\mu} = 0.30$,

or $\sigma_{lnRGS\mu c} = 0.54$.

(The value obtained from computing directly $\sigma_{lnRSa\mu}$ from the set of original records was $\sigma_{lnRGS\mu} = 0.49$). For the system, the parameters for g^+ and g^- are: $\alpha^+ = 0.14$; $\alpha^- = 0.35$; and $\beta^+ = 0.82$ (Table 3.24). Combining these and using Eq. 3.35, we obtain:

$\text{E}[\ln(R_{\mu c})] = (1/2) \, \sigma_{lnRGS\mu c} \, [(\alpha^+ - \alpha^-) \, (2/(2\pi)^{1/2}) + \beta^+ \sigma_{lnRGS\mu c}] = 0.074$,

so the estimated bias (i.e., defined as the ratio of the real records' estimate of the median to that of the compatible records') is $\exp(0.074) = 1.08$.

Table 3.24 shows that the actual median ratio, using median-shape matched accelerograms, is 1.14. Although this value is not statistically significantly different from

1.08 (due to the large SEE —approximately equal to 0.1 for avg(ln(R_μ))—) the fact that all the predictions are consistently lower than the observed bias estimates suggests that the difference in this case is more than a statistical phenomenon.

Notice that the predictions are (consistently) lower (around 90%) than those empirically observed, yet they are capturing the relative variation of the observed bias., they seem to work reasonably well in general. For one case (1Hz MDoF stick, global ductility), the estimated ratio was actually lower than unity; the negative value of $\Delta\alpha$ (for the linear model) coincides with the (under-) prediction of the quadratic model.

As was the case for the attempt to generalize the conclusions for angle-correction (section 3.7) few general observations can be made. In general, in terms of the simplistic linear model, values of $\Delta\alpha$ seem to be larger for higher frequency systems. Although this might at first sight appear to be a reason for systematically higher biases for the higher frequency systems, this was not the case either for the empirical observations or for the predicted values. The effect of the higher values of $\Delta\alpha$ for the 4Hz systems with respect to that of the 1Hz systems (e.g., for $\mu_D \approx 4$, $\Delta\alpha(4\text{Hz}) \approx 0.3$ vs. $\Delta\alpha(1\text{Hz}) \approx 0.2$) are sometimes offset by the lower standard deviations of the logarithms of the spectral accelerations ($\sigma_{lnSao}(4\text{Hz}) = 0.5$, vs. $\sigma_{lnSao}(1\text{Hz}) = 0.6$), as indicated by the attenuation laws used (Abrahamson, 1997). Notice *that* for the same level of ductility, the coefficient of correlation is the same for both cases (Eq. 3.28).

The model seemed to work best for SDoF systems. Also, the model seems to work better for the interstory ductility bias estimation. In general, the worst represented system was the 2-D frame. As previously stated, more systems would need to be studied in order to identify any useful patterns (e.g., in $\Delta\alpha$) that the limited information here does not allow us to find.

3.9 Conclusions.

The use of spectrum compatibilized records has in practice been easily taken for granted. This study presented results that may be taken as a warning. For the estimation of the ductility demands that correspond to a scenario event, spectrum matched records, whose target is that of the scenario M-R bin median shape, will generate results that predict an **unconservatively biased** estimate of median displacement-based nonlinear responses. Typical values for ductilities around 4 and above are 1/1.15 to 1/1.2 (and may increase with the displacement level) that of the bin-records' results. This warning, however, is accompanied by a very useful reduction in the observed variability of response. This allows a large reduction in the required number of nonlinear analyses to estimate such median with an equivalent confidence (typical reduction of the order of 4:1). The reduction allowed is large, but not large enough to use single spectrum compatible records as some seismic codes call for.

As was discussed in Shome, 1999, spectral accelerations other than the one at the structure's fundamental frequency may be important to consider for the efficient prediction of nonlinear demands. This implies that spectral shape in general may be important. In this study it was found that a primary contributor to the apparent aforementioned biased estimation relies on the *global-shape.* A simple descriptor of this shape was proposed, the *global-shape* ratio, in terms of the spectral accelerations at the fundamental frequency, f_0, and at the softened *effective* frequency, $f_\mu = f_0 / \mu^{1/2}$.

The effect of such shape is *asymmetric*; in an absolute sense, the above-unit valued global-shape ratios have a stronger effect on ductility demands than their below-unit valued counterparts leading the median ductility to be larger than that anticipated from a record with unit shape value. Because spectrum matched accelerograms suppress the natural variability that M-R bin records have in shape, the asymmetry has no effect on the overall median ductilities. As a consequence the median ductilities that they produce are biased *low*.

Local variations (i.e. in the close vicinity of the fundamental elastic frequency) of the spectral shape did not seem to have any major effect on the observed bias. However, different descriptors of these local variations may need to be tested, to confirm this finding.

The empirical observation of the observed bias for a large range of systems, permits the correction of the estimate of the median ductilities, by the use of simple methods derived in part from the spectrum-matched-based results. Some options are (1) by scaling the records appropriately given a particular " $\mu = a \, Sa^{\, b}$ " model (including the *equal-displacement* model with $b = 1$), and (2) by simply correcting directly the estimate of median demands observed. A third method proposed, which proved to be highly system-dependent, allows for the modification of the target spectral shape, such that the "corrected" spectrum compatibilized accelerograms directly allow the unbiased estimate of the median demands to be computed. Correction curves were computed for a few systems. However, these did not appear to show a useful pattern for allowing a generalization of the correction for other systems not studied. Further, the scheme does not always correct appropriately different response measures in the same system (e.g., global and interstory ductilities in a MDoF system). This is suggested by the differences in bias in the factors observed in Figs. 3.27 through 3.32.

For the model proposed for the correction of the target, only a linear variation of the "factor function" was considered. It could be argued, however, that different shapes of such functions might influence differently the response that the records modified by them would produce. Also, an improved global-shape parameter could be investigated, such that the inclusion of the frequency-variation in global shape (perhaps by introducing, for example, parameters such as a *global-shape-curvature* measure) is considered (involving not only the end-point-computed parameter, f_μ).

An analytic model for the expected asymmetry-effect, in terms of the under-prediction of the median estimate by bin-median spectral shape compatibilization, was presented. It reflects directly the effect of the asymmetry as well as the level of ductility (in terms of

the softened frequency range) on this under-prediction. The model was tested with a few systems, and captured part of the characteristics of the bias (the relative values), however, under-predicted the empirically observed bias. The model, too, may benefit from the improvement of the global-shape definition. A further improvement in the model may consider the additional variability introduced by the finite-width M-R bin because the model considered a variability associated to ideal single-scenario-event bins.

Chapter 3 Figures.

Figure 3.1a. Force deformation characteristics of the bilinear hysteresis model. The post-yield slope considered is that of 3% of the elastic slope.
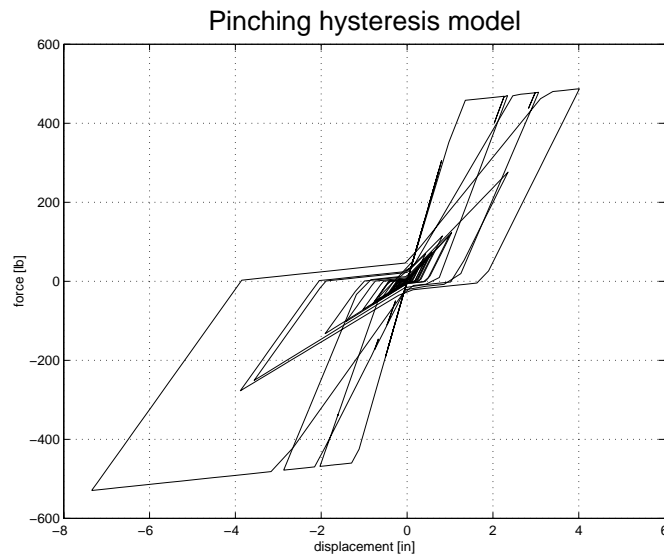
Figure 3.1b Force-deformation characteristics of the pinching hysteresis, stiffness degrading model. The post-yield slope considered is that of 3% of the elastic slope. See Foutch, 1996, for examples of stiffness degrading and pinching algorithms.

Bilinear System; program: RASCAL; Contours:$\mu_{orig} \setminus \mu_{compat}$
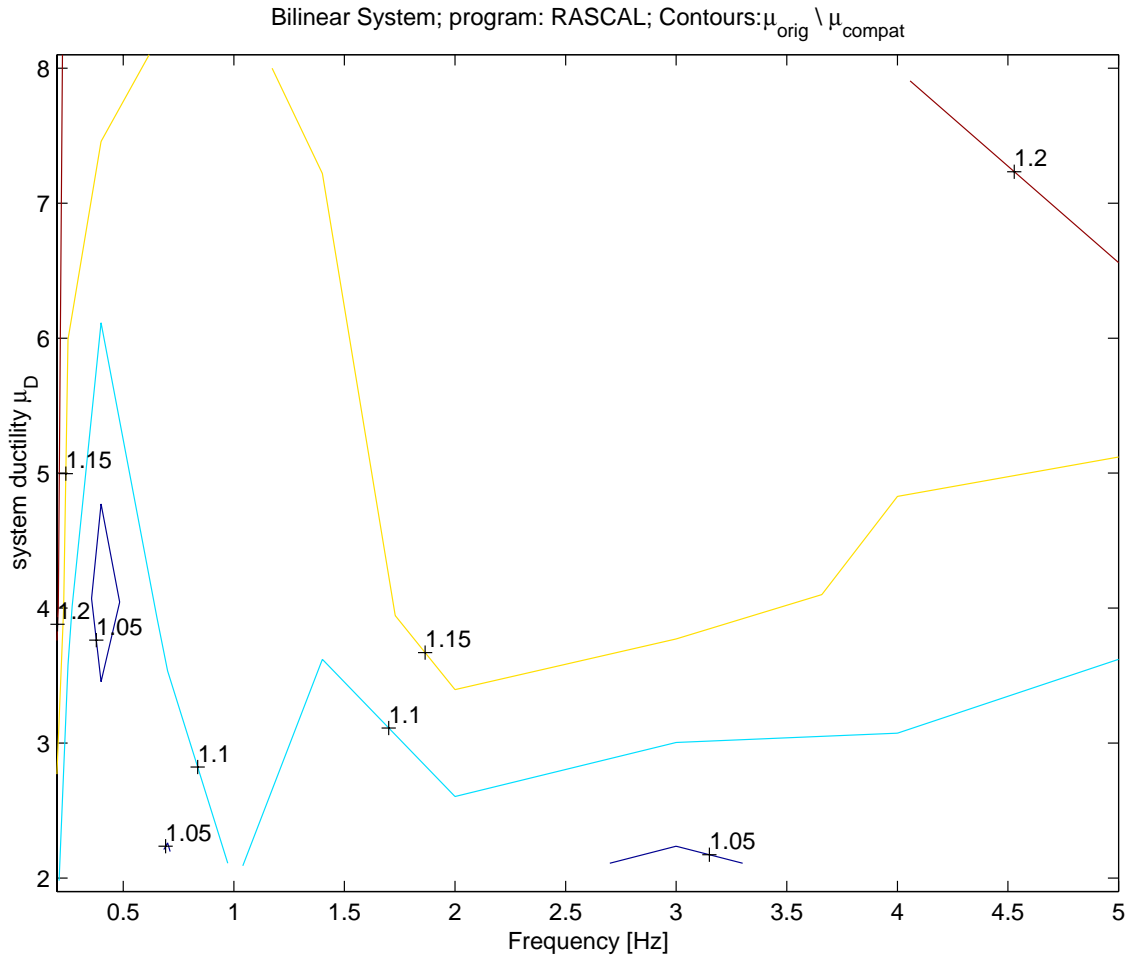
Figure 3.2a-i. Contour plot for ductility bias (ratio of original to compatibilized medians) for the bilinear hysteretic loop SDoF systems, 63 frequency-domain (RASCAL)-matched accelerograms. μ_D represents the *nominal* design level. Data taken from Table 3.2a.
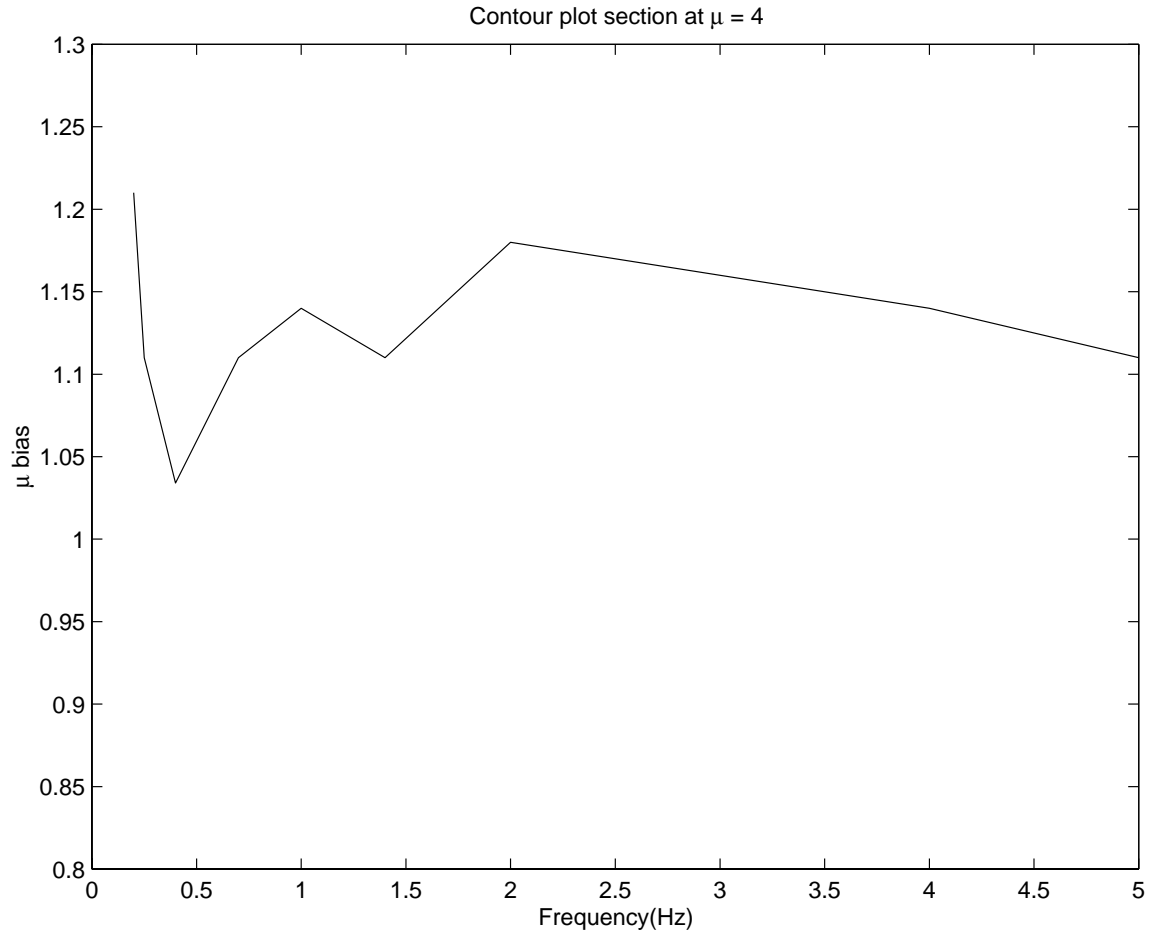
Figure 3.2a-ii. Section of Figure 3.2a-i at ductility $\mu = 4$. This slice represents the variation of *bias* observed for median ductility (ratio of original records' median ductility to spectrum matched records' median ductility).
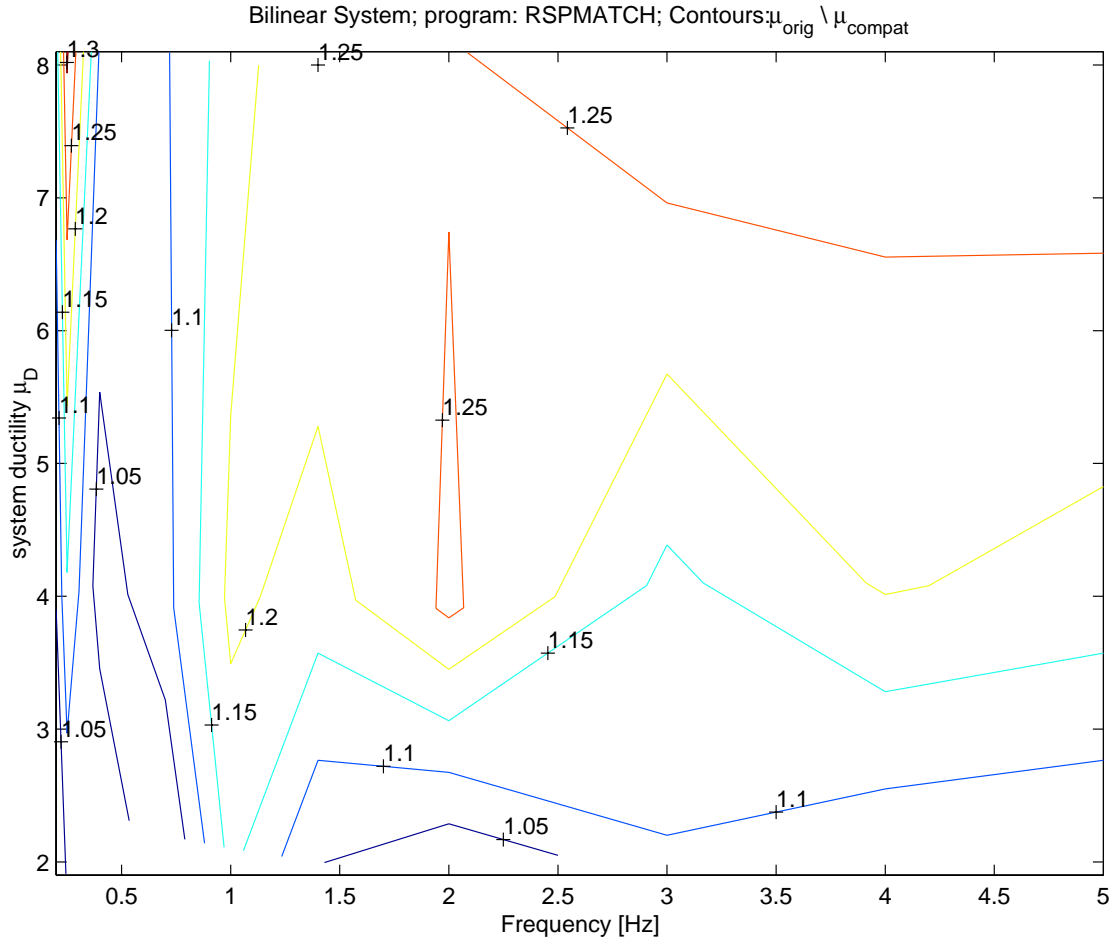
Figure 3.2b. Contour plot for ductility bias (ratio of original to compatibilized medians) for the bilinear hysteretic loop SDoF systems, 63 time-domain (RSPMATCH)-matched accelerograms. μ_D represents the *nominal* design level. Data taken from Table 3.2b.
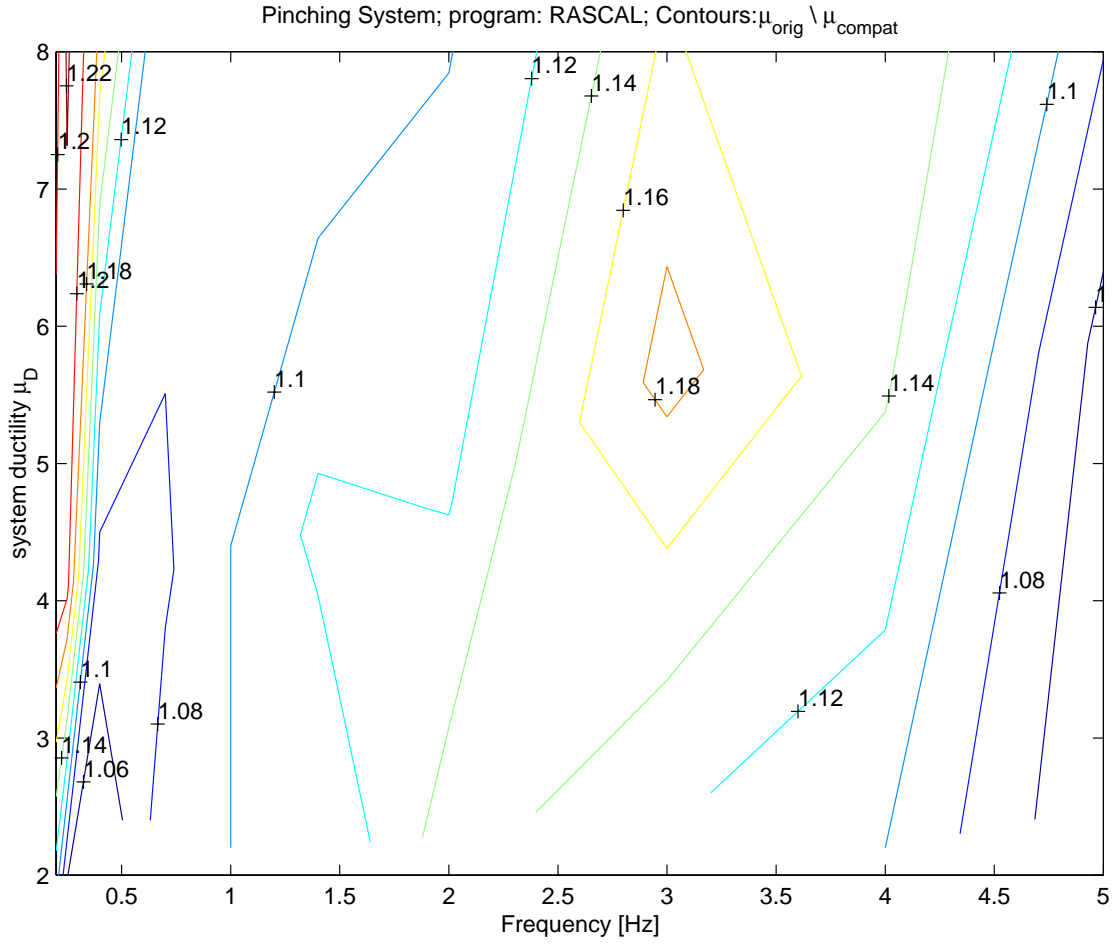
Figure 3.3a. Contour plot for ductility bias (ratio of original to compatibilized medians) for the pinching hysteretic loop SDoF systems, 63 frequency-domain (RASCAL)-matched accelerograms. μ_D represents the *nominal* design level. Data taken from Table 3.3a.
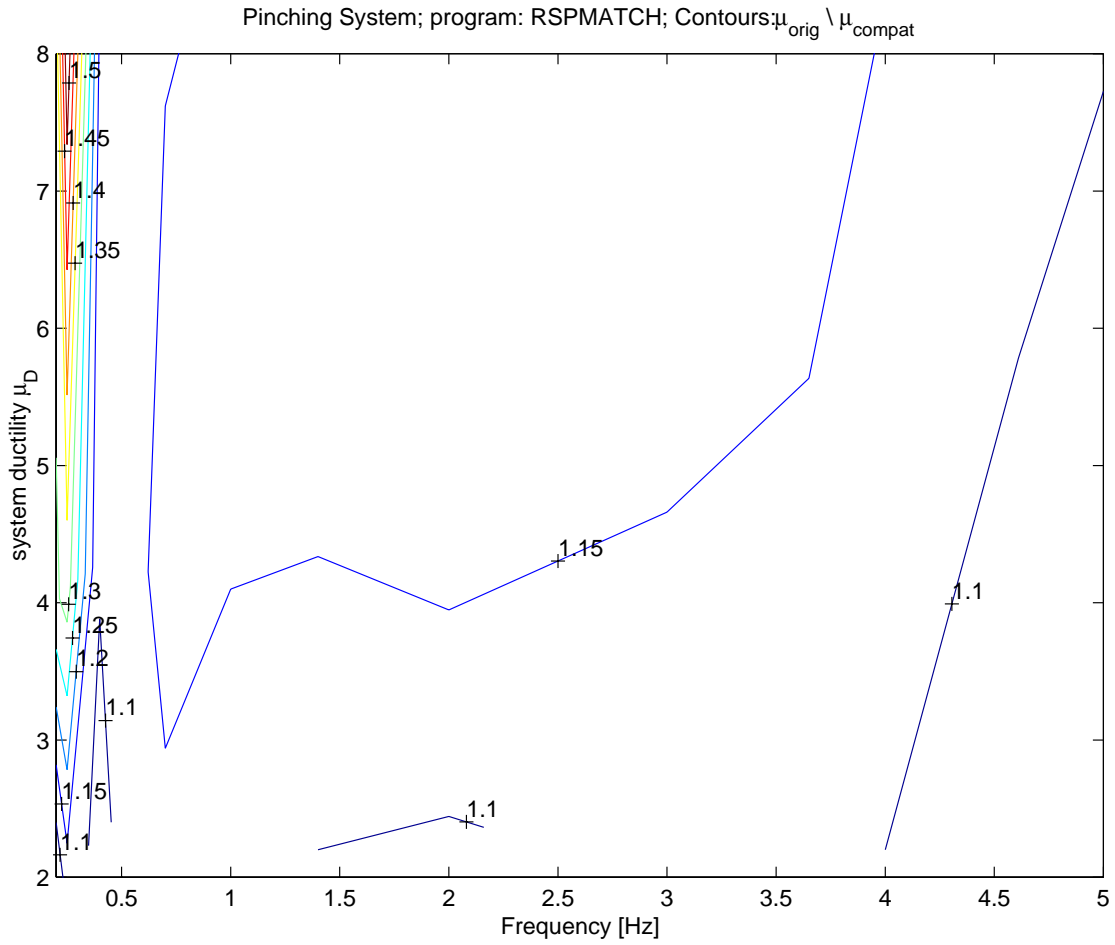
Figure 3.3b. Contour plot for ductility bias (ratio of original to compatibilized medians) for the pinching hysteretic loop SDoF systems, 63 time-domain (RSPMATCH)-matched accelerograms. μ_D represents the *nominal* design level. Data taken from Table 3.3b.
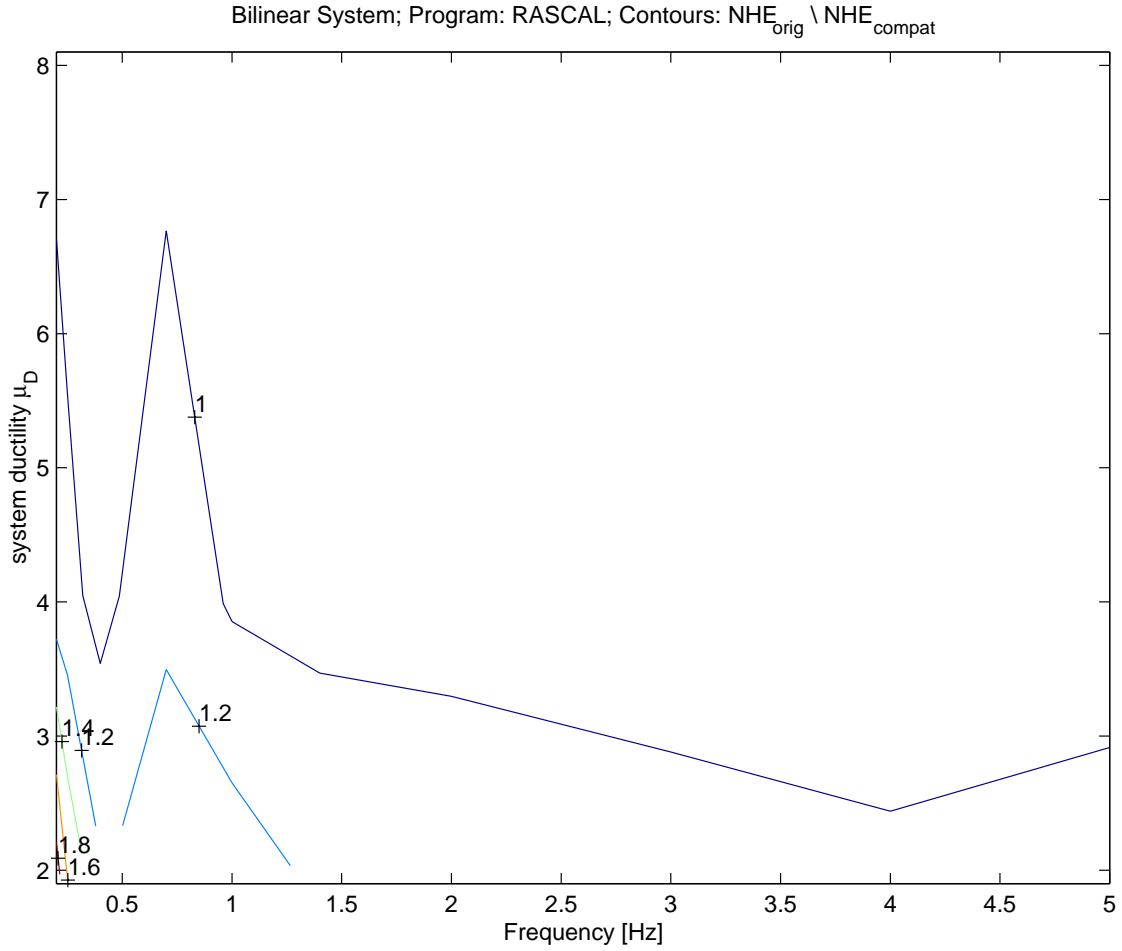
Figure 3.4a. Contour plot for normalized hysteretic energy bias (ratio of original to compatibilized medians) for the bilinear hysteretic loop SDoF systems, 63 frequency-domain (RASCAL)-matched accelerograms. μ_D represents the *nominal* design level. Data taken from Table 3.2a.
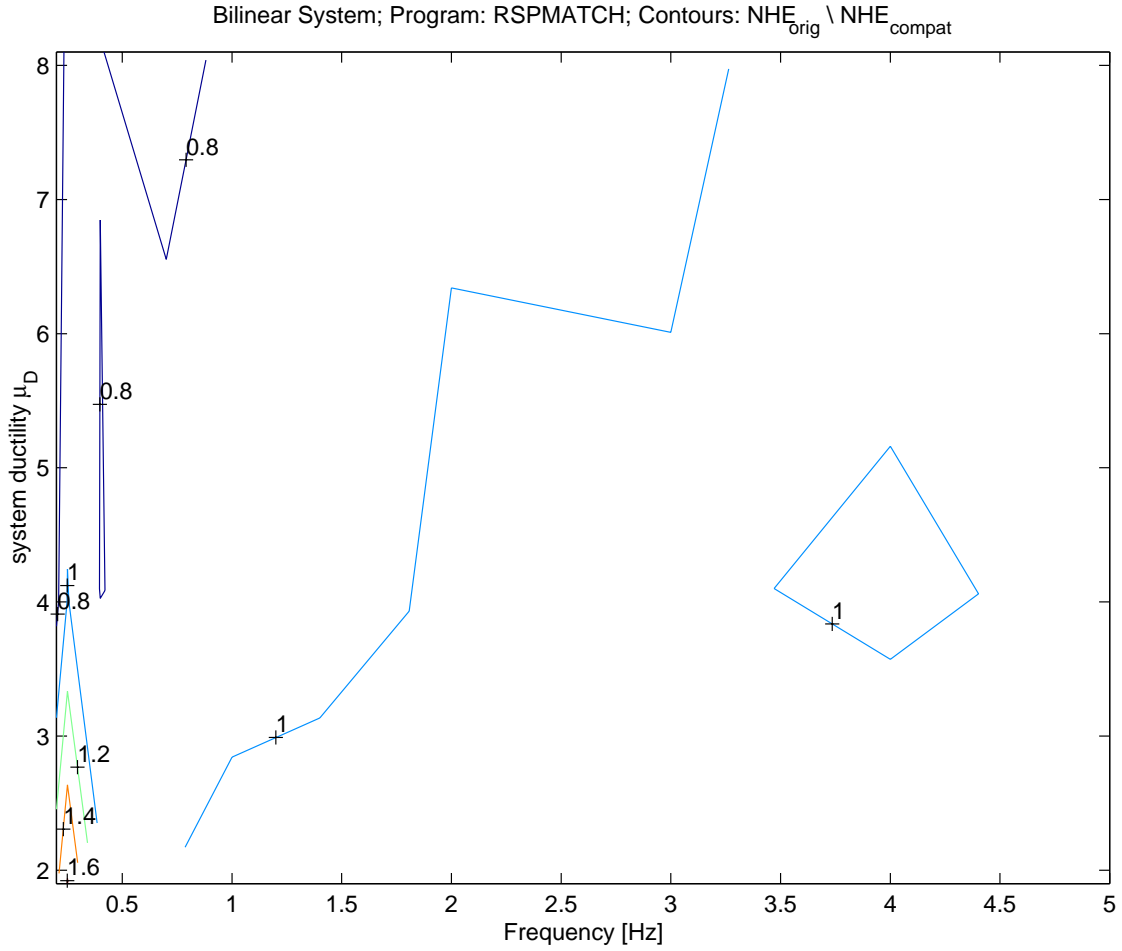
Figure 3.4b. Contour plot for normalized hysteretic energy bias (ratio of original to compatibilized medians) for the bilinear hysteretic loop SDoF systems, 63 time-domain (RSPMATCH)-matched accelerograms. μ_D represents the *nominal* design level. Data taken from Table 3.2b.
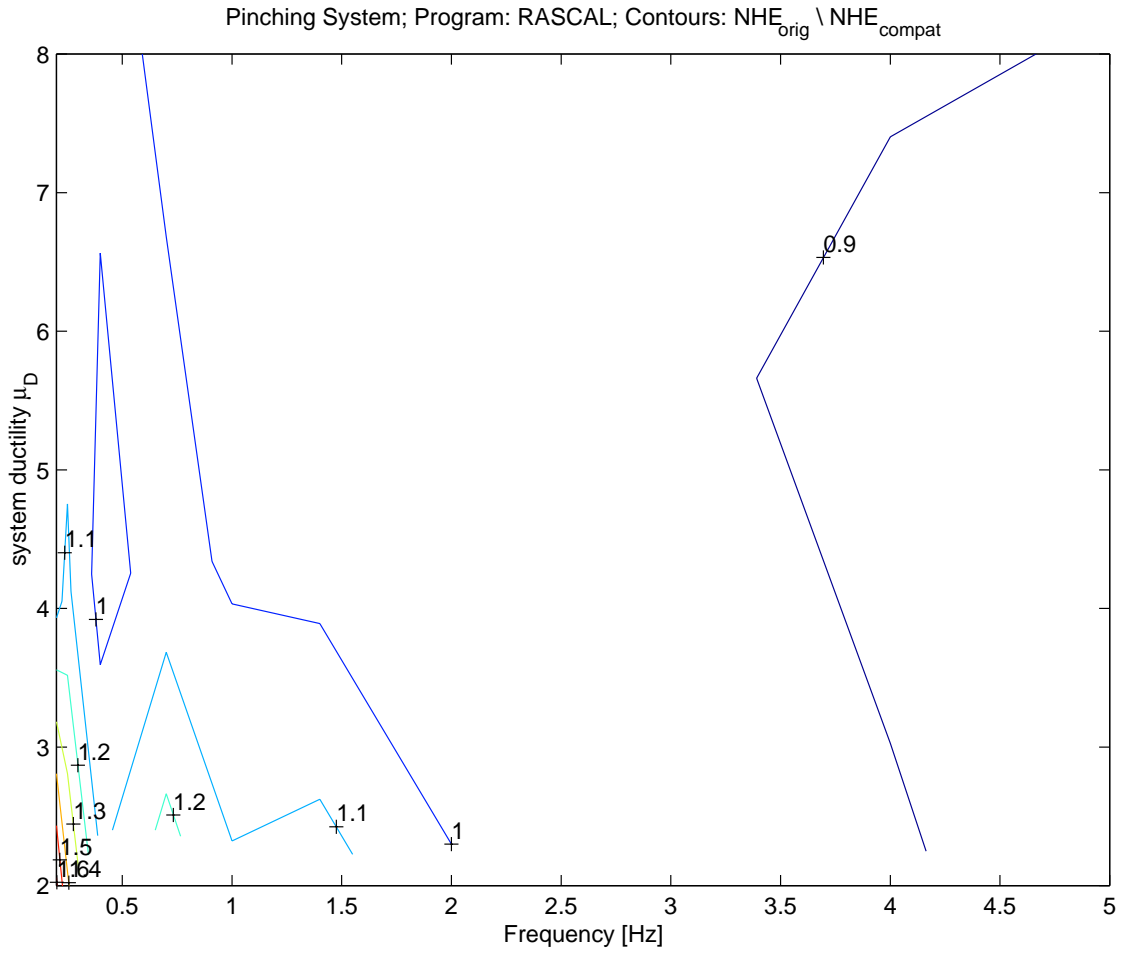
Figure 3.5a. Contour plot for normalized hysteretic energy bias (ratio of original to compatibilized medians) for the pinching hysteretic loop SDoF systems, 63 frequency-domain (RASCAL)-matched accelerograms. μ_D represents the *nominal* design level. Data taken from Table 3.3a.

Pinching System; Program: RSPMATCH; Contours: NHE$_{orig}$ \ NHE$_{compat}$
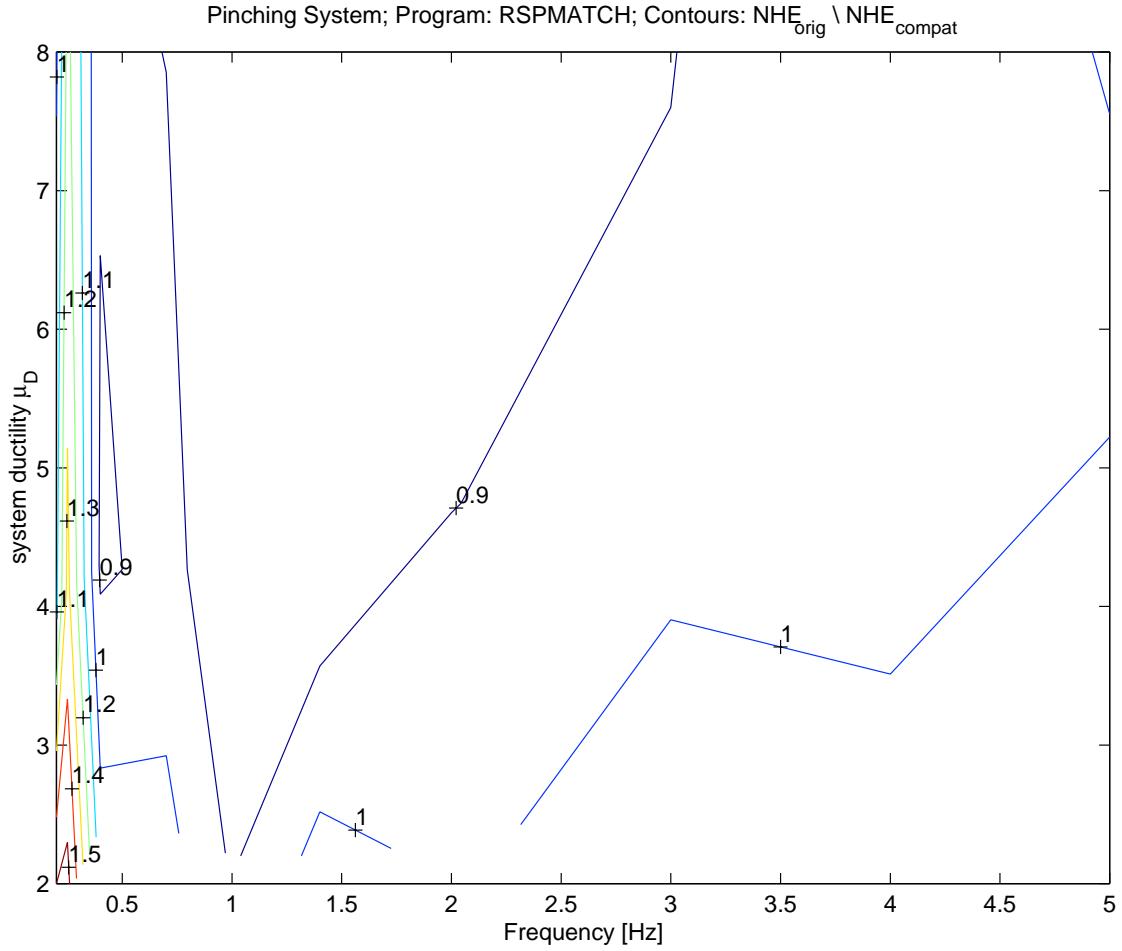
Figure 3.5b. Contour plot for normalized hysteretic energy bias (ratio of original to compatibilized medians) for the pinching hysteretic loop SDoF systems, 63 time-domain (RSPMATCH)-matched accelerograms. μ_D represents the *nominal* design level. Data taken from Table 3.3b.
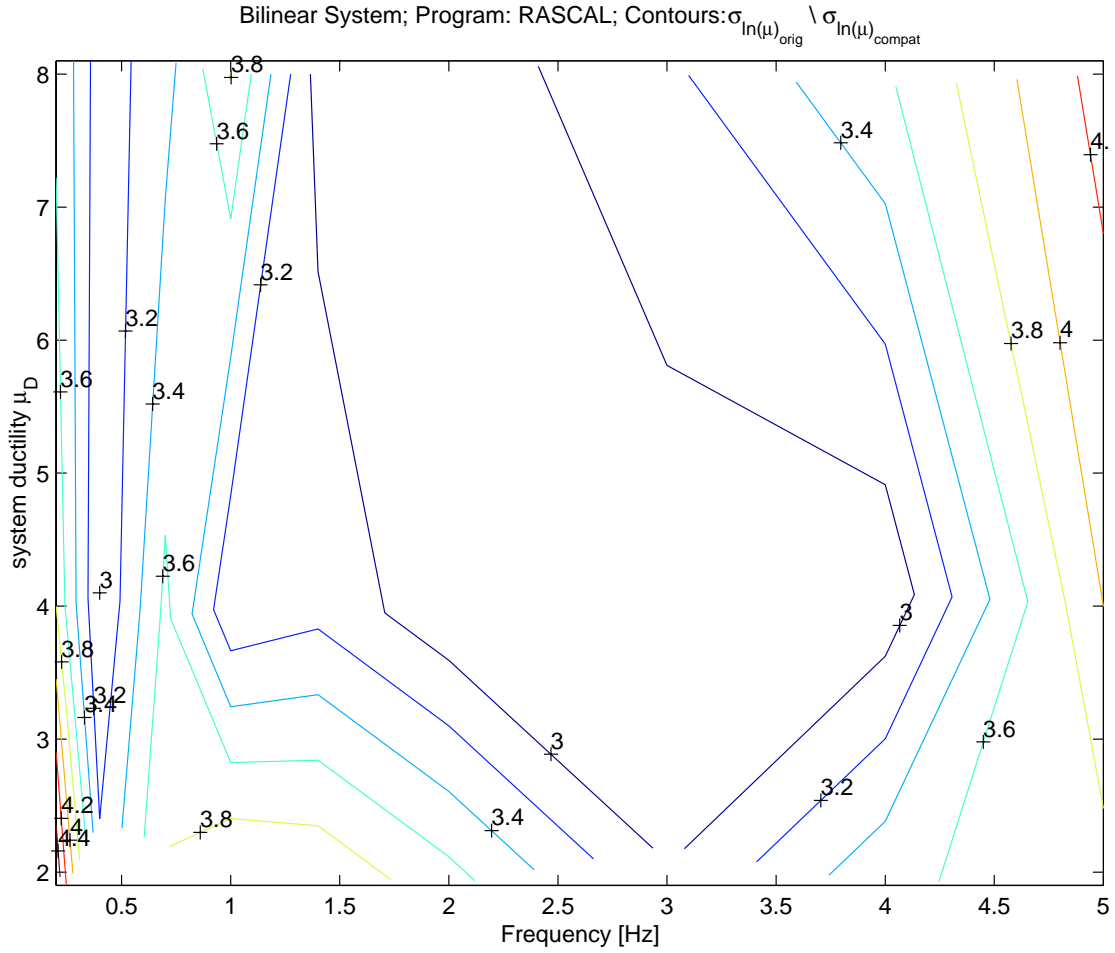
Figure 3.6a. Contour plot for the dispersion reduction ratios for ductilities (of original to compatibilized medians) for the bilinear hysteretic loop SDoF systems, 63 frequency-domain (RASCAL)-matched accelerograms. μ_D represents the *nominal* design level. Data taken from Table 3.2a.
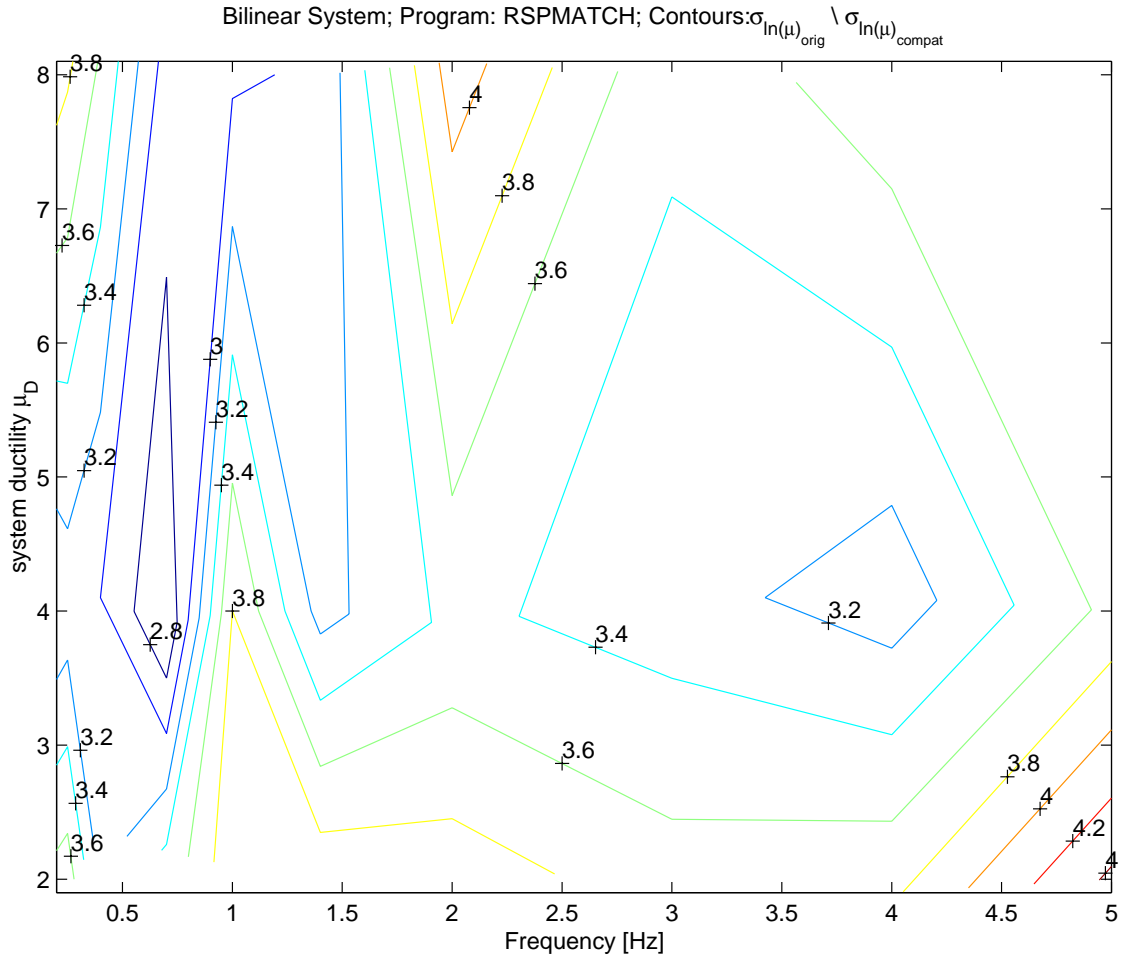
Figure 3.6b. Contour plot for the dispersion reduction ratios for ductilities (of original to compatibilized medians) for the bilinear hysteretic loop SDoF systems, 63 time-domain (RSPMATCH)-matched accelerograms. μ_D represents the *nominal* design level. Data taken from Table 3.2b.
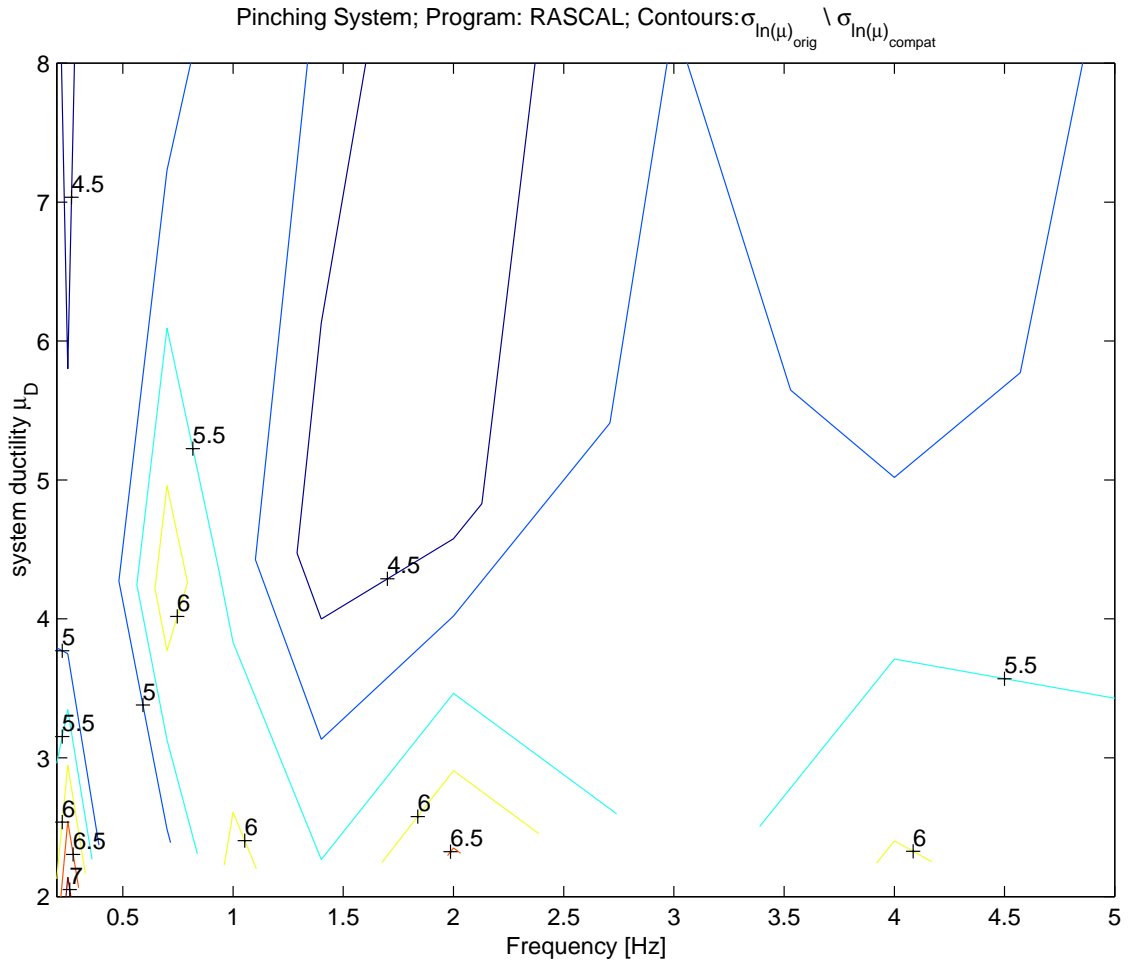
Figure 3.7a. Contour plot for the dispersion reduction ratios for ductilities (of original to compatibilized medians) for the pinching hysteretic loop SDoF systems, 63 frequency-domain (RASCAL)-matched accelerograms. μ_D represents the *nominal* design level. Data taken from Table 3.3a.
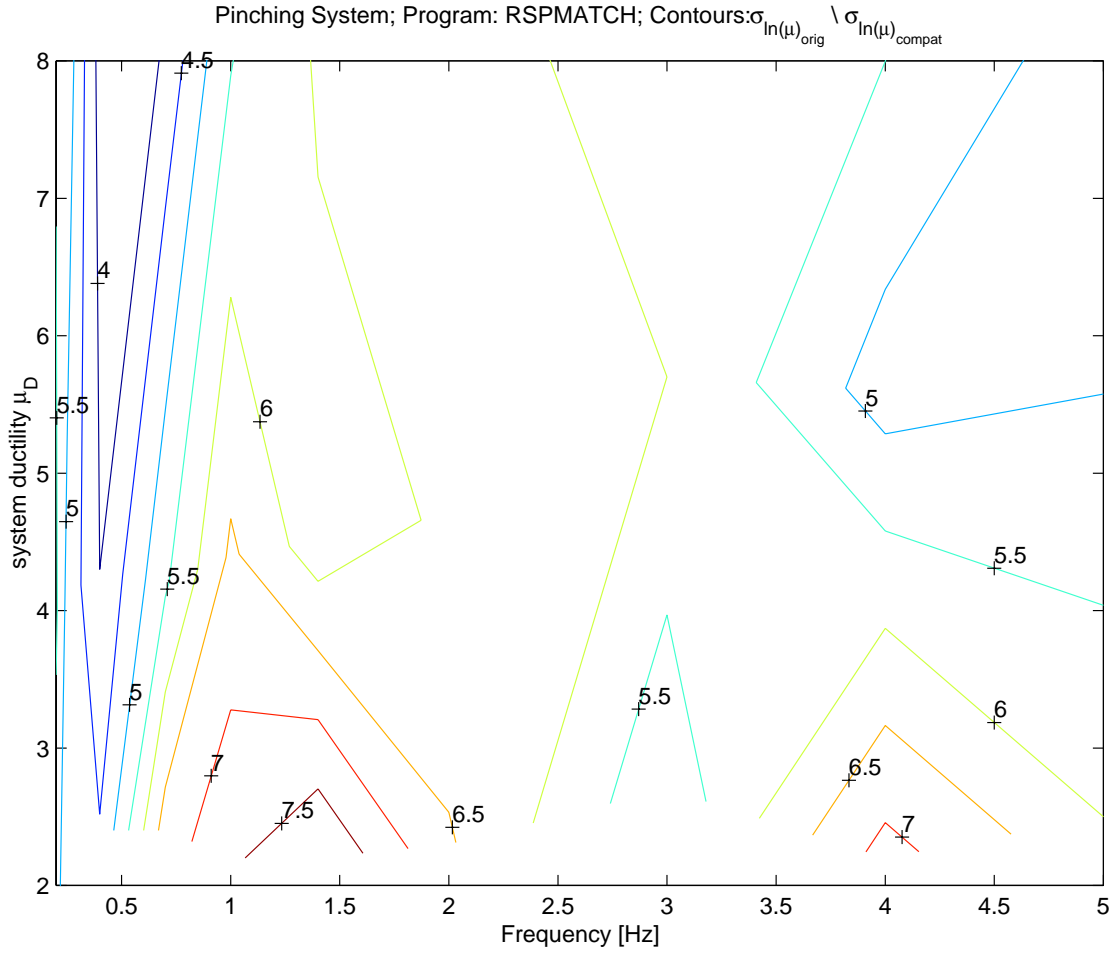
Figure 3.7b. Contour plot for the dispersion reduction ratios for ductilities (of original to compatibilized medians) for the pinching hysteretic loop SDoF systems, 63 time-domain (RSPMATCH)-matched accelerograms. μ_D represents the *nominal* design level. Data taken from Table 3.3b.
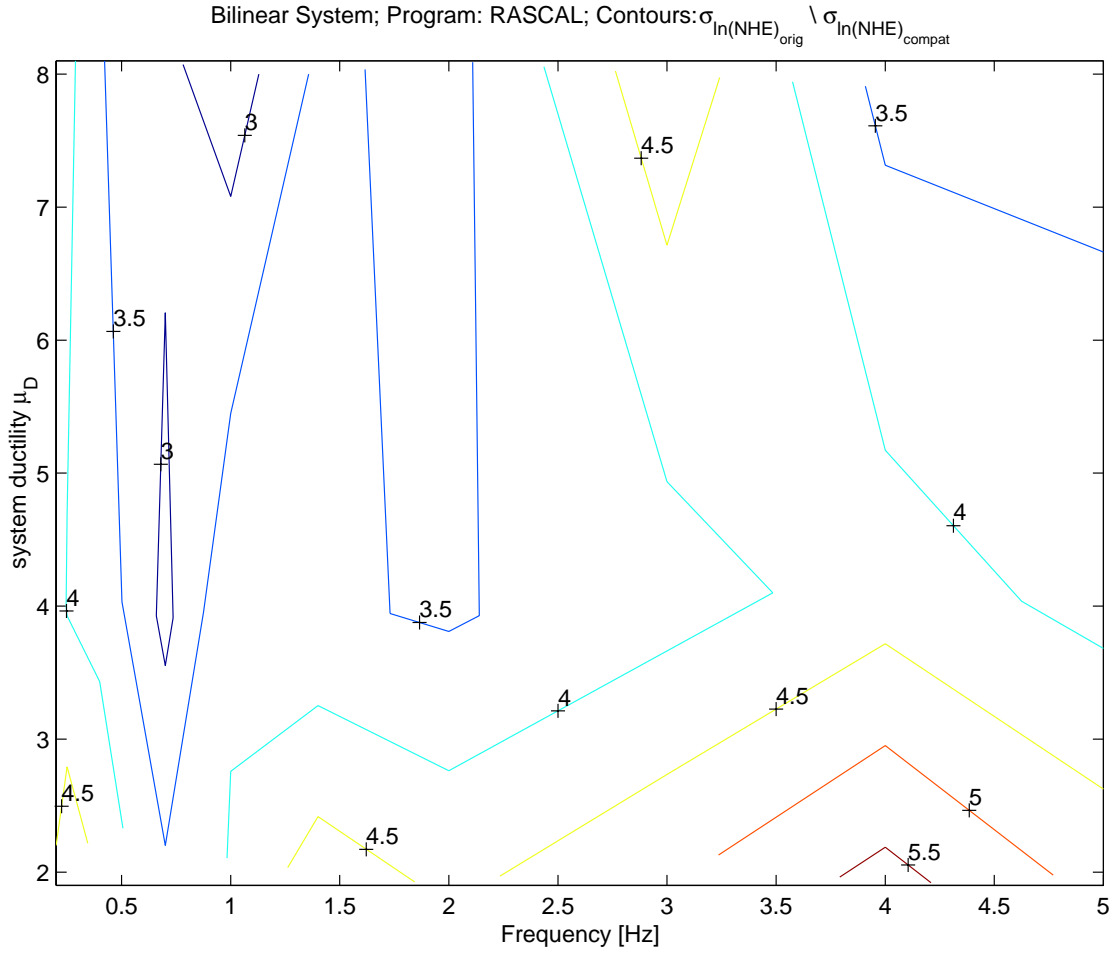
Figure 3.8a. Contour plot for the dispersion reduction ratios for normalized hysteretic energies (of original to compatibilized medians) for the bilinear hysteretic loop SDoF systems, 63 frequency-domain (RASCAL)-matched accelerograms. μ_D represents the *nominal* design level. Data taken from Table 3.2a.
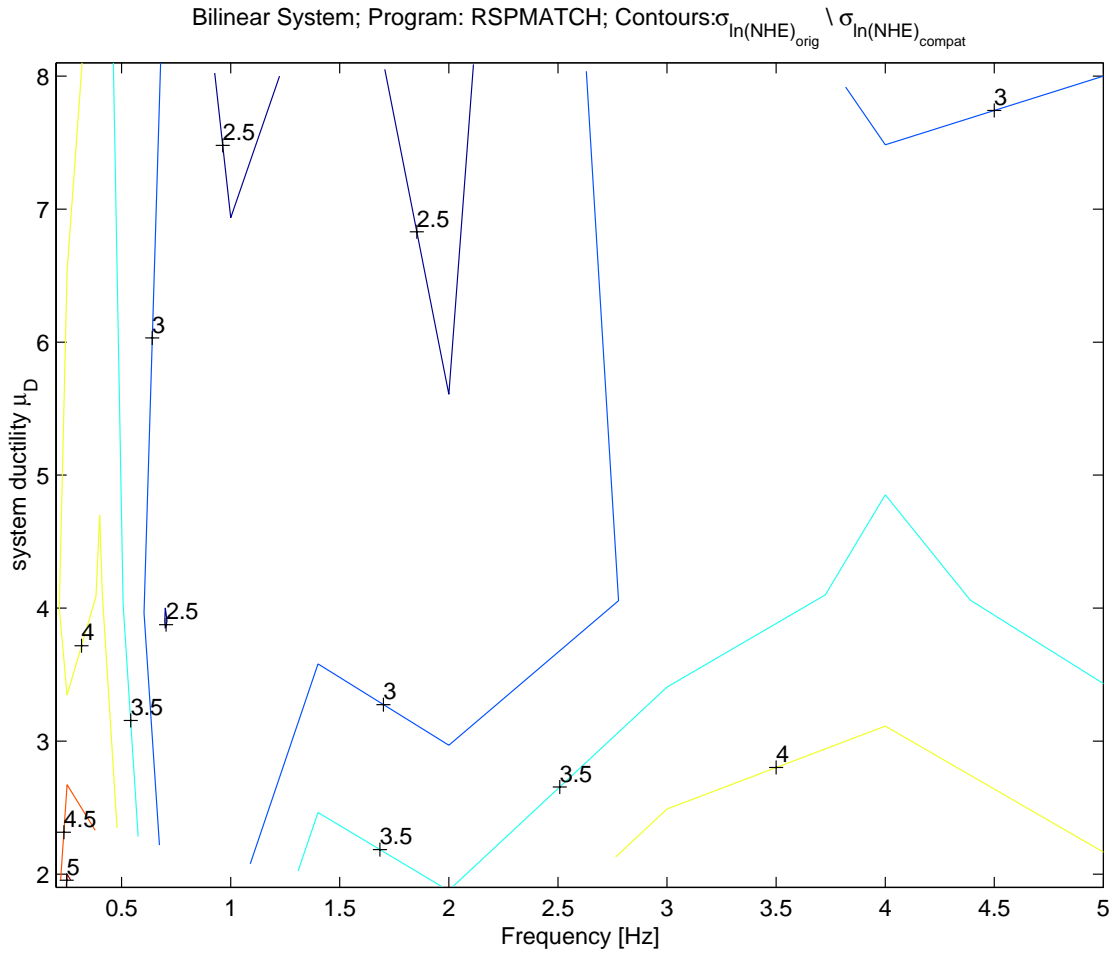
Figure 3.8b. Contour plot for the dispersion reduction ratios for normalized hysteretic energies (of original to compatibilized medians) for the bilinear hysteretic loop SDoF systems, 63 time-domain (RSPMATCH)-matched accelerograms. μ_D represents the *nominal* design level. Data taken from Table 3.2b.
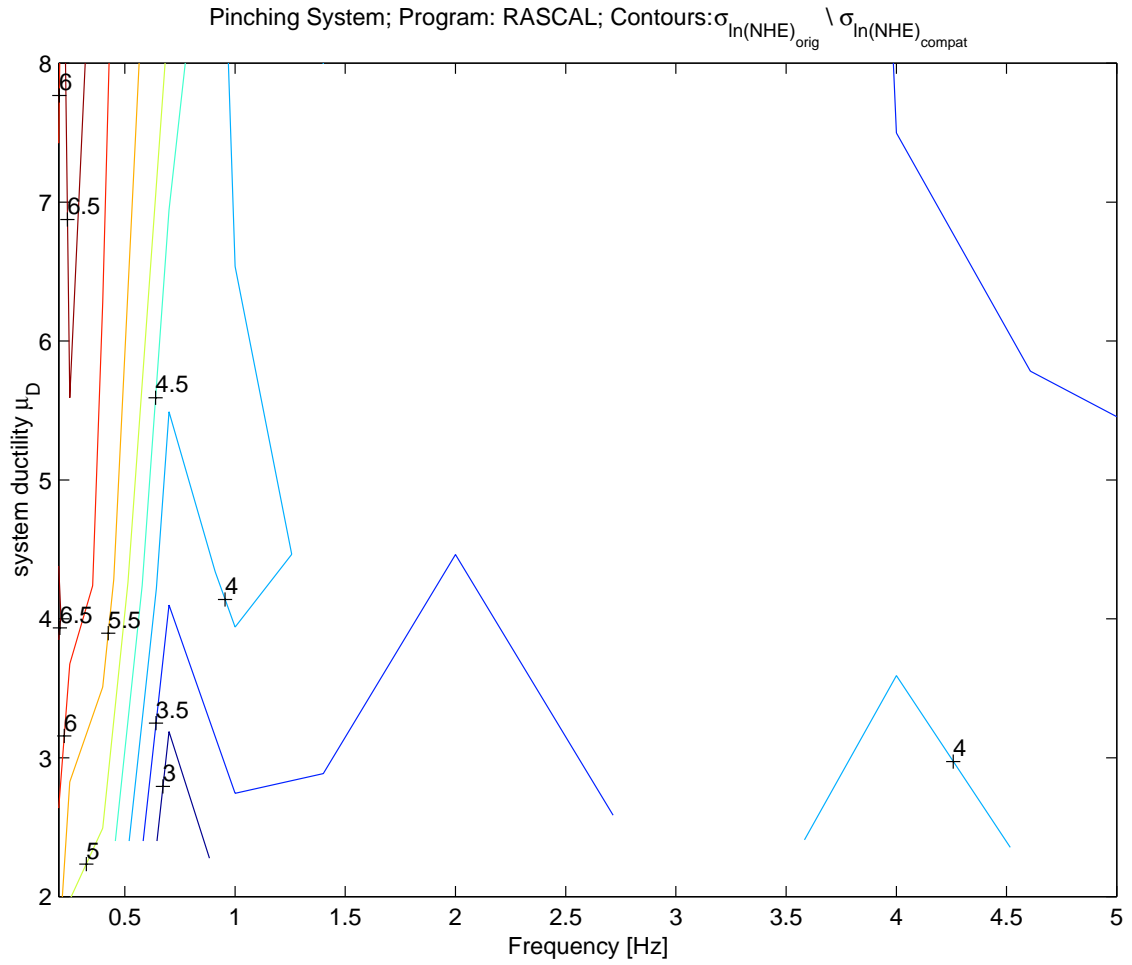
Figure 3.9a. Contour plot for the dispersion reduction ratios for normalized hysteretic energies (of original to compatibilized medians) for the pinching hysteretic loop SDoF systems, 63 frequency-domain (RASCAL)-matched accelerograms. μ_D represents the *nominal* design level. Data taken from Table 3.3a.
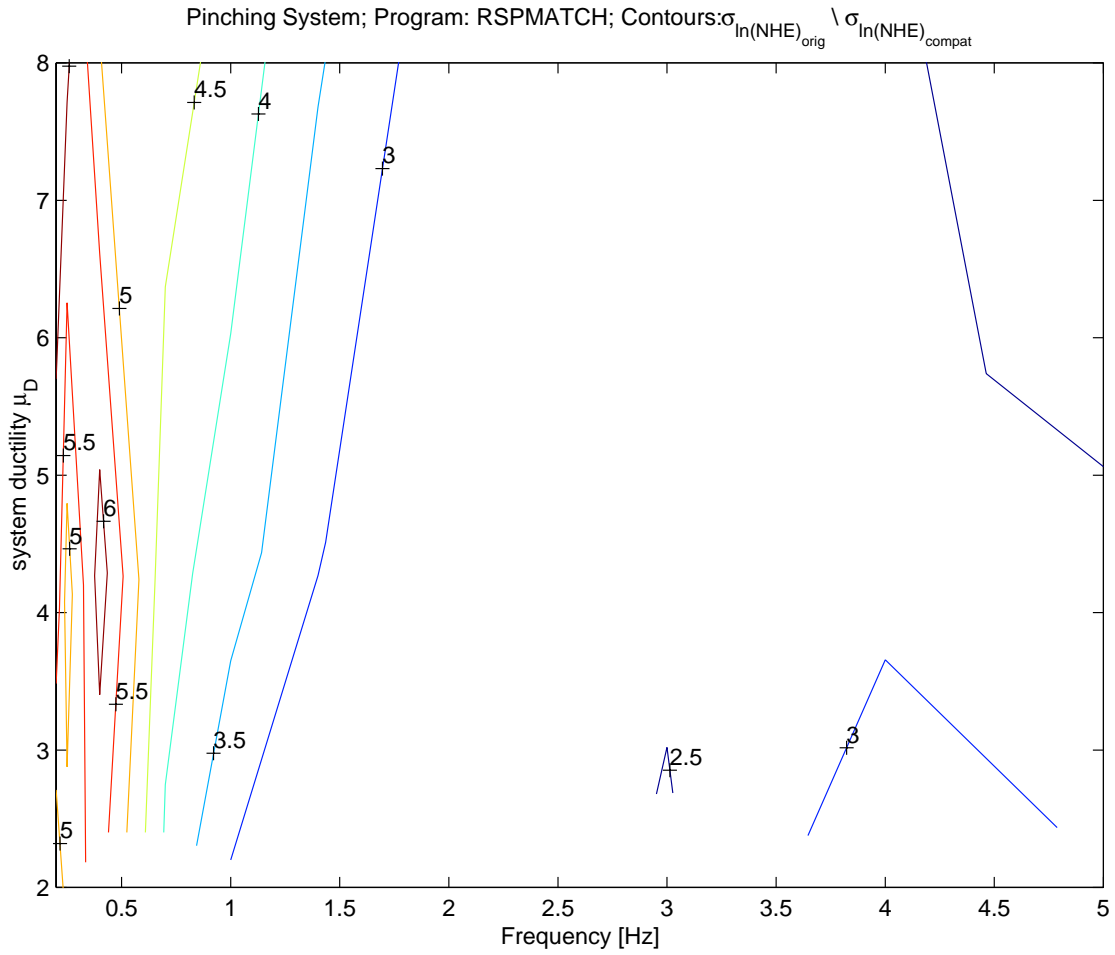
Figure 3.9b. Contour plot for the dispersion reduction ratios for normalized hysteretic energies (of original to compatibilized medians) for the pinching hysteretic loop SDoF systems, 63 time-domain (RSPMATCH)-matched accelerograms. μ_D represents the *nominal* design level. Data taken from Table 3.3b.
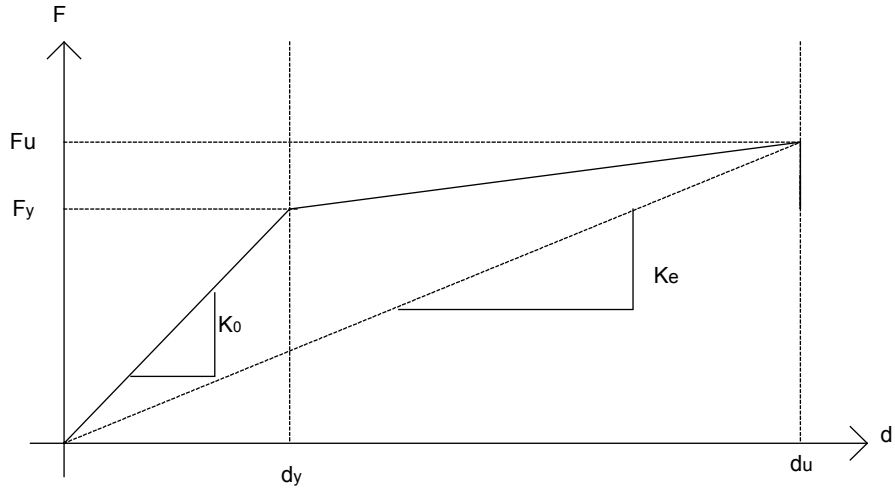
Figure 3.10. The concept of *effective stiffness* is computed based on the nonlinear displacement d_u, and the force that causes it, F_u. The corresponding *effective period* is computed with this value of stiffness: $T_e = (m / K_e)^{1/2}$
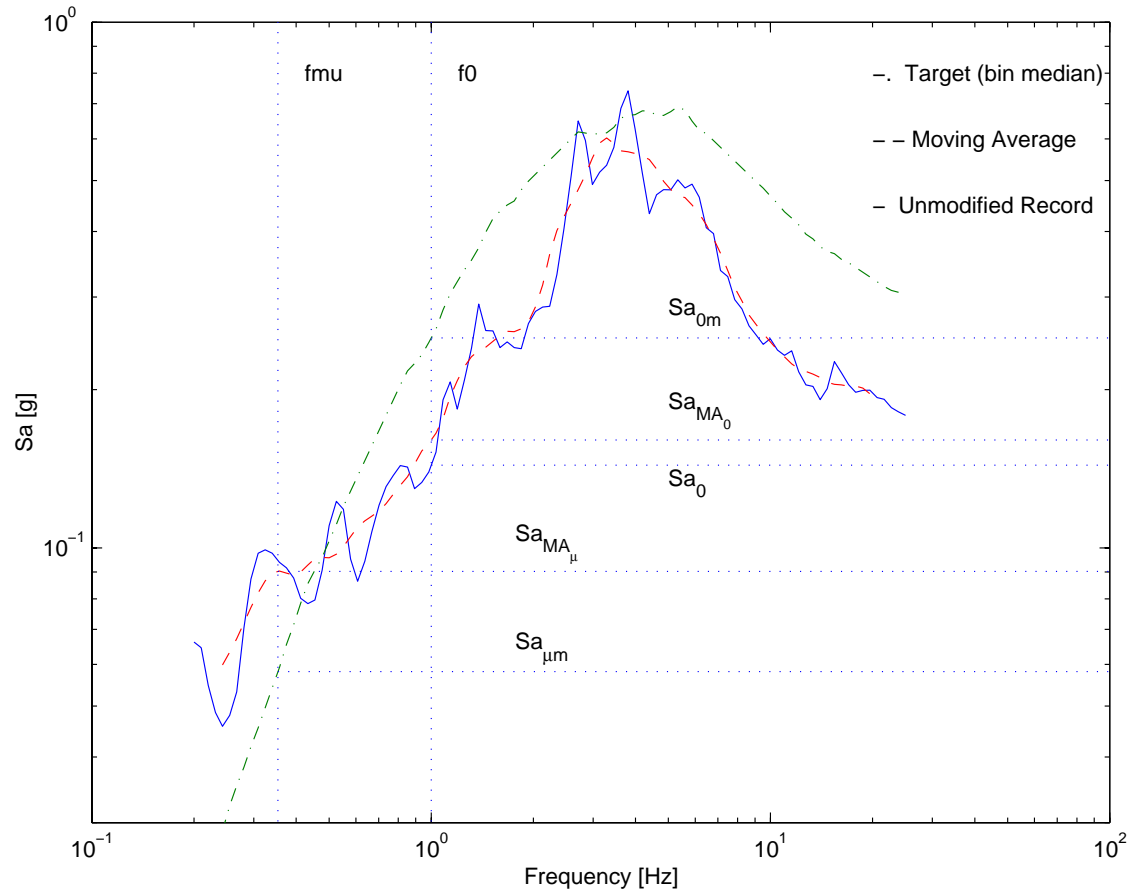
Figure 3.11. Parameters for computing shape and intensity effects. For $f_0 = 1$Hz, and $\mu = 8$, $f_\mu = 0.35$Hz. For this particular record, relative to unity, the ratios are: $R_{GS\mu} > 1$ (*global shape* ratio); $R_{LS} < 1$ (*local shape* ratio. At f_0, the spectral acceleration is at a "valley", although it still decreases a little before increasing again with lower frequencies). Also, $R_{SaMA0} < 1$ (*intensity* ratio).
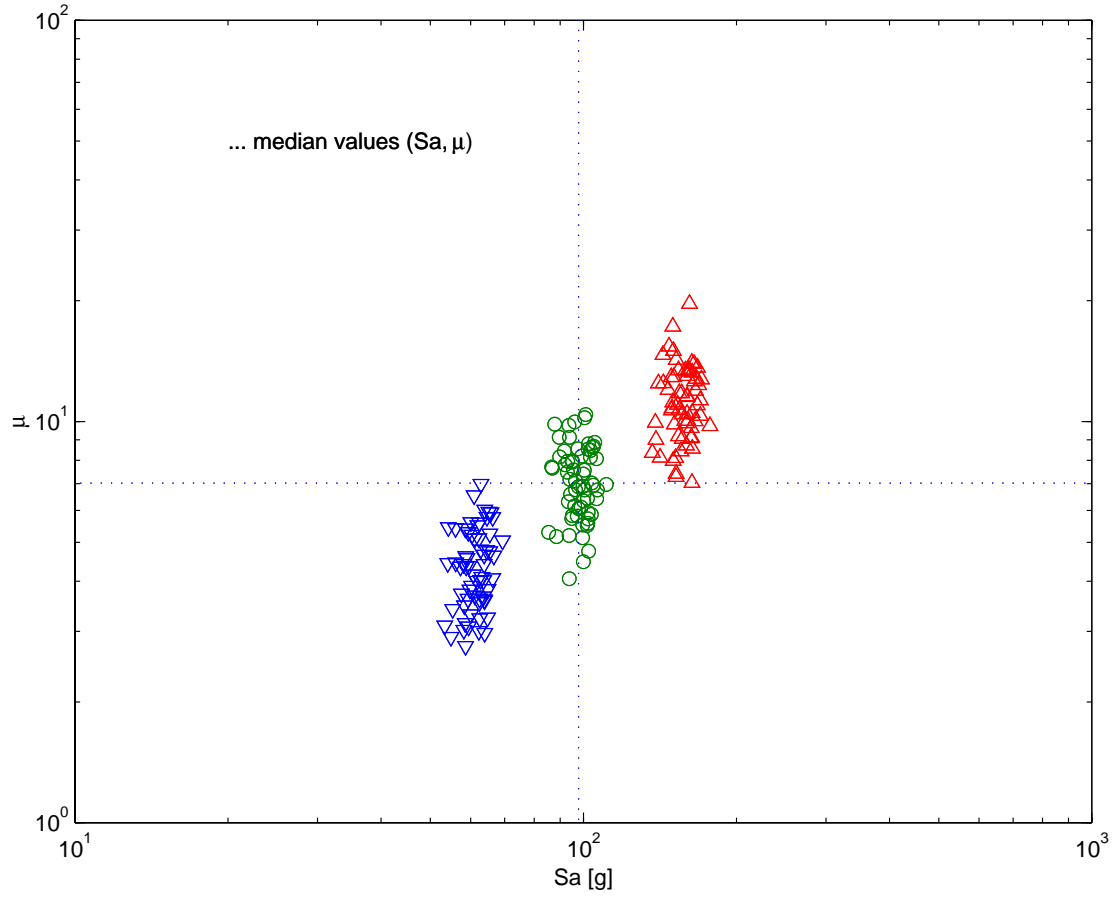
Figure 3.12 Isolated intensity effects. The effect of scaling (i.e., either multiplying or dividing) the records by the same factor causes the same relative effect. For this case, the "same effect" was that of either increasing or decreasing by around 0.5 the value of $\ln(R_{\mu c})$. The control set is the middle "cloud". The system analyzed is the nominal ductility $\mu_D = 8$, SDoF bilinear 1Hz system.
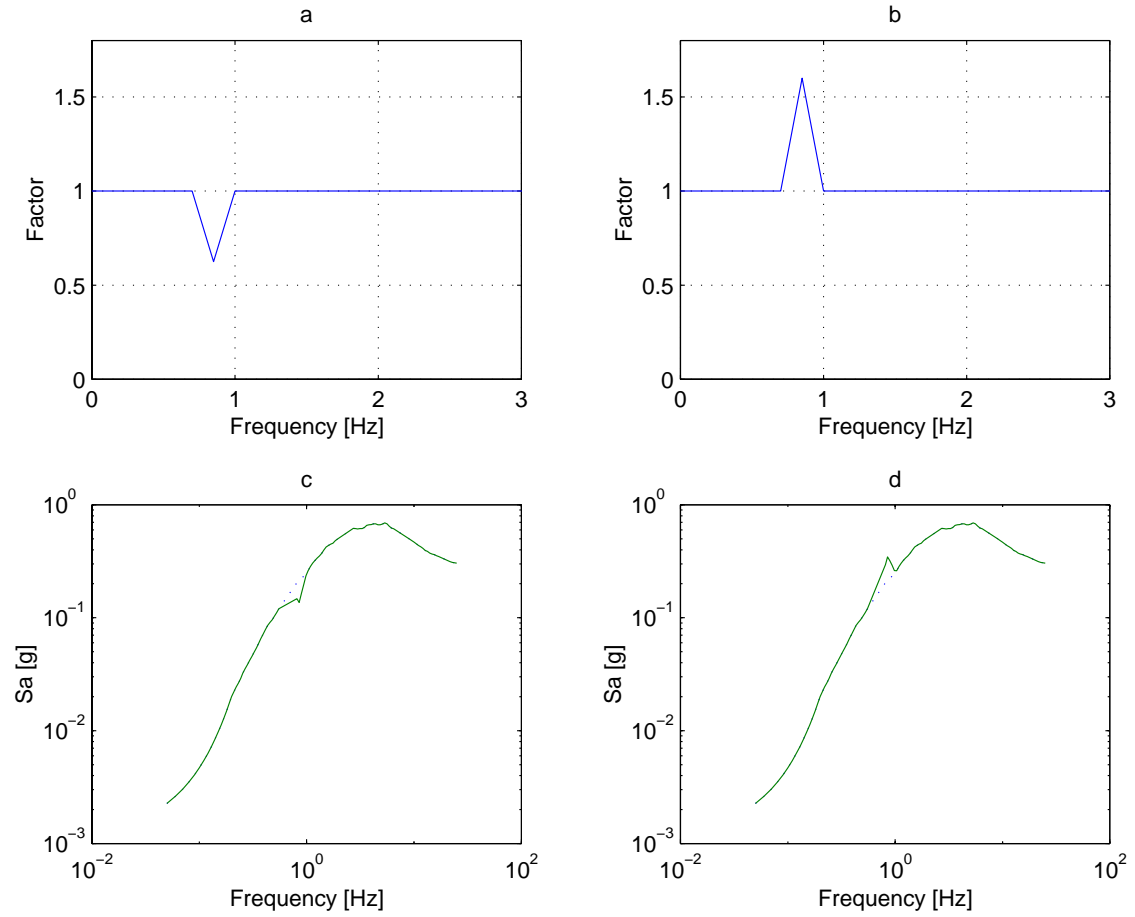
Figure 3.13. a) Factor function for decreasing (in the direction of "softening", i.e., lower frequencies) spectral accelerations. The maximum value is at 1.6, at 0.85Hz (the base of the triangular factor function is 0.3 Hz). b) Factor function for increasing spectral accelerations. The minimum factor is $1/1.6 = 0.625$, at 0.85Hz. . c) Modified target with factor function from a). d) Modified target with factor function from b).
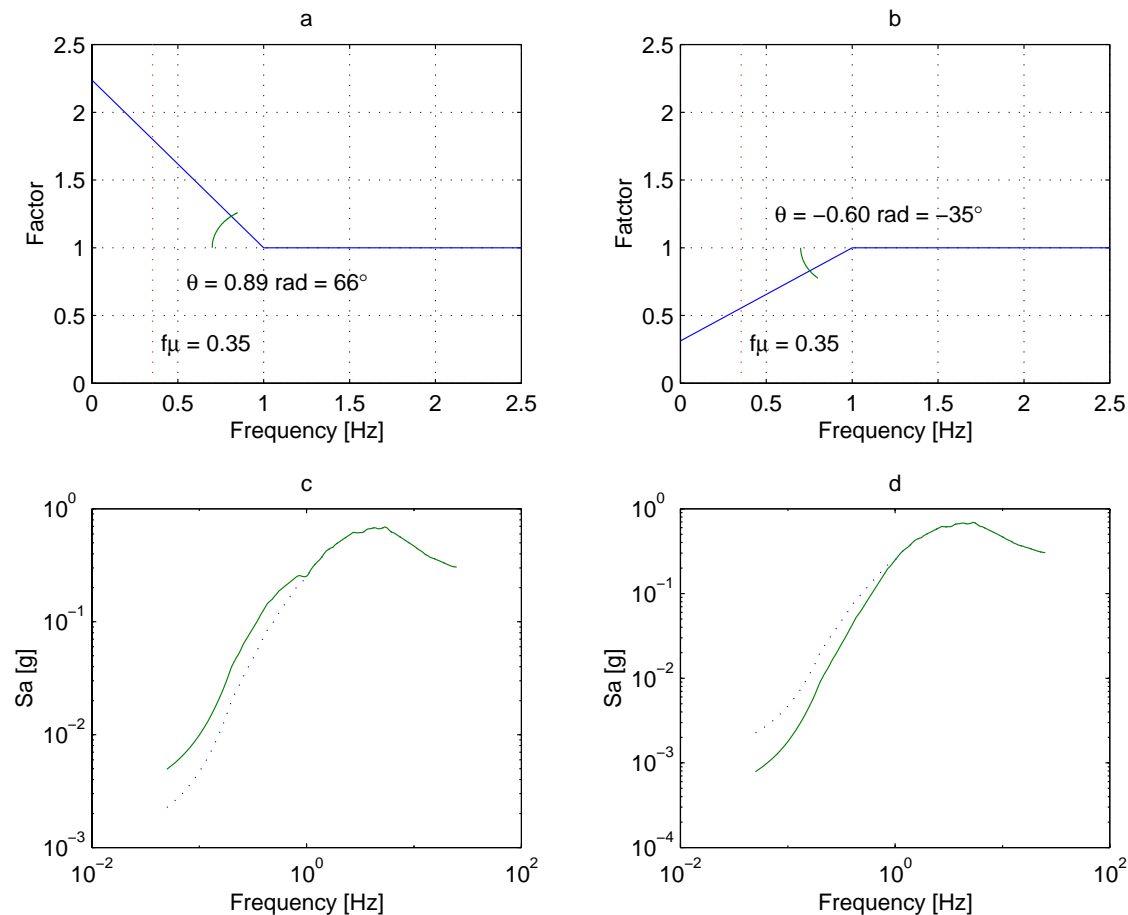
Figure 3.14. *Factor Functions* for the study of isolated *global-shape* effect. These consider linear variations of the factor, starting at unity for the elastic frequency (in this case, f_0 = 1Hz), in the direction of softening. The construction of these factor functions is such that at the softened effective frequency, considered here at 0.35Hz, the value of the factor ($FF(f_\mu)$) is equal to the global shape ratio to be tested ($R_{GS\mu c}$). a) $FF(f_\mu) = FF(0.35Hz) = R_{GS\mu c} = 1.8$; b) $FF(f_\mu) = R_{GS\mu c} = 1/1.8$. In logarithmic terms, these ratios have the same absolute values. c) Modified target with factor function from a); d) modified target with factor function from b). In section 3.7.1 the angle θ will also be used to characterize such factor functions.
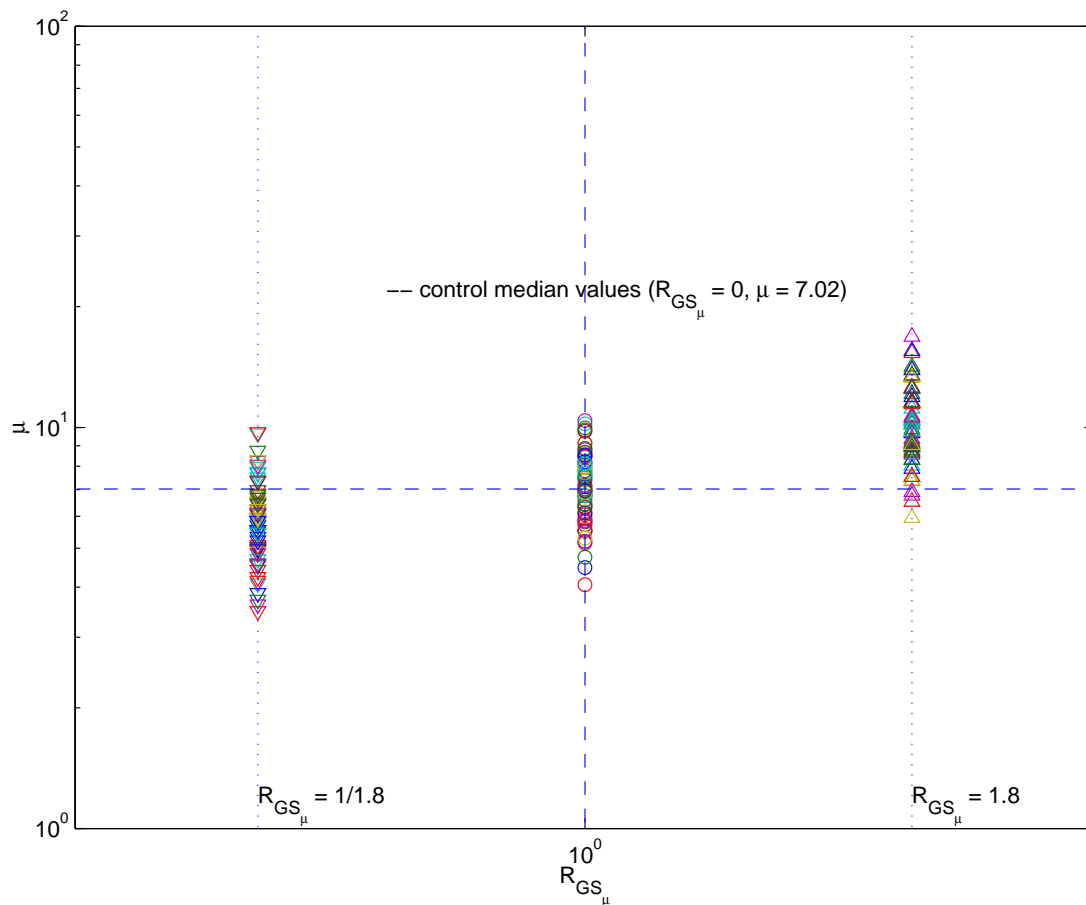
Figure 3.15. Isolated *global-shape* effects. The sought-after asymmetry can be seen by the difference in relative "distances" of the different "clouds" to the control case (the middle "cloud"). The cloud on the right-hand-side corresponds to $R_{GS\mu c} = 1.8$, whereas the left-hand-side cloud corresponds to $R_{GS\mu\ c} = 1/1.8$. The regression returns the value of the slopes (i.e., the value of a_2^+ and a_2^-) of the lines passing through the median values of the clouds; the slope is higher for the above-unit $R_{GS\mu c}$ (right-hand-side "cloud").
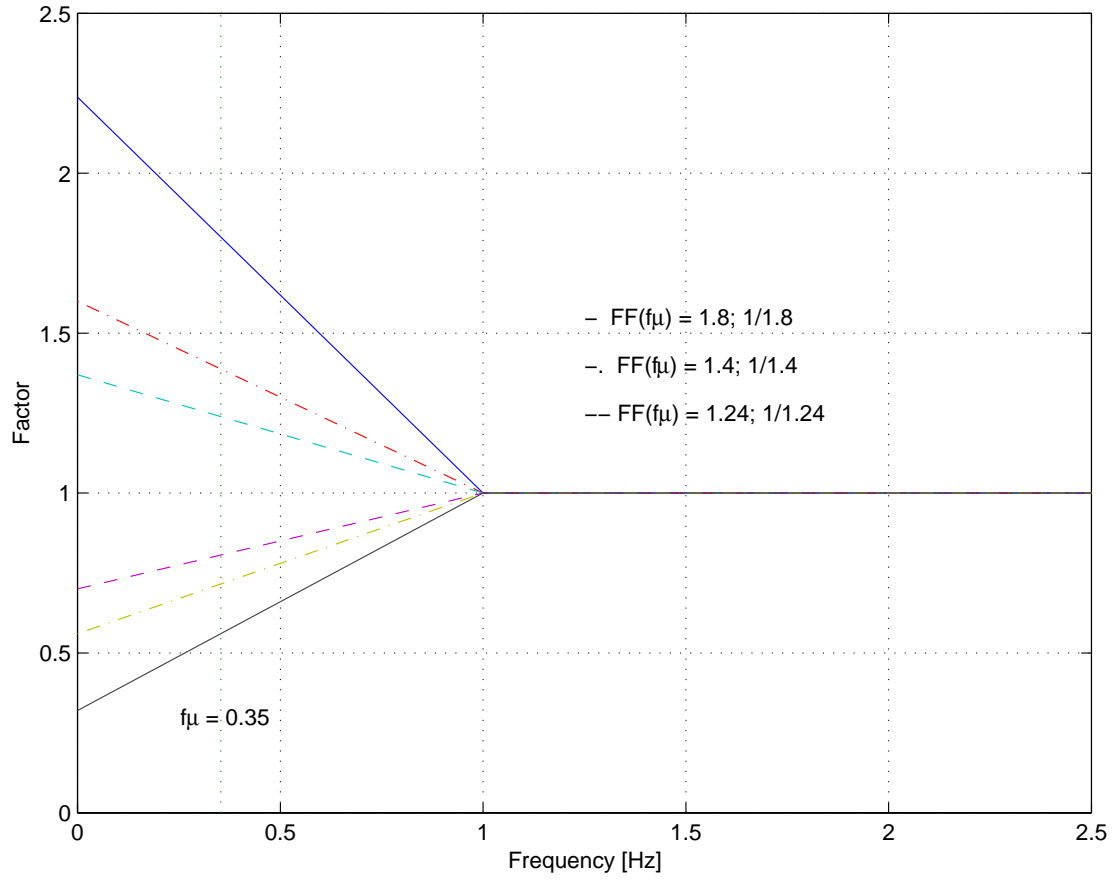
Figure 3.16 New factor functions considered for the parametric study of $R_{\mu c}$ vs. $R_{GS\mu c}$. The value of the factor function at $f_\mu = f_0 / (\mu_D)^{1/2} = 0.35$Hz is equal to the values of $R_{GS\mu c}$ that were considered (i.e., 1.24, 1.4, 1.8, and their reciprocals). The corresponding angles are $\theta = \{0.89, 0.55, 0.35, -0.29, -0.44, -0.60\}$rad.
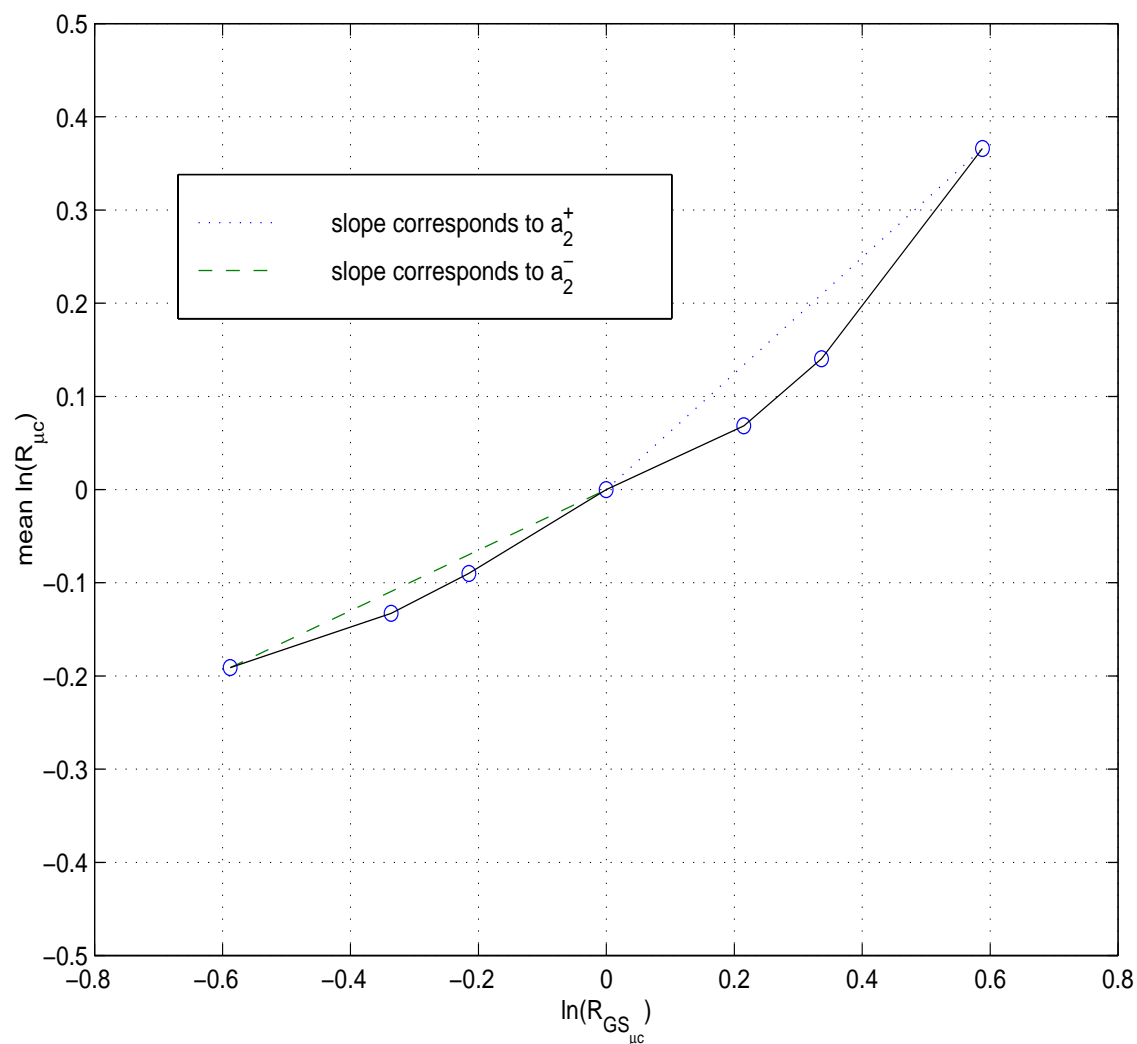
Figure 3.17. Variation of mean $\ln(R_{\mu c})$ at different values of $\ln(R_{GS\mu c}) = \ln(FF(f_\mu))$. The single-parameter regression coefficients a_2^+ and a_2^- correspond to the ratio: $avg(\ln(R_{GS\mu c}))$ / $\ln(R_{\mu c})$ at each of the points computed, and hence to the slope of the secant line. Shown dotted/dashed are the secant lines corresponding to the highest and lowest global-shape ratio of $R_{GS\mu c} = 1.8$, $1/1.8$ (which yield $a_2^+ = 0.623$ for $R_{GS\mu c} = 1.8$ and $a_2^- = 0.325$ for $R_{GS\mu c} = 1/1.8$ (see Table 3.20)). The system analyzed corresponds to the low-resistance 1Hz SDoF oscillator.
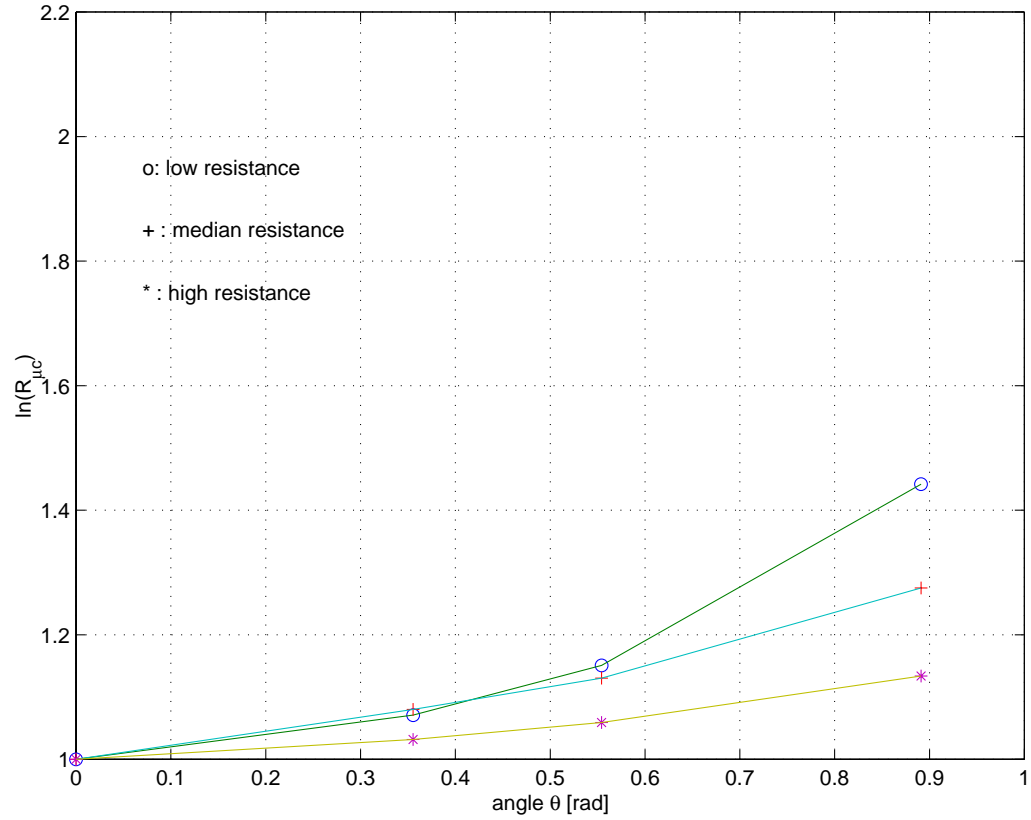
Figure 3.18. Correction-angle curves for the SDoF 1hz systems (low, medium and high resistance). The corresponding ductilities for the uncorrected spectrum matched records were 7.02, 3.5, and 1.9 respectively. The vertical axis corresponds to the value of $\ln(R_{\mu c})$, the log ratio of the median ductility produced by the modified shape compatibilized records, to the median ductility produced by the original shape (bin median spectral shape target) set of compatibilized records.
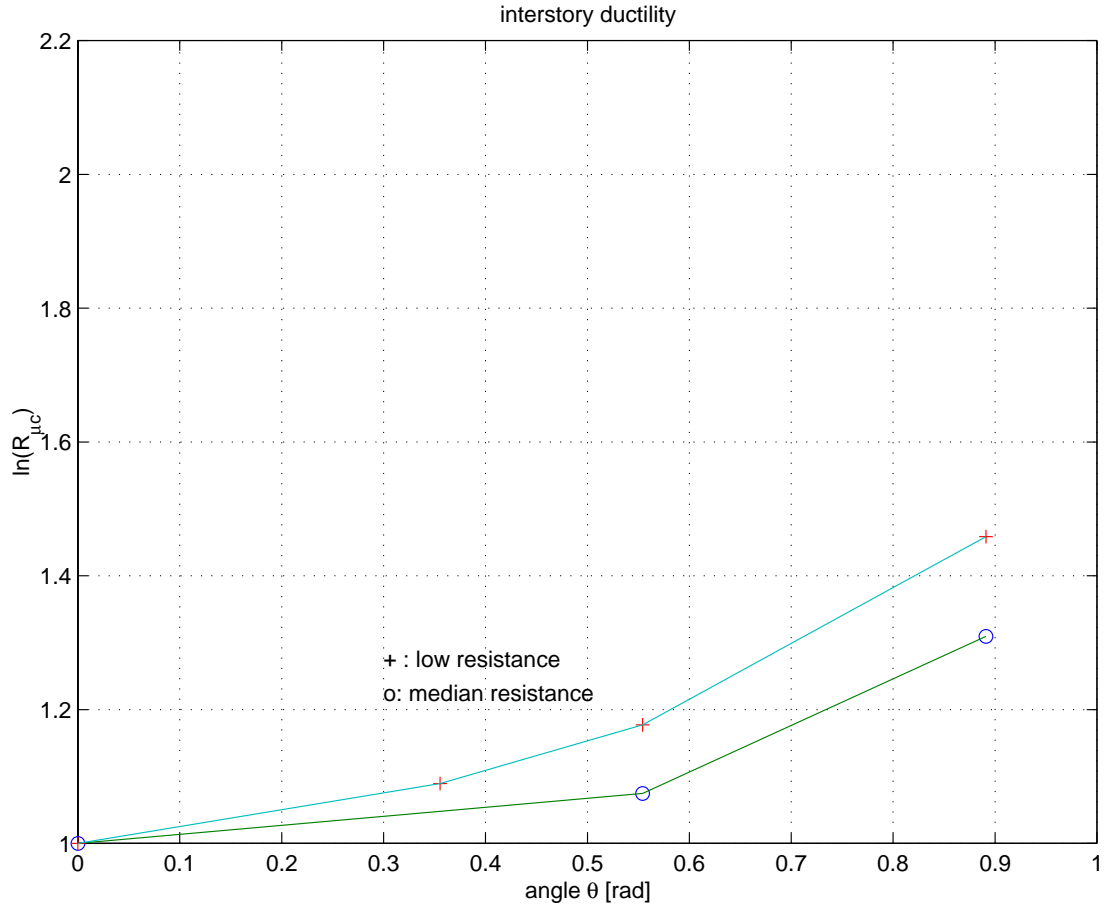
Figure 3.19. Correction angle curves for interstory ductilities, 1Hz stick MDoF model, for the median and low resistance systems. The uncorrected spectrum compatible records median ductilities were 3.75 and 6.58 respectively (from Table 3.21). The vertical axis corresponds to the value of $R_{\mu c}$, the ratio of the median ductility produced by the modified shape compatibilized records, to the median ductility produced by the original shape (bin-median-spectral-shape target) set of compatibilized records.
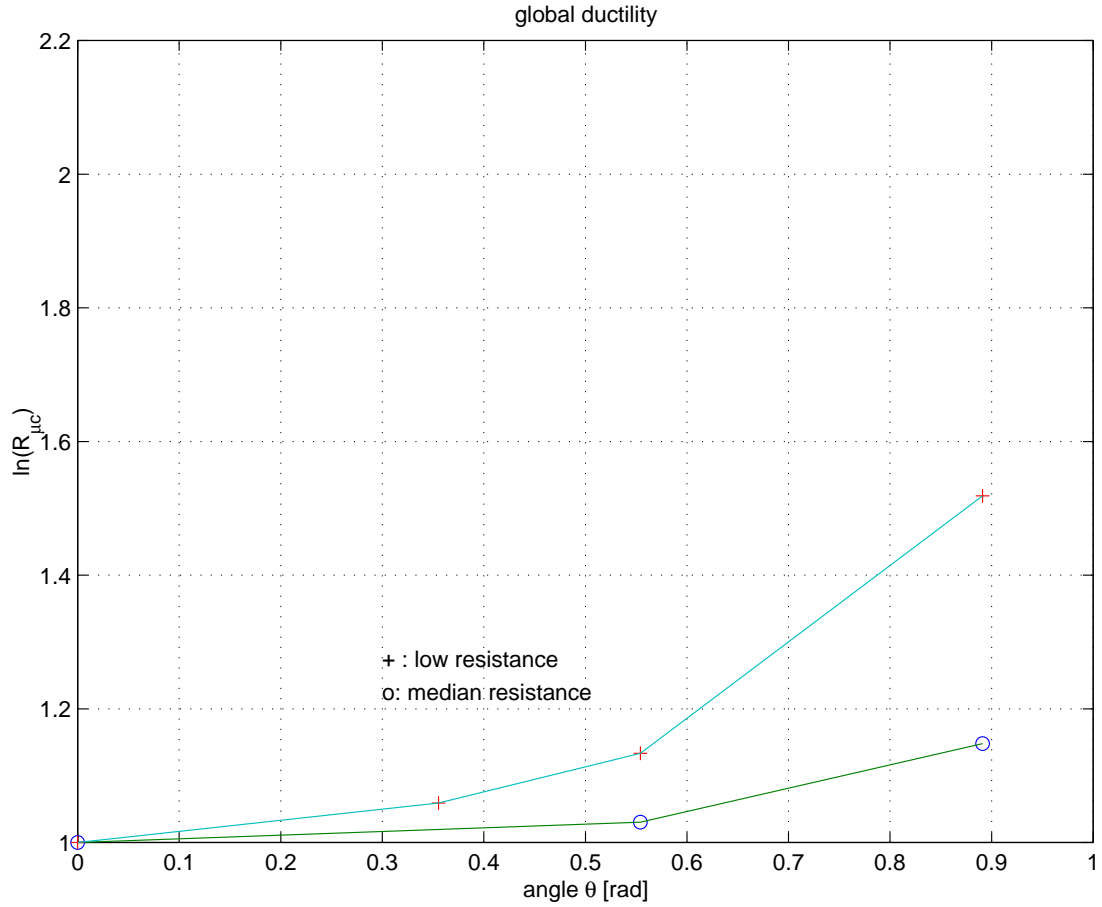
Figure 3.20. Correction angle curves for global ductilities, 1Hz stick MDoF model; median and low resistance systems. The uncorrected spectrum compatible records' median ductilities were 2.3 and 3.22 respectively. The vertical axis corresponds to the value of $R_{\mu c}$, the ratio of the median ductility produced by the modified shape compatibilized records, to the median ductility produced by the original shape (bin-median-spectral-shape target) set of compatibilized records.
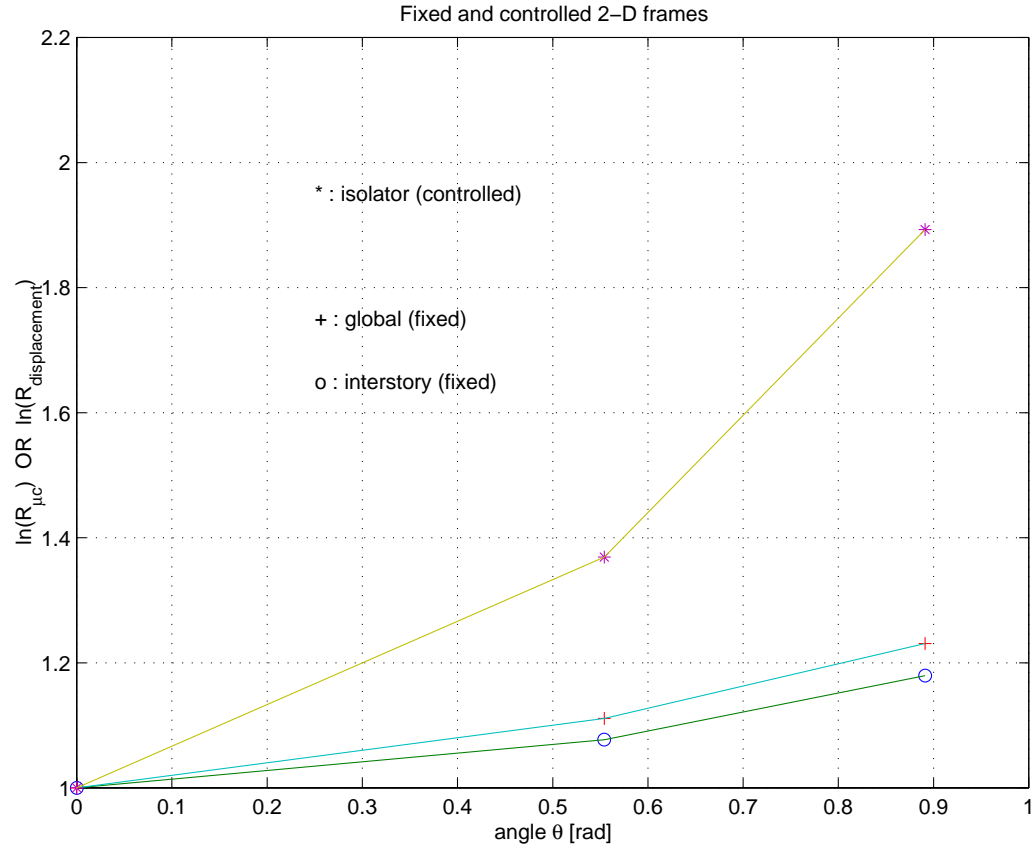
Figure 3.21. Correction angle curves for ductilities and displacement. Global and interstory ductilities are considered for the 1Hz MDoF 2-D fixed frame, and displacement for the friction-pendulum based isolated case. The uncorrected spectrum compatible records median ductilities were 3.9 (maximum interstory) and 2.3 (global), and the maximum displacement in the isolator was 8.4in. The vertical axis corresponds to the logarithm of $R_{\mu c}$ (or of $R_{displacement}$), the ratio of the median ductility (or displacement) produced by the modified shape compatibilized records, to the median ductility (or displacement) produced by the original shape (bin-median-spectral-shape target) set of compatibilized records.
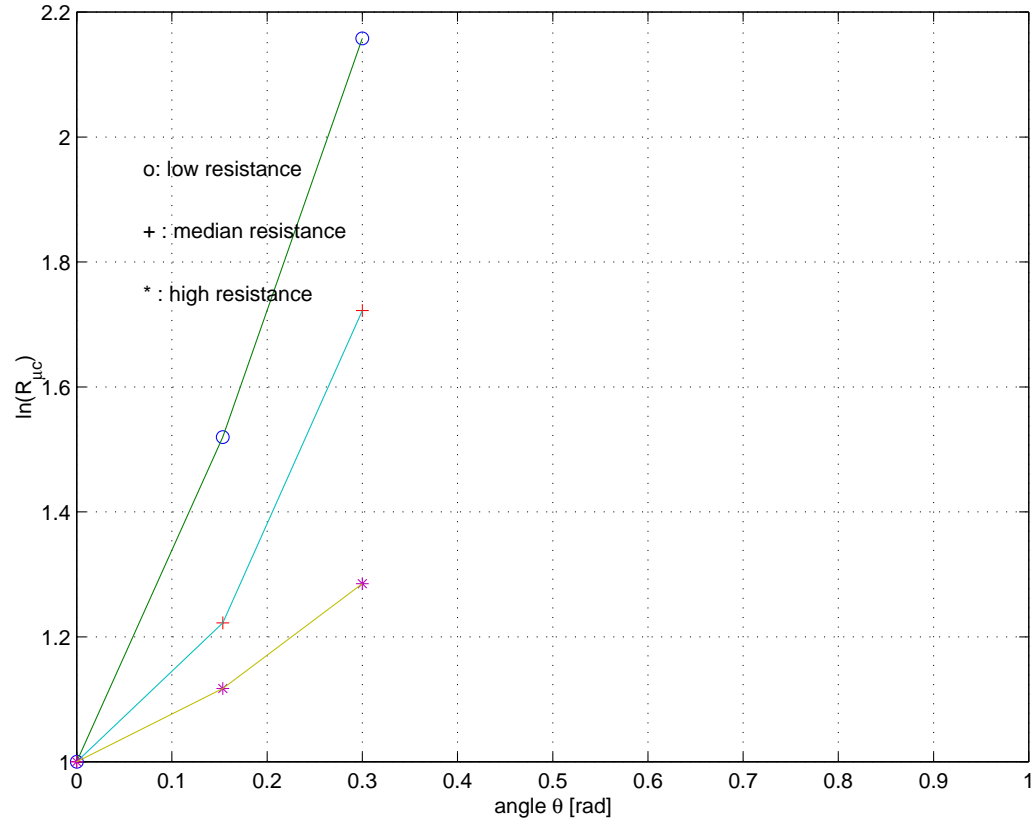
Figure 3.22. Correction angle curves for SDoF 4hz systems (low, medium and high resistance). The corresponding ductilities for the uncorrected spectrum matched records were 6.6, 3.6 and 1.8 respectively. The vertical axis corresponds to the logarithm of $R_{\mu c}$, the ratio of the median ductility produced by the modified shape compatibilized records, to the median ductility produced by the original shape (bin-median-spectral-shape target) set of compatibilized records.
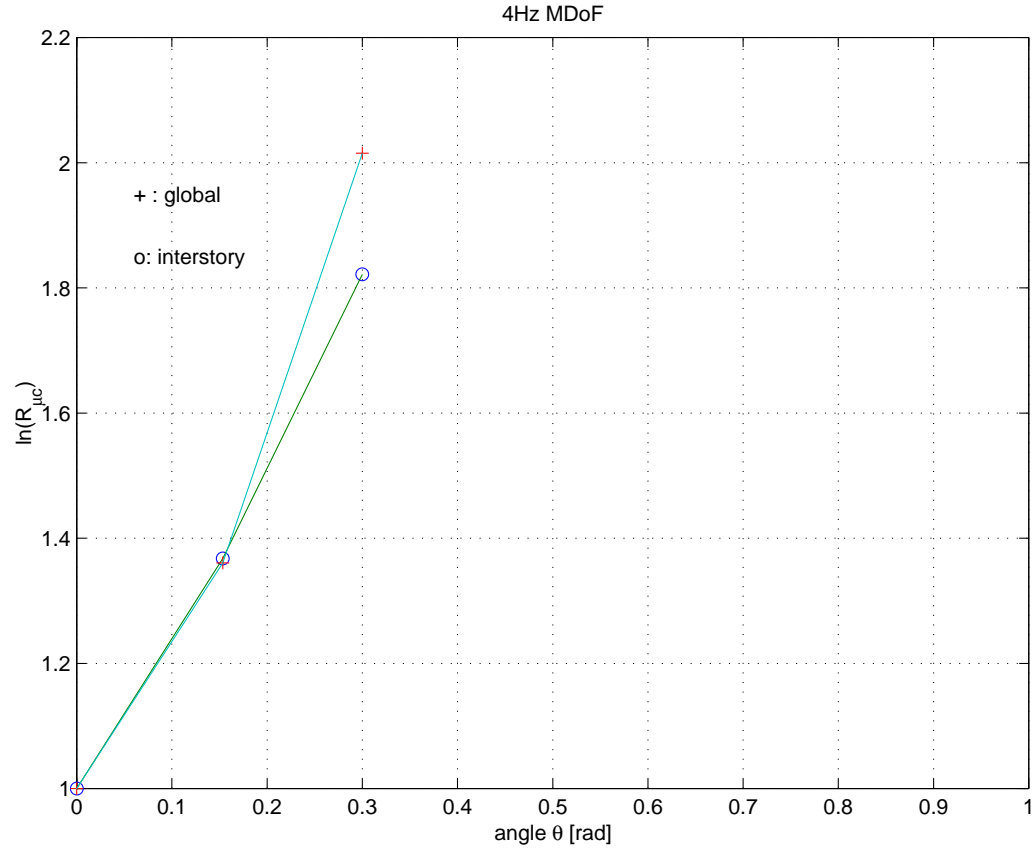
Figure 3.23. Correction angle curves for the 4Hz stick MDoF model. The uncorrected spectrum compatible records' median ductilities were 3.3 (global) and 6.6 (maximum interstory) respectively. The vertical axis corresponds to the logarithm of $R_{\mu c}$, the ratio of the median ductility produced by the modified shape compatibilized records to the median ductility produced by the original shape (bin-median-spectral-shape target) set of compatibilized records.
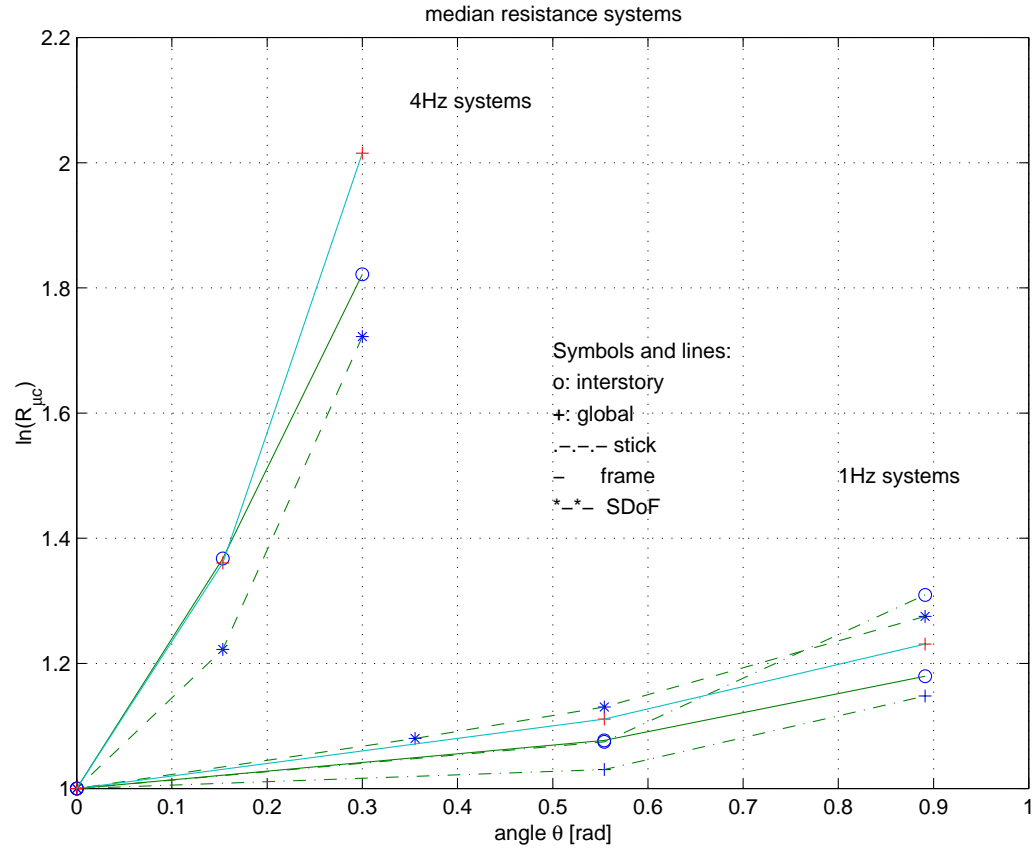
Figure 3.24: Correction angles for all median resistance systems, $\mu_D \approx 4$ (see the corresponding median ductilities in the previous captions). The SDoF curve for the 4hz case over-predicts the required angle, whereas the SDoF curve for the SDoF system under-predicts all MDoF required angles.
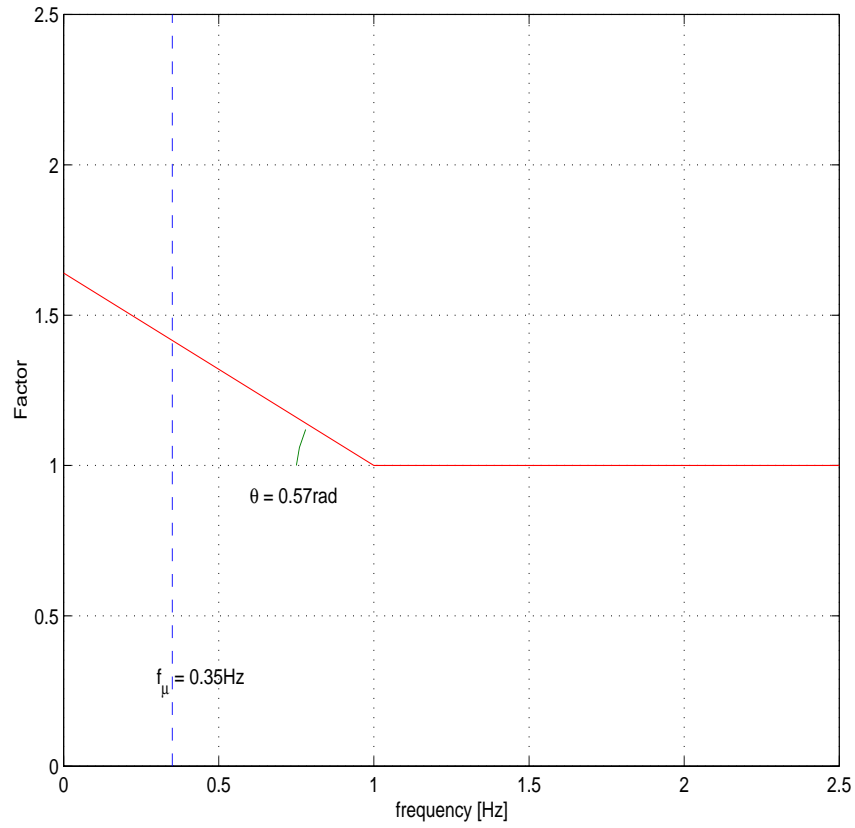
Figure 3.25 Required factor function to correct the bin-median target spectrum for unbiased estimates on high interstory ductility of 1Hz systems. The factor is unit-constant for frequencies higher than $f_0 = 1$hz. The corresponding θ-angle is $\theta = 0.57$rad
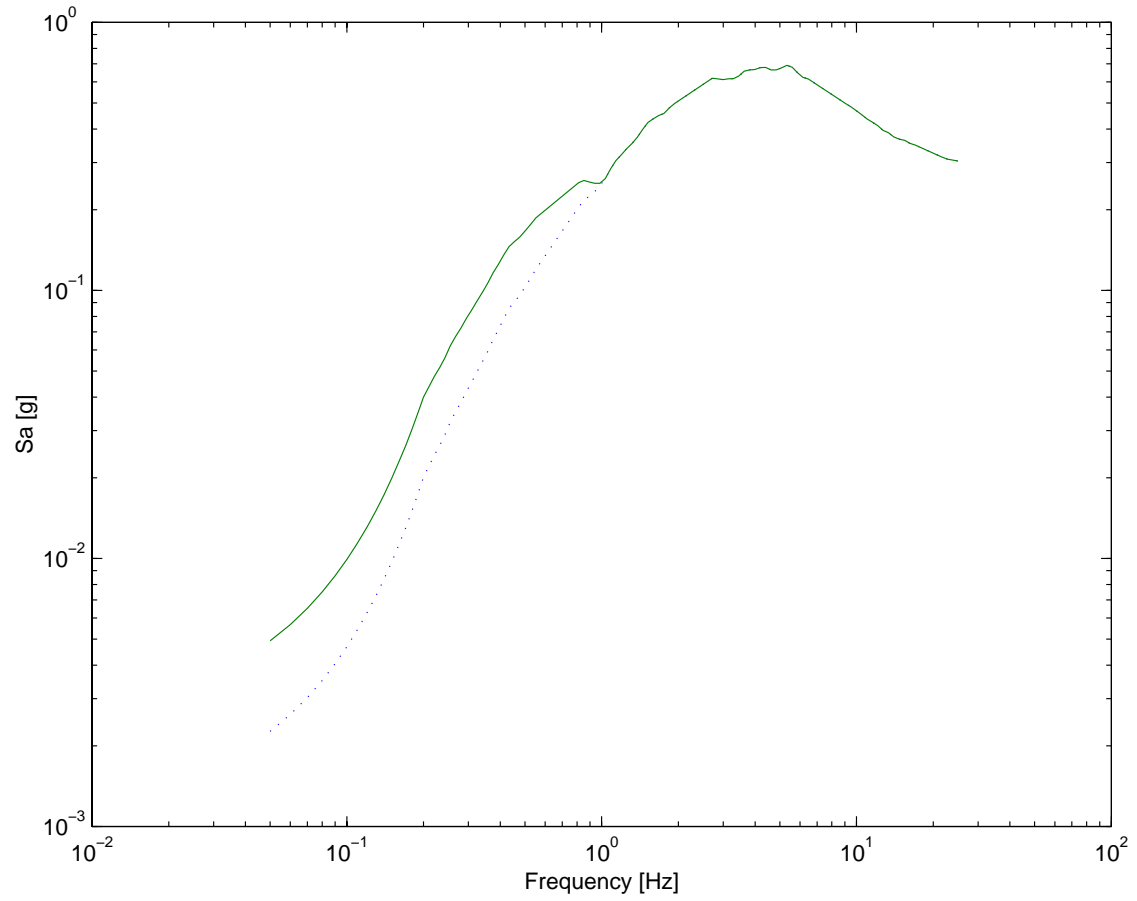
Figure 3.26 Original target (bin median spectral shape) and modified spectral shape. By compatibilizing the M-R bin records to the modified corrected shape, the accelerograms would allow us to generate nonlinear response results that would permit us to compute an unbiased estimate of the median bin ductilities for 1Hz, high-interstory-ductility systems).
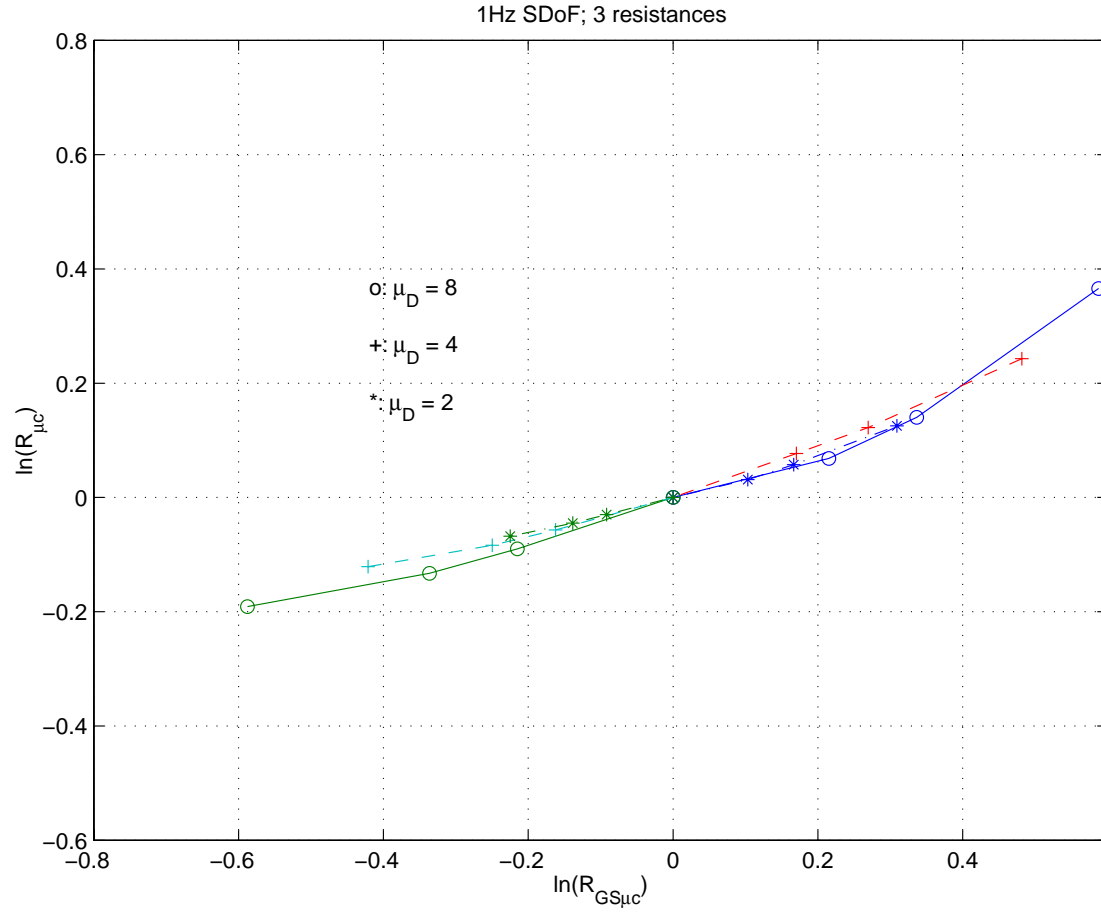
Figure 3.27. g^+ and g^- functions for the SDoF, 1Hz systems: low, median and high resistances (i.e., $\mu_D = 8$, 4 and 2). A single g^+ function could potentially be considered for all cases.
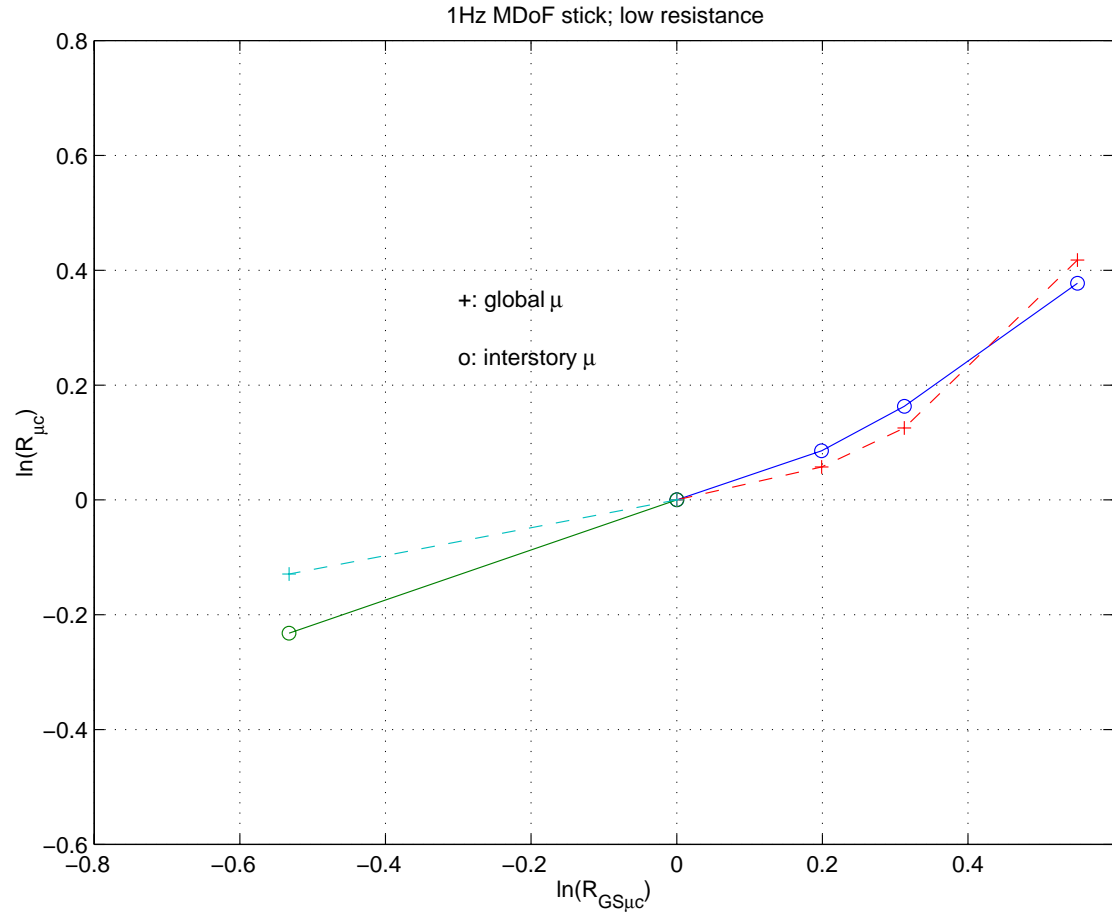
Figure 3.28. g^+ and g^- functions for the MDoF, 1Hz systems: low resistances (i.e., $\mu_{Di} \approx 8$). The high apparent asymmetry in the global ductility may explain the corresponding high introduced bias (1.24). See Table 3.24
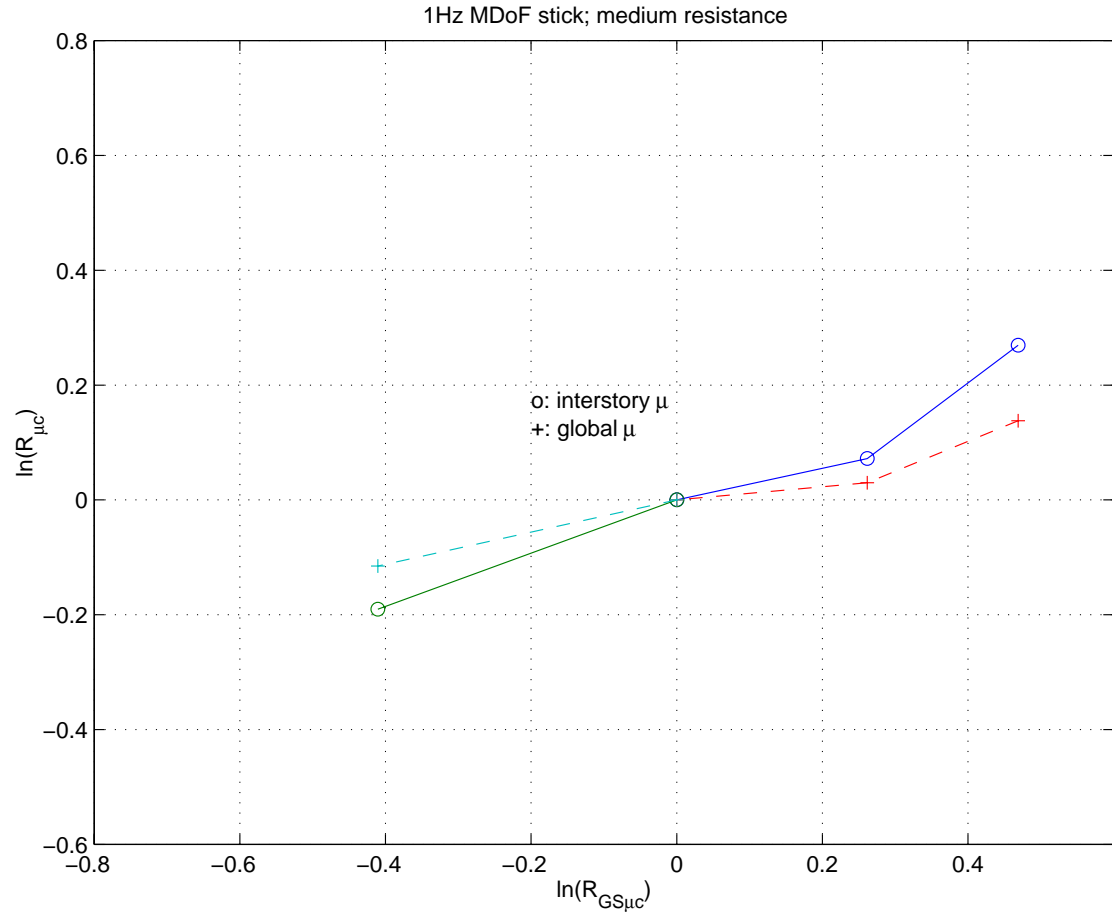
Figure 3.29. g^{+} and g^{-} functions for the MDoF, 1Hz stick systems: median resistances (i.e., $\mu_{Di} \approx 4$). The low apparent asymmetry in the global ductility may indicate a poor prediction of the bias introduced by spectrum compatibilizing to the median bin shape. See Table 3.24
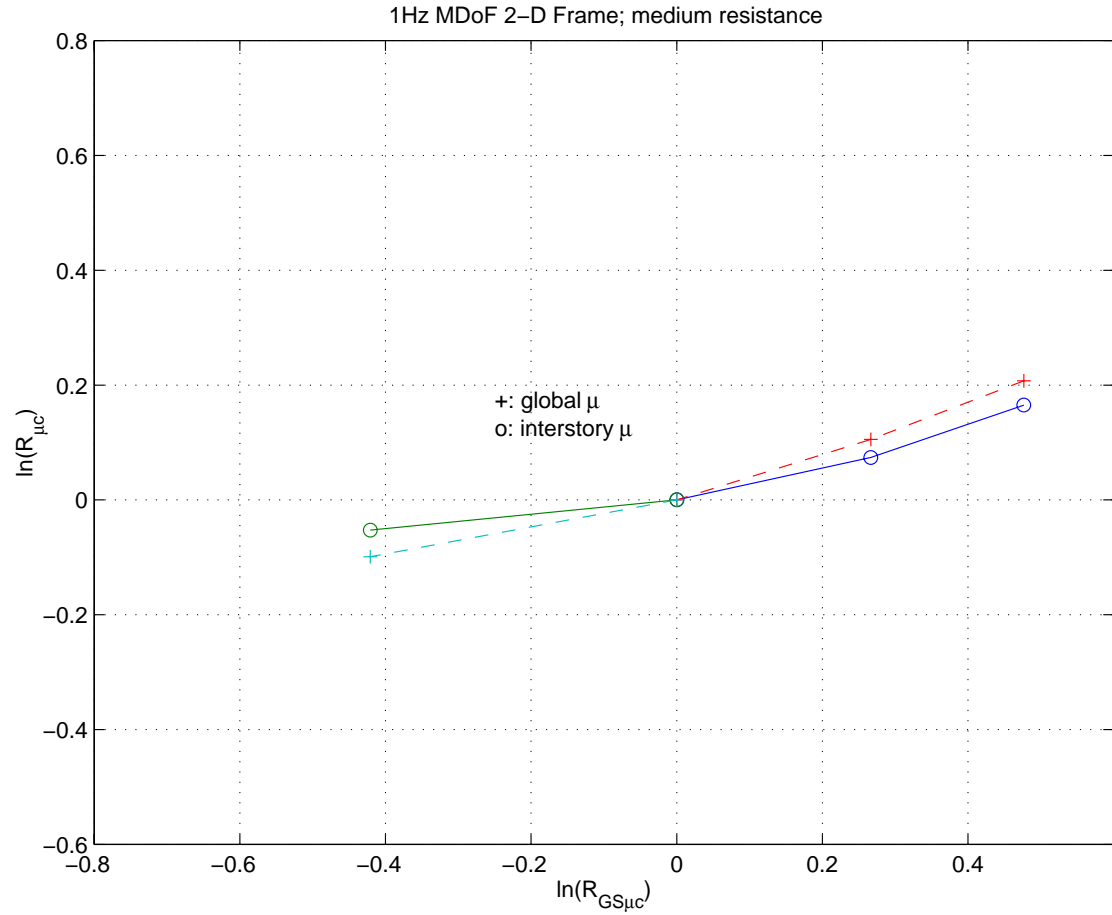
Figure 3.30. g^+ and g^- functions for the MDoF, 1Hz 2-D fixed frame: median resistances (i.e., $\mu_{Di} \approx 4$). The apparent asymmetries (global and interstory) for this system appear to be higher than the ones that the 1Hz stick model in Figure 3.29 showed. Although still low, the prediction model can capture this difference; the actual introduced bias is in fact higher for this system, as can be seen in Table 3.24.
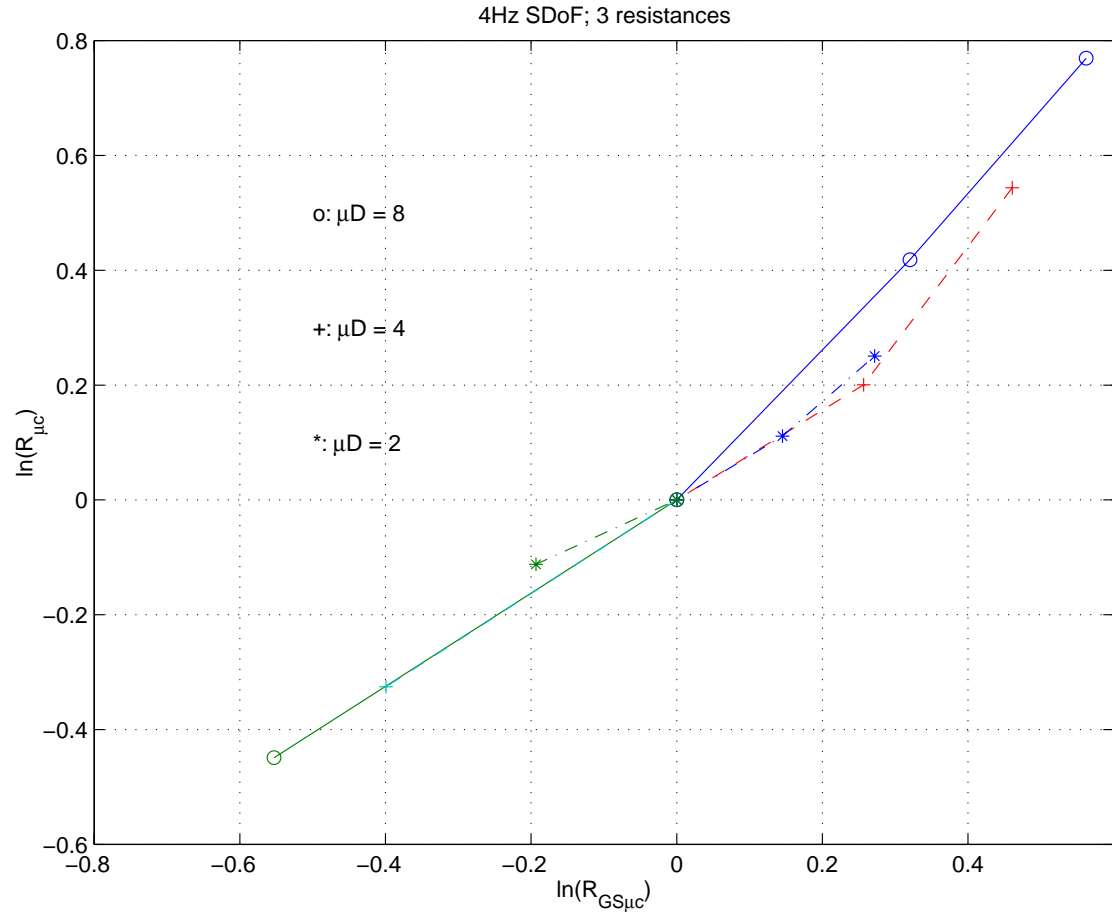
Figure 3.31. g^+ and g^- functions for the SDoF, 4Hz systems: low, median and high resistances (i.e., μ_D = 8, 4 and 2). Unlike the 1Hz case, a single representative g^+ function is not obvious. Notice that with respect to the 1Hz systems the ductility ratios are higher for the same levels of global-shape ratios.

4Hz MDoF stick; medium resistance

o: interstory μ
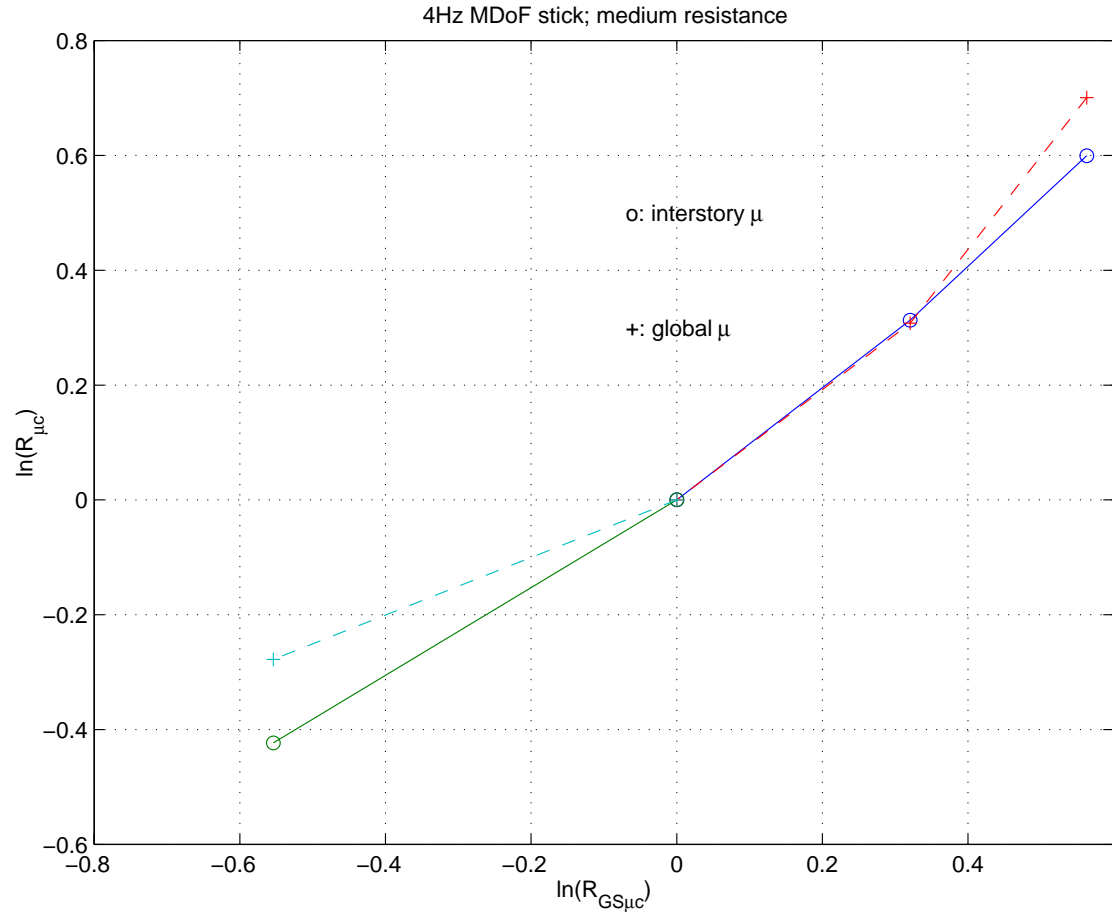
+: global μ

Figure 3.32. g^+ and g^- functions for the MDoF, 4Hz stick system: median resistances (i.e., $\mu_{Di} \approx 4$). The global ductility curve (+) shows a larger *asymmetry* which is reflected in a larger bias introduction, with respect to that of the interstory ductility, as can be seen in table 3.24.

Chapter 3 Tables.

Freq. [Hz]	$\mu_D = 2$				$\mu_D = 4$				$\mu_D = 8$			
	μ_m	$\sigma_{ln\mu}$	NHE_m	$\sigma_{ln(NHE)}$	μ_m	$\sigma_{ln\mu}$	NHE_m	$\sigma_{ln(NHE)}$	μ_m	$\sigma_{ln\mu}$	NHE_m	$\sigma_{ln(NHE)}$
0.20	2.00	0.77	3.20	1.31	4.00	0.76	10.90	1.26	8.10	0.78	39.10	1.22
0.25	1.90	0.71	2.90	1.37	4.00	0.71	11.20	1.23	8.10	0.73	36.90	1.29
0.40	2.40	0.64	4.30	1.41	4.10	0.66	13.10	1.30	8.10	0.68	40.70	1.13
0.70	2.20	0.72	4.40	1.26	3.90	0.73	13.90	1.12	8.10	0.73	42.80	1.18
1.00	2.10	0.71	3.10	1.37	4.00	0.76	12.00	1.42	8.00	0.80	46.00	1.06
1.40	2.00	0.67	3.00	1.52	4.00	0.72	11.90	1.35	8.00	0.76	42.20	1.15
2.00	1.90	0.59	3.10	1.50	3.90	0.69	13.00	1.21	8.10	0.78	47.20	1.10
3.00	2.20	0.62	3.80	1.58	4.10	0.69	15.40	1.28	8.00	0.79	45.50	1.41
4.00	1.90	0.64	2.30	1.82	4.10	0.74	12.90	1.53	7.90	0.82	48.60	1.11
5.00	2.00	0.71	3.20	1.87	4.00	0.84	14.00	1.54	8.00	0.90	47.30	1.23

Table 3.1a. Results for the bilinear hysteretic loop SDoF systems, 63 recorded accelerograms. μ_D represents the *nominal* design level .(By *nominal* we mean that the systems were tuned, by varying their yield displacement, such that the median responses were for all cases close to the corresponding nominal level).

Freq. [Hz]	$\mu_D = 2$				$\mu_D = 4$				$\mu_D = 8$			
	μ_m	$\sigma_{ln\mu}$	NHE_m	$\sigma_{ln(NHE)}$	μ_m	$\sigma_{ln\mu}$	NHE_m	$\sigma_{ln(NHE)}$	μ_m	$\sigma_{ln\mu}$	NHE_m	$\sigma_{ln(NHE)}$
0.20	2.00	0.79	2.10	1.09	4.00	0.78	5.30	1.05	8.10	0.82	15.10	1.06
0.25	1.90	0.73	2.00	1.09	4.10	0.73	5.70	1.00	8.20	0.75	14.70	1.11
0.40	2.40	0.68	3.00	1.09	4.30	0.72	6.80	1.06	8.50	0.72	17.20	0.98
0.70	2.40	0.74	3.80	0.95	4.20	0.76	8.50	0.96	8.70	0.74	21.50	0.97
1.00	2.20	0.74	3.10	1.08	4.40	0.79	9.10	1.09	9.10	0.82	25.80	0.98
1.40	2.20	0.72	3.40	1.10	4.50	0.80	9.90	1.09	9.30	0.81	27.80	1.01
2.00	2.30	0.72	3.80	1.17	4.70	0.79	11.60	1.02	10.00	0.84	33.80	1.00
3.00	2.70	0.77	5.70	1.14	5.70	0.84	16.60	1.10	11.20	0.85	39.30	1.17
4.00	2.20	0.79	4.10	1.38	5.60	0.86	18.00	1.10	11.70	0.86	50.60	0.95
5.00	2.50	0.90	5.90	1.52	5.90	0.93	22.70	1.11	12.40	0.87	60.00	0.94

Table 3.1b. Results for the pinching hysteretic loop SDoF systems, 63 recorded accelerograms. μ_D represents the *nominal* design level. The different SDoF (pinching hysteresis) models were generated based on the yield displacements that the corresponding bilinear systems had, which causes the observed ductilities to deviate from the *nominal* level. For example, the observed median ductility for the 1Hz, $\mu_D=4$ system is actually $\mu_m = 4.4$. This is due the fact that the yield displacement of the model was not tuned for the median ductility to be 4.0, but rather the same yield displacement from the bilinear model was kept.

Freq. [Hz]	$\mu_D = 2$				$\mu_D = 4$				$\mu_D = 8$			
	μ bias	μ σ bias	NHE bias	NHE σ bias	μ bias	μ σ bias	NHE bias	NHE σ bias	μ bias	μ σ bias	NHE bias	NHE σ bias
0.20	1.11	4.53	1.88	4.52	1.21	3.80	1.09	4.34	1.21	3.55	0.95	4.07
0.25	1.06	4.18	1.61	4.89	1.11	3.55	1.06	3.97	1.19	3.48	0.91	4.16
0.40	1.09	3.20	1.13	4.27	1.03	3.00	0.94	3.82	1.17	3.09	0.92	3.53
0.70	1.05	3.79	1.33	3.50	1.11	3.65	1.16	2.87	1.14	3.32	0.93	3.11
1.00	1.11	3.94	1.29	4.03	1.14	3.04	0.98	3.94	1.14	3.81	0.91	2.72
1.40	1.05	3.94	1.15	4.75	1.11	3.13	0.94	3.55	1.16	2.92	0.90	3.59
2.00	1.06	3.69	1.07	4.41	1.18	2.88	0.97	3.46	1.19	2.89	0.90	3.33
3.00	1.05	2.95	1.06	4.79	1.17	2.88	0.90	3.76	1.19	3.16	0.85	4.86
4.00	1.06	3.56	1.05	5.69	1.14	2.85	0.86	4.25	1.20	3.57	0.95	3.36
5.00	1.05	3.74	1.07	4.79	1.11	4.00	0.92	3.85	1.25	4.29	0.97	3.32

Table 3.2a. Bias and dispersion ratios (original to compatibilized) for the bilinear hysteretic loop SDoF systems, 63 frequency-domain (RASCAL)-matched accelerograms. μ_D represents the *nominal* design level.

Freq. [Hz]	$\mu_D = 2$				$\mu_D = 4$				$\mu_D = 8$			
	μ bias	μ σ bias	NHE bias	NHE σ bias	μ bias	μ σ bias	NHE bias	NHE σ bias	μ bias	μ σ bias	NHE bias	NHE σ bias
0.20	1.00	3.67	1.33	4.09	1.05	3.04	0.75	4.20	1.13	3.90	0.68	4.07
0.25	1.06	3.74	1.61	5.07	1.14	3.09	1.01	3.51	1.31	3.84	0.86	4.30
0.40	1.09	3.05	0.93	4.41	1.03	3.00	0.79	4.06	1.09	3.58	0.80	3.65
0.70	1.00	3.43	0.96	2.86	1.08	2.61	0.88	2.49	1.09	2.92	0.75	2.95
1.00	1.17	3.94	1.11	2.80	1.21	3.80	0.83	2.90	1.18	2.96	0.83	2.36
1.40	1.05	3.94	1.11	3.71	1.18	3.13	0.92	2.81	1.25	3.04	0.86	2.61
2.00	1.00	3.93	1.11	3.49	1.26	3.45	1.04	2.57	1.25	4.11	0.97	2.39
3.00	1.10	3.65	1.12	4.16	1.14	3.29	1.03	3.12	1.29	3.43	0.97	3.36
4.00	1.06	3.76	1.10	4.44	1.21	3.08	0.97	3.64	1.27	3.73	1.08	2.92
5.00	1.05	4.44	1.19	4.07	1.18	3.65	1.04	3.28	1.29	3.75	1.11	3.00

Table 3.2b. Bias and dispersion ratios (original to compatibilized) for the bilinear hysteretic loop SDoF systems, 63 time-domain (RSPMATCH)-matched accelerograms. μ_D represents the *nominal* design level.

Freq. [Hz]	$\mu_D = 2$				$\mu_D = 4$				$\mu_D = 8$			
	μ bias	μ σ bias	NHE bias	NHE σ bias	μ bias	μ σ bias	NHE bias	NHE σ bias	μ bias	μ σ bias	NHE bias	NHE σ bias
0.20	1.11	6.08	1.62	5.74	1.21	4.88	1.08	6.56	1.19	4.56	1.01	5.89
0.25	1.06	7.30	1.43	4.95	1.21	4.56	1.12	6.25	1.22	4.41	1.01	6.94
0.40	1.04	4.86	1.07	4.95	1.08	4.50	0.96	5.89	1.18	4.80	1.04	6.13
0.70	1.09	4.93	1.23	2.57	1.08	6.33	1.05	3.56	1.09	4.35	0.96	5.11
1.00	1.10	6.17	1.11	3.27	1.10	5.27	0.98	4.19	1.08	5.13	1.00	3.77
1.40	1.10	5.54	1.13	3.33	1.13	4.21	0.95	3.89	1.07	5.06	0.97	4.04
2.00	1.15	6.55	1.00	3.34	1.12	4.39	0.98	3.52	1.09	4.20	0.96	3.85
3.00	1.13	5.13	0.95	3.56	1.19	5.25	0.92	3.67	1.13	4.72	0.91	4.33
4.00	1.10	6.08	0.91	4.31	1.14	4.78	0.87	3.55	1.15	4.78	0.98	3.39
5.00	1.04	5.63	0.84	3.71	1.05	5.17	0.86	3.47	1.14	4.83	0.97	3.13

Table 3.3a. Bias and dispersion ratios (original to compatibilized) for the pinching hysteretic loop SDoF systems, 63 frequency-domain (RASCAL)-matched accelerograms. μ_D represents the *nominal* design level.

Freq. [Hz]	$\mu_D = 2$				$\mu_D = 4$				$\mu_D = 8$			
	μ bias	μ σ bias	NHE bias	NHE σ bias	μ bias	μ σ bias	NHE bias	NHE σ bias	μ bias	μ σ bias	NHE bias	NHE σ bias
0.20	1.05	5.27	1.50	4.54	1.29	5.57	1.08	5.83	1.33	5.47	0.99	6.24
0.25	1.12	4.56	1.54	5.19	1.32	4.87	1.33	4.76	1.55	5.36	1.23	6.17
0.40	1.09	4.53	1.03	5.74	1.10	4.00	0.88	6.24	1.15	3.79	0.91	4.90
0.70	1.14	6.73	1.03	3.96	1.17	5.43	0.93	4.17	1.14	3.89	0.89	4.85
1.00	1.10	7.40	0.89	3.00	1.16	6.58	0.83	3.76	1.15	5.13	0.88	4.45
1.40	1.10	8.00	1.03	2.75	1.15	5.71	0.81	3.03	1.16	6.23	0.82	3.74
2.00	1.10	6.55	0.97	2.93	1.18	6.08	0.90	2.55	1.15	6.00	0.84	2.94
3.00	1.13	5.13	1.06	2.48	1.16	6.00	0.92	2.68	1.20	5.67	0.87	3.08
4.00	1.10	7.18	1.05	3.29	1.14	4.78	0.92	2.62	1.16	6.62	0.99	2.44
5.00	1.09	6.00	1.04	2.92	1.07	4.89	0.99	2.36	1.17	5.12	1.03	2.35

Table 3.3b. Bias and dispersion ratios (original to compatibilized) for the pinching hysteretic loop SDoF systems, 63 time-domain (RSPMATCH)-matched accelerograms. μ_D represents the *nominal* design level.

a) Global Ductility					
Original		RL		rspM	
μ_o	$\sigma_{ln(m)}$	μ_o/μ_c	σ_o/σ_c	μ_o/μ_c	σ_o/σ_c
1.14	0.61	1.01	4.87	0.96	3.70
1.95	0.59	1.17	3.80	1.08	3.11
3.91	0.71	1.26	3.91	1.15	3.08
5.86	0.79	1.28	4.47	1.12	3.54

b) Interstory Ductility					
Original		RL		rspM	
μ_o	$\sigma_{ln(m)}$	μ_o/μ_c	σ_o/σ_c	μ_o/μ_c	σ_o/σ_c
2.03	0.62	1.09	4.33	1.02	3.66
4.10	0.62	1.28	3.38	1.21	2.95
10.27	0.73	1.30	3.04	1.24	2.94
16.50	0.77	1.24	3.67	1.17	3.76
Bilinear hysteresis; 0.25Hz					

Table 3.4 Bias (ratio of original records' median ductility to compatibilized records' median ductility (denoted by μ_o/μ_c)) and dispersion reduction ($\sigma_{ln(\mu)}$ from original records to $\sigma_{ln(\mu)}$ from compatibilized records (denoted by σ_o/σ_c)). a) Global ductility, and b) Interstory ductility, for the 0.25Hz bilinear system. Results from frequency domain scheme (program RASCAL, RL) and time domain scheme (program RSPMATCH, rspM).

a) Global Ductility					
Original		RL		rspM	
μ_o	$\sigma_{\ln(m)}$	μ_o/μ_c	σ_o/σ_c	μ_o/μ_c	σ_o/σ_c
0.70	0.59	0.94	4.72	0.94	4.52
1.25	0.53	0.98	5.13	0.96	5.65
2.57	0.61	1.12	3.04	1.19	3.94
4.00	0.69	1.24	3.31	1.29	3.46

b) Interstory Ductility					
Original		RL		rspM	
μ_o	$\sigma_{\ln(m)}$	μ_o/μ_c	σ_o/σ_c	μ_o/μ_c	σ_o/σ_c
0.84	0.60	1.04	6.35	1.06	4.43
1.69	0.60	1.06	4.36	1.08	5.03
4.40	0.69	1.17	2.91	1.26	3.30
7.21	0.74	1.19	2.95	1.28	3.24
Bilinear hysteresis; 1.0 Hz					

Table 3.5 Bias (ratio of original records' median ductility to compatibilized records' median ductility (denoted by μ_o/μ_c)) and dispersion reduction ($\sigma_{\ln(\mu)}$ from original records to $\sigma_{\ln(\mu)}$ from compatibilized records (denoted by σ_o/σ_c))) and dispersion reduction ($\sigma_{\ln(\mu)}$ from original records to $\sigma_{\ln(\mu)}$ from compatibilized records). a) Global ductility, and b) Interstory ductility, for the 1.0Hz bilinear system. Results from frequency domain scheme (program RASCAL, RL) and time domain scheme (program RSPMATCH, rspM).

a) Global Ductility					
Original		RL		rspM	
μ_o	$\sigma_{\ln(m)}$	μ_o/μ_c	σ_o/σ_c	μ_o/μ_c	σ_o/σ_c
1.90	0.55	1.06	4.60	1.12	4.46
4.38	0.79	1.32	3.83	1.34	3.80

b) Interstory Ductility					
Original		RL		rspM	
μ_o	$\sigma_{\ln(m)}$	μ_o/μ_c	σ_o/σ_c	μ_o/μ_c	σ_o/σ_c
2.95	0.73	1.10	3.13	1.13	3.06
7.47	0.79	1.13	3.94	1.12	3.72
Bilinear hysteresis; 4.0 Hz					

Table 3.6 Bias (ratio of original records' median ductility to compatibilized records' median ductility (denoted by μ_o/μ_c)) and dispersion reduction ($\sigma_{\ln(\mu)}$ from original records to $\sigma_{\ln(\mu)}$ from compatibilized records (denoted by σ_o/σ_c)). a) Global ductility, and b) Interstory ductility, for the 4.0Hz bilinear system. Results from frequency domain scheme (program RASCAL, RL) and time domain scheme (program RSPMATCH, rspM).

a) Global Ductility					
Original		RL		rspM	
μ_o	$\sigma_{ln(m)}$	μ_o/μ_c	σ_o/σ_c	μ_o/μ_c	σ_o/σ_c
0.72	0.62	0.96	4.99	0.96	4.77
1.36	0.60	1.05	5.15	1.05	9.31
3.12	0.69	1.08	6.09	1.11	6.66
5.07	0.76	1.09	4.76	1.15	7.14

b) Interstory Ductility					
Original		RL		rspM	
μ_o	$\sigma_{ln(m)}$	μ_o/μ_c	σ_o/σ_c	μ_o/μ_c	σ_o/σ_c
0.86	0.64	1.07	6.78	1.09	4.58
1.85	0.66	1.09	4.58	1.15	4.76
4.82	0.71	1.10	3.36	1.19	4.76
8.18	0.74	1.17	4.23	1.28	4.29
Pinching hysteresis; 1.0 Hz					

Table 3.7. "Bias" (ratio of original records' median ductility to compatibilized records' median ductility (denoted by μ_o/μ_c)) and dispersion reduction ($\sigma_{ln(\mu)}$ from original records to $\sigma_{ln(\mu)}$ from compatibilized records (denoted by σ_o/σ_c)). a) Global ductility, and b) Interstory ductility, for the 1.0Hz pinching system. Results from frequency domain scheme (program RASCAL, RL) and time domain scheme (program RSPMATCH, rspM).

system	original records				Matched records (ratios)			
	global		interstory		global		interstory	
	μ_m	$\sigma_{ln\mu}$	μ_m	$\sigma_{ln\mu}$	μ_o/μ_c	σ_o/σ_c	μ_o/μ_c	σ_o/σ_c
SDoF	-	-	4	0.76	-	-	1.14	3.04
MDoF stick	2.57	0.61	4.4	0.69	1.12	3.04	1.17	2.91
MDoF 2D	2.9	0.83	4.6	0.6	1.24	2.13	1.18	3.16

Table 3.8 Comparison of the different 1Hz systems SDoF, 5DoF (a stick model), a MDoF 2-D frame, bilinear hysteresis systems. Shown are the "biases" (ratio of original records' median ductility to compatibilized records' median ductility), as well as the dispersion reductions ($\sigma_{ln(\mu)}$ from original records to $\sigma_{ln(\mu)}$ from compatibilized records). Only results for the frequency domain scheme-compatibilized records are shown.

records	isolator		superstructure	
	μ	$\sigma_{ln(\mu)}$	μ	$\sigma_{ln(\mu)}$
original	5.79	0.78	0.82	0.39
RL	4.85	0.23	0.76	0.08
Ratios	1.19	3.4	1.08	4.9

Table 3.9. Median displacement ductilities and dispersions of the 2DoF Base isolated system (elastomeric bearing) for the original set of records and the spectrum compatible set (RASCAL, denoted by RL).

records	isolator		Superstructure			
	d [in]	$\sigma_{ln\,d}$	μ_i	$\sigma_{ln\mu}$	μ_g	$\sigma_{ln\mu}$
original	10.1	0.92	1.8	0.58	1.15	0.61
compat'd	8.4	0.29	1.5	0.13	0.96	0.17
Ratios	1.2	3.2	1.2	4.5	1.2	3.6

Table 3.10. 2-D SMRF, base isolated (friction pendulum) system. Comparison of results for the 63 original bin-records and the same (time-domain-scheme) compatibilized accelerograms.

	R_{SaMA0}	$R_{GS\mu}$	R_{LS}
R_{SaMA0}	1.00	-0.28	-0.10
$R_{GS\mu}$	-0.28	1.00	0.04
R_{LS}	-0.10	0.04	1.00

Table 3.11. Correlation matrix of the shape and intensity ratios (for the entire data set of original records).

	Coefficients	Standard Error	Lower 95.0%	Upper 95.0%
Intercept	-0.07	0.04	-0.15	0.02
a_1	1.15	0.06	1.03	1.27
a_2	0.54	0.08	0.38	0.69
a_3	-0.27	0.33	-0.93	0.38

Table 3.12. Regression coefficients for a_0, a_1 and a_2 for Eq. 3.15.

	R^2	a_1	SEE	a_2	SEE	a_3	SEE
R $_{SaMA0}$	0.87	1.04	0.07	-	-	-	-
R_{SaMA0}, $R_{GS\mu}$	0.93	1.16	0.06	0.53	0.08	-	-
R_{SaMA0}, $R_{GS\mu}$, R_{LS}	0.93	1.15	0.06	0.54	0.08	-0.27	0.33

Table 3.13 Incremental regressions for the entire data set. No further improvement to the model seems to be added by the introduction of parameter R_{LS}. The coefficient for R_{LS} (i.e., a_3) is not significant due to its high standard error of estimation (SEE).

	$R_\mu < 1.0$ $n = 29$		$R_\mu > 1.0$ $n = 34$	
	Coeff.	SEE	Coeff.	SEE
a_1	1.18	0.11	1.05	0.06
a_2	0.41	0.14	0.66	0.08
a_3	0.30	0.54	-0.72	0.32

Table 3.14. Regression of coefficients a_1 through a_3 for above- and below-unit R_μ subsets. n is the number of records in each subset (which add to 63)

	$R\mu < 1.0$; $n = 29$						
	a_1^-	SEE	a_2^-	SEE	a_3^-	SEE	SSE
R_{SaMA0}	1.09	0.11	-	-	-	-	4.97
R_{SaMA0}, $R_{GS\mu}$,	1.19	0.10	0.41	0.14	-	-	3.72
R_{SaMA0}, R_{LS}	1.08	0.11	-	-	0.38	0.61	4.90
R_{SaMA0}, $R_{GS\mu}$, R_{LS}	1.18	0.11	0.41	0.14	0.30	0.54	3.68

Table 3.15: Incremental regressions for partial data set, corresponding to $R_\mu < 1$. As was seen for the entire data set case (Table 3.13) there was no obvious gain in adding the variable R_{LS}. Do not confuse the headings "SEE" (standard error of estimation) and " SSE" (the sum of squares of the errors). The minus-sign superscript on the coefficients (a_i^-) refers to the below-unit normalized ductilities record set (i.e., those with negative logarithmic values)

	$R\mu > 1.0$; $n = 34$						
	a_1^+	SEE	a_2^+	SEE	a_3^+	SEE	S<u>SE</u>
R_{SaMA0}	0.98	0.10	-	-	-	-	4.67
R_{SaMA0}, $R_{GS\mu}$,	1.11	0.06	0.66	0.08	-	-	1.56
R_{SaMA0}, R_{LS}	0.92	0.11	-	-	-0.79	0.57	4.40
R_{SaMA0}, $R_{GS\mu}$, R_{LS}	1.05	0.06	0.66	0.08	-0.72	0.32	1.38

Table 3.16: Incremental regressions for partial data set, corresponding to $R\mu > 1$. As was seen for the entire data set case (Table 3.13) there was no significant gain in adding the variable R_{LS}. Do not confuse the headings "S<u>EE</u>" (standard error of estimation) and " S<u>SE</u>" (the sum of squares of the errors). The plus-sign superscript on the coefficients (a_i^+) refers to the above-unit normalized ductilities record set (i.e., those with positive logarithmic values).

Factor (= R_{Sa0c})	n	$\ln(R_{Sa0c})$	$\sigma_{\ln(RSa0c)}$	$\ln(R_{\mu c})$ (mean)	$\sigma_{\ln(R\mu c)}$	a_1	SEE
1.6	63	0.47	0	0.454	0.16	0.97	0.04
1.0	63	0	0	0	NA	NA	NA
1/1.6	63	-0.47	0	-0.5	0.21	1.06	0.06

Table 3.17 Isolated intensity effects. As was expected from the results in section 3.6.1, no asymmetry was found for the value of the coefficient a_1. This is in agreement with the findings of Shome, 1999, because *normalization* of records does not introduce bias in the estimate of median displacement demands. n is the number of data points, which correspond to the number of compatibilized records.

Case (with respect to "softening" direction)	n	$\ln(R_{\mu c})$ (mean)	$\sigma_{\ln(R\mu c)}$	SEE
Increasing Sa	63	0.13	0.22	0.03
Decreasing Sa	63	-0.10	0.18	0.02

Table 3.18. Isolated *local-shape* effects. No apparent asymmetry can be identified for the local shape effect. "Increasing" or "Decreasing" of Sa is in the direction of softening

154

f_μ	μ_D	control μ	Case (with respect to softening direction)	n	$\ln(R_{\mu c})$ (mean)	$\sigma_{\ln(R\mu c)}$	SEE
0.5	4	3.47	Increasing Sa	63	0.17	0.22	0.03
			Decreasing Sa	63	-0.12	0.17	0.02
0.707	2	1.94	Increasing Sa	63	0.10	0.16	0.02
			Decreasing Sa	63	-0.06	0.14	0.02

Table 3.19. *Local-shape* effects; higher resistance systems. μ_D refers to the median ductility the systems show when subjected to the unmodified bin records. "Increasing" or "Decreasing" of Sa is in the direction of softening.

$FF(f_\mu)$ = $R_{GS\mu c}$	n	$\ln(R_{\mu c})$ (mean)	$\sigma_{\ln(R\mu c)}$	a_2	SEE
1.8	63	0.366	0.2	0.623	0.04
1.0	63	0	NA	NA	NA
1/1.8	63	-0.19	0.158	0.325	0.03

Table 3.20. Isolated *global-shape* effects. The observed response satisfies $\ln(R_{\mu c}) = a_2 * \ln(R_{GS\mu c})$; in other words $R_{\mu c} = \mu / \mu_m = \mu / 7.02 = R_{GS\mu c}{}^{a2}$. As expected from the results obtained in section 3.6.1, the asymmetry in the estimated coefficients a_2 is evident: for the above-unit $R_{GS\mu c} = 1.8$, $a_2^+ = 0.623$ (compare to $a_2^+ = 0.66$ from Table 3.16) and for the below-unit $R_{GS\mu c} = 1/1.8$, $a_2^- = 0.325$ (compare to $a_2^- = 0.41$ from Table 3.15).

μ_D	control μ_c	$FF(f_\mu)$ = $R_{GS\mu c}$	Case	n	$\ln(R_{\mu c})$ (mean)	$\sigma_{\ln(R\mu c)}$	a_2	SEE
4	3.47	1.62	$R_{GS\mu}>1$	63	0.24	0.20	0.5	0.05
		1/1.62	$R_{GS\mu}<1$	63	-0.12	0.14	0.25	0.04
2	1.94	1.36	$R_{GS\mu}>1$	63	0.13	0.14	0.41	0.06
		1/1.36	$R_{GS\mu}<1$	63	-0.07	0.09	0.22	0.04

Table 3.21. Isolated *global-shape* effects on the higher resistance systems. μ_D refers to the median ductility that the systems show when subjected to the unmodified bin records.

		SDoF			MDoF			
		low resistance	medium resistance	high resistance	Stick low resistance	Stick medium resistance	2-D fixed-base medium resistance	2-D Friction Pendulum-isolated
Real records	μ_g	-	-	-	4.01	2.57	2.90	1.15
	$\sigma_{\ln\mu}$	-	-	-	0.69	0.61	0.83	0.61
	μ_i	8.00	4.0	2.1	7.21	4.4	4.60	1.80
	$\sigma_{\ln\mu}$	0.80	0.76	0.71	0.74	0.69	0.60	0.58
	isolator [in]	-	-	-	-	-	-	10.10
	$\sigma_{\ln(d)}$	-	-	-	-	-	-	0.92
Original target spectrum-matched records	μ_g	-	-	-	3.22	2.3	2.34	0.96
	$\sigma_{\ln\mu}$	-	-	-	0.18	0.2	0.39	0.17
	μ_i	7.02	3.5	1.9	6.04	3.7	3.90	1.50
	$\sigma_{\ln\mu}$	0.21	0.22	0.17	0.21	0.24	0.19	0.13
	isolator [in]	-	-	-	-	-	-	8.40
	$\sigma_{\ln(d)}$	-	-	-	-	-	-	0.29
Modified target spectrum-matched records	μ_g	-	-	-	3.65	2.37	2.60	0.96
	$\sigma_{\ln\mu}$	-	-	-	0.20	0.18	0.41	0.15
	μ_i	8.10	3.9	2	7.12	4.03	4.20	1.46
	$\sigma_{\ln\mu}$	0.23	0.22	0.18	0.21	0.21	0.18	0.13
	isolator [in]	-	-	-	-	-	-	11.48
	$\sigma_{\ln(d)}$	-	-	-	-	-	-	0.24

Table 3.22 Comparison of results of all 1Hz systems using the set of compatibilized records corrected for the 1Hz, $\mu_D = 8$, SDoF system. The correction is designed to produce an un-biased estimate of the median ductilities that the 1Hz SDoF, low resistance system would display for a bin set of unmodified records. The factor function used is the one that corresponds to FF(0.35Hz) = 1.4, in Figure 3.16.

system	location	bin-records observed median response	bias	θ req'd [rad]
		μ or *d* [in]		
1Hz SDoF	-	8.00	1.14	0.53
	-	4.00	1.14	0.58
	-	2.00	1.11	0.78
1Hz MDoF (stick)	global	4.00	1.24	0.65
	inter	7.21	1.19	0.57
	global	2.57	1.12	0.81
	inter	4.40	1.17	0.69
1Hz 2-D frame, fixed	global	2.90	1.24	0.90
	inter	4.60	1.18	0.90
1Hz 2-D Isolated (FP)	isolator	10.10	1.20	0.30
4hz SDoF	-	8.00	1.20	0.06
	-	4.00	1.14	0.10
	-	2.00	1.06	0.08
4hz MDoF (stick)	global	4.40	1.32	0.14
	inter	7.47	1.13	0.05

Table 3.23 Required angles for the modification of the bin-median spectral shape in order to remove the bias observed by use of the bin-median shaped matched records. The bin-records' observed median response reflects the system's resistance level. The values in the *bias* column correspond to the ratio of the bin-records' median to the bin-median-shape-matched records' median, and were taken from Tables 3.2 through 3.10.

system	location	bin-records observed median response (μ or d[in])	bias observed	ratio estimation parameters						
				α^+	β^+	α^-	bias computed	α_l^+	bias computed	$\Delta\alpha$
1Hz SDoF	-	8.00	1.14	0.14	0.82	0.35	1.07	0.55	1.04	0.20
	-	4.00	1.14	0.41	0.20	0.30	1.04	0.49	1.03	0.18
	-	2.00	1.11	0.26	0.46	0.31	1.01	0.38	1.01	0.08
1Hz MDoF (stick)	global	4.00	1.24	-0.03	1.42	0.24	1.08	0.64	1.07	0.39
	global	2.57	1.12	-0.11	0.87	0.28	1.00	0.25	1.00	-0.03
	inter	7.21	1.19	0.30	0.71	0.44	1.07	0.63	1.04	0.19
	inter	4.40	1.17	-0.10	1.45	0.46	1.04	0.50	1.01	0.04
1Hz 2-D frame, fixed	global	2.90	1.24	0.34	0.19	0.23	1.03	0.43	1.03	0.19
	inter	4.60	1.18	0.19	0.32	0.13	1.04	0.33	1.04	0.21
4hz SDoF	-	8.00	1.20	1.23	0.25	0.81	1.10	1.35	1.10	0.54
	-	4.00	1.14	0.28	1.95	0.81	1.05	1.09	1.04	0.27
	-	2.00	1.06	0.58	1.24	0.58	1.04	0.89	1.03	0.31
4hz MDoF (stick)	global	4.40	1.32	0.58	1.17	0.50	1.09	1.17	1.10	0.67
	inter	7.47	1.13	0.86	0.37	0.76	1.05	1.04	1.05	0.28

Table 3.24. For the different models analyzed for $R_{\mu c}$ vs. $R_{GS\mu c}$, i.e., their g^+ and g^- functions (Figs. 3.27 through 3.32) the values of α^+, α^-, and β^+ were obtained. Also, a linear fit was made for the function g^+, for which the value of α_l^+ was obtained. The two-parameter g^+, in general, works better. In general, although the model presents lower bias predictions, the model is able to capture the relative variation of the asymmetry effect.

Appendix 3.A. Recorded Accelerograms Used in Chapter 3.

	Event	year	month	day	M^1	Station	R^2 [km]	PGA [g]
1	Morgan Hill	1984	4	24	6.2	Coyote Lake Dam (SW Abut.)	0.1	0.71
2	Morgan Hill	1984	4	24	6.2	Gilroy Array #2	15.1	0.16
3	Morgan Hill	1984	4	24	6.2	Gilroy Array #3	14.6	0.19
4	Morgan Hill	1984	4	24	6.2	Gilroy Array #6	11.8	0.22
5	Morgan Hill	1984	4	24	6.2	Gilroy Gavilan Coll.	16.2	0.11
6	Morgan Hill	1984	4	24	6.2	Gilroy Array #7	14.0	0.19
7	Morgan Hill	1984	4	24	6.2	Hollister Diff. Array	28.3	0.09
8	N. Palm Springs	1986	7	8	6.0	Joshua Tree	29.8	0.05
9	Superstition Hills	1987	11	24	6.7	El Centro Imp. Co. Cent	13.9	0.36
10	Superstition Hills	1987	11	24	6.7	Wildlife Liquef. Array	24.4	0.18
11	Superstition Hills	1987	11	24	6.7	Westmorland Fire Sta.	13.3	0.17
12	Loma Prieta	1989	10	18	6.9	Agnews State Hospital	27.0	0.17
13	Loma Prieta	1989	10	18	6.9	Anderson Dam (L. Abut.)	21.4	0.06
14	Loma Prieta	1989	10	18	6.9	Anderson Dam (Downstr.)	21.4	0.24
15	Loma Prieta	1989	10	18	6.9	BRAN	10.3	0.45
16	Loma Prieta	1989	10	18	6.9	Capitola	14.5	0.53
17	Loma Prieta	1989	10	18	6.9	Coyote Lake Dam (Downst.)	22.3	0.16
18	Loma Prieta	1989	10	18	6.9	Gilroy Array #4	16.1	0.42
19	Loma Prieta	1989	10	18	6.9	Gilroy - Historic Bldg.	12.7	0.28
20	Loma Prieta	1989	10	18	6.9	Fletcher Dr	28.2	0.25
21	Loma Prieta	1989	10	18	6.9	Hollister - South & Pine	28.8	0.37
22	Loma Prieta	1989	10	18	6.9	Saratoga - Aloha Ave.	13.0	0.51
23	Loma Prieta	1989	10	18	6.9	Sunnyvale - Colton Ave.	28.8	0.21
24	Loma Prieta	1989	10	18	6.9	UCSC	18.1	0.31
25	Loma Prieta	1989	10	18	6.9	WAHO	16.9	0.37
26	Loma Prieta	1989	10	18	6.9	Saratoga - W Valley Coll.	13.7	0.26
27	Cape Mendocino	1992	4	25	7.1	Fortuna - Fortuna Blvd.	23.6	0.12
28	Cape Mendocino	1992	4	25	7.1	Rio Dell Overpass - F	18.5	0.39
29	Landers	1992	6	28	7.3	Coolwater	21.2	0.28
30	Landers	1992	6	28	7.3	Desert Hot Springs	23.2	0.17
31	Landers	1992	6	28	7.3	North Palm Springs	24.2	0.14
32	Landers	1992	6	28	7.3	Sunland - Mt Gleason Av.	151.1	0.03
33	Landers	1992	6	28	7.3	Morongo Valley	19.3	0.19
34	Landers	1992	6	28	7.3	La Crescenta - New York	147.9	0.02
35	Landers	1992	6	28	7.3	Big Tujunga, Angeles Nat.	144.3	0.03
36	Landers	1992	6	28	7.3	LA - N Westmoreland	159.2	0.04
37	Landers	1992	6	28	7.3	Yermo Fire Station #	24.9	0.25
38	Northridge	1994	1	17	6.7	LA - Century City CC	25.7	0.26
39	Northridge	1994	1	17	6.7	Tarzana-Cedar Hill Nursery A	17.5	1.78

Table 3.A.1. List of recorded accelerograms used in Chapter 3. Notes: (1) M = Moment Magnitude; (2) R = Closest distance from fault-rupture to site.

	Event	year	month	day	M[1]	Station	R[2] [km]	PGA [g]
40	Northridge	1994	1	17	6.7	LA - Chalon Rd	23.7	0.23
41	Northridge	1994	1	17	6.7	N. Hollywood-Coldwtr. Can.	14.6	0.30
42	Northridge	1994	1	17	6.7	Canoga Park - Topanga	15.8	0.36
43	Northridge	1994	1	17	6.7	LA - N Faring Rd	23.9	0.27
44	Northridge	1994	1	17	6.7	Fletcher Dr	29.5	0.16
45	Northridge	1994	1	17	6.7	Lake Hughes #12A #	22.8	0.17
46	Northridge	1994	1	17	6.7	LA - Hollywood Stor F.	25.5	0.23
47	Northridge	1994	1	17	6.7	Lake Hughes #9	26.8	0.17
48	Northridge	1994	1	17	6.7	Canyon Country - W Lost Cany.	13.0	0.41
49	Northridge	1994	1	17	6.7	Moorpark - Fire Sta.	28.0	0.19
50	Northridge	1994	1	17	6.7	Beverly Hills - 12520	20.8	0.62
51	Northridge	1994	1	17	6.7	Beverly Hills - 14145	19.6	0.42
52	Northridge	1994	1	17	6.7	Castaic - Old Ridge R	22.6	0.57
53	Northridge	1994	1	17	6.7	Glendale - Las Palmas	25.4	0.36
54	Northridge	1994	1	17	6.7	Sun Valley - Roscoe Blvd	12.3	0.30
55	Northridge	1994	1	17	6.7	17645 Saticoy St	13.3	0.48
56	Northridge	1994	1	17	6.7	Stone Canyon #	22.2	0.25
57	Northridge	1994	1	17	6.7	Santa Susana Ground #	19.3	0.28
58	Northridge	1994	1	17	6.7	Santa Monica City Hal	27.6	0.88
59	Northridge	1994	1	17	6.7	LA - Saturn St	30.0	0.47
60	Northridge	1994	1	17	6.7	Pacific Palisades - S	26.2	0.47
61	Northridge	1994	1	17	6.7	Topanga - Fire Sta #	23.4	0.36
62	Northridge	1994	1	17	6.7	Vasquez Rocks Park #	24.2	0.15
63	Northridge	1994	1	17	6.7	Hollywood - Willoughb	25.7	0.14

Table 3.A.1 (cont.). List of recorded accelerograms used in Chapter 3. Notes: (1) M = Moment Magnitude; (2) R = Closest distance from fault-rupture to site.

Appendix 3.B. Structural Details.

The structural details for the structures considered in Chapter 3 are as follows, for the different systems considered:

1) SDoF systems. Oscillators were designed arbitrarily modifying masses and stiffnesses in order to tune the frequency of vibration. The yield displacements were adjusted in order to produce the desired median ductilities.

2) MDoF stick models. The 1Hz, 5-DoF stick system was based on the design of a 5-storied, 4-bay SMRF model (see details in Shome, et al, 1997). A step-by-step static nonlinear pushover analysis provided the parameters for the bilinear backbone. In order to produce the 0.25Hz and the 4.0Hz systems, the masses considered for the 1Hz system were scaled. The configuration and the parameters (for the 1Hz system) considered are as follows
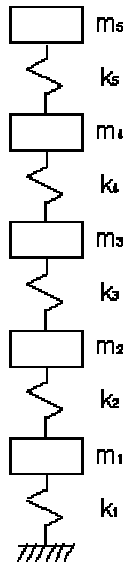
Figure 3.A.1 Spring-mass configuration for MDoF stick-models.

Story	δ_{yi} [in]	K_i [k/in]	K_{pi} [k/in]	m_i [ks^2/in]
1	1.2	302	24	0.58
2	1.8	182	19	0.58
3	1.7	169	15	0.58
4	1.6	148	10	0.58
5	1.6	112	8	0.24

Table 3.B.1. Parameters used for the MDoF model of the 1Hz stick systems

3) Two dimensional MDoF frame. The model was taken from Barroso, 1999. It represents a 3-story SMRF ductile 1Hz system designed as part of the SAC steel project for the Los Angeles area. The frame consists of three fully moment-resisting bays and one simply-connected bay (see Figure 3.B.2). The expected yield strength for the columns' steel was 57.6ksi, and for the beams' steel was 49.2ksi. The column and beam sections are shonw in Table 3.B.2.
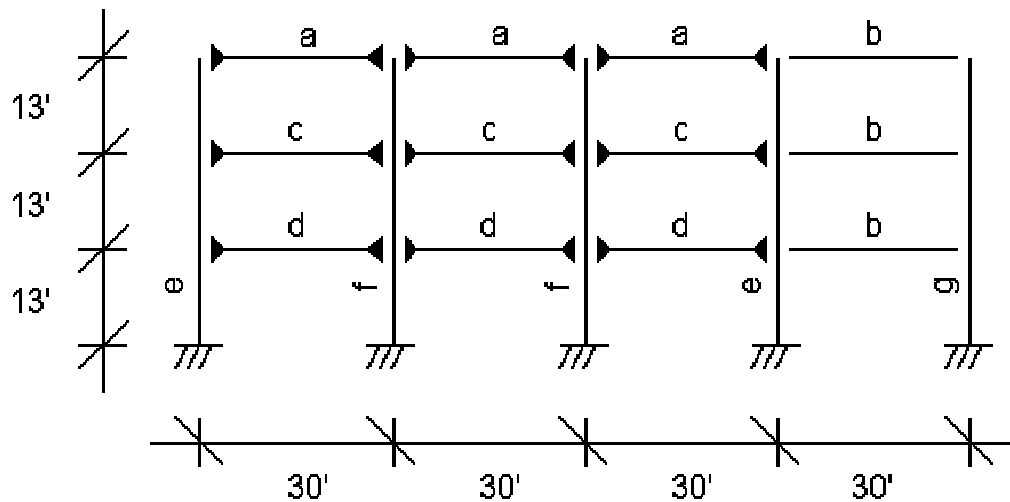
Figure 3.B.2. Configuration of the two-dimensional SMRF used in Chapter 3 (for further details see Barroso, 1999).

Beams		Columns	
type	section	type	section
a	W24x68	e	W14x257
b	W21x44	f	W14x311
c	W30x16	g	W14x68
d	W33x118		

Table 3.B.2. Column and Beam sections for the 2-dimensional SMRF used in Chapter 3.

Chapter 4

A Direct Probabilistic Seismic Design Procedure

4.1 Introduction.

A design procedure is presented for structures in a seismic environment, which ensures that a prescribed probability of *failure* is met. The proposed approach is a "top-down" approach in that, starting from an *appropriate* failure-level ground motion intensity, a value for a specific gross measure of the behavior of the structural configuration is assumed (and subsequently verified). This measure spans from the highly nonlinear domain at failure down to the elastic domain, permitting one to establish site and structure-specific (lower) *design-level loads* for detailed sizing in the conventional manner (e.g., via typical, linearly based Working Stress Design or Load and Resistance Factor Design based codes). In general, traditional design schemes are, in contrast, "bottom-up", starting with a standard annual-probability-based *ground motion intensity* for the member-sizing level, and, at best, checking via nonlinear dynamic analysis to see if the failure probability achieved is satisfactory.

First, the methodology will be presented, and then its application will be exemplified in order to illustrate and clarify it (with a three dimensional model of an offshore steel jacket). For transparency, detailed issues that may arise in the implementation of the method are discussed in appendices to this chapter and in Chapter 5. For example, the

best seismic intensity to consider, and the most appropriate response to observe; these are problems that need to be addressed in the three-dimensional case. The focus here, however, is on the method itself.

Traditional structural seismic design schemes have considered the actions that could be related to a single earthquake design level. These schemes introduce a major inconsistency in terms of the probability of failure for systems designed in different seismic regions, even though the different region-based design level earthquake loads consider adequately the respective seismic environments. Due to the differences in the overall seismic hazard (which can be characterized, for example, by a hazard curve like that of Fig. 4.1) for two regions, the ground motions that are likely to be associated to failure level intensities, may have very different return periods. Even though the design loads might have had the same return periods, the previous fact may be reflected in potentially very different probabilities of failure.

Current typical building design provisions define earthquake design levels as ground motions associated to a probability of exceedence (PE) of 10% in 50 years (or, equivalently, a 475 year mean return period) (e.g., SEAOC, 1996). The corresponding seismic forces to consider are permitted to be reduced to allow for the consideration of energy dissipation due to structural nonlinear behavior. Other than for such reduction, such postelastic behavior is not explicitly considered in the sizing. It isn't even always tested or verified by nonlinear structural analyses. Typically, the assumption on the force reduction given a ductile behavior (provided for example, by appropriate detailing) will be considered valid.

Current trends recognize the need to quantify the response at higher ground motion levels: those related to less frequent but stronger intensities. For example, current bridge design criteria (e.g., ATC-32, 1996), have evolved in the past ten years from the single 10% in 50 year consideration (ATC-6, 1986). The former recommends that member sizing be made taking into account the less frequent *Safety Evaluation* level ground motion which is defined "probabilistically as an earthquake with a 1000- to 2000-year

return period" (or a PE of 2.5 to 5% in 50 years). At the lower level, the more frequent *Functional Evaluation* level loads (with return periods around 100 years, or PE of 40%-in 50 years) are assumed to be adequately resisted by ordinary bridges.

For fixed offshore structures, recommendations for seismic design are by means of the lower return period ground motion (200 years in this case or PE of around 20% in 50 years), namely, the *Strength Level Earthquake (SLE)* (API, 1993). Such recommendation will, however, require that ductility assumptions do indeed hold for the "rare, intense earthquake without collapsing". They require that sufficient reserve strength for the structure be verified, which is done with the strong and infrequent *Ductility Level Earthquake (DLE)* (with average return periods in the range of a few thousand years (Bea, 1995)).

The actions to consider for design are associated with fixed probabilities of exceedence of the *ground motion*. In contrast to these previous procedures, the method that is described here prefixes a probability of *response* of the structure itself. This takes into account both its uncertain seismic environment, and its response to the irregular ground shaking. In what follows it is presumed that the topology and global geometry of the structure to be designed have been selected.

4.2 Methodology.

The criterion of failure for the design scheme proposed is defined here as the event where a particular deformation of the structure exceeds a certain limit; that limit is the deformation "capacity". The value of *Pt* is the starting point from which one can derive a related target *intensity*-capacity (i.e., in terms of the ground motion) of the structure, and subsequently an initial design parameter for sizing the structure such that the goal is likely to be met. The process is done in two stages: the first involving a design based on preliminary trial parameters for representing the global behavior of the structure, and the

second stage consisting of verifying that the detailed design meets the target *Pt* and modifying the structure if it doesn't.

For the first stage, initial (preliminary) values for the parameters that represent the global behavior of the structure, responding to the site's seismic environment, are chosen. Such a seismic setting can be described in terms of a seismic hazard curve associated with a spectral acceleration at a particular reference frequency, which for this study will be taken at or near the fundamental frequency of the structure. Thus, one (trial) parameter required is the fundamental frequency, f_0, of the structure, in order to select the appropriate hazard curve to use. For these purposes the value of f_0 can be estimated sufficiently adequately by past experience (e.g., for a fixed jacket with known configuration in a given water depth, a building with a known structural system and given height, etc.; it is common to find empirical equations for this value in current codes). The response of the structure to the environmental actions (described in terms of the spectral acceleration) can be represented adequately by an appropriate scalar value. For example, for the illustration presented in section 4.3 this scalar was chosen to be the offshore jacket's deck maximum displacement (*dmd*) in either direction (see Appendix 4.A for a further discussion on this selection). For buildings the maximum interstory displacement is the logical candidate.

In a manner that will become apparent later, the target probability of failure is linked to a sought-after capacity of the structure, a capacity represented in terms of the seismic intensity measure, the spectral acceleration[1] at f_0. The (capacity) spectral acceleration is the one we will calibrate the structure to, so we call it the "target spectral acceleration capacity", Sa_{ct}. Such a capacity can be understood in a dynamic sense: it is the spectral acceleration of a seismogram that is "expected" in some sense (to be more carefully defined below) to cause the structure to be on the verge of failure.

---

[1] Equivalently, this might be expressed in spectral displacement terms, $Sd = Sa /(f_0^2 \, (2\pi)^2)$. Spectral acceleration is perhaps to be preferred for traditional force-based design schemes.

To reach the bottom of the top-down design procedure, where a design spectral acceleration, Sa_d, is proposed, one needs to have a preliminary estimate of the reserve "strength" of the structure from design level up to failure level, in terms not of force but of spectral acceleration (i.e., in a dynamic sense). In the fixed offshore structures wave design realm, there is an analogous quantity, in terms of base shear force: the *Reserve Strength Ratio, RSR* (as defined, for example, in Stahl, et al, 1998). We will denote this *spectral acceleration* reserve strength by ρ_{Sa}. This parameter will allow us to deduce a spectral acceleration for sizing from the target spectral acceleration capacity, Sa_{ct}, i.e., $Sa_d = Sa_{ct} / \rho_{Sa}$. The estimation of ρ_{Sa} will is discussed below.

A less sensitive third assumption needed is related to the particular way the probability of the structure's failure is computed, and to how the target spectral acceleration capacity, Sa_{ct}, is deduced from the target probability of failure. The probability of failure is the annual likelihood that the structure's maximum dynamic response exceeds the capacity. This probability can be expanded (by the familiar total probability theorem) into an integral over the product of the probability distribution of the ground motion intensity and the conditional distribution, given intensity, of the structure's dynamic response. This can be seen as a random variable given the input spectral acceleration. If this input-to-response relationship were deterministic, then the probability of failure could be identically described either by the probability of the response exceeding capacity, or by the probability of the spectral acceleration exceeding the spectral acceleration corresponding to such capacity. In the more general random intensity-to-response case, however, the probability of the structure to fail can be conveniently decomposed into the product of (1) the probability of exceedence of a median or similar such central estimate of the ground spectral acceleration that causes failure (such probability being given by the hazard curve evaluated at this value), and (2) a *correction factor* that takes into account the aforementioned randomness in the relationship between the response and the ground motion (Cornell, 1995) (described in more detail ahead, Eq. 4.10). The value of this correction factor, which we will refer to as *Cf*, will also be estimated a priori, and then confirmed or re-evaluated at a second step.

In the subsequent sections it will become apparent how these estimates are utilized in generating the important first iteration of the design. Once this first sizing is completed, compliance with the target probability of failure needs to be verified. If the desired performance is not met then the structure is modified until it is, either by trial and error or iterating the procedure using more informed (updated) estimates of the various factors.

4.2.1 First Iteration: Original Design.

The first trial value needed, the value of first modal frequency, f_0, will allow us to collect the appropriate seismic hazard information. This will be in terms of a hazard curve, describing the exceedence probability for any level of the spectral acceleration associated with the fundamental frequency of the structure.

As mentioned earlier, the target probability of failure is the starting point to determine a capacity of the structure we are aiming for, in terms of spectral acceleration. For the moment, let's assume we already know what the spectral acceleration capacity of the structure ought to be, in order to explain how the design parameter is computed.

The sizing of structural elements can also be done in terms of a spectral acceleration, which we will call the *design spectral acceleration*, or Sa_d. Such a value is customarily used in conjunction with a design spectrum, for elastic response spectrum analysis, by scaling the design spectrum to have the same value as Sa_d at the structural frequency f_0. Alternatively, it could be used in linear dynamic analyses, scaling appropriate accelerograms in a similar manner. Hence, once the value of Sa_d is determined we have the means for generating our original design. Clearly, Sa_d is a fraction of the capacity Sa_c, and can be related to it by a factor, the dynamic reserve strength ratio, ρ_{Sa}, as given by the following relationship:

$$Sa_d = Sa_c / \rho_{Sa}. \tag{4.1}$$

The reserve strength ratio is a property of the structure; it should reflect the ability of the structure to perform adequately in the nonlinear range. Such ratio is related to the design method (e.g., WSD or LRFD), to how efficient the design was made (e.g., how close the members' interaction ratio values were to 1.0), and to a lesser extent, to how the internal actions were found, e.g., whether the chosen analysis scheme was an elastic dynamic analysis or simply response spectrum based. The initial trial value of ρ_{Sa} may perhaps be estimated simply from engineering experience.

The ρ_{Sa} ratio is in spectral acceleration terms; the designing engineer is likely, however, to feel more comfortable estimating relationships among displacements. An alternative approach to estimating the value of ρ_{Sa} relies on establishing an approximate functional relationship between the displacement response of the structure (e.g., a maximum offshore platform deck displacement, or an interstory building drift, etc.) and the spectral acceleration. In a median sense (since the response of the structure will be in general somewhat different for different time histories used in the dynamic analyses) we can adopt a convenient functional form (analogous to Eq. 3.16):

$$\delta_{med} = a \, Sa^b ,$$
(4.2)

in which δ_{med} is the median maximum response given ground motions of intensity Sa, and a and b are empirical constants. We can use this relationship to deduce the ρ_{Sa} from the ratio of the displacement capacity to the design displacement. Such a displacement ratio is best thought of as being the product of two factors, one representing the linear range and the other the post-elastic response range. The latter is the familiar (system) ductility factor, μ (the ratio of capacity displacement, δ_c, to yield displacement, δ_y). It is the most prevalent coefficient used to characterize and compare the seismic "robustness" of different systems. Therefore it is presumed that this may be the preferred starting point for trial estimates. The capacity ductility will be denoted μ_c. Besides μ_c, we need the ratio between the effective elastic limit displacement (i.e., the displacement at the onset of a

significant non-linear force-deformation dependence), and the displacement at the design level loads. This relationship is commonly better understood in terms of forces; for a linear system it just equal to the base shear at first yield divided by the base shear at the design level, and will be denoted by N. The value of N is typically between 1.0 (the lower bound value) and 1.5 depending on the design code employed and the efficiency of the design.

The capacity to design level displacement ratio is the product $\mu_c * N$:

$$\delta_c / \delta_{design} = (\delta_c / \delta_y) * (\delta_y / \delta_{design}) = \mu_c * N ,$$
(4.3)

or, using Eq. 4.2,

$$\delta_c / \delta_{design} = (Sa_c / Sa_d)^b = \rho_{Sa}^b ,$$
(4.4)

yielding:

$$\rho_{Sa} = (\mu_c * N)^{1/b} .$$
(4.5)

In order to compute the value of ρ_{Sa}, we need then to use estimates of the values of μ_c, N and the exponent b. The value of b in Eq.4. 2 is of course simply unity if, as is commonly observed in simple ductile oscillators in period ranges above 0.5sec (Chopra, 1995), the inelastic displacements are approximately equal to the displacements of the corresponding elastic oscillator. This may be a reasonable value for initial trial purposes. Experience with MDoF systems has shown that this factor may range from about 0.7 to 1.5.

Finally, whether ρ_{Sa} is estimated directly from experience or via Eq. 4.5, we can compute the design parameter from the target capacity from Eq. 4.1. Repeating,

$$Sa_d = Sa_c / \rho_{Sa}.$$ (4.1, 4.6)

Returning to the capacity sought for the structure, it can be recognized that it will depend directly on the specified level of the target failure probability, *Pt*. Hence, it can be thought of as a *target* spectral acceleration capacity, or Sa_{ct}. As mentioned earlier, if the structural dynamic response were deterministically given to us by a relationship such as Eq. 4.2, we could directly compute its value by using the appropriate hazard curve and the target probability of failure, *Pt*. The computation of probability of failure can be written for this hypothetical case as:

$$Pf = P[\delta > \delta_c] = P[a\,Sa^b > a\,Sa_c{}^b] = P[Sa > Sa_c] = H[Sac],$$ (4.7)

where H[*y*] (the spectral acceleration hazard curve) is the probability that the ground motion intensity (represented by spectral acceleration, *Sa*) exceeds the value *y*. Here Sa_c is the spectral acceleration that causes the structure to reach its displacement capacity.

Setting the probability of failure to the prescribed target, and using the previous equation inversely, we can solve for the target spectral acceleration capacity *required* to meet *Pt*:

$$Sa_{ct} = H^{-1}[Pt].$$ (4.8)

Here H^{-1} is the inverse of the function H[*y*], i.e., H^{-1}[*Pt*] is the spectral acceleration exceeded with probability *Pt*. Thus, combining equations (4.6) and (4.8), for this simplistic case the design level spectral acceleration to be used for member sizing would simply be:

$$Sa_d = H^{-1}[Pt] / \rho_{Sa}.$$ (4.9)

This may be considered to be a first-order estimate of Sa_d. The computation of the probability of failure and subsequently of Sa_{ct} and Sa_d can, however, be refined to a second-order approximation by including the randomness in the response and in the displacement capacity.

As mentioned above, the computation of the probability of the structure to fail can be conveniently decomposed into the probability of the capacity target spectral acceleration to be exceeded, H[Sa_c], multiplied by a correction factor, *Cf*. This factor carries information on the level of dispersion of the displacement response given the level of the ground motion intensity and the uncertainty on the capacity itself, as well as the sensitivity of the response to the ground motion. The more general computation of the probability of failure can be written therefore in the following way:

$$P_f = P[\delta > \delta_c] = P[demand\ displacement > capacity\ displacement] = H[Sa_c] * Cf \quad (4.10)$$

Previous empirical knowledge of the value of *Cf* can provide for a good estimate. Such values can typically range from 1.2 to 3.5 (see Cornell, 1995). Also, an estimate of *Cf* can be analytically computed by an approximate approach (see Appendix A), via the following equation:

$$Cf = e^{[\frac{1}{2}(\frac{K_0 \sigma_t}{b})^2]} \quad , \quad (4.11)$$

in which K_0 is the slope (in a region surrounding the target probability of failure) of the hazard curve in a log-log-scale (Fig. 4.1); *b* is the estimated exponent of the median displacement given spectral acceleration, as described by Eq. 4.2; and

$$\sigma_t^2 = \sigma_\delta^2 + \sigma_{\delta_c}^2 \quad , \quad (4.12)$$

in which σ_δ is the standard deviation of the natural logarithm of the maximum response given spectral acceleration and σ_{δ_c} is the standard deviation of the natural logarithm of

the displacement capacity. These standard deviations are approximately equal to the coefficients of variation (c.o.v.) of these random quantities.

These last equations allow us to arrive at an analytic estimate of the value of Cf, provided we assume values for b and σ_t (or σ_δ and $\sigma_{\&}$), and by finding an appropriate value of K_0 from the corresponding hazard curve. Eq. 4.11 has been derived by approximating the hazard curve H[y] by a linear function in logarithmic space, using the slope of the curve in the region of failure (near Sa_c), as well as considering lognormal distributions for the displacement capacity and for the displacement given spectral acceleration of the ground motion. (See Appendix A for a derivation).

It is worthwhile noting that including such a correction factor is effectively only a second-order refinement in that it will normally not dramatically change the value of the target spectral acceleration capacity sought. We can see this in terms of the hazard curve slope, K_0. For representative relatively small values of σ_t (e.g., 0.3 to 0.4), and for values of b close to unity, the value of Cf increases exponentially in K_0^2, e.g., about $\exp(K_0^2/20)$. Under the assumed linear approximation in logarithmic space of the hazard curve, however, the implied effect on the target spectral acceleration is only $\exp(K_0/20)$. For typical values of K_0 (e.g., 2 to 4) this is a factor of only 1.1 to 1.2. The second-order estimate is only about 10% to 40% larger than the first-order estimate. In particular, the target spectral acceleration is insensitive to uncertainty in the estimates of σ_t, K_0 and b. Therefore, one might simply choose to use the first order estimate (i.e., Eq. 4.9) increased by 25%.

As done previously, by setting the probability of failure to the prescribed target, and using Eq. 4.10 inversely, we can solve for the target spectral acceleration capacity required to meet Pt:

$$Sa_{ct} = H^{-1}[Pt/Cf],$$
(4.13)

and finally, the design spectral acceleration can be computed as before by using the reserve strength ratio:

$$Sa_d = Sa_{ct} / \rho_{Sa} = H^{-1}[Pt/Cf]/\rho_{Sa} \ .$$
(4.14)

This was our objective. This value can be used as the level of a traditional design spectrum. One can use it for a response-spectral based structural analysis, or as a basis to scale the record(s) to use for a linear dynamic analysis. Consistent with this design level, member sizing should be based on conventional guidelines (e.g., API RP-2A, UBC, etc). It should be noted that, in contrast to Sa_{ct}, Sa_d may be somewhat sensitive to uncertainty in the estimate of b (if the ρ_{Sa} is determined via Eq. 4.5). A mis-estimation of Sa_d may affect the gross first-trial member sizes, but it will have a lesser effect on relative member sizes. Any such mis-judgements in these first trial values will be identified in the subsequent analyses of the trial design. Also noteworthy is the fact that this spectral intensity may be related to return periods not typical of the design-level earthquake (for example H[Sa_d] 1/200 , the value that API, 1993, would suggest).

4.2.2 Subsequent Iterations : Updated Information.

Once the original design is completed the most important verification needed to be made is that of the compliance to the desired performance. In this case this is defined by the failure probability. If the probability of failure is not that of the target, the design may need to be adjusted.

Computation of *Pf* can be a difficult task. However, various simplifications can be made in order to find an estimate with reasonable effort. For example, as mentioned above, the factor *Cf* in Eq. 4.11 to be used in the computation of probability as described by Eq. 4.10, was derived by making some of these simplifications.

The median response of the structure was considered to be described by Eq. 4.2. The parameters of such a relationship can be obtained by performing nonlinear dynamic analyses on the structure at various levels of spectral acceleration. For a fixed level of intensity (*Sa*), the response of the structure will vary for the different ground motion time histories employed in the analysis. It is reasonable to assume that, given the spectral acceleration of the input, the response of the structure is lognormally distributed (Shome et al, 1998) and that in a median sense Eq. 4.2 holds. A simple linear regression of the logarithm of the response on the logarithm of the spectral acceleration of the ground motion will provide us with estimates of the required parameters, based on the following transformation of Eq. 4.2:

$$\ln(\delta_{med}) = \ln(a) + b \ln(Sa) .$$
(4.15)

Given the typical level of record-to-record dispersion about this regression line (i.e., more or less 30 to 40%) one would prefer to have on the order of 10^+ "data" points to estimate $a' = \ln(a)$ and b. When the nonlinear analyses are resource intensive, engineering experience can be used to allow the regression to be performed based on an even smaller set of runs. The value of the slope b can be reasonably assumed, so only a few runs (about 5) can permit us to find the missing value of a. Another result given to us by the regression is an estimate of the dispersion, σ_δ, which is defined as the standard deviation of $\ln(\delta)$. Such a small sample result, however, has a wide confidence interval, and hence should be used with care. Previous experience should also guide us in the estimation of this parameter when only a few data points are used in the regression. As discussed, however, this estimate affects only the "second-order" factor *Cf*.

Since we are ultimately interested in the near-failure behavior of the structure, we can perform the nonlinear runs with records having spectral accelerations around the computed value of Sa_{ct}, where failure is expected to occur. Recall that Sa_{ct} is relatively insensitive to the trial parameter estimates. One can use a different record at each of several Sa values in this region of interest, or multiple scaled levels of each of several records. A criterion for the selection of records can be based on choosing those from

events with a magnitude and distance combination that contributes most importantly to the hazard at Sa_{ct} (e.g., McGuire, 1995, Bazzurro and Cornell, 1999).

It is also assumed here that, independently from the value of the displacement given spectral acceleration (i.e., the displacement "demand"), there is a random value of the displacement *capacity*, considered to be lognormally distributed. This random variable (δ_c) is described by a median value, δ_{cm}, and the standard deviation of the logarithm, $\sigma_{\delta c}$. (used in Eq. 4.12). Lacking today better options, the value of the median δ_{cm} can be reasonably estimated from inspection of the results of a nonlinear *static* "pushover" analysis (e.g., as described for bridges in ATC-32). Once again, engineering experience will provide us with a sensible value of the dispersion, taking into account not only the variation of the capacity of the structure, from (a real) event to event, but also the fact that the median value was estimated from a static approach, and not a dynamic one.

A first-order check to verify that the target probability of failure constraint has been met can be done in terms of confirming that the median displacement associated with the target spectral acceleration is in fact lower than the median displacement capacity. If the nonlinear dynamic runs are all performed exactly at the target spectral acceleration capacity, then the median observed displacement can be directly compared to the median capacity; otherwise, solving for the median displacement by means of Eq. 4.2 evaluated at Sa_{ct}, with the selected value of *b*, and the regressed value of *a*, will allow us to perform such a comparison. It is worth mentioning that in terms of this first-order check, the selection of the value of *b* is not critical. Because these runs have been made with *Sa* values at or near Sa_{ct} the regression will adjust the value of *a* to the data accordingly, as will be seen in the next section's example.

With the information gathered thus far, the computation of the probability of failure can be written out in terms of an integral, using the total probability theorem:

$$P_f = P[\delta > \delta_c] = \int_0^\infty P[\ln(\delta) - \ln(\delta_c) > 0 \,|\, Sa = u] f_{Sa}(u) du \tag{4.16}$$

where f_{Sa} is the (absolute value of the) derivative of the hazard curve, and represents the probability density function of spectral acceleration. Because $\ln(\delta)$ is normally distributed given spectral acceleration, and is independent of the also normally distributed $\ln(\delta_c)$, their difference is also normal, so the integrand reduces to a cumulative normal density with standard deviation, σ_t, given by Eq. 4.12, multiplied by the density function of the spectral acceleration.

The probability of failure can now be computed numerically with Eq. 4.16 or it may be estimated analytically under the assumptions in Appendix A, which can be written as:

$$P_f = H[(\delta_{cm}/a)^{1/b}] Cf , \tag{4.17}$$

where Cf is given by Eq. 4.11. The value of σ_t may have been updated based on the observed scatter about the regression discussed above. The argument in H[.] corresponds to the value of Sa that would cause a median displacement with a value of δ_{cm}.

By definition of the problem, it is required that Pf be less or equal than Pt. If this is not the case, then the structure needs to be improved from a reliability point of view. This means that either the displacement demands on the structure need to be reduced, or the displacement capacity needs to be increased, or a combination of both needs to occur. Displacement-based redesign is not a straightforward task. Increasing the *force* capacity typically also increases the stiffness, which has a counteracting effect on the yield displacement capacity. Increasing the stiffness typically does, however, reduce the elastic displacement demand for moderate to long period structures. This depends somewhat on the spectral content of the records. If the original design's analysis, which should include a static (nonlinear) pushover as well as the dynamic analyses, suggests that only one or two components (braces, piles, etc) are failing significantly prior to others, then they

alone might be reinforced accordingly. This can increase yield force capacity "faster" than it increases stiffness. The net effect of such local strengthening on the post-yield displacement capacity is, however, still more difficult to predict.

One global approach to displacement-based re-design to consider is based on the same general scheme discussed above. It requires computation of an updated design spectral acceleration, Sa_d'. Such a design parameter is computed in the same way the original value was computed using, however, not the initial empirical/trial values in equations (4.13) and (4.14) of the correction factor, Cf, and the dynamic reserve strength, ρ_{Sa}, but the actual implicit values found from analysis of the first design of the structure.

The actual capacity of the structure can be expressed in terms of spectral acceleration, which will be denoted by Sa_{c0}; it is obtained by solving for the spectral acceleration in Eq. 4.2, using the corresponding displacement capacity found in the static nonlinear pushover analysis. The result is $Sa_{c0} = (\delta_{cm} / a\ )^{1/\,b}$ which is just the argument of H[.] in Eq. 4.17. Note that if the Pf has been obtained by numerical integration rather than by Eq. 4.17, we can solve for the implicit correction factor, Cf_0:

$$Cf_0 = Pf / H[Sa_{c0}].\qquad(4.18)$$

The updated target spectral acceleration capacity required to meet the target probability of failure is computed as previously done, by means of Eq. 4.13, using now the updated correction factor Cf_0 (e.g., Eq. 4.18). In order to find the updated design spectral acceleration we need to compute the actual dynamic reserve strength ratio for the structure, ρ_{Sa0}. This is done by dividing the current spectral acceleration capacity, Sa_{c0}, by the original (initial) design spectral acceleration that was used to design the structure initially:

$$\rho_{Sa0} = Sa_{c0} / Sa_d.\qquad(4.19)$$

This revised ρ_{Sa0} value (for this first design) contains implicitly updated information on the design-to-elastic-limit and elastic-limit-to-failure ratios (Eq. 4.3), which initially were simply assumed trial values.

The updated design spectral acceleration required to meet the target Pt is computed with Eq. 4.14. The ratio between this updated value and the original design spectral acceleration can be used as a guideline for increasing the strengths of the structural elements. As discussed in Appendix 4.B, the relationship is not simply one-to-one. That is, because of the issues discussed above, if the updated value is 50% larger than the first it does not imply that a simple 50% force capacity increase should be applied. Appendix 4.B discusses this further.

Having improved the structure, once again the probability of failure should in principle be verified by a new set of non-linear analyses to confirm that the target has been met.

4.2.3 Summary.

Summarizing the procedure described in the previous sections, the design steps are as follows:

1) Define the target probability of failure, Pt, to be met.

2) Make assumptions about the structure to estimate the initial trial values of: (a) the structure's first natural frequency, f_0; (b) the correction factor Cf (or alternatively, use Eq. 4.11 with assumed values of the parameter b and σ_t, as well as the hazard curve slope K_0), and (c) the dynamic reserve strength ratio, ρ_{Sa} (or alternatively Eq. 4.5) with the required assumed values). Of the three, ρ_{Sa} is the only one to which there is a first-order sensitivity.

3) Find the required spectral acceleration capacity, Sa_{ct}, associated to Pt (Eq. 4.13), and then the value of the design spectral acceleration, Sa_d, (Eq. 4.14) for member-sizing of the original structure using conventional linear elastic procedures and design codes and guidelines.

4) Perform several dynamic nonlinear analyses (e.g., using records with spectral acceleration equal or close to the target capacity, and use log-linear regression to estimate a, and possibly to revise the values of b and σ_δ). Perform a static nonlinear pushover analysis to estimate the "median" value of the displacement capacity, δ_{cm}.

5) Compute the probability of failure, using either the analytical approximate approach (Eqs. 4.10 and 4.11), or by numerical evaluation of the integral in Eq. 4.16, to verify compliance with the target value.

6) Resize elements if the target reliability is not met; if appropriate update trial values above for revision of the level of the design spectral acceleration, Sa_d, for subsequent resizing.

4.3 Numerical Example.

The following example considers a steel offshore jacket for design using the proposed scheme. The objective is to illustrate the steps and clarify the procedure. The behavior of wave-exposed fixed offshore systems can be characterized in a similar manner, and an example for a reliability-based design scheme for such loads of a similar structure is presented in Manuel, et al,1999.

4.3.1 Definition of the Target Probability of Failure, Pt.

For this example the target probability of failure, *Pt*, is selected to be 1/2000 (0.0005) per year (as suggested in Stahl, et al, 1998). The definition of failure considered here is the exceedence of a capacity related to a deck maximum displacement (*dmd*), which will be selected from a static nonlinear pushover analysis.

4.3.2 Problem modeling assumptions and initial trial values.

The hypothetical structure in consideration is a fixed steel jacket for offshore oil production, presumed to be located off the California coast. The structural configuration consists of a regular 3-dimensional, 5-tiered k-braced system, 310 feet tall, and cross section tapering from a 135' by 135' base to a 72' by 72' deck level top. The assumed trial dynamic properties of the jacket are first mode elastic period $T_0 = 2.0$ seconds, and damping of 2% of critical. The jacket is based on a design employed in Dalane, 1993 (which is also the basis for the example presented in Manuel, et al, 1999). See Appendix 4.D for structural member details. Figure 4.2 shows a schematic of the structural configuration.

The hazard corresponds to the seismic threat at a site in the California Sta. Barbara Channel. From the site seismic hazard analysis, a hazard curve for 2.0sec (0.5 Hz) was computed (Fig. 4.1), and a scenario event representative of the hazard was selected, with a magnitude M = 6.85, and distance R = 4.0 km. Four different earthquake events corresponding to the scenario event were chosen (although corresponding to larger distances, to avoid near-source issues that were not dealt with here) (see Appendix 4.C).

Once the structural dynamic frequency of the system was assumed and the environmental hazards identified, the probability correction factor, *Cf*, and the reserve dynamic reserve strength ratio, ρ_{Sa}, were estimated in order to find an associated target spectral acceleration capacity, and subsequently the design spectral acceleration.

For this example, the assumption that the dynamic nonlinear characterization of the structure can be represented by the functional form given by Eq. 4.2 was made, hence an estimate of the correction factor computed by means of Eq. 4.11 was used. From the hazard curve, the absolute value of the slope K_0, in a region of probabilities close to Pt, is estimated to be 3.17. Several studies (e.g., Luco and Cornell, 1998) and results generated for this structure (Appendix 4.A.3) indicate that an estimation of the exponent b in Eq. 4.2 can be taken to be less than unity, e.g., $b = 0.7$. Also, a total standard deviation, σ_t, was assumed to be 0.38, based on experience. With the above values, we can compute an initial estimate of the value for the correction factor, by means of Eq. 4.11:

$$Cf = e^{\left[\frac{1}{2}\left(\frac{K_0\sigma_t}{b}\right)^2\right]} = 4.4 \ .$$

(Note: this value of Cf may be larger than typical values, due to the lower-than-unit value of b assumed).

In order to find the value of the design spectral acceleration, Sa_d, we need to estimate a value of the reserve dynamic strength ratio, ρ_{Sa}, by using Eq. 4.5. We can reasonably assume an initial trial value of the capacity ductility to be $\mu_c = 2.0$, given the non-ductile nature of the braced frame structural configuration. Also, let's assume a value for the ratio of elastic-limit displacement to design level displacement of $N = 1.5$, for member sizing based on API RP2A-WSD, i.e., a working-stress design guideline. Using Eq. 4.5 we have:

$$\rho_{Sa} = (\mu_c * N)^{1/b} = (2 * 1.5)^{1/0.7} = 4.8$$

4.3.3 Design Spectral Acceleration.

Having the initial assumptions of the numbers we need, we can now compute the design spectral acceleration. Using the hazard Eq. 4.10 inversely, to solve for the target spectral acceleration capacity, as indicated by Eq. 4.13, we obtain:

$$H[Sa_{ct}] = Pt \,/\, Cf = 1/8640 = 0.00012.$$

Therefore,

$$Sa_{ct} = H^{-1}[1/8640] = 980 \text{ cm/s}^2 \approx 1 \text{ g.}$$

Finally, via Eq. 4.14 the design spectral acceleration was:

$$Sa_d = Sa_{cr} \,/\, \rho_{Sa} = 980 \text{ cm/s}^2 \,/\, 4.8 = 204 \text{ cm/s}^2 \approx 0.2 \text{ g.}$$

It may be noted that the annual probability of exceeding this design level is close to 1/160 (≈ 0.0063), 26% higher than the 1/200 *Strength Level Earthquake,* specified by API-RP2A-WSD, hence the seismic intensity for design is lower than that normally considered for the *SLE.*

This spectral acceleration value, Sa_d, is now used for sizing the structural elements. In our case, the jacket was designed based on a response spectrum analysis. The design spectrum was taken to be the spectral shape associated to the scenario event scaled to the design spectral acceleration. The sizing criteria correspond to API's working stress design code (API RP 2A-WSD). See Appendix 4.A.1 for details on the properties of the sized elements.

4.3.4 Structural Analyses.

The static and dynamic analyses performed on the structure were required to compute the probability of failure of the designed structure, and to verify that it was close to the target value. For these analyses, the nonlinear finite element code *CAP* was used (PMB-Bechtel, 1994).

Firstly, a static nonlinear pushover analysis provided us with information on the displacement capacity of the structure. Figure 4.3 shows us the pushover curve for the structure, on which we can identify the elastic limit for the displacement as well as select a "representative" (albeit difficult to identify with precision) displacement capacity.

The corresponding values, taken from the curve are:

$\delta_y = 0.72'$,
$\delta_{cm} = 1.4'$.

Although the elastic limit can be precisely identified, the value for the capacity was selected by judgment; it corresponded to the "last" highest strength drop that occurs at the buckling of diagonals. It also corresponds, coincidentally, to the ductility capacity considered in step 4.3.2, since $\mu = 1.4/0.72 \approx 2$. Throughout the example, the definition of δ_{cm} will be kept as the elastic limit multiplied by such value of ductility capacity.

Indirectly, compliance to the target probability of failure can be "verified" (in a first order approximation) by comparing the median displacement of the structure, responding to records with spectral acceleration at the estimated target spectral acceleration capacity, to the displacement capacity indicated by the pushover curve (see Fig. (4.4)).

In a dynamic sense, we're interested in knowing the (random) response of the structure to ground motions of different specified intensities, as given for example by the spectral

acceleration at, or near, the fundamental frequency of the un-yielded structure[2]. Failure was anticipated to occur at spectral accelerations around Sa_{ct} of 1g, because our design is keyed to this target value. Therefore nonlinear dynamic analyses were performed with the selected seismograms scaled such that their spectral accelerations were around this value (see Shome, et al, 1998, for a discussion on record scaling). The results allowed us to fit the displacement vs. intensity model in that region, and hence estimate the median displacement at spectral accelerations around $Sa_{ct.,}$ to verify that the probability of failure is below the target (i.e., that *Pf* is less or equal to *Pt*). The results of six nonlinear runs (See Appendix 4.C for the description of the records) (two time histories are scaled to two different values and two time histories are used only once) in terms of deck maximum displacement (*dmd*) are shown in Table 4.1.

For this example we relied on previous "knowledge" of the value *b* in the linear regression of the logarithms, in order to estimate the value of *a* in Eq. 4.2 for determining the best fit for the displacement given spectral acceleration. The regression yields, for a fixed value of $b = 0.7$:

$a = 2.00$ (for *dmd* in feet and *Sa* in g),

$\sigma_{ln\delta} = 0.34$.

It should not be forgotten that the value of the dispersion obtained with a regression with such limited data points has a very broad confidence interval, and should be used with care, when computing the total probability of the structure to fail.

Figure 4.4 shows us the data points and the regression model. It can also be seen in the figure that the median displacement associated to the target spectral acceleration value

---

[2] An eigenvalue analysis of the initial structural design confirms that its fundamental period (1.9 sec) is close to the trial assumption of 2 seconds. However, it is not critical that the fundamental period of the structure be within more than about ± 20% than that of the frequency related to the spectral acceleration used to define the intensity of the ground motion (in the hazard curve, response spectrum, and time histories). (See Shome, et al, 1998). The definition of ground motion intensity was defined to be fixed, at the spectral acceleration related to the initial trial fundamental frequency of the structure, and kept throughout the whole procedure.

(i.e., 1g) exceeds that of the displacement capacity (i.e., 1.4') obtained from the pushover analysis, which already indicates that the probability of failure is anticipated to exceed the target. It is also worth indicating that the selection of *b* was not crucial in determining an estimate of the displacement in the region of expected failure. A second regression model where *b* was pre-assigned a value of 1.0, indicates a very close value for the displacement at Sa_{ct} (Fig. 4.4). As discussed previously, the chosen value of *b* becomes important only to a second order when it is used to compute the more "refined" probability of failure indicated by Eq. 4.10.

4.3.5 Computation of the Probability of Failure.

We have now enough information to compute the performance of the initial design of our structure in probabilistic terms. Remember that the target probability of the deck's displacement to exceed the value of δ_c was set to 1/2000. The probability of the structure to fail was computed next numerically with Eq. 4.16, where the following relationships are assumed:

    i) $\delta = a * Sa^b * \varepsilon$, where ε is lognormally distributed error term with parameters $\varepsilon \sim LN \, (1.0, \, \sigma_{ln\delta \, | \, lnSa})$.

    ii) δ_c is assumed to be lognormally distributed, with parameters $\delta_c \sim LN \, (\delta_{cm} = 1.4; \, \sigma_{\delta_c} = 0.2)$, and

    iii) *Sa* has a complementary cumulative distribution equal to the hazard curve H[*y*].

From the regression, even though the estimated standard deviation is considered to have small confidence (due to the limited data) it turned out to have a reasonable value and was used for the computation of the probability of failure (see Appendix 4.A for a larger data set regression that justifies this decision).

The numerical computation of integral (Eq. 4.16) with the above assumptions results in:

Pf = 1/875 > 1/2000,

which indicates that the structure needs to be modified to increase its reliability. (The approximation of *Pf*, using the analytical approach of calculating *Cf*, yields a more conservative value of *Pf* = 1/376).

4.3.6 Modification of the Structure to Achieve Target, and Updating of the Trial Values.

The computed probability of failure, *Pf*, suggests that the structure needs to be "bettered" from a probability of failure point of view. Such improvement can be attained either by increasing its displacement capacity, by reducing the displacement demands on the structure given the seismic environment, or by a combination of the above. Based on the reasoning described in Appendix 4.B that explains the reduction in demands by increasing the resistance of a SDoF system, a partial strengthening of the jacket was performed. Since the sizing of the legs of the jacket are typically governed by towing and launching loads or due to their use as guides for piles, rendering them relatively strong for "operational" loads, the increase in resistance will be done by increasing the cross section of the braces and horizontals alone (which are the members that fail first). A lower-bound of the necessary increase in resistance needed in these elements can be found by computing the required increase of the whole system treating it as a SDoF system, and applying it to the aforementioned elements. The improvement of the structure is based on re-computing an updated design spectral acceleration, Sa_d', given that the actual spectral acceleration capacity, Sa_{c0}, is known.

Sa_{c0} is computed solving for the value of spectral acceleration in Eq. 4.2, such that the displacement corresponds to the value of the displacement capacity, so:

$Sa_{c0} = (\delta_c / a)^{1/b} = (1.4 / 2.00)^{1/0.7} = 0.6g$ (which is lower than Sa_{ct}, as expected).

In order to calculate the updated design level (Sa_d') needed to achieve the target sought, updated values for Cf and ρ_{Sa} need to be found as well (i.e., the *actual* values of Cf_0, and ρ_{Sa0}, respectively). Eqs. 4.17 and 4.18 yielded:

$Cf_0 = (1/874)/$ H$[0.6] \approx 2.0$, and

$\rho_{Sa\,0} = 0.6$ g $/ 0.2$ g $= 3.0$

The new updated capacity target was then found by solving for it as done in step 4.3.2, adhering to the original performance target but using the revised value of Cf:

$Sa_{ct}' =$ H$^{-1}[Pt / Cf_0] =$ H$^{-1}[(1/2000) / 2] \approx 0.8$ g

Finally, we find the corresponding design value by using the actual reserve strength ratio:

$Sa_d' = Sa_{ct}' / \rho_{Sa0} = 0.8$g $/ 3.0 = 0.27$g,

which is approximately 30% stronger than the first design, i.e., $Sa_d' \approx 1.3 * Sa_d$.

The increase in resistance was done simplistically by associating the moment of inertia to the strength of horizontals (modeled here for bending) and diagonals (for buckling). For this, the thicknesses of the corresponding tubular members were increased by 30%, in order not to increase the diameter/thickness (D/t) ratio.

The strengthened design was analyzed as the original design was. As expected, there was a slight increase in stiffness ($T_0' = 1.8$ sec), and the static nonlinear pushover analysis indicates a new yield displacement and a new displacement capacity of:

$\delta_y = 0.8'$,

$\delta_c = 1.6'$.

The nonlinear dynamic analyses were done with records scaled in the region of spectral accelerations close to the updated target capacity. The new deck maximum displacements (*dmd*) found are shown in table 4.2.

As before, fixing the value of the exponent in Eq. 4.2 to $b = 0.7$, we regress and find the following values:

a= 1.8 (for *dmd* in feet and *Sa* in g), and
$\sigma_\delta = 0.22$.

In Figure 4.5 we can see the data set, as well as the regressed fit for the assumptions of b = 0.7 and $b = 1.0$. (Notice the comparatively small value of the dispersion. Once again, the small data set makes this estimate's confidence band be broad). Also notice once more that the estimation of the median displacement at the target spectral acceleration capacity is not very sensitive to the value of b (the estimates of the median displacements are 1.57' and 1.52' respectively). For the improved design we can also notice that the estimated displacement (i.e., $aSa_c^{\,b}$) is closer to the updated displacement capacity (1.6'), than was the case for the original design.

The computation of probability of failure was computed as before, keeping the same values of the standard deviations, which yields:

$Pf \approx 1/1700,$

still a little higher than our target but much closer and probably close enough for most purposes.

4.4 Conclusions.

Traditional structural design has considered as a ground motion levels for design those earthquake intensities related to a fixed relatively low return period. Actions from these are then used as an input for elastic design. Inelastic behavior is typically only assumed by using an elastic-force reduction for the design, and at best (but uncommonly) verified for less frequent and higher intensity earthquake loads (e.g., *Ductility Level Earthquake*, for offshore structures; *Safety Evaluation* level, for bridges, *Rare* to *Very Rare,* for buildings).

In contrast, the procedure presented here allows for the setting the desired *structural* performance, in terms of a *failure* probability. The method explicitly takes into account the structural inelastic behavior in order to propose design level seismic actions for design, for use with conventional elastic design methods, as described by WSD- or LRFD-based codes.

The iterative nature of the method allows for incorporation of updated information on the structure. Means for estimating initial trial values are offered, but these can be estimated directly from engineering experience as well. It should be mentioned that the choice of the parameter $b = 1$, which is a good "representative" value in general for describing nonlinear displacements, would have allowed a faster convergence. Although we had data to consider $b = 0.7$, for this particular case, it is to the best of our (current) knowledge that a unit value is a better proposal to be considered for, at least, the initial trial values.

The methodology is not limited to the offshore system presented in the example, it is as applicable for buildings and bridges. Although not discussed here, the method can be naturally extended to consider other performance levels. Such extension would allow to verify, for example, the compliance to a particular *seismic performance objective* that the owner of the structure decides for it, in a *performance based design* framework (as described by SEAOC, 1996).

Although the method itself is straightforward, its implementation may not be obvious. Details arising in such implementation, such as the best descriptor of response, are not discussed here. Some of these issues are discussed in Appendix 4.A.

Chapter 4 Figures.
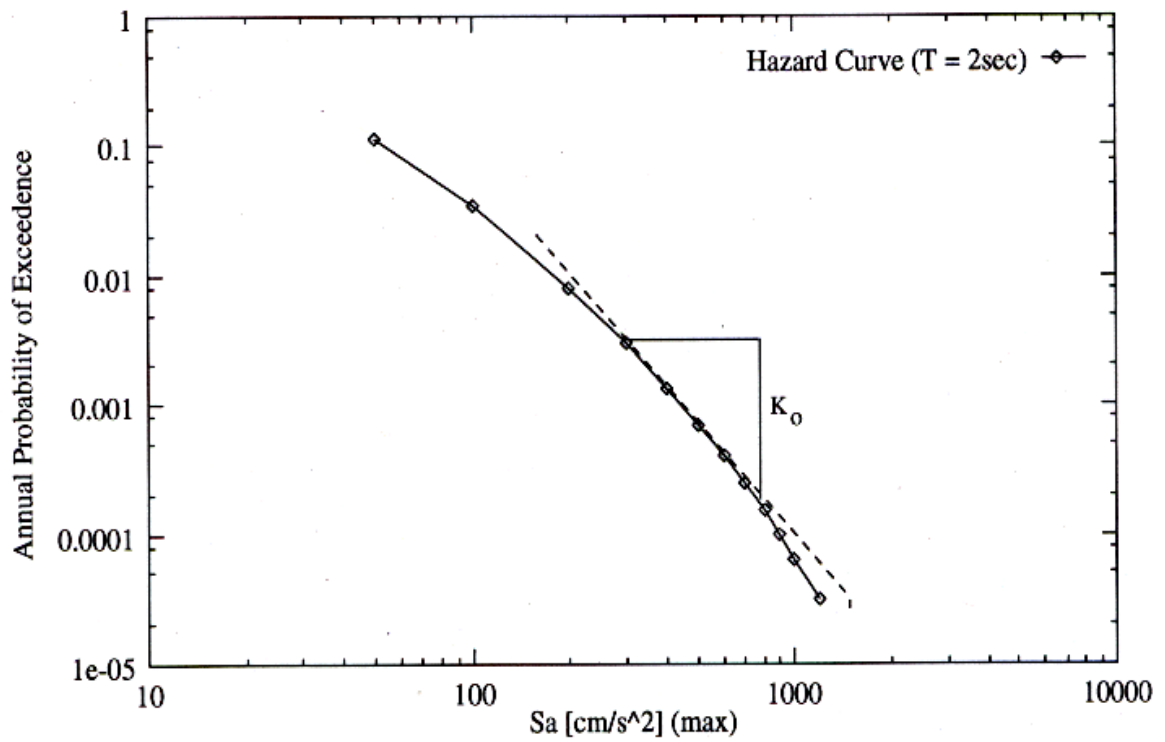
Figure 4.1 Typical seismic hazard curve, and representation of logarithmic slope K_0, in a region of 0.0002 annual probability of exceedence. This particular curve corresponds to the hazard at a site in the Sta. Barbara Channel, and corresponds to a structural period of 2sec ($f_0 = 0.5$ Hz), and damping of 5%.
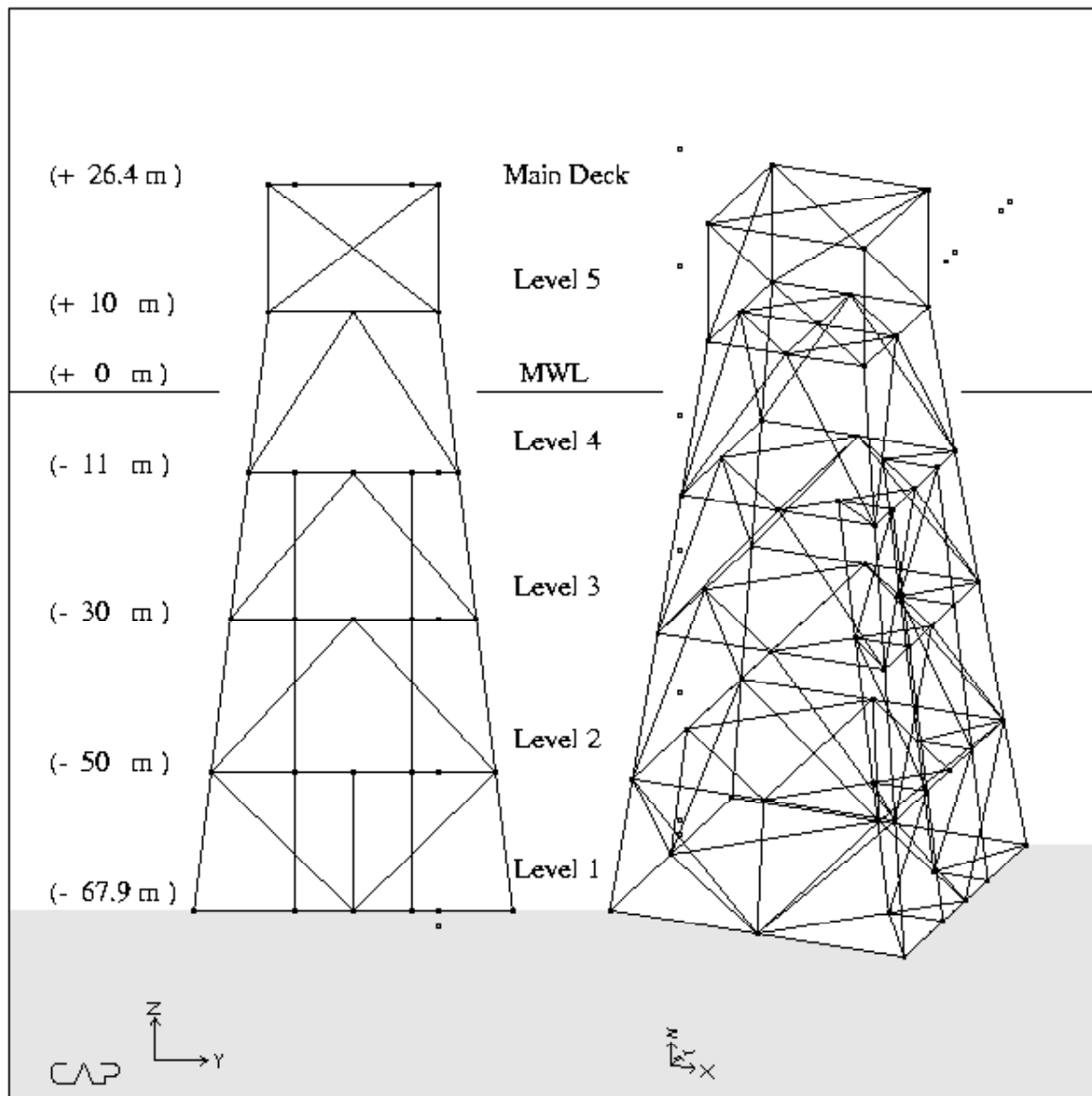
Figure 4.2. Structural configuration of the steel jacket, taken from Manuel, et, al, 1999.
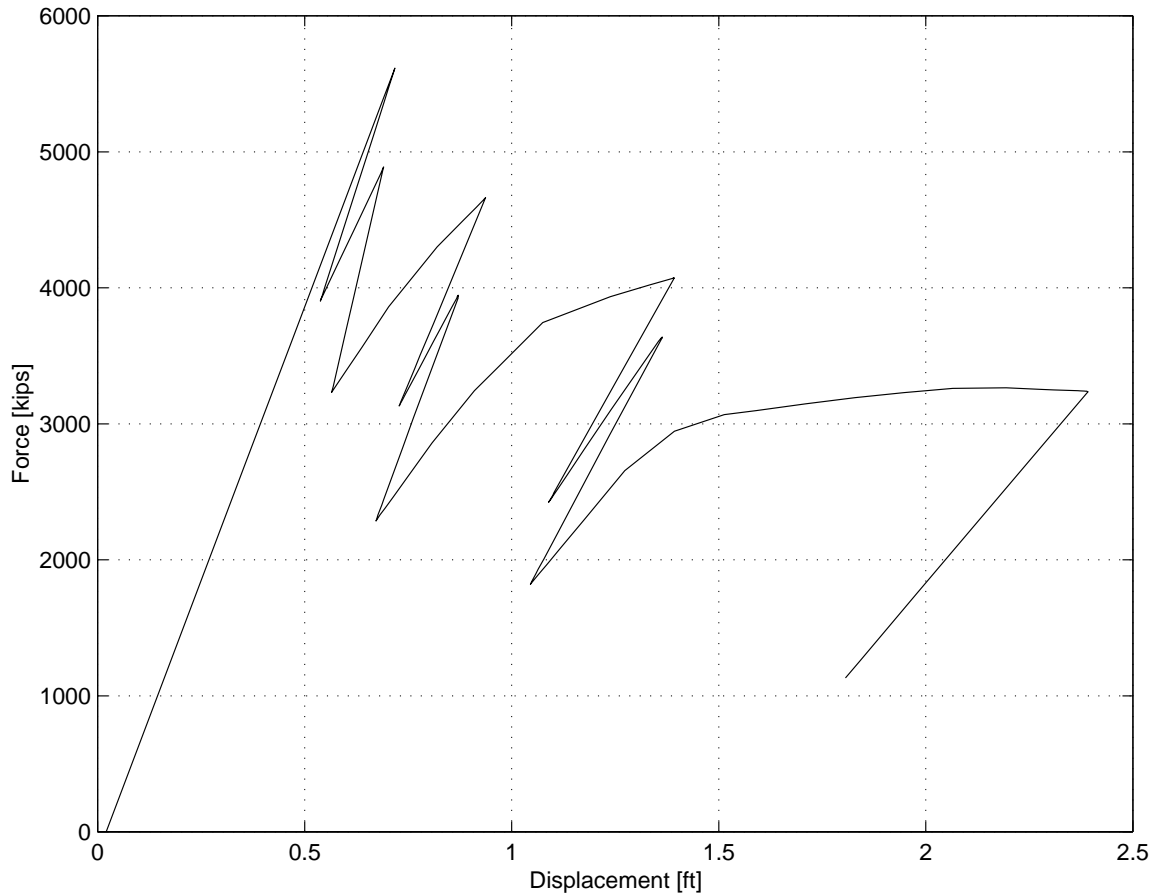
Figure 4.3 Nonlinear static "pushover " analysis on the offshore platform considered in the example. Notice the unusual load-deflection curve for the braced frame, with respect to pushover curves for moment-resisting frames. As elements buckle, the negative stiffness of these elements require that the load needs to be decreased in order to maintain equilibrium, showing a non-monotonic behavior. The stages of reduced displacement at reduced loads are the only responses consistent with the given element force-deformation characteristics of the diagonals (modeled as Marshall struts) that satisfy the requirements of static equilibrium. See Simons and Powell, 1982, for a discussion on non-monotonic displacements on statically loaded nonlinear structures.
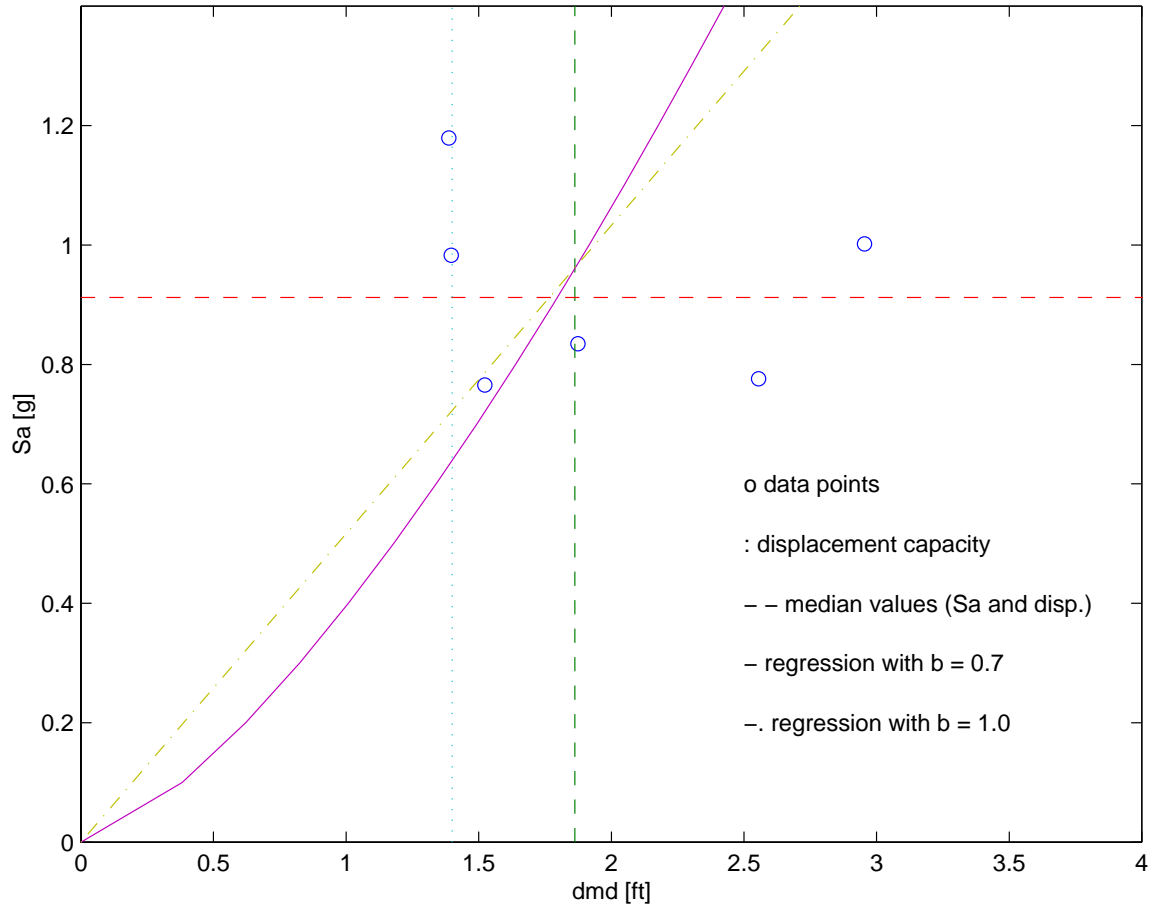
Figure 4.4 Nonlinear Dynamic Analysis results, and model fitting. (Note: Although the regression was done as *dmd* on *Sa*, the plot is presented in the more familiar "force-deflection" format with displacement as the ordinate and spectral acceleration as the abscissa).
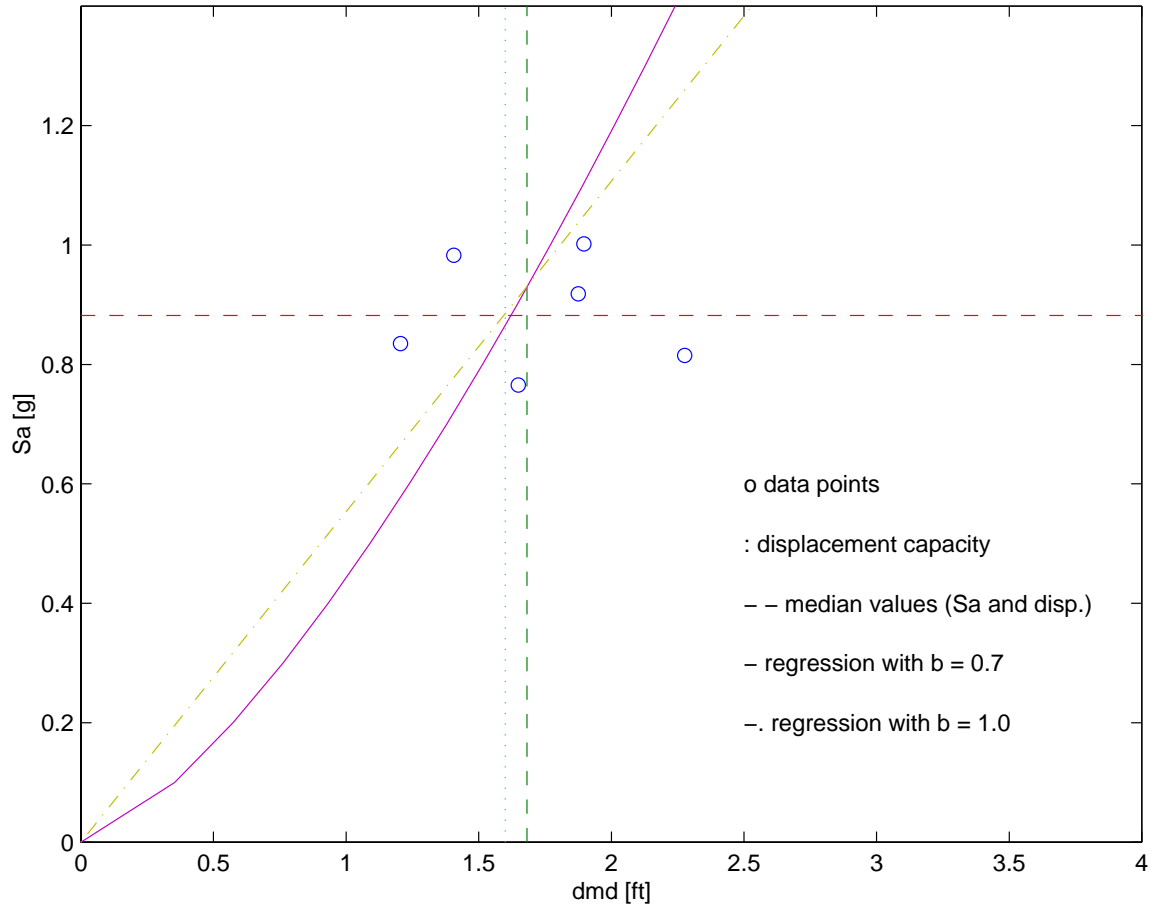
Figure 4.5. Nonlinear Dynamic Analyses results for the upgraded structure, and regression curves for the displacement response. Notice that the displacement capacity is closer to the "cloud" of displacements (which are related to spectral accelerations close to the calculated capacity) suggesting a better design than the first-iteration one.

Chapter 4 Tables.

Sa [g]	dmd [ft]
0.98	1.40
1.18	1.39
0.83	1.87
1.00	2.95
0.77	1.52
0.78	2.56

Table 4.1. Deck Maximum Displacements (*dmd)* vs. Sa. Original design. See figure 4.4 for the plot of these data points and the model obtained from regression.

Sa [g]	dmd [ft]
0.98	1.41
0.84	1.21
1.00	1.90
0.77	1.65
0.92	1.88
0.82	2.28

Table 4.2. Displacements vs. Sa. Updated Design. See figure 4.5 for the plot of these data points and the model obtained from regression.

Appendix 4.A. Issues on Scalar Representation of Seismic Input and Output (I/O) in PSDA

4.A.1 Scalar Representation of Seismic Input and Output (I/O) for PSDA in Chapter 4

Current practice of PSHA considers ground motion intensity to be described by a single scalar quantity, i.e., spectral acceleration. The attenuation laws used in PSHA produce estimates of such a quantity based on the observed geometric average (which has been indistinctively referred to in this work as the *median*) of two orthogonal horizontal directions. The use of attenuation laws thus produced should be limited to cases where it is not important to discern between orthogonal components as well as cases for which such a statistic (i.e., the median acceleration) is the one of primary interest.

The possibility of considering seismic input parameters other than only the first-mode frequency spectral acceleration in the contribution to response, in a PSDA framework, is considered, for example, in Shome (1999). This requires the description of hazard in terms of a multi-variable representation, e.g., spectral accelerations at the first-mode as well as the second-mode structural frequency. Systems that present important high-mode effects can benefit from describing their response in these terms.

The effect on PSDA from an improved representation of seismic hazard is the reduction of observed dispersion of response. For example, it is known that first-mode spectral acceleration is a better parameter for predicting response than is peak ground acceleration, because it yields a smaller dispersion in observed conditional response. This reduces the computational expense required for the prediction of estimates of median response (needed to couple to PSHA).

On the other hand, and depending on the needs of the structural analyst, the response of interest required may also be best represented by a multi-variable set. For example, a

definition for total damage in a building may require not only the estimation of maximum inter-story drift, but also the drift at several inter-stories. Typical damage indices (e.g., Park and Ang, 1985) consider scalar combinations of ductility and hysteretic energy measures.

The example considered in section 4.3 obviously involved the handling of multi-dimensional parameters, both on the seismic input side, as well as on the structural response side (output). Such parameters, however, were collapsed into scalar representations for use in the current-practice format of PSDA. The following sub-section discusses different possibilities for such a scalar description. The vectorial description of PSDA is beyond the scope of this work.

4.A.1.1. Scalar Representation of Seismic Input.

The scalar representation considered in Chapter 4 was that of observing the *maxima* of both maximum orthogonal input and output. The input considered the maximum spectral acceleration at the fundamental frequency, for both horizontal components of ground motion. The scalar parameter for seismic output was the maximum nodal displacement at the deck (observed throughout the duration of motion) for both directions.

In order to make use of PSHA incorporating available attenuation laws, a "typical" modification factor (with assumed zero standard deviation) was considered in order to translate *maximum* spectral acceleration to *median* spectral acceleration. The translation factor was based on Table 4.A.1, which shows the ratios of maximum spectral acceleration of the two components to median spectral acceleration for a set of 26 records of magnitudes ranging from 6.7 to 7.3, distances from 10 to 30km, on stiff soil sites.

For simplicity, the assumption of zero standard deviation on the ratio of maximum median spectral acceleration was made (although, as was seen, it is typically ≈ 0.1) which

allowed the direct use of the existing *median* spectral acceleration hazard curves (i.e., H[.]) by means of the following simple assumption:

$$H_{Sam}[y] = H[y/r_{ma}],$$ (4.A.1)

where $H_{Sam}[.]$ is the hazard curve for *maximum* spectral acceleration, and r_{ma} is the maximum-to-(geometric)-average (i.e., maximum-to-median) spectral acceleration ratio. Based on table 4.A.1, the value considered in Chapter 4 was $r_{ma} = 1.2$ (for the 0.5Hz system).

	Frequency [Hz]					
	0.2	0.5	1	5	10	25
$r_{ma} = $ Sa_{max}/Sa_{av}	1.17	1.23	1.16	1.14	1.09	1.11
σ	0.12	0.1	0.1	0.09	0.06	0.09

Table 4.A.1 Median ratio of maximum spectral acceleration to average orthogonal spectral accelerations (r_{ma}). These results correspond to a set of records with magnitudes in the [6.7,7.3] range and distances in the [10,30] km range.

4.A.1.2. Scalar Representation of Seismic Output.

As mentioned earlier, the scalar parameter for seismic output was the maximum nodal displacement at the deck (observed throughout the duration of motion) for both directions.

The rationale behind the consideration of output was, on one hand, based on the objective of the PSDA, which was to establish the probabilistic description of *failure*. On the other hand, it was based on the definition of failure itself. The objective could have been different, for example a *pre-failure*, intermediate performance level. The definition of failure was based on the two uni-dimensional static pushover analyses for the system

(done for each direction independently). The system was assumed to fail if the displacement in either direction exceeded its corresponding displacement capacity. The capacities were judged to be equal for the two directions. Failure will then occur if and only if the maximum displacement exceeds the common capacity. Therefore the sole use of maximum displacement is a special case that follows from the nearly identical N-S, E-W directions of the structure. More generally one might like to use the maximum of both orthogonal horizontal demand-to-capacity ratios.

Although the attenuation laws typically describe the *geometric average* of the horizontal orthogonal components of strong ground-motion, the *maximum* was considered for the description of input. As can be seen in table 4.A.2, the direction of the deck's maximum displacement (*dmd*) typically coincided with the direction of maximum spectral acceleration. This was the justification for using the maximum ground motion measure with this output measure. However, as will be discussed below, this is not always the case, even for large differences in the orthogonal (first-mode) intensities. We can observe in table 4.A.2 that the direction of maximum displacements start off coinciding with that of the maximum spectral acceleration, but can change when the system incurs in non-linear behavior. For this particular near-symmetric structure one expects to observe the same direction for maximum response and maximum spectral acceleration while in the elastic range.

	dmd_x	Sa_x	dmd_y	Sa_y	Sa_x/Sa_y	Sa_y/Sa_x
EQ 1	0.32	0.13	1.06	0.49	0.26	3.82
	0.50	0.21	1.43	0.79		
	0.85	0.26	1.40	0.98		
	0.76	0.31	1.39	1.18		
	2.02	0.41	1.98	1.57		
	2.41	0.46	2.28	1.77		
EQ 2	0.84	0.42	0.47	0.20	2.06	0.49
	1.87	0.83	0.86	0.41		
	2.95	1.00	1.16	0.49		
EQ 3	0.62	0.24	0.76	0.38	0.62	1.61
	0.90	0.47	1.52	0.77		
	2.22	0.85	3.05	1.38		
	1.35	0.95	3.18	1.53		
EQ 4	0.49	0.20	0.31	0.15	1.32	0.76
	1.75	0.42	1.14	0.32		
	1.34	0.56	1.80	0.43		
	2.76	0.71	1.55	0.53		
	2.56	0.78	2.04	0.59		
	3.89	0.92	1.46	0.70		

	intensity-ratio indicating direction of maximum Sa (Sa_m)
	matches direction of Sa_m
	does not match direction of Sa_m

Table 4.A.2 Maximum deck displacements (*dmd*) and spectral accelerations. Notice that although typically the direction of maximum spectral acceleration coincides with the direction of the maximum displacement (grid shading), this is not always so (vertical shading) for nonlinear displacements. The right-most two columns are the ratios of the orthogonal components of spectral acceleration. Ratios greater than unity indirectly indicate the maximum direction (diagonal shading).

Although the different data points came from scaling the available accelerograms to different intensity levels, the parameters required in order to represent the relationship between intensity and response (i.e., *a*, *b*, and σ_δ) were computed from considering all observed displacements independently (see the data points in Table 4.A.2). We can trace the displacements caused by each of the accelerograms at different levels of intensity (which describes an *Incremental Dynamic Analysis (IDA)*, see for example Luco and Cornell, 1998). It may be surprising to note that as the intensities increase the (scalar) responses not necessarily do so monotonically. Actually, for some cases the demand may

indeed *decrease* for a range of increased intensities. This is one effect of considering a limited number of variables for describing nonlinear response. Observe for example the trace corresponding to record EQ-4 (see table 4.A.2) in figure 4.A.1.
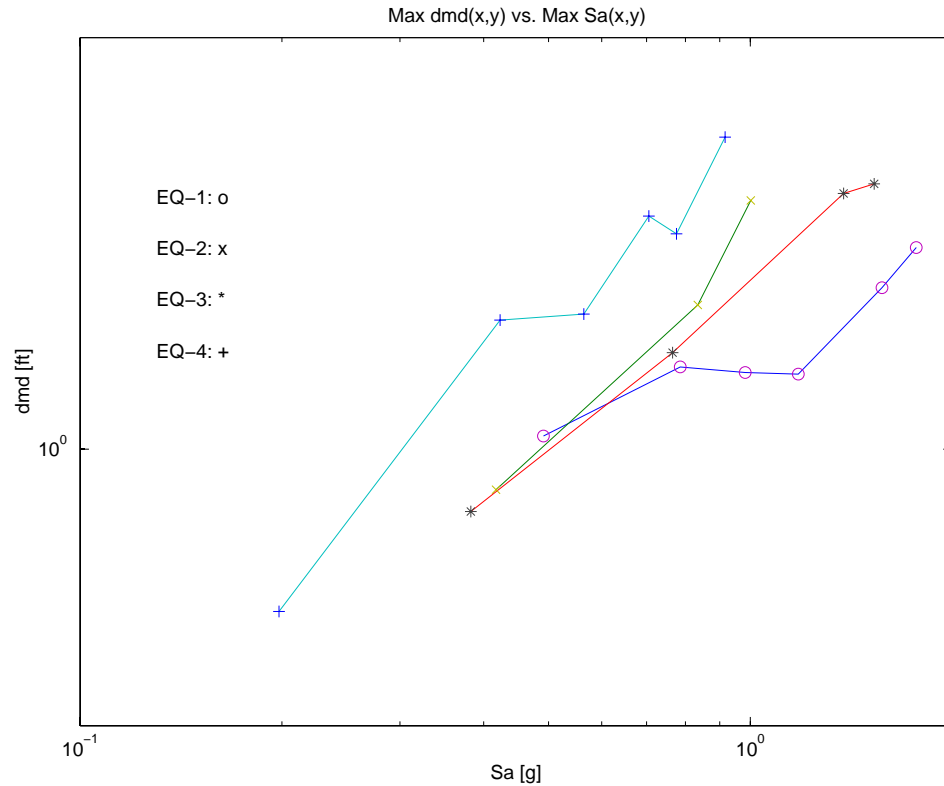
Figure 4.A.1. *Incremental Dynamic Analyses* considered for the design example of Chapter 4. Notice that responses may not always increase with intensity. In fact, for EQ-4 (represented by the '+' symbol), the response decreased at Sa ≈ 0.7. The plot corresponds to the data points from Table 4.A.2

The reason for the non-monotonic possibility for response given increasing intensities can be explained by looking at Figure 4.A.2. It corresponds to the dynamic response histories of the nodal displacements at the deck, corresponding to two (out of 4) diagonally opposed corner nodes. The time histories for EQ-4 are shown in Figure 4.A.3.
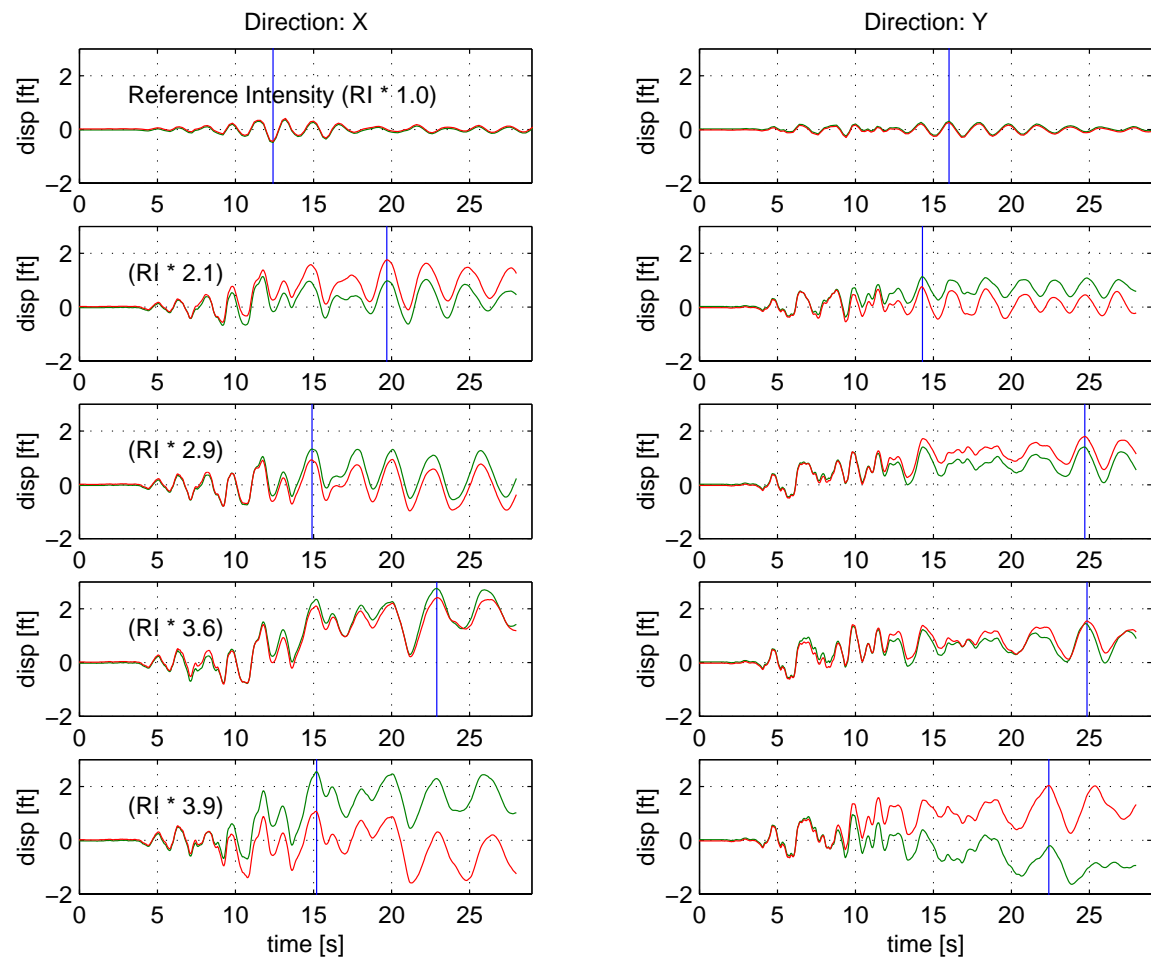
Figure 4.A.2. Response time-histories for the deck nodes, corresponding to the nonlinear *Incremental Dynamic Analysis* with EQ-4. The vertical solid line in each time history indicates the occurrence of the maximum absolute displacement. Notice the shift of maximum displacement in time as well as in direction after RI*2.1 and RI*2.9. Each plot represents the response of two different deck nodes, diagonally opposed.
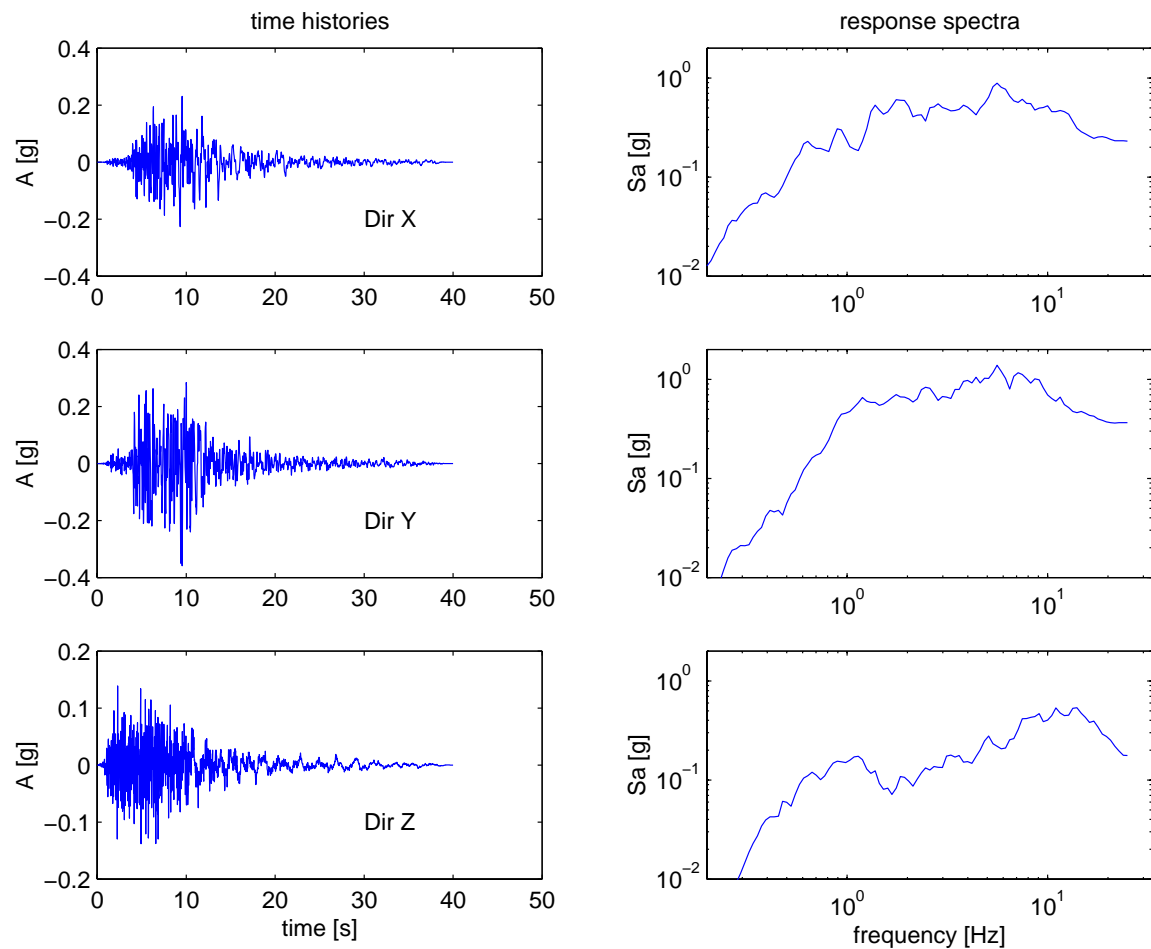
Figure 4.A.3. Accelerograms and response spectra for EQ-4 (Northridge 1/17/94; M = 6.7; R = 25.5) which was the seismic input for the responses depicted in figure 4.A.2. Although the spectral acceleration for the X direction is 1.32 times higher than that for the Y direction (see Table 4.A.2), the intensity case *RI**2.9 caused the Y direction to have the largest response (see Fig. 4.A.2). Shown here are the spectra corresponding to *RI**1.0, with $Sa_x = 0.2g$ and $Sa_y = 0.15g$.

In figure 4.A.2 we see the responses for incremental intensities, the first being a reference intensity (namely, RI * 1.0) that does not cause nonlinear behavior in the structure (Sa_{max} = Sa_x = 0.2g). As intensity increases, the temporal *location* and *direction* (*x* or *y*) of the maximum deck displacement shift. For example, comparing RI*1.0 and RI*2.1, the time at which the maximum displacement occurs shifted from 12.4s , to 19.7s, as the system responded nonlinearly.

An apparent decrease in the rate of change of (maximum) response with intensity is caused by an increasing response of a different *node*, or an increasing response in a different *direction* for the same node, or an increasing response in the same node, same direction, but at a different *time*.

For example, at RI*2.9 there was a direction shift with respect to RI*2.1, for the maximum response of the same node. Although the maximum displacement remained at the same node, at RI*3.9 the opposing node started to build up large nonlinear displacements. At RI*3.6, the maximum *X*-direction displacement of the node shifted from just before 15 seconds (RI*2.9) to around 23 seconds.

Also worth mentioning is the response to the torsional mode (third mode of vibration). Its elastic frequency (0.57Hz) was not too different from the first two translational modes (almost identical, at 0.52Hz). The separation of the node displacement time history-lines indicates a rotational displacement which was the main cause of the maximum displacement at RI*3.9.

4.A.2. Other I/O Scalar Representations for Intensity-to-Response Parameter Estimation.

Other representations for both input and output could have been considered. Some different possibilities include, but are not limited to, the square root of the sum of the squares (SRSS) of displacements and/or spectral accelerations; the averages, or any combination of these. For comparison purposes the following combinations were chosen: SRSS for *Sa* and displacement (SRSS-SRSS); (geometric) averages for *Sa* and displacement (AVG-AVG); (geometric)-average spectral acceleration and maximum displacement (AVG(*Sa*)-Max(*dmd*)); and finally the previously described maximum spectral acceleration and maximum response (Max-Max).

With respect to considering only the maximum values, the average and SRSS schemes will "stretch out" the axes for each *IDA*, since the values thus combined will be higher than the maximum. The *Sa* axis will be evenly stretched for each record, since the ratio of both directions' spectral accelerations remains constant for each intensity considered. However, the amount of stretching in the response dimension will in general change with intensity as the different possible responses change. For these comparison schemes, the stretching may still not cause strict monotonic response with increasing intensity. Figure 4.A.3 shows the effect of considering these different schemes, vis-à-vis the Max-Max model described earlier.
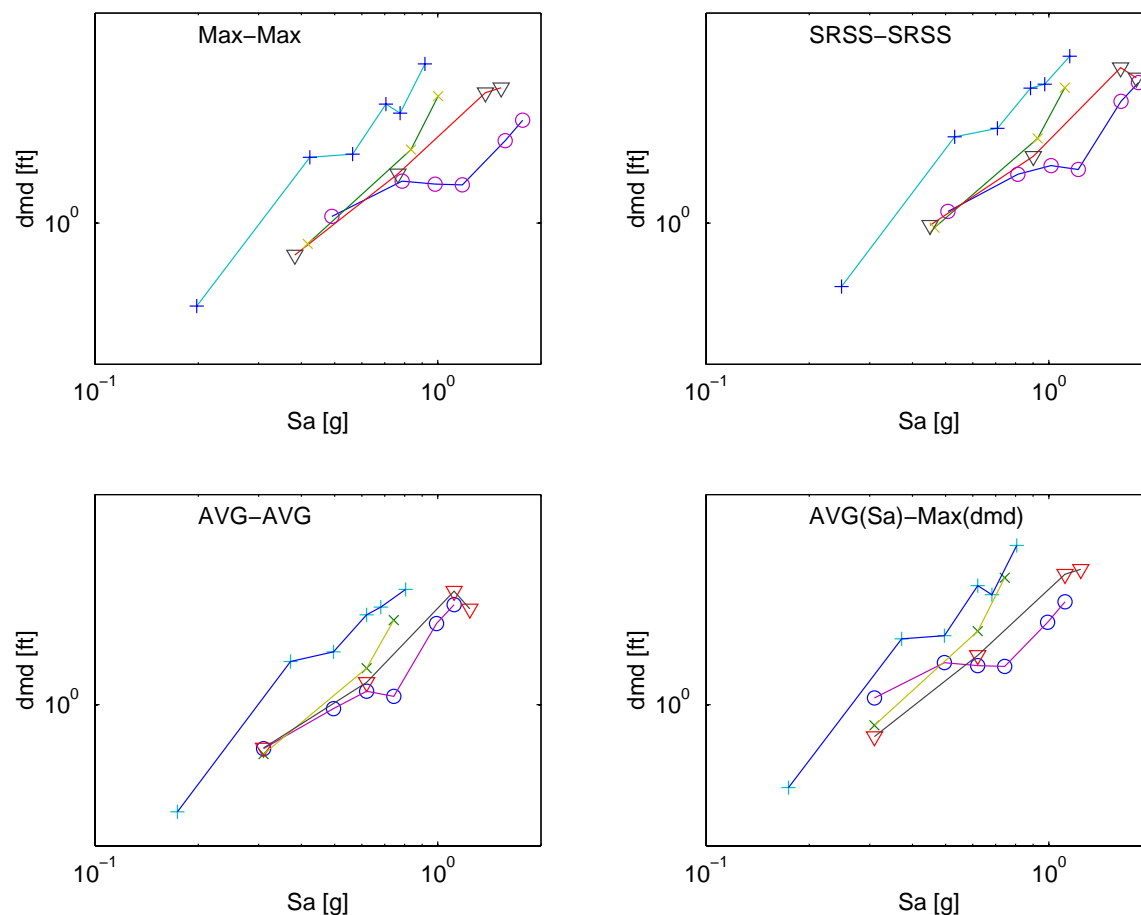
Figure 4.A.4 Different combination schemes for seismic I/O measures. The manner in which the I/O measures are collapsed to scalar values will, to some extent, affect the shape of the *IDA* traces.

The parameter estimation tends to be mildly better (in terms of a lower dispersion) for these new different combinations, for the same intensity-to-response model $(\delta = a\,Sa^{\,b})$. In general, the parameter b will tend to be higher as the relative stretching cause relatively higher displacements, as may be expected especially for relating near-collapse displacements to intensity (i.e., a "softening" value of $b > 1$). As long as response is potentially not monotonic, even considering a single-record IDA for the estimation of parameters, the model fitting cannot be perfect. Table 4.A.3 shows the estimation of the parameters for the different cases.

Combination	a	b	σ_δ
Max-Max	2.09	0.72	0.37
SRSS-SRSS	2.27	0.86	0.31
AVG-AVG	2.28	0.93	0.27
AVG(*Sa*)-Max(*dmd*)	2.81	0.89	0.29

Table 4.A.3 Parameter estimates from regression of *dmd* vs. *Sa* for the different combination schemes. As a combination scheme tends to produce higher displacements, the value of b will tend to be higher.

These different combinations may show apparently lower dispersions of the fitted models than that of the Max-Max case (although one needs to be careful with such values due to the relative small sample size). However, they may not all make as much sense to consider. The average and SRSS of response and spectral acceleration combine parameters that do not occur simultaneously. Hence, depending on the relative responses and ground motion time histories, the resulting prediction may even be unconservative. The maximum displacement was desired because it is judged to be the best predictor of system failure. Also, the maximum spectral acceleration was chosen over the geometric average because the direction of such maximum in general coincided with that of the maximum direction (see table 4.A.2). For structures that present higher asymmetries in lateral behavior, and hence present a lower correlation between the direction of maximum input to maximum output, the AVG(*Sa*)-Max(*dmd*) case may be preferred.

Of course other combinations not mentioned can also be considered (e.g., SRSS(*Sa*)-Max(*dmd*), etc.). A particular option not considered here traces *throughout the time*

history the vectorial sum of orthogonal horizontal input and/or output (e.g., Wang and Wen, 1998).

Appendix 4.B. Reliability Improvement from a Seismic Demand Reduction Approach.

In order to increase the reliability of the structural system we can identify the sources for potential reduction of the value of *Pf*, the probability of failure. For the reliability to improve (i.e., for *Pf* to decrease), either the displacement capacity, δ_c, must be increased or the conditional probability of displacements exceeding a given value must be decreased, as indicated in equation 4.16:

$$P_f = P[\delta > \delta_c] = \int_0^\infty P[\ln(\delta) - \ln(\delta_c) > 0 \mid Sa] f_{Sa}(Sa) dSa \tag{4.16}$$

A reduced probability of failure translates into either (1) reducing the displacement demand for all levels of spectral acceleration or (2) by increasing the capacity. From equation 4.17:

$$Pf = H[(\delta_c / a)^{1/b}] Cf \tag{4.17}$$

we can see that since the hazard curve is a monotonically decreasing function (for example, see figure 4.1) either the argument of H[.] needs to be increased or the value of *Cf* needs to be lowered for the probability of failure to decrease. For the argument of H[.] to increase we need to, again, either increase the value of the displacement capacity or decrease the value of the parameter *a* (from $\delta = a\, Sa^b$) , which corresponds to a reduction in demands for any level of spectral acceleration (assuming an uncontrollable and fixed value of the system-dependent *b*). The value of *Cf* is really out of our control (Eq. 4.11), because the hazard value of K_0 is fixed by the seismic environment, and the values of *b* and σ_δ depend on the structural configuration and the natural complexities of the nonlinear problem and the randomness in the seismic input.

The approach considered was based on controlling the displacements of the system. Displacement control is conceptually possible either on the displacement *demand*, which is related to the seismic input, or on the *capacity*, which, as defined here, does not depend on the actual loads that the structure may be exposed to. Only the former was considered. Directly increasing the displacement capacity appears more viable for structures under certain static loads, such as wave loads, where critical members can be identified and directly "strengthened" by stiffening. For our re-design example, due to the dynamic and random character of the seismic actions and responses, the identification of critical elements that could be "improved" would not have been straightforward. For cases like ours there very well might be, however, a particular "weak link" in the system that can potentially be improved. To identify such a critical element one needs to study the temporal sequence of element failures for the different seismic dynamic loadings and then try to systematically identify problematic components. Observing the dramatic load-displacement discontinuities in the nonlinear static pushover analyses (e.g., Fig. 4.3), such critical links can only be associated with the brittle nature of the buckling diagonals. However, in the dynamic case, in the example considered in Chapter 4 there was no consistent single brace (or small subset of braces) that could be identified as the sought-after weak link.

Thus, the approach considered was that of reducing the demands, i.e., reducing the value of the parameter *a*, in Eq. 4.17 above. For the particular case of an elastic system where *b* = 1, the value of *a* will be inversely proportional to the structural stiffness. In other words, for a particular level of intensity (for example, spectral acceleration), the displacement demand is inversely proportional to stiffness, i.e., *a* is proportional to *flexibility*.

An elastic SDoF system subjected to a single seismic dynamic loading will show a higher displacement with respect to a stiffer system for periods below the *displacement sensitive* region (where response is most related to ground displacements, typically above around 2 to 3 sec.) of the loading's response spectrum (e.g., Chopra, 1995). Notice that such reduction in demand is not the same as the reduction in the parameter *a*, because, for the

same record, the spectral acceleration of the stiffer system has a different value. The reduction will be proportional to the increase in stiffness only for regions of constant spectral acceleration ($Sa = \omega^2 D$ where ω^2 is proportional to stiffness), and lower than this for the *velocity sensitive* region, where the reduction will be proportional to the square root of the increase in stiffness.

The reduction in displacement demands for a nonlinear system is not as straightforward as for the elastic case. From a static point of view, demands can always be reduced either by increasing the resistance (e.g., the yield force), or by increasing the stiffness, assuming that the post-elastic behavior does not change (e.g., a same fraction of initial stiffness for the post-elastic stiffness). Of course, for a given structural element's design, higher resistance typically means higher stiffness (e.g., higher brace cross-sectional area implies higher axial stiffness; higher moment of inertia implies higher flexural stiffness, etc.). For these cases, the reduction in demand is due to the force-deformation curve of the strengthened system always lying above that of the original system.

For the dynamic loading case the situation is even more complicated. Even though the force-deformation curve for the individual elements of a structural system (or that of a SDoF system) presents a "softening" effect (i.e., a decreasing *effective* stiffness; see Chapter 3), the dynamic intensity-to-response curves may not have such a softening effect. For example, Seneviratna and Krawinkler (1997) report cases for inelastic SDoF and MDoF systems of different characteristics (levels of ductility and frequency) where the response (e.g. roof displacement) is either lower than (i.e., it is then a "hardening" system) or higher than (i.e., it is then a "softening" system) their elastic counterpart, as a function of structural period. Sewell (1989) also found a frequency-dependent *nonlinear damage effectiveness of ground motion*. In this reference it is reported that higher frequency SDoF systems (for two kinds of hysteresis: bilinear and stiffness degrading) present higher demands than those of lower frequency oscillators (for the same level of resistance), with respect to higher-resistance systems (larger yield displacements). The fact that some systems present "hardening" is not surprising because results for the jacket

yielded values of b lower than unity ($b = 0.72$) from the regression of 19 data points (see Appendix 4.A).

Assuming for simplicity in the following discussion a unit value for b, hardening systems would have smaller values for a than their elastic counterparts (elastic a, or a_e). The value of a would represent the slope of the best linear fit for the available data points. For these nonlinear, hardening SDoF systems the data set necessarily lies on a straight line (with slope a_e) for displacement demands lower than the elastic limit, and the best-fit slope would show $a < a_e$. Once a structure is strengthened, not only does the stiffness increase (reflected in the reduction of the new value of a_e), but also the elastic-limit displacement may increase. Such larger displacement would "delay" the offset of hardening, such that the updated value of the nonlinear a is closer to that of the elastic slope, a_e. Supposing that the strengthened system remains a hardening system (i.e., the change in period is not too dramatic), there may even be overlapping regions of response for both systems, i.e., there may be regions of intensity where the original system actually had lower displacement demands than the strengthened version. In general for hardening systems, and even for the hypothetical case where the elastic-limit displacement does not change, the reduction in slope a from the original system to the strengthened system will not be as large as the reduction for the elastic case.

The best displacement-demand reduction possible may even be larger than the elastic-case reduction. For "softening" systems, the value of the inelastic slope a will be higher than that of their elastic counterpart, a_e. For the strengthened version of the system, and assuming that the elastic-limit displacement is increased, its inelastic slope, a, will be closer to its own elastic counterpart slope. This means that the overall demand reduction, as given by the reduction of the inelastic slopes, would be higher than the reduction for the elastic case.

The strengthening proposed for the steel jacket is based on augmenting the resistance by means of the updated value of the design parameter Sa_d. For the numerical example (section 4.3) this resulted in a value about 30% higher than the original design's value,

and, strictly, this value should be applied to the whole structure. However, the design of the jacket's legs are typically governed by actions other than seismic, such as those imposed by vertical loads, transportation and launching, etc., so for a more efficient re-design, the increase in resistance shouldn't be considered for the leg members. The whole structural system can be thought of as two subsystems in parallel: that of the legs (and foundation and deck), and that of the diagonals and horizontals. The total flexibility is then composed of the addition of the sub-systems' flexibilities.

In order to increase the resistance of the braces (mainly governed by buckling) and horizontals (mainly governed by bending), the proposed approach was to increase the thickness of these tubular members (see Appendix 4.D for sizing details). Everything else remaining constant (external diameters and structural configuration) the moment of inertia of these elements is approximately directly proportional to the thickness, and hence so is the buckling resistance. (This scheme also guarantees that the local buckling resistance is increased). The cross-sectional area being proportional to the thickness as well makes the axial stiffness of the elements also proportional to the elements. It follows that the elastic-limit displacement should approximately remain equal to that of the original structure, which makes the scheme for the reduction in demands more effective, for this hardening system, vis-à-vis the increasing elastic-limit displacement case. An upper bound for the total system's stiffness increase is the afore considered 30%. Neglecting the increase in mass, the corresponding increased structural frequency for a SDoF system would be proportional to the square root of the increased stiffness, i.e. $1.3^{1/2}$ = 1.14. Hence, for constant spectral velocity records (i.e., constant *Sv* around the first-mode structural frequencies of interest here) the elastic SDoF displacement demands would decrease by 14%.

In order to illustrate the previous ideas, two SDoF cases were studied. The first case corresponded to a 30% stiffness increase for an elastic system. The second case corresponded to the nonlinear version of the first case. Lacking a SDoF model of a strength degrading system for representing the buckling element-based jacket, a ductile bilinear model was chosen for the nonlinear case, for the same level of elastic-stiffness

increase. A set of 63 records having the same characteristics that the jacket might be exposed to (California records, stiff soil, moment magnitude range: [6.7.7.3], distance range: [10,30] kms; see Appendix 3.A) was selected and run through both cases, for two SDoF systems each. The original system for each case had a structural frequency of 0.53 Hz (close to the jacket's fundamental frequency), and the 30% stronger/stiffer system had a frequency of 0.6Hz. Damping was set at 2%.

For the elastic case (Table 4.B.1) we notice the expected 30% decrease in demands given spectral acceleration. However, due to the non-constant spectral velocity in the range of interest (i.e., an increase around 8% of $Sv = Sa/\omega$), the reduction in overall displacement demands was lower than the expected 14% reduction, at approximately a 5% reduction. The data points can be seen in Figure 4.B.1.

	f	ω	T	Sa_{med}	Sa_{med}/ω	Sa_{med}/ω^2	δ_{med}	a
	[Hz]	[sec^{-1}]	[sec]	[in/sec^2]	[in/sec]	[in]	[in]	[sec^2]
	0.53	3.31	1.90	42.91	12.89	3.87	3.93	0.09
	0.60	3.77	1.67	53.19	14.11	3.74	3.74	0.07
ratio	1.14	1.14	0.88	1.24	1.09	0.97	0.95	0.77
1/ratio	0.88	0.88	1.14	0.81	0.91	1.03	1.05	1.30

Table 4.B.1 Elastic SDoF demand reduction associated with a 30% increase in stiffness (i.e., 14% increase in frequency). Notice that the reduction in overall displacement demands (i.e., 5%) is less than the 14% decrease expected had the records presented constant spectral velocity. The median spectral velocity ($Sv_{med} = Sa_{med}/\omega$) in fact increased 9%, which explains the difference. As expected, however, the demand reduction *given* spectral acceleration as given by the value of a (from the regression $\delta_{med} = a\ Sa^{\ b}$) was 30%.
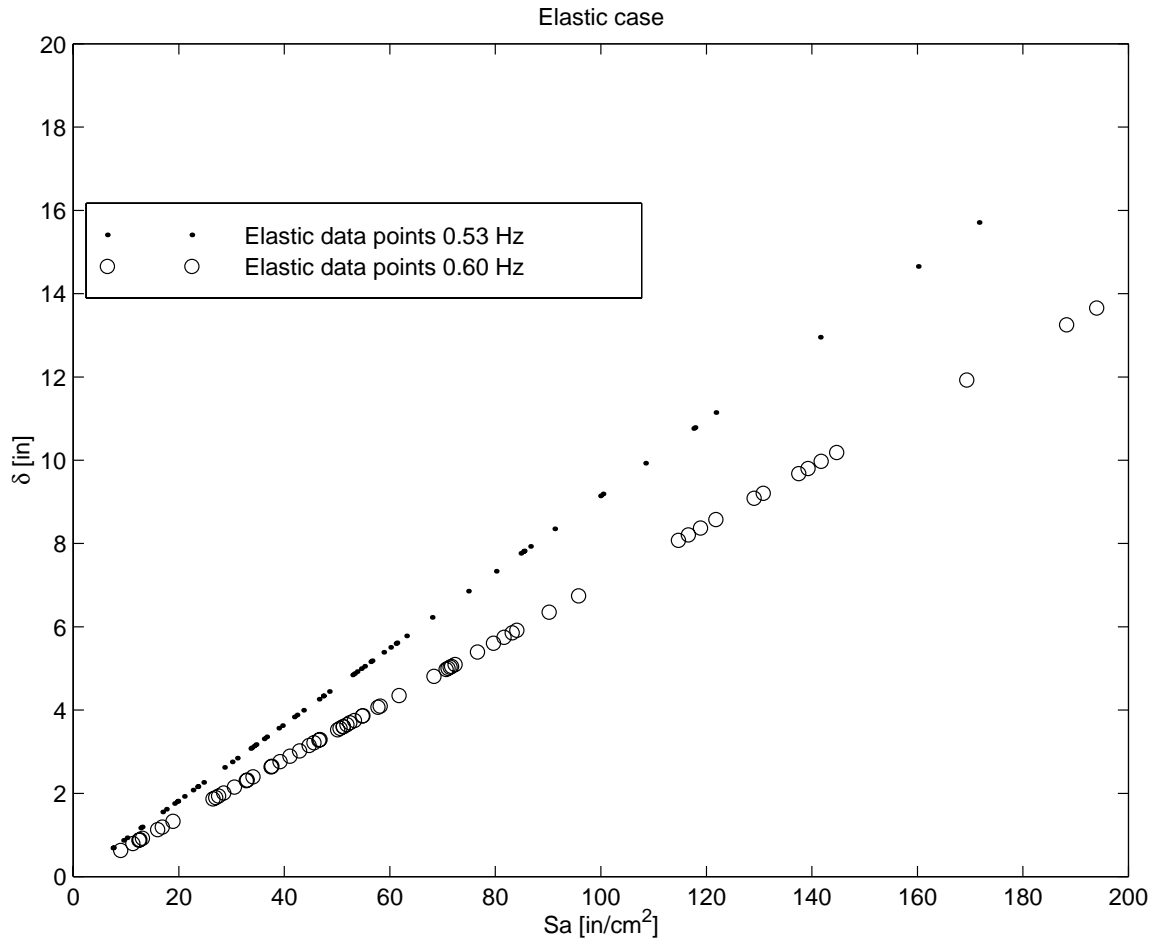
Figure 4.B.1. Reduction in displacement demands by increasing stiffness in the elastic system. Notice that the data points for one system do not match the spectral accelerations, *Sa(f)*, of the other system due to the difference in structural frequencies. (Perfect fit) regression lines are shown in Fig. 4.B.2, for comparison to the nonlinear case.

For the nonlinear case, a constant elastic-limit displacement of $\delta_y = 1.7$ was selected for both systems for a median ductility of around $\mu = 2$. Table 4.B.2 shows the results for the nonlinear case.

f	ω	T	Sa_{med}	Sa_{med}/ω	Sa_{med}/ω^2	δ_{med}	a
[Hz]	[sec^{-1}]	[sec]	[in/sec^2]	[in/sec]	[in]	[in]	[sec^2]
0.53	3.31	1.90	42.91	12.89	3.87	3.56	0.077
0.60	3.77	1.67	53.19	14.11	3.74	3.46	0.062
ratio	1.14	1.14	0.88	1.24	1.09	0.97	0.97	0.81
1/ratio	0.88	0.88	1.14	0.81	0.91	1.03	1.03	1.23

Table 4.B.2 Ductile bilinear SDoF demand reduction associated with a 30% increase in elastic stiffness (i.e., 14% increase in frequency). Notice that vis-à-vis the elastic case, the demands are lower, suggesting a hardening system (as was the jacket). The reduction in overall displacement demands is even lower than for the elastic case (i.e., 3%). Also, as expected for hardening systems, the demand reduction *given* spectral acceleration as indicated by the value of a (from $\delta = a\ Sa^b$; $b = 1$, chosen for simplicity) was *lower* than the elastic 30% reduction. (The 23% reduction in the value of a is significant at a 95% confidence level.)

The results in Table 4.B.2 show that the nonlinear SDoF structures considered (i.e., for the particular level of resistance and elastic frequency) corresponded to "hardening" systems, such that the nonlinear demands were *lower* than the demands of their elastic counterparts. The "hardening" found is consistent, for example, with findings of Seneviratna and Krawinkler (1997) for SDoF and MDoF systems of similar period and ductility levels. The hardening characteristic causes the reduction in the demands to be *lower* than for the elastic case for the *same* level of strengthening. For comparison purposes, the value of the exponent b was fixed at unity. Hardening systems in general will present a b value lower than unity, as was the case for the 3-D jacket ($b = 0.72$ for the first design, see Appendix 4.A). We can see that the level of hardening (by comparing a values) was lower for the strengthened system (0.6Hz: approx. 20%) with respect to its elastic counterpart (Table 4.B.1), than for the original system (0.53Hz: approx. 13%). Figure 4.B.2 shows the results for the nonlinear analyses, juxtaposed to the elastic-case best-fit lines. Although the plots extend to spectral accelerations at about 200in/sec^2, and displacements around 18in, the regression is controlled by data points closer to the median values (i.e., between 40 and 50 in/sec^2 and around 4in).
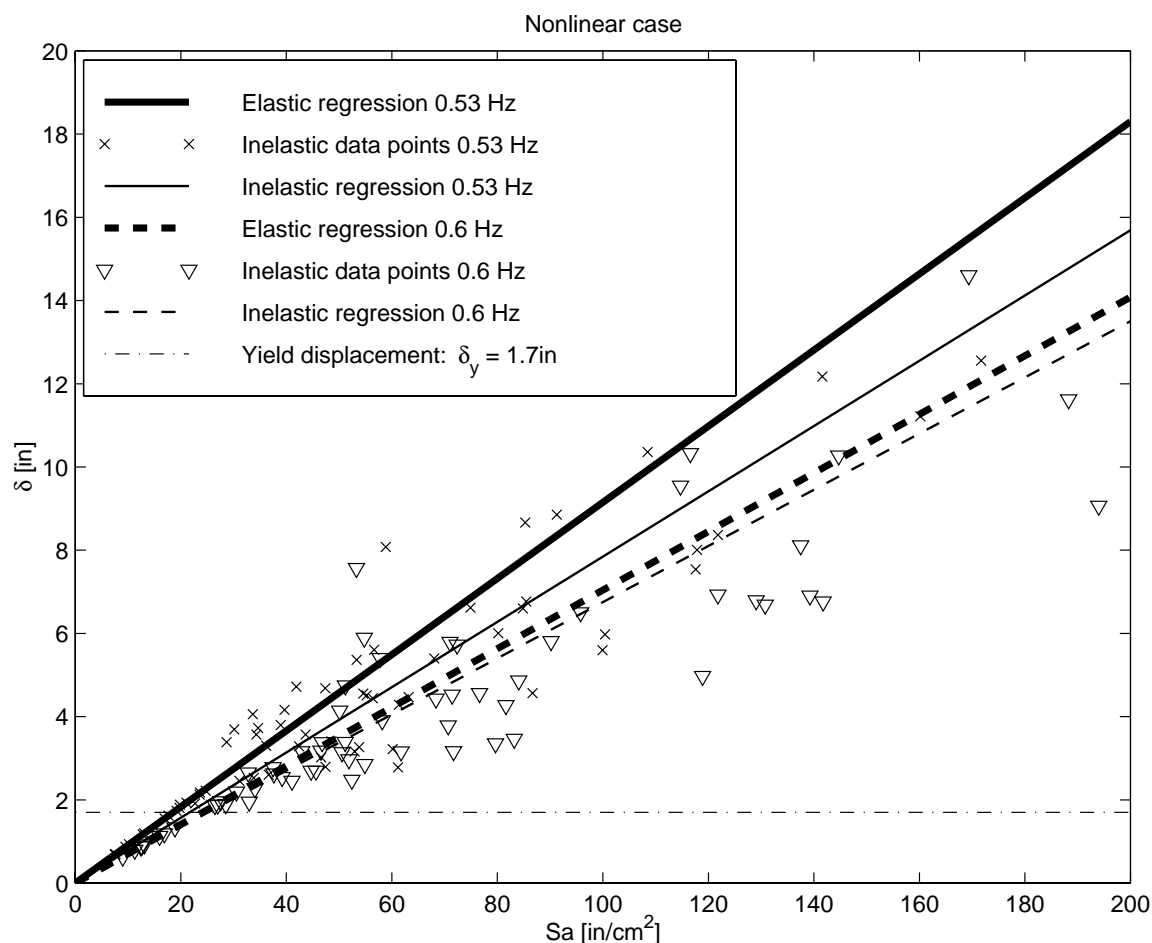
Figure 4.B.2. Reduction in displacement demands for the nonlinear case. The systems showed "hardening" with respect to their elastic counterparts, as seen by the lower slopes (given by the value of *a*) of the linear best fit (solid lines: 0.53Hz system; dashed lines: 0.6Hz system). The decrease in displacement demands for the inelastic case is lower than the decrease for the elastic case, because the increase in strength "postpones" the opportunity for the "hardening" induced by inelastic behavior to benefit the system.

We have shown that the reduction in displacement demands by stiffening, in nonlinear systems, is difficult. The stiffening changes the frequency, which may change the (median value of) *Sa* or *Sv* by unanticipated degrees (e.g., there may not be constant *Sv*). Further, the change in strength (yield force) that typically accompanies stiffening may in itself reduce or increase the demands, but "typically" for structures of moderate periods (where "hardening" occurs) the reduction in displacement demands may be lower than anticipated due to the "delaying" of the (perhaps surprising) "benefits" of nonlinearity.

Appendix 4.C. Selection of Earthquake Records for Nonlinear Dynamic Analyses.

The seismic threat posed to the structure was chosen to be described in terms of the spectral acceleration at approximately the fundamental response frequency (0.5Hz), and its probabilistic representation is given by the hazard curve (Fig. 4.1) for the site (Sta. Barbara Channel). Such a curve integrates the contribution of all potential sources and magnitudes of seismic excitation and their probable effects at the site. Consistent with modern seismic regulations (e.g., BSSC, 1997, API-RP 2A 1993) the selection of adequate earthquake records should be based on identifying those that are likely to contribute most to the threat, especially at levels near the capacity spectral acceleration considered. This selection is today often aided by seismic hazard disaggregation (e.g., Bazzurro and Cornell, 1998).

Based on such a procedure, the following nearby thrust-fault event scenario was identified:

Mw = 6.85
R = 4.0 Km

Although the disaggregation procedure indicated the importance of near fault earthquake scenarios, we used records from beyond 10 km, since the potential special effects of near-field records are beyond the scope of the procedure. However, these effects are important and, strictly, should have been considered in the structural responses obtained.

Records with characteristics in the vicinity of the scenario magnitude (Mw = 6.7 to Mw = 7.3), as well as distances in a range of 10 to 30 km, for deep broad soil were identified from (Silva, 1995). Four recordings were selected, with three orthogonal components, corresponding to the following events:

Record	Event	yyyy mmdd	*Mw*	Description	Closest *R* [km]	*PGA* [g]	*Sa* [g]
1	Northridge	1994 0117	6.7	LA - Hollywood Stor FF #	25.5	0.139	-
						0.231	0.160
						0.358	0.088
2	Northridge	1994 0117	6.7	Canoga Park - Topanga Can	15.8	0.489	-
						0.356	0.241
						0.42	0.095
3	Loma Prieta	1989 1018	6.9	Gilroy Array #3	14.4	0.338	-
						0.555	0.097
						0.367	0.060
4	Loma Prieta	1989 1018	6.9	Hollister - South & Pine	28.8	0.197	-
						0.371	0.242
						0.177	0.167

Table 4.C.1. Earthquake records selected for dynamic nonlinear analyses of 3-D steel jacket in Chapter 4.

Appendix 4.D. Structural Properties.

The jacket platform consists of an A-36 steel three-dimensional tubular-member truss. At its base (mudline) the platform is 135' by 135' in plan (41m by 41m). It consists of 5 tiers and its total elevation is 310' (94m) at the deck, carrying a total mass of 10.0 tons. Structural analyses were performed by the nonlinear finite element program CAP (PMB 1996). See figure 4.D.1.
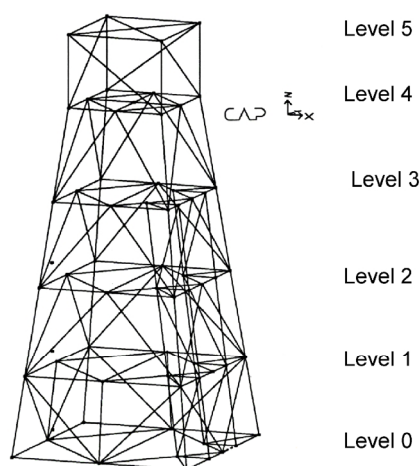

Figure 4.D.1. Five-tiered spatial tubular member truss steel jacket. Level 0 corresponds to the mudline; level 5 corresponds to the deck.

Designs are for both designs (original and upgraded) as indicated by the following table:

| Member | D [ft] | Design 1 | | Design 2 | | tier/level |
		t [ft]	D/t	t [ft]	D/t	
Legs	6.23	0.18	34.56	0.18	34.56	all
Diagonals	2.72	0.13	21.27	0.17	16.36	4-5
	2.46	0.06	43.87	0.07	33.74	3-4
	2.20	0.05	43.99	0.06	33.84	1-3
Horizontals	5.89	0.16	36.00	0.21	27.70	5 ext/int
	2.13	0.11	18.58	0.15	14.29	4 ext
	1.50	0.04	36.06	0.05	27.74	0,1,2,3,4 int
	1.80	0.09	19.64	0.12	15.11	0,1,2,3 ext

Table 4.D.1. Element sizing for original and upgraded designs. Levels as indicated are 0 at the bottom, and 5 at deck level (i.e., tier 1 is from level 0-1).

The dynamic properties from the eigenvalue analysis for both designs at the first 3 periods are:

Mode	Design 1		Design 2	
	T [sec]	f [Hz]	T [sec]	f [Hz]
1.00	1.90	0.53	1.77	0.56
2.00	1.90	0.53	1.77	0.56
3.00	1.76	0.57	1.57	0.64

Table 4.D.2. Structural frequencies for first 3 modes.

Chapter 5

Three-Dimensional Spectrum Matching

5.1 Introduction.

It was shown in the previous chapter that the consideration of a three-dimensional model of a structural system requires regard to additional issues that need to be taken into account for the implementation of PSDA. Since the computational expense involved is high, and matters of efficiency are of natural concern, questions such as the following arise: Can one benefit from the use of spectrum compatible accelerograms? Does one also observe unconservative predictions of response by using this scheme? How is multi-dimensional input to be considered for PSDA? This chapter addresses these issues.

We shall subject a three-dimensional structural model of a steel jacket structure to two sets of three-component records. The second set will be a spectrum compatibilized version of the original set. Both the relative variability of the responses and potential bias in the second set are of interest.

5.2 The Three-Dimensional Spectrum-Compatible Record Set[1].

Planar structural analysis, including seismic input, has typically been performed with simplistic representations of actual systems. In the dynamic analysis case the effects of the orthogonal horizontal component (out-of-plane) of the ground motion used (in-plane) are considered to be uncoupled from the in-plane analysis. Typically, although within the same plane, the effects of the vertical component are also considered not important, such that this direction of ground motion is not included in the analysis. This simplistic one-dimensional ground motion representation provides no conflict with the use of currently available attenuation laws when considering a scenario-based spectral shape as a spectral target to use for compatibilization (see Chapter 3).

Even disregarding the vertical component, for the 3-dimensional structural case one should legitimately question the use of the attenuation-law-based spectral shape of a scenario event. For the scenario-based analysis of both the 1- and 2-dimensional structural cases, the single median shape provided by the corresponding attenuation law was sufficient to represent (in the limit) a relatively large suite of earthquakes from a narrow bin. The typical construction of these laws considers the average (log) spectral acceleration from both horizontal components as a single data point and disregards their ratio.

The following subsections consider two cases of 3-D spectrum matched record sets for dynamic analysis. The first one takes into account the possible variation in spectral intensity for all three orthogonal components of ground motion as indicated by a small scenario-based suite of records. The second case considers the single shape that typical attenuation laws provide for the same scenario. The 3-dimensional problem related questions that this chapter intends to answer are limited to the simple case of near-

---

[1]Throughout this chapter we will be meaning by the three-dimensional set of records (either original or compatibilized), or simply just "set of records", the use of the *three* orthogonal components of ground motion for the structural analysis of the three-dimensional structural model of the steel jacket structure.

symmetric, first-mode (or rather, first-two-mode) dominated systems. The structural system considered is approximately the same as the original design of the steel 3-D 5-tier K-braced offshore jacket in Chapter 4 ($f_0 = 0.53$Hz).

5.2.1 Median Spectral Shape of Available Accelerograms.

As previously mentioned, the structural responses obtained when using artificial representations of ground motion need to be benchmarked against some sort of "reality". Thus, the problem of verifying the validity of spectrum compatible records on 3-dimensional systems for estimation of response becomes somewhat limited due to the major additional computational expense; one does not have the luxury we had in Chapter 3 of comparing a large set of results from both original records ("reality") and the artificial ones.

For verifying the use of spectrum compatible records on the 3-D system, the same small set of records employed in Chapter 4 was used (see Appendix 4.C for the description of the accelerograms). Despite the fact that the records were selected to represent a particular magnitude-distance scenario event, a limited size set may cause their median response spectral shape to not exactly match that of the attenuation law's prediction. Figure 5.1 compares the individual records of the records employed and their median spectrum to the median attenuation law-based scenario shape. The records are on average somewhat stronger than the predicted shape, mostly at higher than the fundamental frequencies. Also, the limited number of records will produce a more jagged median shape.

The component used for any given direction was not taken from the traditional orientation convention (e.g., NS and WE), which introduces the natural variability in the intensity due to direction. Instead, we selected the stronger components (as indicated by the spectral acceleration of interest) for the ground motion input in one structural direction and the weaker components for the other direction. This was done in order to

avoid using a spectral shape that could be potentially either too strong or too weak relative to the selected set of components (for any one direction). Hence, the horizontal target spectral shapes that were used to create spectrum compatible records correspond to the median shapes of these two subsets of stronger and weaker components. Figures 5.2a and 5.2b show the target shapes for the two components. Notice that (although not so much the case in our particular range of primary interest, i.e., below 0.53Hz) the targets are not as smooth as typical target shapes based on a large set of records are (e.g., an attenuation law-based shape). Also shown in figures 5.2a and 5.2b are the spectra of the original records scaled to a reference frequency close to the structure's first mode frequency (0.53Hz).

The runs that were performed correspond to pre-assigned intensity values. Intensity was defined by the scalar selected as per Chapter 4, i.e., the maximum or larger (horizontal) spectral acceleration. For the original (non-compatibilized) records, all record sets were scaled such that the larger-component spectral accelerations corresponded to 0.6g and to 0.8g. All orthogonal (weaker) components were scaled by the same factor such that the relative intensities for all component pairs remained unchanged for each record set (this relative intensity was not the same for all records).

In contrast, the spectrum-compatible versions of the original records show constant ratios of orthogonal spectral accelerations, as those of the median spectral shapes obtained (x, y and z direction) for all records. In other words, the intensity in one direction was the predetermined intensity (0.6 or 0.8g) while the intensities of the other horizontal direction and the vertical direction were determined by the relative intensities of the median shapes. Recall that the criterion for selecting the component to be used in each direction for analysis was the maximum (stronger) spectral acceleration for one (horizontal) direction, e.g., x, and the other components in the remaining corresponding directions, i.e., y and z.

Four original record sets were used to analyze the structure. Each was scaled to two levels, 0.6 and 0.8g at 0.5Hz. Then their corresponding spectrum-compatible versions

were also scaled to these two levels. The results obtained are summarized in table 5.1, and are also plotted in Fig. 5.3. An additional data point was added by considering an alternate spectral acceleration to scale to for one of the records (record # 4) because for this record numerical convergence within the analysis was not attained for the pre-selected intensities of the SCR versions[2]. This translates into a total of 7 data points for the spectrum matched records' runs, and not 8 data points as was the case for the original records.

As one can observe in table 5.1 (a), b) and c)) and figure 5.3, there is a degree of reduction in dispersion, as indicated by the values of the square root of the mean square error for the different cases (in table 5.1c $MSE^{1/2}$ is the estimate of $\sigma_{ln(dmd) \,|\, ln(Sa)}$), although the estimated reduction, perhaps, was not as large as could have been expected. For this particular case, one does not expect to see the dispersion ratios of the level observed in the results of Chapter 3 (for which a typical value would be around 4). In Chapter 3 the responses corresponded to accelerograms whose intensities are actually observed in a pooled set of scenario-based narrow-bin records. In contrast, the numbers presented above correspond to runs performed at predetermined levels of intensity, such that the records (original and SCR versions) are all scaled or *normalized*. The spectrum compatibilizing technique produces a dispersion reduction that is caused solely by the effect of making uniform the *shape* of the response spectra, because the reduction effect from homogenizing the *intensity* has already been taken care of by the normalization.

---

[2] The non-convergence refers to a high equilibrium-error within the nonlinear dynamic analysis. The error exceeds a pre-established tolerance employed in the step-by-step integration strategy of the analysis. Based on inspecting the time-histories of response for SCR record # 4 (for both 0.6 and 0.8g intensities) and for the other records, a collapse-level high displacement was not expected. There was no attempt to alter the analysis parameters (e.g., iteration steps, tolerance limits, etc.) for any analysis, such that all results generated were from equal-parameter runs. This distinction is important because the discussion in this chapter assumes no collapses occur among the runs performed. Without this assumption the analysis of displacement results would have had to be performed *conditioning* on the non-observance of collapse. Another way that collapses could have been considered would be to identify a lower-bound for the value of displacement that SCR records #4 would have produced, in order to make an overall comparison as done in table 5.1.

From results in Shome (1999) the typical dispersion reduction for normalization is approximately 2, and as seen in Chapter 3, the typical value of total reduction is of approximately 4. This means that the effect of shape uniformization alone should account for a similar reduction of around 2 as well. Notice that the sample size is small (i.e., 7 to 8 data points) for this example; therefore one cannot definitely establish if the reduction has been less than expected or not.

One can observe a typical value of bias (ratio of median response to the suite of original records and the median response to the compatibilized suite) in the previous response results. For the individual values of intensity, the observed bias (ratio of the median response from the original records to the median response from SCR) ranges from around 10% (for the records scaled to 0.8g) to around 35% (for the records scaled to 0.6g). The overall bias for the pooled data set was established by comparing the values of the slope a, since for a value of $b = 1.0$, the median displacement given spectral acceleration is directly proportional to it. The value observed, $bias = 1.14$, falls between those observed for MDoF bilinear hysteretic systems between 0.25Hz and 1.0Hz and for levels of ductility between 2 and 4 (see tables 3.4 and 3.5). This observed bias differs from the ones reported in Chapter 3 in that a distinction is not being made for the level of ductility considered. In other words, by comparing the value of a, the bias reported is given on an average sense for the levels of displacement observed in the data set. Also remember that the structure is not of a bilinear hysteretic type. It corresponds to a fragile braced frame system that would present a strong strength reduction in the backbone of its hysteretic loop. Such cases were not considered earlier. It needs to be noted, however, that the observations presented are not as robust as the results in Chapter 3, due to the much smaller sample sizes.

As mentioned previously, the region of primary interest for these analyses corresponds to frequencies lower than 0.53 Hz (the frequency of the system). In order to perform an analysis of the effects of global shape on the response to spectrum matched records (which was not done here) one should not expect to be able to consider the value of the softened effective frequency to be $f_\mu = f_0 / \mu^{1/2}$. Such a relationship is an ad-hoc rule

based on the bilinear backbone of the hysteresis systems considered in Chapter 3, and does not apply to the strength-degrading braced frame system. Following the rationale behind the relationship of the softened effective frequency for ductile systems one would expect a lower frequency for a given level of ductility.

Although the components of ground motion were selected in order to separate the effect of additional variability due to the relative orthogonal intensities, a direction of maximum response "jump" was observed in two of the seven spectrum matched record runs. In other words, the maximum response was not parallel to the stronger record. For all the cases using original records the strong component caused the largest response, i.e., the direction of maximum response corresponded to the direction of maximum input. For the original records the intensity ratios of strong to weak directions ranged from 1.48 (for record 2) to 4.104 (record 4). On the other hand, for all cases of spectrum-matched records the ratio was by design fixed at 2.3 (compare figures 5.2a and 5.2b). The fact that no "jumping" was observed for the original records may be due to the limited sample size. The occurrence of "jumping" was present in the original-record runs in Chapter 4 (see Appendix 4.A). Figure 5.4 shows an example of the response direction "jumping" for record 2.

A natural extension to the exploration of the use of spectrum matched records beyond the effect of the global spectral shape in structural response for the 3-D case is an investigation of the effect of the reduced variability of the *relative* intensities of the orthogonal components of strong ground motion. The limited sample size does not allow us to perform a confident multivariate regression analysis that could determine such an additional effect. For the preferred case of performing analyses with a random selection of ground motion principal direction (for $Sa(f_0)$, for example) the cases of closer to unity orthogonal intensity ratios may be more damaging than those of higher valued ratios. However, for current standards of record selection by a traditional 1-dimensional PSHA-based disaggregation scheme, the value of spectral acceleration considered would be the median of both components. This selection results in unity ratios that would have a smaller largest component than would larger ratios. Although this effect may be likely to

be of a 3rd order importance, it warrants further study. This problem is addressed to some extent in the following section.

5.2.2 Attenuation Law-based Scenario Spectral Shape.

Given the PSHA-based disaggregated M-R scenario a more natural selection of target spectral shape for spectrum matching records is that of the corresponding attenuation law median prediction. Current state-of-the-practice PSHA is performed uni-dimensionally and, as mentioned earlier, traditional attenuation laws estimate the average (logarithmic) intensity of both orthogonal directions of horizontal ground motion. The loss of information on the relative intensity is unfortunate for the 3-D case, since it does not permit a rational selection of relative intensities given the average. It also leaves one with the sole choice of the median shape for both horizontal directions, which may not be appropriate, especially in near-source cases, where the ratio may be particularly large (Sommerville, 1997).

Given the lack of information, one possible way to consider the single spectral shape provided is to compatibilize both components of all available records to it and analyze the structure with them. Traditional code consideration of *simultaneous* orthogonal components of ground motion is done through response spectrum analysis (for linear analysis) and considers 100% of ground motion in one direction and 30% of ground motion in the other (e.g., SEAONC, 1996). Notice that this yields an intensity ratio (1:0.3 or 3.33:1) that is unconservative with respect to the ratio considered in the previous section (1:0.41 or 2.41:1). For the particular case of our near-symmetric system, the unit ratio seems to be overly conservative with respect to the results of the dynamic analyses that used the records' original intensity ratio. Table 5.2 shows the results corresponding to five runs for two different cases with records that are spectrum-matched to the attenuation-law median spectral shape. The first case considered the same level of intensity (*Sa*) for both orthogonal directions, whereas the second case considered the relative intensities that the unmodified records had. In both cases the larger spectral

acceleration was set equal to that of the larger spectral acceleration in the original records. The attenuation law used for the determination of the median scenario shape was taken from Abrahamson (1997).

All vertical components of ground motion were compatibilized to the corresponding vertical-motion attenuation law; the ratio of horizontal to vertical intensity, for the unit horizontal intensity ratio case, was directly taken from there as well.

As can be seen in table 5.2 one can directly see the higher response that the unit ratio causes with respect to the case of considering a more rational set of intensity ratios. Similar to the regression analysis performed on the results shown on table 5.1 (previous section), values of the slope *a* and the mean square error (MSE) were obtained for a *dmd* = *a Sa*^{b} model (with *b* = 1). The difference in response can be summarized by the relative values of the slope *a*. For this case if we consider valid an introduced average bias (due to the effect of spectrum matching) of the order of 1.2 (for the level of response observed), then the unit ratio case would even yield conservative results with respect to the use of real records (i.e., the hypothetical "real" records would have produced a median slope of *a* = 3.57 * 1.2 = 4.3 , which is less than 5.12).

We can see in the original-ratio portion of table 5.2 that the spectrum compatible records used there seem to produce a higher median estimate of response (as given by the value of *a*) than those used in the previous section (table 5.1c). This comparison is not strictly valid, due to the high standard error of estimation of these medians caused by the small sample sizes, and the use of (slightly) different target spectral shapes (perhaps even neglecting, due to the symmetry of the structure, the effect of considering the strong component for the same direction in the latter case). Also, having observed the much higher responses of the unit ratio case a hypothesis that can arise is the possible additional reduction of bias (with respect to actual records) from the use of fixed orthogonal intensity ratios for the SCR set.

The large response produced by the unit orthogonal intensity ratio case may be a result of the structure being near-symmetric[3]. The observed typical failure mode for the unit ratio case was based on yielding in the leg elements, as opposed to the brace buckling failure mode more typical for the other case observed for the steel jacket. From an elastic point of view, a corner tubular leg member of a symmetric system for the unit-ratio example would be affected by internal actions $2^{1/2}$ times larger than its infinite-ratio counterpart (i.e., using only one component). Systems with large asymmetries may not introduce as large a factor for the internal actions on the corner legs (e.g., a structure with many bays, longer in one direction).

The same way one would not use the same accelerogram of one component of ground motion simultaneously in both directions, one should not use the same level of spectral target for both directions. Strictly, the shapes to be considered should be generated by attenuation laws constructed with different sets of ground motion records (e.g., fault-parallel and fault-normal). As mentioned earlier, it should be expected, however, that their spectral shapes are similar except for the near-source case.

5.3 Conclusions.

The main objective of this chapter was to explore the validity of findings from Chapter 3 regarding the use of spectrum matched records, considering what we learned in Chapter 4 on the 3-dimensional system. The higher level of complexity of the 3-dimensional system involves not only structural modeling issues but also includes considerations on the ground motion input for the structural analyses.

---

[3] Unless one has a firm knowledge of the actual possible differences in the orthogonal ground motion intensities (as perhaps would be the case in a near-source situation), one would perform such analyses twice, one for each horizontal direction. Of course this would not be necessary for a strictly symmetric system.

The limited size of the suite of records used did not allow us to establish the findings with as much confidence as was shown in Chapter 3. The use of such a small sample size also introduced "noise" in the results that was not present before, such as, possibly, the use of not-so-smooth target spectra for the 3 components of ground motion in section 5.2.1. It was not established in Chapter 3 how much reduction in dispersion by using spectrum matched records was from the elimination of jaggedness in the spectral shape, versus the reduced variability in the *overall* shape factor (which does not include a measure of jaggedness).

The limited sample size did not allow a rigorous test of the significance of the 1.14 value of bias (ratio of observed median displacements from real records to median displacements from the use of SCR) for the strength and stiffness degrading structure (due to brace buckling) not considered in Chapter 3. This value is consistent, however, with the results from Chapter 3. It raises the question of the potential importance of an additional source of bias due to the suppressed variability in the spectral acceleration ratios of the intensity of both components. The effect of this suppressed variability merits further study. The issues raised can also be taken as a call to our suppliers of attenuation laws for (previously considered unimportant) information on both strong and weak components.

The classic representation of ground motion intensity, as considered by typical PSHA uses a scalar value of spectral acceleration. This procedure is dictated by the traditional seismological delivery of attenuation laws based on average spectral accelerations from two orthogonal directions. One example of the limitation of such attenuation laws is their use in studying directivity effects, important in near-source sites, for which special attenuation laws are just beginning to be developed (Somerville, 1997).

Although the experiment in section 5.2.2 could have been performed using the median shapes produced for section 5.2.1, the use of smooth attenuation law-based shapes may be of a more practical use. The main focus of section 5.22 was to establish the inadequacy of adhering to only the information that conventional attenuation laws

provide, i.e., the median spectral acceleration of the two components. Recall that from Chapter 4 an empirical value of the average ratio of the maximum spectral acceleration to the average spectral acceleration was approximately 1.2 (at least for a [6.7, 7.3] magnitude range and a [10,30] distance range for soil sites). Such a value, which requires an average ratio for the minimum intensity of 0.8, could then be considered for the relative intensities to consider for the simultaneous analysis of both orthogonal directions while using the same scenario spectral shape. This could be done, for example, by setting the weak intensity level at $1/(1.2/0.8) = 1/1.5$. The unlikely case of having not only the same spectral intensity (at the fundamental elastic frequency) but also the same shape would yield not only relatively high displacements but failure modes/sequences (e.g., based on the yielding of the corner legs) that are unlikely to occur with the more typical large-small orthogonal intensity couple (of different relative values) of actual ground motion.

The M-R scenario-based selection of records that was used throughout this work has been typical for current practice for the planar structural system case, when a single (horizontal) spectral intensity and shape usually suffice. It is beyond the scope of this study to establish an analogous procedure for the selection of appropriate accelerograms for 3-D analyses. State-of-the-practice disaggregation of hazard for the selection of a "representative" M-R scenario pair does not consider the conditional probability of observing one or two components of ground motion (e.g., Sa_y, Sa_z) given the observance of the orthogonal component (i.e., Sa_y, Sa_z).

Chapter 5 Figures.
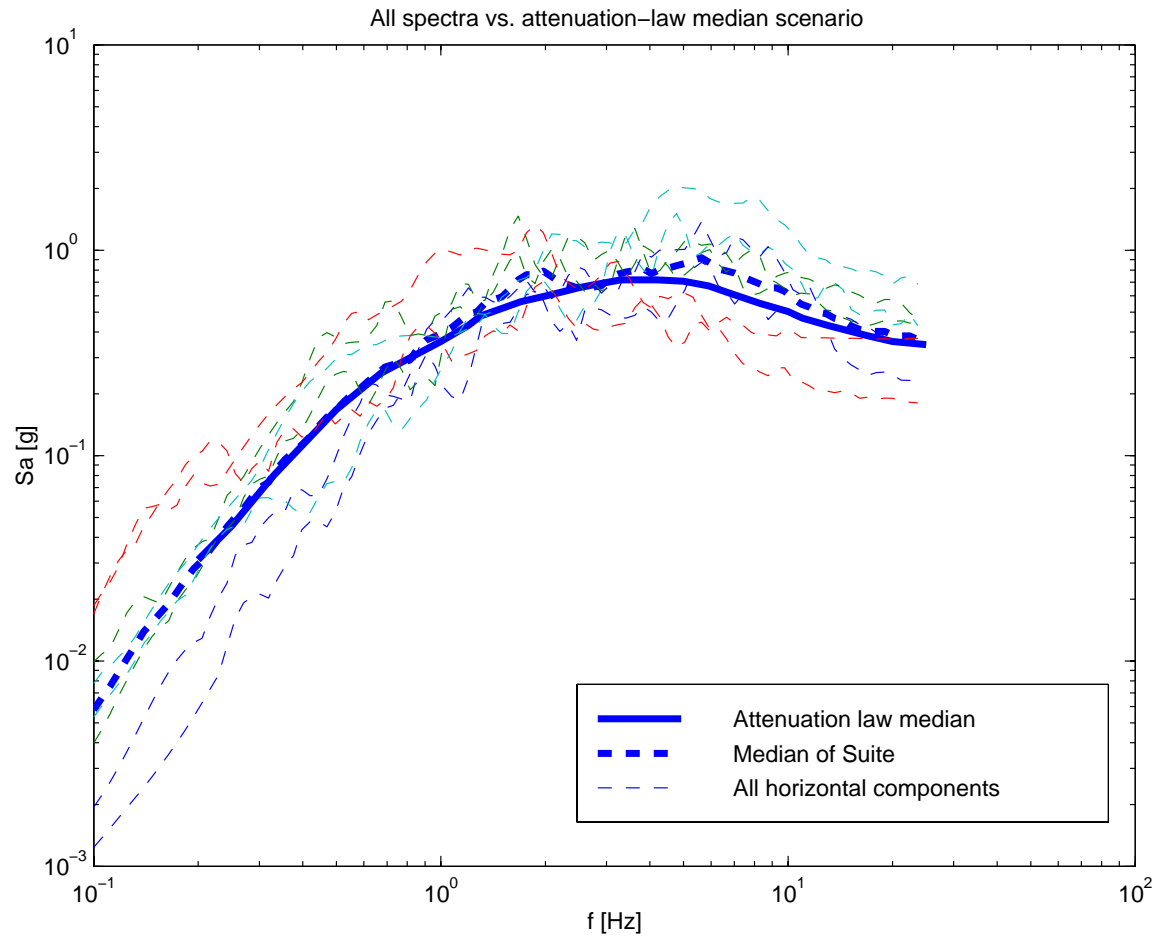
Figure 5.1. All records' spectra (both orthogonal directions) vs. attenuation law-based scenario shape. The attenuation-law median shape has been normalized to the records' median value at 0.5Hz, close to the jacket's fundamental frequency (0.53Hz). The records are on average somewhat stronger than the predicted spectrum at higher frequencies, although the shape is quite similar.
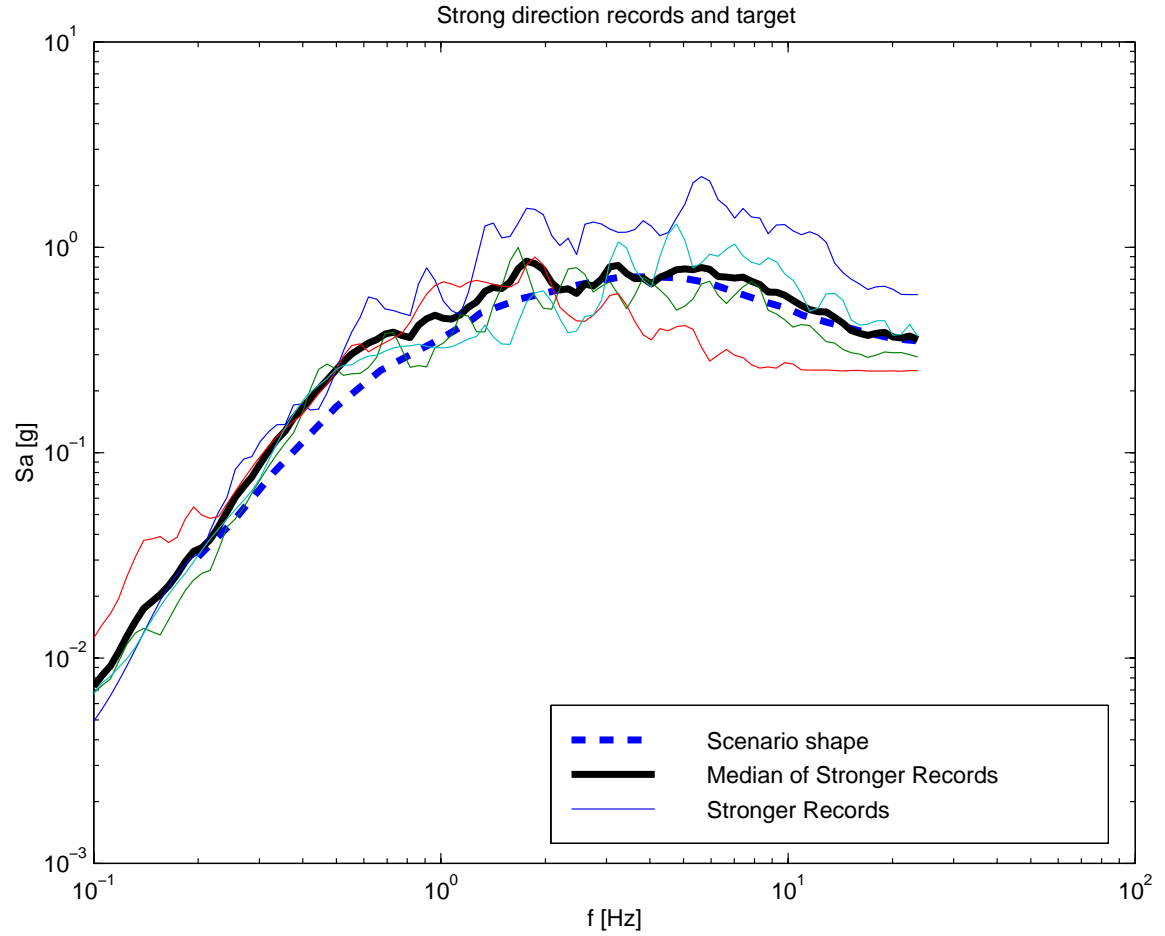
Figure 5.2a. Target shape (median of stronger records) for compatibilizing stronger horizontal components to. The spectra are scaled to the median value at a reference frequency of 0.5Hz, close to the fundamental elastic frequency of the structure (0.53Hz), except for the scenario shape which is scaled at the median of all horizontal components, as in Fig. 5.1.
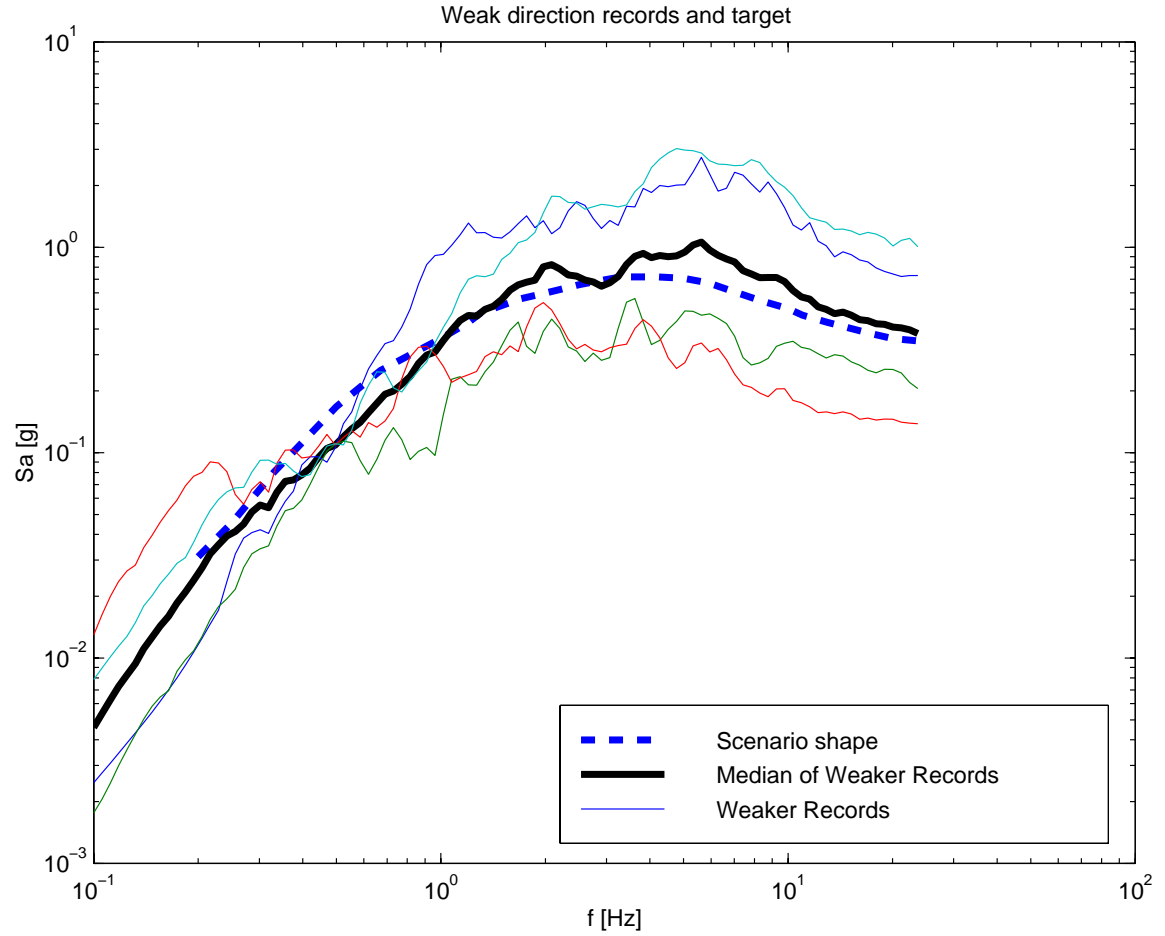
Figure 5.2b. Target shape (median of weaker records) for compatibilizing weak horizontal components to. The spectra are scaled to the median value at a reference frequency of 0.5Hz, close to the fundamental elastic frequency of the structure, except for the scenario shape which is scaled at the median of all horizontal components, as in Fig. 5.1.

Runs for Original records and Compatibilized records
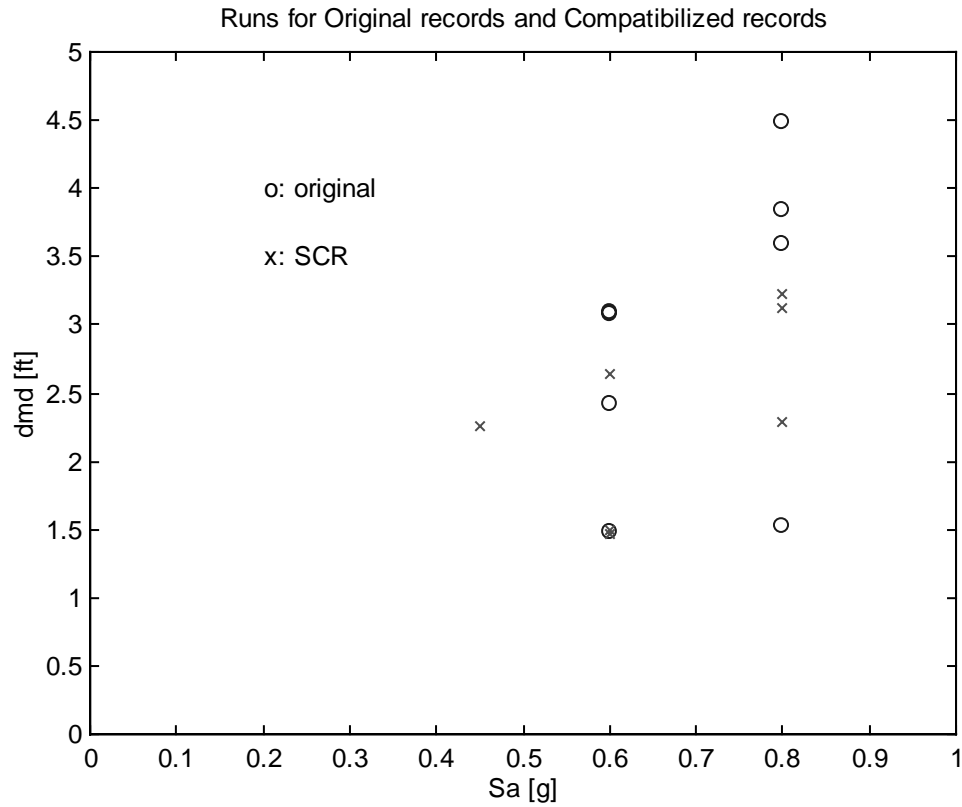
Figure 5.3. Response from original records and compatibilized records (SCR). Numerical convergence was not attained for the response corresponding to the SCR runs for record #4, so an additional intensity of 0.45g was considered for this record. The values of the *Sa-dmd* pairs are given in table 5.1a). Note that at *Sa* = 0.6g, there two original-record data points are very close to each other (around *dmd* = 3.1'), and so are two SCR data points (around *dmd* = 1.5').
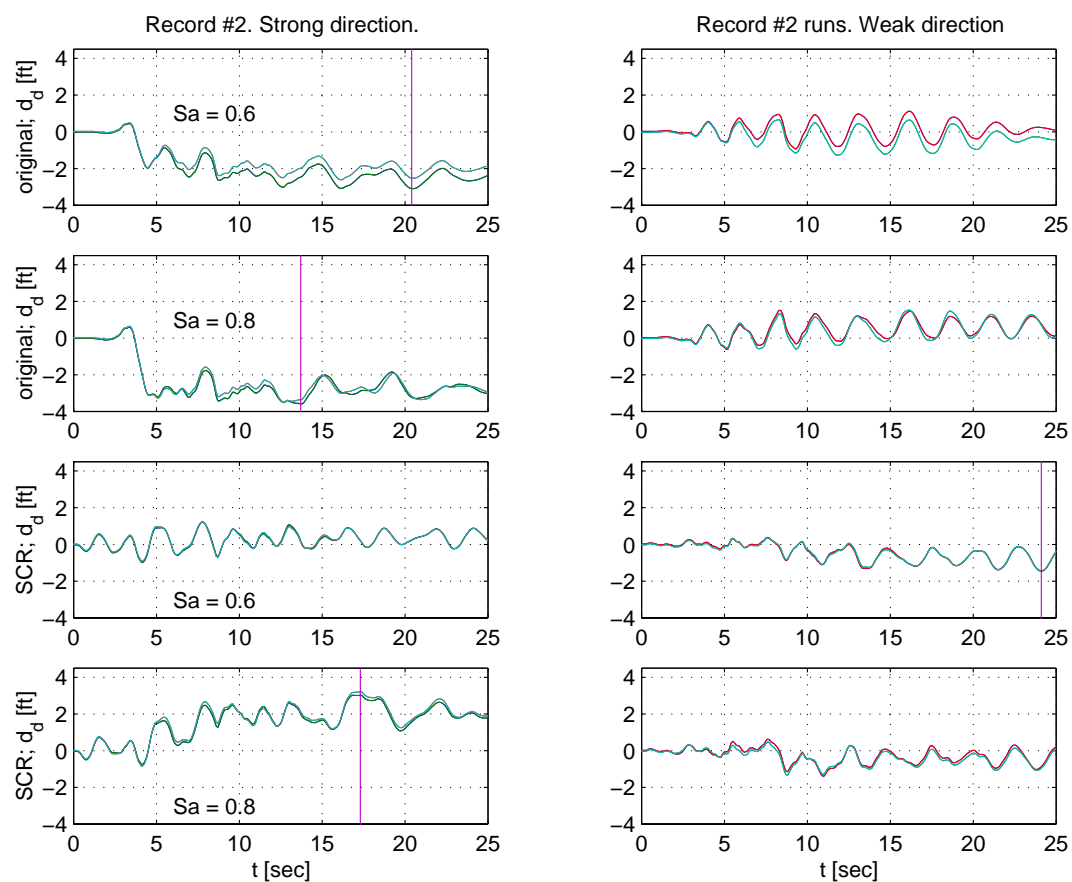
Figure 5.4 "Jump" in (maximum) response direction for a spectrum compatible version (SCR) of record 2 (at *Sa* = 0.6g). d_d represents deck displacement (as given by two diagonally opposed nodes). The vertical line indicates the time at maximum deck displacement in *either direction*. The weak direction of the original records had spectral accelerations of 0.6/1.48 = 0.41 and 0.8/1.48 = 0.54 (from the ratio 1.48 for record 2). For the SCR case the intensities were actually lower, at 0.6/2.3 = 0.26 and 0.8/2.3 = 0.35 (from the fixed ratio 2.3 for all SCR cases).

Chapter 5 Tables.

Data from nonlinear dynamic analyses					
Original records				Compatible records	
record	*Sa [g]*	*dmd [ft]*	record	*Sa [g]*	*dmd [ft]*
			4	0.45	2.25
1	0.6	2.42	1	0.6	2.63
2	0.6	3.10	2	0.6	1.47
3	0.6	1.48	3	0.6	1.49
4	0.6	3.08	4	0.6	N/A
1	0.8	3.85	1	0.8	3.13
2	0.8	3.59	2	0.8	3.23
3	0.8	1.53	3	0.8	2.29
4	0.8	4.48	4	0.8	N/A

a) Results from nonlinear analyses: Deck maximum displacements (*dmd*) for all records.

	Original records				SCR			
Sa	dmd_a [ft]	dmd_m [ft]	$MSE^{1/2}$	n	dmd_a [ft]	dmd_m [ft]	$MSE^{1/2}$	n
0.45	-	-	-	0.00	2.25	2.25	0.00	1
0.60	2.52	2.42	0.35	4.00	1.86	1.79	0.33	3
0.80	3.36	3.12	0.49	4.00	2.88	2.85	0.19	3
Total			0.39	8.00			0.24	6.00

b) Cross-comparison of statistics between same-level intensity results. Notice the reduction in dispersion for both cases, 0.6 and 0.8g. dmd_a represents the average deck maximum displacement. dmd_m represents the median displacement (modeled here as the exponential of the average of the logarithms). $MSE^{1/2}$ corresponds to the square root of the mean square error, and takes into account for each case the reduced number of data points (*n*-1).

(Table 5.1. See caption below)

	Original	SCR
a [ft/g]	3.96	3.47
MSE$^{1/2}$	0.39	0.29

c) Statistics for all pooled data. A regression model based on $\ln(dmd) = \ln(a\ Sa^b) = \ln(a) + b\ \ln(Sa)$ was considered, and for simplicity, the value of *b*=1 has been assigned. *MSE* was computed with (*n*-1) = 7. *MSE*$^{1/2}$ corresponds to the mean square error of the regression, which is the estimate of $\sigma_{ln(dmd)\ |\ ln(Sa)}$.

Table 5.1 (cont.). Results from the nonlinear dynamic analyses for the original records as well as for the spectrum compatible records (SCR). N/A indicates that the value of the displacement was not available due to the numerical non-convergence within the analysis (see footnote (2)), and the data point was treated as non-existent.

Unit ratio				orig. ratio			
record	*Sa [g]*	*Sax/Say*	*dmd [ft]*	record	*Sa [g]*	*Sax/Say*	*dmd [ft]*
1	0.78	1	4.80	1	0.78	1.80	2.50
2	0.77	1	3.80	2	0.77	0.67	4.00
3	1.18	1	5.60	3	1.18	0.24	4.30
3	0.98	1	4.70	3	0.98	0.24	2.20
4	0.83	1	4.20	4	0.83	2.58	3.50

a	5.12
MSE$^{1/2}$	0.11

a	3.57
MSE$^{1/2}$	0.32

Table 5.2 Response for 2 cases of intensity ratio: unit horizontal intensity ratio, and varying ratios obtained directly from the seeds' horizontal relative intensities as well as vertical relative intensity. *Sa* corresponds to the maximum of the two horizontal spectral accelerations. The vertical intensity for the unit ratio case was taken directly from the attenuation law (Abrahamson, 1997). All responses correspond to spectrum matched records with the median scenario shape from the attenuation law.

Chapter 6

Summary and Final Conclusions

The trend in modern seismic design is to incorporate procedures that address the nonlinear response of structural systems more so than has been done in the past. *Probabilistic Seismic Demand Analysis (PSDA)* is a recently developed tool that permits incorporating in a rational way the complex nonlinear seismic response of structures into both *evaluation* and *design*. In its simplest form, PSDA couples the probabilistic description of ground motion (i.e., Probabilistic Seismic Hazard Analysis, PSHA) to the conditional response of the structural system in order to provide a probabilistic description of structural response (see Chapter 1 and Appendix A). Findings from the previous chapters address questions on either evaluation or design as the ultimate goal for PSDA.

The following paragraphs do not intend to summarize in detail the findings of each chapter. Instead, the intention of this chapter is to thread them together for a clearer overview.

6.1 PSDA and Spectrum Matching.

Chapters 2, 3 and 5 dealt with issues regarding the *evaluation* of structures. One aspect of structural evaluation is the identification of the relationship between response and ground motion intensity, which is a necessary element of PSDA. In particular, these chapters

addressed the *efficiency* and *accuracy* that the use of some seismological representations of possible ground motion (e.g., Spectrum Compatible Records, SCR, or Spectrum Matched Records) may or may not have in the description of structural response.

Response spectral shape is a valuable property of ground motion, which has an important contribution to structural displacement demands. Its importance, coupled with the scarcity of recorded ground motion, leads to the interest in the use of artificially created accelerograms with a desired spectral shape, i.e., spectrum matched records.

In Chapter 2, the use of SCR was proposed for the "correction" of available records of particular magnitude-distance and soil type (the *seeds*) for the representation of ground motion of different characteristics (the *objective*). It was found that the corrected records could be used for an *accurate* estimation of displacement demands that the corresponding recorded ground motion would produce.

Another factor that greatly contributes to the interest in the use of SCR is the computational expense involved in nonlinear structural dynamic analyses. As a result, artificial accelerograms are intended to be used for the *efficient* estimation of seismic demands, in addition to the accuracy of the estimation required. Chapter 3 investigated the previously unverified validity of the use of SCR for these purposes. It was found that the use of SCR does present an important reduction in the variability of nonlinear response vis-à-vis the use of actual recorded ground motion for dynamic analyses, for the particular case of a M-R scenario-based shape and suite of records. The typical reduction in the coefficient of variation of displacement-based response is on the order of 4:1 (and a little higher for hysteretic-energy demands). This reduction allows the analyst to employ as few as $1/4^2$ or 1/16 the number of records that would be required for the same level of confidence in the estimate of median demands obtained by using original recorded accelerograms. It is important to mention that although the reduction in dispersion is significant, it is not low enough to warrant the use of only a *single* spectrum matched record to obtain an estimate of median displacement demands with a reasonable confidence interval.

The efficiency gain produced by this reduction in dispersion, however, does not come without a price. The estimation of displacement demands is no longer accurate: it is ***biased***. The effect of using a set of accelerograms matched to the median shape of the M-R scenario is to observe an ***unconservative*** bias in the estimate of displacement demands. (The results showed no consistent effect on the estimation of hysteretic energy-based centralized statistics). The typical bias in displacement demands introduced by use of SCR is on the order of 1.2:1 (for levels of ductilities around 4 and above). In other words, the displacement demands that a sample of actual recorded ground motions from a particular M-R scenario would yield are around 20% larger than those predicted by SCR's. The cause of the bias was identified. It was found that there is an asymmetric effect of the *global shape* of the spectrum on the displacement demands, such that the effect of *compatibilization* introduces such a bias in the estimates of demands. Although the target spectral shape can be modified in order to have the SCR produce unbiased estimates of median displacements, it did not appear to be a practical solution. The level of bias across different systems seemed reasonably stable such that the values for displacement demands could instead be directly and simply corrected, in order to obtain an approximated unbiased estimate of the median.

Chapter 3 was limited to planar SDoF and MDoF systems of bilinear and pinching hysteresis types, with and without base isolation. The analyses performed relied on a large data set of accelerograms in order to make the observations more robust. Chapter 5 dealt with a more complicated 3-dimensional system (albeit near-symmetric), which included a strength-degrading behavior due primarily to the braced-frame configuration. Although Chapter 5 did not have the luxury of using a large data set, the results obtained seemed to support the findings of unconservative bias that spectrum compatible records may introduce. It was found in this chapter that one has to be careful when assigning relative intensities to orthogonal-SCR, because actual recorded ground motions generally present differences in relative intensity.

It has to be mentioned that the results presented in this work did not include findings with respect to some important cases, such as the use of near-source records. Also, in terms of spectral shape, only the smooth M-R scenario-based median spectral shape was considered. Other smooth spectral shapes not studied here that are of typical current use include code-based design spectra and uniform hazard spectra, for which the "right" answer is more difficult to establish.

6.2 PSDA and Design.

Chapter 4 studied the use of PSDA as a tool for structural design by decomposing its constituents for identifying a required (elastic) design level (e.g., by means of determining a seismic intensity for member-sizing) in order to meet a performance goal. In particular, the goal considered in Chapter 4 was that of a prescribed probability of *failure*. The method proposed in that chapter contrasts with current design schemes in that the design level is not known a priori, but is a function of the goal, and of course, the expected nonlinear behavior (focusing at the near-failure behavior, i.e., not elastic) of the structure to be designed.

The method proposed is iterative in nature, and one can reduce iterations from a better understanding of the nonlinear behavior of systems, not limited to response but including capacity. Briefly addressed in this chapter was the importance of determining if the structural system behaves in a *hardening* or in a *softening* manner upon the offset of nonlinearity, which will have an effect on subsequent design iterations.

It was found in Chapters 4 and 5, from having used a more complex 3-dimensional system for the numerical design example, that definitions of seismic input and output (e.g., spectral intensity and top displacement) need to be carefully selected when not performing the more common planar structural analyses.

Appendix A

Derivation of the Correction Factor *Cf.*

Probabilistic Seismic *Demand* Analysis (PSDA) builds upon the existing probabilistic characterization of ground motion as described by Probabilistic Seismic *Hazard* Analysis (PSHA). Such hazard is commonly expressed in terms of *hazard curves*, which are plots of the probability that a seismic intensity Y (e.g., spectral acceleration) exceeds some value y. In other words, the hazard curve (represented by H [y]) is equal to $P[Y > y]$.

The interface between PSDA and PSHA can be seen as the correction factor, *Cf*, as utilized in Chapter 4 for the probabilistic description of *failure*. Such *Cf* "inflates" the probability H[y] to account for the variability in the conditional response *given* intensity.

The probability of response, in *failure* terms, was written in Chapter 4 as:

$$P_f = P[\delta > \delta_c] = H[Sa_c] * Cf ,$$

(A.1, 4.10)

where Sa_c is the spectral acceleration capacity of the system. The correction factor, in terms of the probability of failure is then:

$$C_f = P_f / H[Sa_c].$$

(A.2)

For the particular case where the log-linear relationship between the median displacement, δ, and spectral acceleration, Sa, is assumed to hold (Eq. A.3) and when the integral of total probability for finding Pf (Eq. A.4) is expanded, the value of H[Sa_c] appears explicitly and *Cf* can be analytically obtained. Recall,

$$\delta = aS_a^{\ b},$$

(A.3)

and,

$$Pf = P[\delta > \delta_c] = \int_0^\infty P[\ln(\delta) - \ln(\delta_c) > 0 \mid Sa = u] fsa(u) du$$

(A.4, 4.16)

Since the probability density function of *Sa* (i.e., $f_{Sa}(u)$) can be written in terms of the hazard curve (unity minus the cumulative probability) we can re-write Eq. A.4 as:

$$Pf = P[\delta > \delta_c] = \int_0^\infty P[\ln(\delta) - \ln(\delta_c) > 0 \mid Sa = u](-\frac{dH(u)}{du}) du$$

(A.5)

Using integration by parts and recognizing that in the limit:

$\lim_{Sa \to 0} P[\ln(\delta) - \ln(\delta_c) > 0] = 0$, and

$\lim_{Sa \to \infty} H[Sa] = 0$, we have:

$$Pf = \int_0^\infty \frac{d}{du}(P[\ln(\delta) - \ln(\delta_c) > 0 \mid Sa = u]) H[u] du.$$

(A.6)

For the assumption that both the displacement capacity, δ_c, and the displacement given spectral acceleration, $\delta(Sa)$, are lognormally distributed (such that their logarithmic difference has a normal distribution with variance given by Eq. A.7, and with median

values equal to δ_{cm} and aSa^b, respectively), we can anticipate $P[\ln(\delta) - \ln(\delta_c) > 0 \mid Sa]$ to be a lognormal CCDF (complementary cumulative distribution function) as a function of Sa (which can be seen as a *fragility curve*), with the median value $Sa_{50} = (\delta_{cm} / a)^{1/b}$, and to be able to easily find the value of *Cf* as done in Appendix A of (Bandyopadhyay, et al, 1993). For small values of Sa, the probability of the aforementioned event tends to zero; for high values of Sa it tends to unity, and when $Sa = (\delta_{cm}/ a)^{1/b}$ this probability is one half. The total variability of the logarithmic difference of displacement given Sa and displacement capacity is:

$$\sigma_t^2 = \sigma_\delta^2 + \sigma_{\delta c}^2 . \tag{A.7, 4.12}$$

Let $z(y) = \ln(\delta(y)) - \ln(\delta_c)$, such that, as mentioned above, it is normally distributed with parameters $E[z(y)] = \ln(a\, y^b) - \ln(\delta_{cm})$, with a *homoscedatic* variance: $VAR[z(y)] = \sigma_t^2$ (i.e., constant variance throughout the range of possible Sa values). Call $g(y)$ the normal distribution density function with the above parameters. By renaming the variable of integration for clarity, we have:

$$P[z(y) > 0 \mid Y = y] = \int_0^{+\infty} g(\tau)\, d\tau = \int_{-E[z(y)]}^{+\infty} g(u - E[z(y)])\, du = \int_{-E[z(y)]}^{+\infty} f(u)\, du , \tag{A.8}$$

where $f(u) = g(u - E[z(y)])$ is a normal distribution with the same variance as $g(\tau)$ but now centered at the origin. Due to the symmetry of the normal distribution, we can re-write:

$$\int_{-E[z(y)]}^{+\infty} f(u)\, du = \int_{-\infty}^{+E[z(y)]} f(u)\, du . \tag{A.9}$$

The fundamental theory of calculus lets us easily differentiate this function with respect to y, so:

$$\frac{d}{dy}[\int_{-\infty}^{+E\{z(y)\}} f(u)\,du] = f(E[z(y)])\frac{d}{dy}E[z(y)] \ . \tag{A.10}$$

By using Eq. A.10 and Eq. A.8, we get:

$$\frac{d}{dy}P[z(y)>0\,|\,Sa=y]=[\frac{1}{\sigma_t\sqrt{2\pi}}]e^{-\frac{1}{2}(\frac{\ln(a)+b(\ln(y))-\ln(\delta_m)}{\sigma_t})^2}\frac{b}{y} \tag{A.11}$$

which is the sought-after derivative of the lognormal fragility curve in Eq. A.6.

By assembling the original probability of failure and utilizing the linear approximation of the hazard curve, which is stated as:

$$H[y] = K_1 y^{-K_0} \ , \tag{A.12}$$

we obtain:

$$Pf = \int_{-\infty}^{+\infty} K_1 y^{-K_0}\frac{1}{(\sigma_t/b)\sqrt{2\pi}}e^{-\frac{1}{2}(\frac{\ln(y)-\ln(\delta_m/a)^{1/b}}{\sigma_t/b})^2}\frac{dy}{y} \ . \tag{A.13}$$

With the change of variable $\ln(y) = t$, our probability of failure is given by:

$$Pf = \frac{K_1}{(\sigma_t/b)\sqrt{2\pi}}\int_{-\infty}^{+\infty}e^{-K_0 t}e^{-\frac{1}{2}(\frac{t-\ln(\delta_m/a)^{1/b}}{\sigma_t/b})^2}dt \ . \tag{A.14}$$

The integrand can be reduced and solved by the following equivalence (see, for example, Elishakoff, 1983):

$$\int_{-\infty}^{+\infty} e^{-\frac{1}{2}(At^2+2Bt+C)} \, dt = \sqrt{\frac{2\pi}{A}} \, e^{-(AC-B^2)/2A} \ . \tag{A.15}$$

So, finally:

$$Pf = K_1 e^{K_0(\delta_{cm}/a)^{1/b}} e^{(K_0\sigma_t/b)^2/2} = H[(\delta_{cm}/a)^{1/b}] e^{[\frac{1}{2}(\frac{K_0\sigma_t}{b})^2]} \ . \tag{A.16}$$

Hence, by (A.2), recognizing that $Sa_c = (\delta_{cm}/a)^{1/b}$, we can find the value of the correction factor:

$$Cf = e^{[\frac{1}{2}(\frac{K_0\sigma_t}{b})^2]} \ . \tag{A.17}$$

Appendix B

On the selected ground motions for Chapter 3 and the effect of bin width on bias.

The assumed importance of the use of accelerograms from a *narrow* magnitude-distance bin is to be able to associate the results obtained from nonlinear analyses to the particular magnitude-distance pair of a seismic event of interest (i.e., to a scenario event) and to clarify the study of non-linear responses by avoiding potential magnitude-distance dependencies. Therefore, the selected width of a bin (i.e., the range for magnitudes and/or for the distance) has potential implications on the results obtained in Chapter 3. Two important statistics that were discovered in this study to impact the bias introduced by the use of spectrum-matched records are identified in Chapter 3. They are (1) the dispersions of and (2) the correlation between the spectral accelerations at the fundamental frequency of the structure and at a lower frequency associated with the general level of nonlinearity introduced by the ensemble of records. The larger the dispersions of spectral acceleration at these frequencies, the larger the *bias* introduced. Also, the smaller the correlation coefficient between the two spectral accelerations the larger the *bias*. The "width" of the bin changes these three statistics somewhat, and therefore could affect the bias.

For clarity of the argument in Chapter 3, it was perhaps unfortunate that not all of the 63 records were precisely of the same bin (only 44 were). In fact, 4 records had distances

larger than 144 kms, implying low intensities; 8 had magnitudes between 6.0 and 6.2 (of which one record was soil type A, as per FEMA-273, 1996, at a distance of 0.1km); and 4 other records were of soil type A while 3 were unclassified, for a total of 19 records outside the bin for one reason or another.

The following tables, however, indicate that the inclusion of the 19 out-of-bin records had negligible impact on the existence or the amount of bias. The conclusions presented in Chapter 3 hold, therefore, even for a purely bin-based ensemble of accelerograms. The practical importance of this statement is that it allows the engineer to use records available to her (within sensible limits), even though they may not strictly belong to a particular bin, e.g., a bin enclosing a particular scenario of interest.

Results shown in Table B.1 below show the biases and the dispersion reduction obtained by the use of the 44 strictly-in-bin records, and their comparison to the results obtained from the use of all 63 records. Shown are results for selected bilinear, SDoF and MDoF systems, with fundamental structural frequencies of 1Hz and 4Hz. The ductilities considered range from 2 to 8, as do the results in section 3.5. The records from these sets were compatibilized to the spectral shapes shown in Figure B.1[1].

---

[1] Although the median spectra corresponding to both sets of records are not precisely the same, their shapes are virtually identical, albeit offset (the 63-record median shape being a little lower as seen in Fig. B.1). Hence, only one spectrum was used (that of the 63-record set) as target for compatibilization. The spectrum-compatible records were scaled upwards by the amount of the offset at the corresponding frequency for use in the non-linear analyses corresponding to the 44-record set.
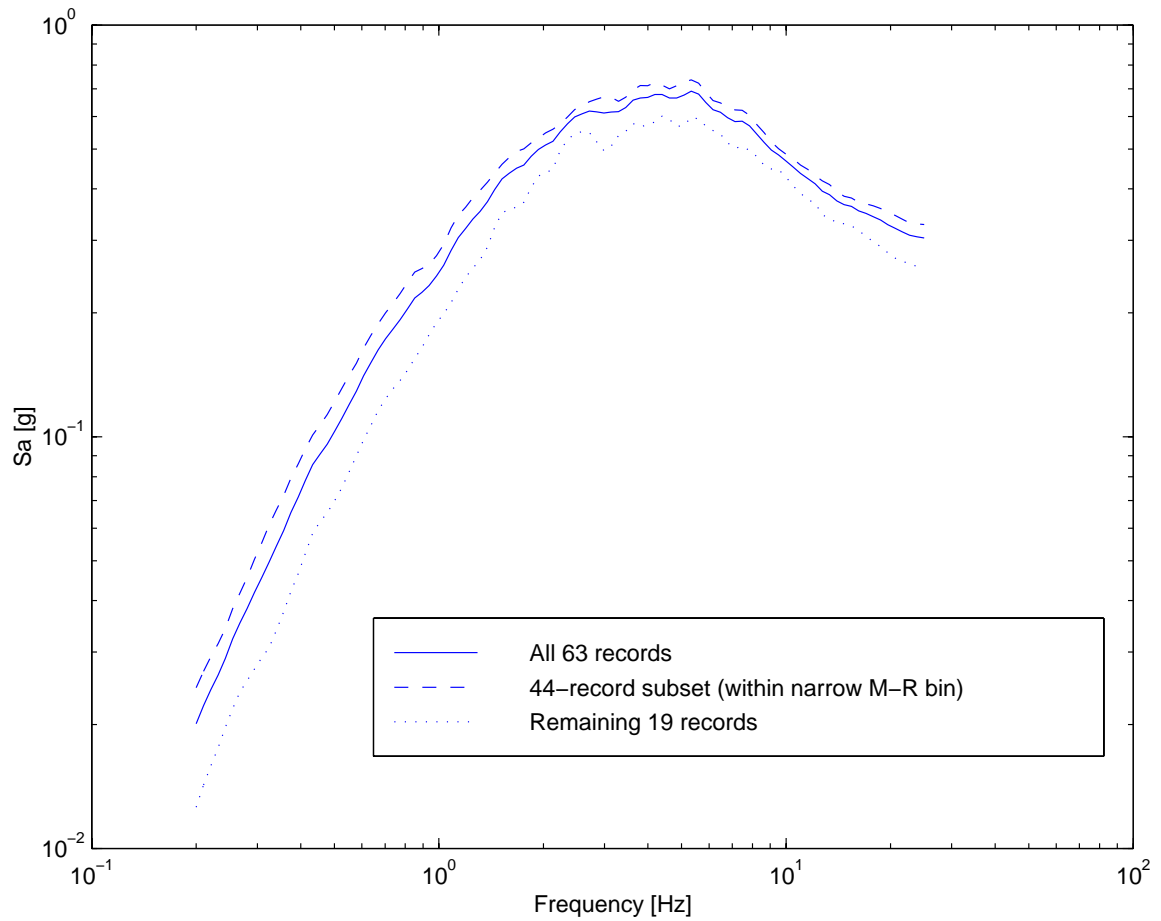
Figure B.1. Median response spectra for the 63-record and 44-record sets. The 63-records' median spectrum is a little lower due to the inclusion of the lower-magnitude and higher-distance records. Notice, however, the virtually identical shapes.

	SDoF 1Hzep				SDoF 4Hzep			
	Original	Compat'ed	Ratios 44 recs.	Ratios 63 recs.	Original	Compat'ed	Ratios 44 recs.	Ratios 63 recs.
μ	2.35	2.12	1.11	**1.11**	2.03	1.98	1.03	**1.06**
σ	0.70	0.18	3.84	**3.94**	0.64	0.18	3.54	**3.56**
μ	9.63	7.94	1.21	**1.14**	8.81	7.49	1.18	**1.20**
σ	0.77	0.23	3.38	**3.81**	0.81	0.23	3.49	**3.57**
				(From table 3.2a)				(From table 3.2a)
	MDoF 1Hzep				MDoF 4Hzep			
	Original	Compat'ed	Ratios 44 recs.	Ratios 63 recs.	Original	Compat'ed	Ratios 44 recs.	Ratios 63 recs.
μ (max intstry.)	1.88	1.76	1.07	**1.06**				
σ	0.59	0.14	4.38	**4.36**				
μ (global)	1.37	1.37	1.00	**0.98**				
σ	0.52	0.11	4.89	**5.13**				
μ (max intstry.)	5.12	4.00	1.28	**1.17**	3.21	2.96	1.08	**1.10**
σ	0.67	0.22	3.06	**2.91**	0.72	0.22	3.21	**3.13**
μ (global)	2.89	2.41	1.20	**1.12**	2.02	1.86	1.08	**1.06**
σ	0.62	0.15	4.18	**3.04**	0.56	0.12	4.52	**4.60**
μ (max intstry.)	8.40	6.75	1.24	**1.17**	8.12	7.34	1.11	**1.13**
σ	0.71	0.25	2.82	**2.91**	0.78	0.18	4.35	**3.94**
μ (global)	4.67	3.55	1.32	**1.24**	4.83	3.58	1.35	**1.32**
σ	0.69	0.20	3.41	**3.31**	0.81	0.20	3.98	**3.83**
				(From table 3.5)				(From table 3.6)

Table B.1. Results from nonlinear analyses for MDoF and SDoF systems for the 44-record set, strictly corresponding to the narrow magnitude and distance bin (*M* between 6.7 and 7.3, *R* between 10 and 30km) indicated in section 3.4. The ratios indicated are of the results (median ductilities and standard deviations of the logarithm) for original records divided by those of the spectrum-compatible records. The "bias" was defined in Chapter 3 as the ratio of the median ductilities (original to compatible). Also shown (in bold) are the ratios obtained from the use of the whole 63-record set which include a few records of lower magnitude as well as records of larger distances, taken from tables 3.5 and 3.6). As can be seen, there are no significant differences between the ratios for the 44 and 63 record sets, for these 1Hz and 4Hz bilinear systems, for both ductility and standard deviation ratios.

As can be seen, for each of the structural cases considered, the observed bias results are not statistically different between the two record sets.

It can be asked if the effects of the two record sets' bin widths on the bias might have been predicted from the formal derivations in this work. The target is the response for a specific M-R pair. In the case of the 44 records a bin of narrow but still finite width was used; in the case of 63 records a still "wider" bin was used. Recall from section 3.8 that the prediction of the level of bias introduced by the use of spectrum-matched records could be linked to the statistical properties of the spectral accelerations of the unmodified records, as follows:

$$E[\ln(R_{\mu})] = \sigma_{\ln R_{GS\mu}}[(\alpha^{+} - \alpha^{-})(2\pi)^{1/2} + (\beta^{+}/2)\sigma_{\ln R_{GS\mu}}], \qquad (3.35)$$

where $R\mu$ is the normalized ductility (with respect to the median ductility from all spectrum-matched records) for a specific record. Therefore $\exp(E[\ln(R\mu)])$ can be associated with the bias. The α's and β are structure-dependent parameters, whereas $\sigma_{\ln R_{GS\mu}}$ corresponds to a parameter dependent on the aforementioned statistics:

$$Var[\ln(R_{GS\mu})] = \sigma^{2}_{\ln R_{GS\mu}} = \sigma^{2}_{\ln Sa_{0}} + \sigma^{2}_{\ln Sa_{\mu}} - 2\rho_{\ln Sa0,\ln Sa\mu}\sigma_{\ln Sa_{0}}\sigma_{\ln Sa_{\mu}}.$$

$$(3.26)$$

As can be seen in these equations, the level of expected bias increases with the level of dispersion of spectral acceleration at the fundamental frequency, f_0, and at the "softened" frequency, f_μ. Both bias and dispersion increase with the level of expected non-linearity. Also, the lower the correlation coefficient the higher the expected bias.

At either frequency f_0 or f_μ, for a specific M-R scenario, the level of spectral acceleration dispersion is the natural variability observed. This is described and estimated by typical published attenuation laws (e.g., Abrahamson and Silva, 1997). In the context of using a

suite of records that do not strictly correspond to the desired scenario, as in records selected for a *bin* of finite width, the variability in observed spectral accelerations for a particular frequency will increase as the width of the bin increases, increasing the bias. Is the increase significant for practical bin widths? In the worst case one might ask: Have the biases observed been caused primarily by this bin width issue, obscuring any purported bias due to the compatibilization per se?

It is not obvious how the width of the bin might alter the coefficient of correlation between the spectral accelerations at the two frequencies of interest, f_0 and f_μ. Shown in the following table are the values of $\rho_{\ln Sa0, \ln Sa\mu}$ for the whole set (63 records) and sub-set of 44 records. The observed values of the standard deviation of the (natural log) spectral acceleration at f_μ, i.e., $\sigma_{\ln Sa_\mu}$, are shown next to the values of $\rho_{\ln Sa0, \ln Sa\mu}$ (the value corresponding to $\mu = 1$ is $\sigma_{\ln Sa_0}$). (See also Figure B.2.) Only for reference, the values given by the Inoue, 1989, model for the coefficients of correlation, as well as the values for $\sigma_{\ln Sa_0}$ and $\sigma_{\ln Sa_\mu}$ predicted by the Abrahamson and Silva, 1997, attenuation model (for *average* of the two horizontal spectral accelerations) (see also Figure B.2) are also shown. As can be seen, there is not a great difference between the coefficients of correlation for the entire set as compared to the smaller subset.

Correlation coefficients from Inoue, dispersion from Abrahamson-Silva, 1997

	f_0:1 Hz			f_0:4 Hz		
μ	f_μ [Hz]	ρ: 1HZ $\rightarrow f_\mu$	$\sigma_{\ln(Sa\mu)}$	f_μ [Hz]	ρ: 4HZ $\rightarrow f_\mu$	$\sigma_{\ln(Sa\mu)}$
1	1.00	1.00	0.59	4.00	1.00	0.50
2	0.71	0.89	0.62	2.83	0.89	0.52
4	0.50	0.77	0.64	2.00	0.77	0.54
8	0.35	0.66	0.68	1.41	0.66	0.56

Correlation coefficients and dispersion from data (entire 63-record set)

	f_0:1 Hz			f_0:4 Hz		
μ	f_μ [Hz]	ρ: 1HZ $\rightarrow f_\mu$	$\sigma_{\ln(Sa\mu)}$	f_μ [Hz]	ρ: 4HZ $\rightarrow f_\mu$	$\sigma_{\ln(Sa\mu)}$
1	1.00	1.00	0.67	4.00	1.00	0.56
2	0.71	0.90	0.73	2.83	0.82	0.61
4	0.50	0.77	0.74	2.00	0.68	0.60
8	0.35	0.71	0.74	1.41	0.53	0.67

Correlation coefficients and dispersion from data (44-record subset)

	f_0:1 Hz			f_0:4 Hz		
μ	f_μ [Hz]	ρ: 1HZ $\rightarrow f_\mu$	$\sigma_{\ln(Sa\mu)}$	f_μ [Hz]	ρ: 4HZ $\rightarrow f_\mu$	$\sigma_{\ln(Sa\mu)}$
1	1.00	1.00	0.66	4.00	1.00	0.54
2	0.71	0.91	0.72	2.83	0.79	0.56
4	0.50	0.77	0.70	2.00	0.58	0.56
8	0.35	0.67	0.67	1.41	0.47	0.61

Table B.2. Coefficients of correlation between Sa_0 and $Sa\mu$, and corresponding standard deviations (of the logarithm) from data observations (whole set and the subset of 44 records). See Figure B.2 for the plot of standard deviations of $\ln(Sa)$ for the entire range of frequencies. For reference only, published empirical models are shown for these statistics (the standard deviations of the log-spectral acceleration from Abrahamson and Silva, 1997, are somewhat lower perhaps due partly to the fact that they correspond to *average* horizontal spectral accelerations).

Notice that the values of the coefficients of correlation are just slightly lower for the 44-record subset for 4Hz only, and virtually identical at 1Hz. Recall (Eq. 3.26) that the lower

the correlation the higher the expected introduced bias. We shall explore below the predicted implication of these statistics on the bias. First, however, we introduce the related finite bin-width question.

Expected effects from bin widths on spectral $\sigma_{ln(Sa)}$ and on bias.

The level of additional dispersion of spectral acceleration introduced by the (necessary) use of records from a bin of finite width can be explained also by the attenuation laws. They describe regression relationships between spectral acceleration and magnitude (as well as distance and soil type; for clarity, these two variables will be left out of this discussion).

For example, a *linear* approximation (taking the slope from the derivative with respect to magnitude) of the Abrahamson and Silva, 1997, attenuation law estimates the following proportionality between the logarithm of spectral acceleration and magnitude (for *M* around 7, and frequency around 1 Hz, at distance $R = 20$km), for strike-slip events on rock sites, as follows:

$$\ln Sa \approx [-.144 - 2(-.102)(8.5 - M) + 0.17(\ln R)]\, M + K + \varepsilon = 0.67M + K + \varepsilon = sM + K + \varepsilon,$$

$$(B.1)$$

where *K* is the ordinate at the origin, which is a function of distance and units (as well as mechanism and soil type if included), ε is the random error term of the model, and the linear slope is $s = 0.67$. It can easily be proven that for such a linearized version of the attenuation relationship, the *additional* variance of (the logarithm of) spectral acceleration introduced by the magnitude-width of the bin is given by the square slope multiplied by the variance of the selected magnitudes of the bin. This translates into a *total* variance of the model for spectral acceleration, for the bin records, of:

$$\sigma_{lnSa}{}^2 = \sigma_\varepsilon{}^2 + s^2\sigma_M^2 ,$$

$$(B.2)$$

where σ_ε^2 is the standard error of the attenuation law regression (associated with a specific M) and σ_M^2 is the variance of the distribution of magnitudes within the finite bin.

To get a sense of the importance of bin width consider a hypothetical bin, containing records with a uniform and continuous distribution of magnitudes, and of bin-width Δ. The variance would be:

$$\sigma_M^2 = \Delta^2/12 \qquad\qquad\qquad (B.3)$$

For example, for a bin width of $\Delta = 0.5$ magnitude units the corresponding variance would be $\sigma_M^2 = 0.02$. This multiplied by $s^2 \approx 0.45$, or 0.009, should be compared to typical values of σ_ε^2 of about 0.3 to 0.5. Clearly, for typical bin widths, this additional dispersion is not large, and its effect on bias would not be great.

For the particular suite of 63 records selected, however, the magnitude distribution was not uniform (or continuous). The actual values of the magnitude bin widths and variances, for the whole (63 record) set and the 44-record bin suite, were: $\Delta = 1.3$ and $\sigma_M^2 = 0.097$, and $\Delta = 0.6$ and $\sigma_M^2 = 0.040$ respectively. Hence, the additional variances introduced (following the model described above, Eq. B.2) were 0.044 (for the 63 records) and 0.018 (for the 44 records), still very low with respect to the (attenuation-law) variances of the spectral accelerations at the frequencies of interest at a specific magnitude. These values represent small fractions of typical values of σ_ε^2 of 4% to 15%. Observe further that the use of the 63 records introduces an additional variance *with respect to* the use of the 44-record subset of $0.044 - 0.018 = 0.026$ (i.e., only between 5% and 9% of typical values of σ_ε^2). We should not anticipate therefore that the bias will be seriously affected by any of these variance increases.

The following figure shows the standard deviation of the log-spectral acceleration for the whole set, and the 44-record and 19-record subsets. As expected, the 44-record subset

presents lower dispersion than the entire 63-record set, due to the variability introduced by the 19 out-of-bin records. Note that although the actual differences in standard deviation may not necessarily follow the model above, the differences are indeed low.
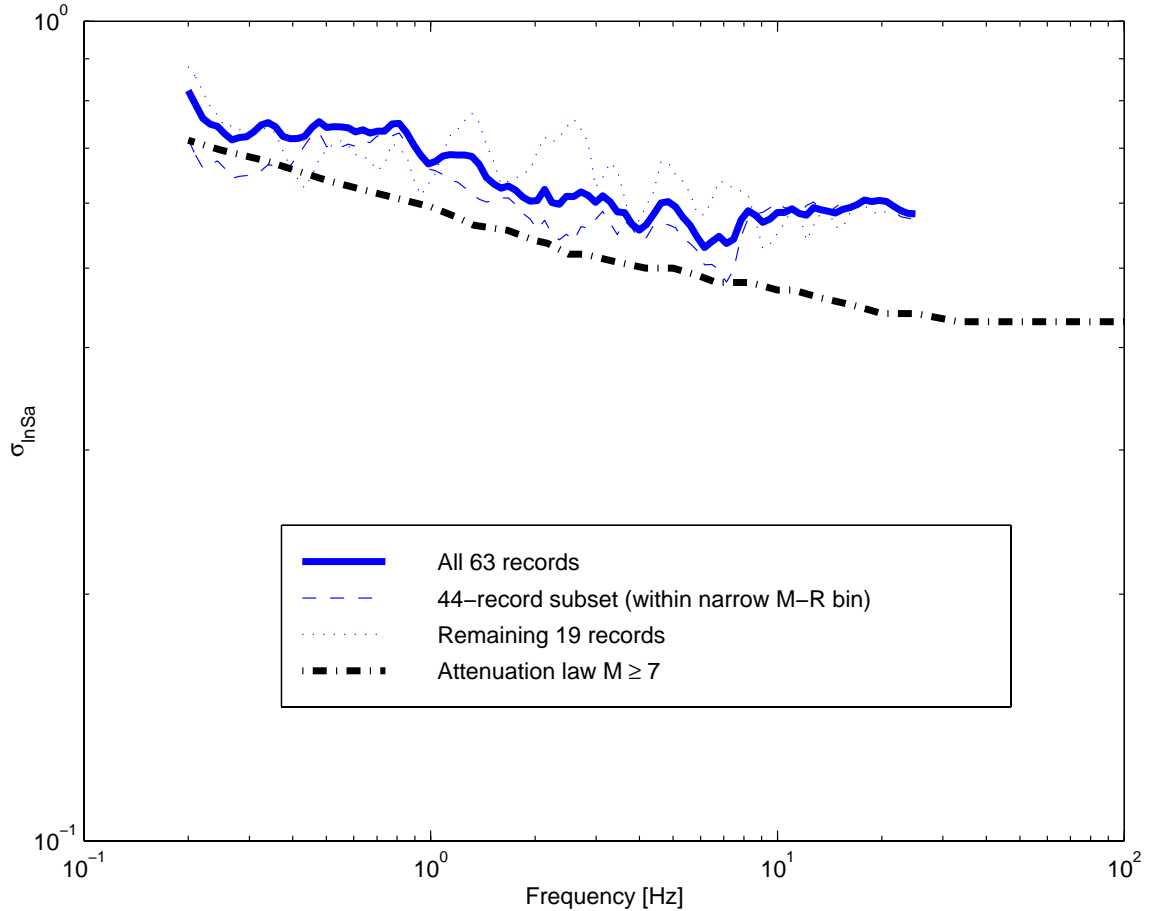
Figure B.2 Standard deviation of the whole set and the two subsets of records used in Chapter 3, compared to the Abrahamson-Silva attenuation law value (for the *average* horizontal component).. Note the higher values for the entire 63-record set due to the increasing of the bin magnitude width (as well as to the different distribution of magnitudes). The differences at 1Hz and 4Hz were particularly low.

Having established the effect on the variance of log-spectral acceleration due to magnitude bin-width, we can calculate its expected effect on the bias (of the 63 records vis-à-vis the use of the 44 records), by means of Eqs. 3.25 and 3.26.

For simplicity, let us assume a hypothetical case where the values of $\sigma_{\ln Sa_0}$ and $\sigma_{\ln Sa_\mu}$ are equal, such that the variance of $\ln(R_{GS\mu})$, in Eq. 3.26, is proportional to $\sigma^2_{\ln Sa_0}$ (assuming that the coefficient of correlation does not vary). If we take the worst case from above, where the additional variance due to the effect of a bin was around 15% of σ^2_ε, then the variance on $\ln(R_{GS\mu})$ is increased also by 15%, or, its standard deviation is increased only in 7% (because $1.15^{1/2} = 1.072$). For simplicity as well, let us use the simplified (linear) version of Eq. 3.35, where β^+ is zero (see Section 3.8.2 for a discussion on this case), the value of $E[\ln(R_\mu)]$ (Eq. 3.35) would then be increased by 7%. This means that the expected (increased) bias is then that of the perfect-bin case (zero-width) raised to the power of 1.07. For a zero-width-bias of, say, 1.2, this 15% variance increase would augment the bias to 1.22, a less than 2% increase.

Let us compute for a pair cases what the increase in variance of $\ln(R_{GS\mu})$ actually was due to the use of the 63-record set vis-à-vis the use of the 44-record subset. Consider the values for ductility $\mu = 8$, for both the 1Hz and 4Hz cases. Recall that not only the standard deviations of the log-spectral accelerations were not constant at different frequencies, but the coefficient of correlation varied for one set to the other as well. The following table shows the relevant variances computed from these statistics using Eq. 3.26 for the selected level of ductility.

$\mathrm{VAR}[\ln(R_{GS\mu})]$

	1Hz	4Hz
63-record set	0.30	0.36
44-record subset	0.29	0.35

Table B.3. Increase in variance in log-global shape ratio (see Section 3.6 for the definition) by the use of larger magnitude (and distance) bin width-set of 63 records, vis-à-vis the use of the narrower bin width-subset of 44 records (see Eq. 3.26). The effects of such small differences should signify negligible differences in biases in median ductility estimates caused by using the spectrum-compatible version of these records.

Needless to say, the effects on the bias given the extremely small differences in VAR[ln($R_{GS\mu}$)], as described by Eq. 3.35 should be (and actually were) negligible.

It has been established then, not only that the use of compatible records from bins with reasonable, finite widths do not introduce significant *additional* bias when used for the estimation of median ductilities, but also, that the relative additional increase in bias from having used the whole 63-record set vis-à-vis the 44-record subset can be predicted to be negligible, as was observed.

References

Abrahamson, N.A., 1993. "Non-Stationary Spectral Matching Program RSPMATCH". Personal communication.

Abrahamson, N.A., Silva, W.J., 1997; "Empirical Response Spectral Attenuation Relations for Shallow Crustal Earthquakes"; *Seismological Research Letters*, Vol. 68, No. 1, Jan/Feb.

American Petroleum Institute (API), 1993; "Recommended Practice for Planning, Designing and Constructing Fixed Offshore Platforms -Load and Resistance Factor Design", API RP 2A-LRFD. First Edition, July.

American Petroleum Institute (API), 1993; "Recommended Practice for Planning, Designing and Constructing Fixed Offshore Platforms -Working Stress Design", API RP 2A-WSD. 20th Edition, July.

Applied Technology Council (ATC) 1986; "Seismic Design guidelines for Highway Bridges"; Report ATC-6.

Applied Technology Council (ATC) 1996; "Improved Seismic Design Criteria for California Bridges: Provisional Recommendations"; Report ATC-32.

REFERENCES

Atkinson, G., Boore, D., 1990;"Recent Trends in Ground Motion and Spectral Response Relations for North America", *Earthquake Spectra*, Vol. 6, No. 1.

Badyopadhyay, K.; Cornell, C.A.; Costantino, C.; Kennedy, R.; Miller, C.; Veletsos, A., 1993; "Seismic Design and Evaluation Guidelines for the Department of Energy High-Level Waste Storage Tanks and Appurtenances"; Department of Nuclear Energy; Brookhaven National Laboratory, Associated Universities, Inc, New York; January.

Barenberg, M.E.., Foutch, D. A., 1988; "Evaluation of Seismic Design Procedures for Highway Bridges"; *ASCE Journal of Structural Engineering*, Vol. 114, No. 7, July.

Barenberg, M.E., 1989; "Inelastic Response of a Spectrum-Compatible Artificial Accelerogram"; *Earthquake Spectra*, Vol. 5, No. 3.

Barroso, L., 1999; ": Performance Evaluation of Vibration Controlled Steel Structures Under Seismic Loading"; Ph.D. Dissertation, Department of Civil and Environmental engineering, Stanford University.

Bazzurro, P., Cornell, C.A., Shome, N., Carballo, J.E., 1998; "A comparison of Three Proposals for Characterization of MDoF Non-linear Seismic Response", *ASCE Journal of Structural Engineering*, Vol. 124, No. 11.

Bazzurro, P.; Cornell, C. A., 1999; " Disaggregation of Seismic Hazard ". *Bulletin of the Seismological Society of America*, Vol. 89, No. 2, pp. 501-520, April.

Bea, R., 1995; "Probability Based Earthquake Load and resistance Factor Design Criteria for Offshore Platforms"; Second International Workshop on Wind and earthquake Engineering for Offshore and coastal facilities; University of California at Berkeley; January 17 - 19.

REFERENCES

Boore, D.M., 1983; "Stochastic Simulation of High-Frequency Ground Motions Based on Seismological Models of the Radiated Spectra", *Bulletin of the Seismological Society of America*, Vol. 73, No. 6, pp.1865-1894, December.

Brune, J.N., 1970; "Tectonic Stress and the Spectra of Seismic Shear Waves from Earthquakes", *Journal of Geophysical Research*, v. 75, pp. 4997-5009.

Building Seismic Safety Council (BSSC); "NEHRP Recommended Provisions for Seismic Regulations for New Buildings and Other Structures"; FEMA 302, 1997.

Chopra, A. K., 1995; "Dynamic of Structures; Theory and Applications to Earthquake Engineering". Prentice Hall. New Jersey.

Cornell, C.A., 1968; " Engineering Seismic Risk Analysis", *Bulletin of the Seismological Society of America*, Vol. 58, No. 5, pp. 1583 - 1606.

Cornell, C.A., 1995; "Structural Reliability - Some Contributions to Offshore Technology". Proceedings of the 27th annual Offshore Technology Conference, OTC 7753.

Dalane, J.I., 1993; "System Reliability in Design and Maintenance of fixed Offshore Structures", Ph.D. Dissertation, University of Trondheim, Norway.

Elishakoff, I., 1983; "Probabilistic Methods in the Theory of Structures"; John Wiley & Sons.

FEMA-273, 1996; "NEHRP Guidelines for the Seismic Rehabilitation of Buildings", Building Seismic Safety Council, Washington, D.C.

Foutch, D. A., Shi, S., 1998; "Effects of Hysteresis Type on the Seiemic Response of Buildings"; 6th National Conference on Earthquake Engineering, Seattle.

REFERENCES

Han, S.W.; Wen, Y.K., 1997; "Method of Reliability-Based Seismic Design. I: Equivalent Nonlinear Systems"; *Journal of Structural Engineering*, March.

Inoue, T., Cornell, C.A.,1990; "Seismic Hazard Analysis of Multi-degree-of-freedom Structures", RMS Report No. 8, Department of Civil Engineering, Stanford University.

Kennedy, R.P., Short, S.A., Mertz, K.L., Tokarz, F.Z., Idriss, I.M., Power, M.S., Sadigh, K., 1984; "Engineering Characterization of Ground Motion -Task I: Effects of Characteristics of Free-Field Motion on Structural Response", NUREG/CR-3805, U.S. Nuclear Regulatory Commission, Washington, D.C..

Kennedy, R. P., Kincaid, R. H., Short, S. A., 1985; "Prediction of Inelastic Response from Elastic Response Spectra Considering Localized Nonlinearities and Soil-Structure Interaction"; Transactions of the 8th International conference on structural Mechanics in reactor Technology, K 9/5, p. 427-434, Brussels, Belgium.

Lee, R., 1996; Personal Communication.

Léger, P., Tayeni, A.K., Paultre, P., 1993; "Spectrum-compatible accelerograms for inelastic seismic analysis of short-period structures located in eastern Canada"; *Can. J. Civ. Eng.,* 20, 951-968.

Lilhanand, K., Tseng, W.S., 1987; "Generation of synthetic time histories compatible with multiple-damping response spectra", SmiRT-9, Lausanne, K1 p.105.

Luco, N., Cornell, C.A., 1998; "Effects of Random Connection Fractures on the Demands and Reliability for a 3-Story Pre-Northridge SMRF Structure"; 6th U.S. National Conference on Earthquake Engineering; Seattle, WA.

REFERENCES

Manuel, L., Schmucker, D.G., Cornell, C.A., Carballo, J.E., 1998; "A Reliability-Based Design Format for Jacket Platforms Under Wave Loads", *Marine Structures*, No. 11, p. 413-428.

Mayes, R., 1989; Chapter 13 of "The Seismic Design Handbook", Naeim, F. ed. Van Nostrand Reinhold, NY.

Mayes, R., 1989; "The Effects of Near Fault Ground Motions on Bridge Columns". Dynamic Isolation Systems, Inc.

Mayes, R., 1998; Personal Comunication.

McGuire, R. K., 1995; "Probabilistic Seismic Hazard Analysis and Design Earthquakes: Closing the Loop", *Bulletin of the seismological Society of America*, Vol. 85 No. 5, pp. 1275-1284, October.

Naeim, F., 1995; "On the Use of Design Spectrum Compatible Time Histories"; *Earthquake Spectra*, Vol. 11, No. 1.

Naumoski, N., 1985; "SYNTH program--Generation of Artificial Acceleration Time Histories Compatible with a Target Spectrum". McMaster Earthquake Engineering Software Library, Department of Civil engineering and Engineering Mechanics, McMaster University, Hamilton, Canada.

NUREG 1.165, 1997; "Identification and Characterization of Seismic Sources and Determination of Safe Shutdown Earthquake Ground Motion", U.S. Nuclear Regulatory Commission, Washington, D.C.

Ostadan, F., Mamoon, S., Arango, I., 1996; "Effect of Input Motion Characteristics on Seismic Ground Responses"; 11th World Conference on Earthquake Engineering, Acapulco, Mexico, June 23-28.

REFERENCES

Park, Y.J.; Ang, A. H. S.; 1985; "Mechanistic Seismic Damage Model for Reinforced Concrete", *Journal of the Structural Division*, ASCE, Vol. 111, No. 4, 722-739.

Park, Y.J., Ang, A. H. S., Wen, Y. K., 1985; "Seismic Damage Analysis for Reinforced Concrete Buildings", *Journal of the Structural Division*, ASCE, Vol. 111, No. 4, 740-757.

PMB Engineering, Inc., 1994; "CAP -Capacity Analysis Program", Technical Manual, San Francisco.

Preumont, A., 1984; "The Generation of Spectrum Compatible Accelerograms for the Design of Nuclear Power Plants", Earthquake Engineering and Structural Dynamics, Vol. 12, 481-497.

Schnabel, P.B., Lysmer, J., Seed, H. B., 1972; "SHAKE -A computer Program for Earthquake Response Analysis of Horizontally Layered Sites" *EERC report No. UCB/EERC-72- 12*, University of California, Berkeley, December.

SEAOC Blue Book, 1996; "Recommended Lateral Force Requirements and Commentary", Sixth edition, Sacramento, CA.

Shome, N., Cornell, C.A., Bazzurro, P., Carballo, J. E., 1997, "Earthquakes, Records and Nonlinear MDoF Responses", Report No. RMS-29, Reliability of Marine Structures Program, Department of Civil Engineering, Stanford University.

Shome, N., Cornell, C.A., Bazzurro, P., Carballo, J. E., 1998; " Earthquakes, Records, and Nonlinear MDoF Responses", Earthquake Spectra, Vol. 14, No. 3, pp. 469-500, August.

REFERENCES

Shome, N., Cornell, C.A., 1999; "Probabilistic Seismic Demand Analysis of Nonlinear Structures"; Report No. RMS-35. Reliability of Marine Structures Program, Department of Civil and Environmental Engineering, Stanford University.

Seneviratna, G.D.P.K., Krawinkler, H.; "Evaluation of Inelastic MDoF Effects for Seismic Design"; Report No. 120, The John A. Blume Earthquake Engineering Center, Department of Civil Engineering, Stanford University; June, 1997.

Sewell, R.T.; "Damage Effectiveness of Earthquake Ground Motion". Ph.D. dissertation. Department of Civil Engineering, Stanford University; January, 1989.

Silva, W., 1987; "WES Rascal Code for Synthesizing Earthquake Ground Motions". US Army Corps of Engineers State-of-the-Art for Assessing Earthquake Hazards in the United States, Report 24; May.

Silva, W.J., 1996; "Pacific Engineering and Analysis Strong-Motion Catalog"; Pacific Engineering and Analysis.

Simons, J. W., Powell, G.H., 1982; "Solution Strategy for Statically Loaded Nonlinear Structures", Earthquake Engineering Research Center, University of California, Berkeley, Report No. EERC 82-22.

Somerville, P.G., Smith, N.F., Graves, R.W., Abrahamson, N.A., 1997; "Modification of Empirical Strong Ground-motion Attenuation Relations to Include the Amplitude and Duration Effects of Rupture Directivity"; *Seismological Research Letters*, Vol. 68, No. 1, Jan/Feb.

Somerville, P., Smith, N., Punyamurthula, S., and Sun, J., 1997; "Development of Ground Motion Time Histories for Phase-2 of the FEMA/SAC Steel Project", *SAC Background Document*, Report No. SAC/BD-97/04.

REFERENCES

Somerville, P., 1998; "Development of an Improved Representation of Near-Fault ground Motions"; Proceedings of SMIP98 Seminar on Utilization of Strong Ground-Motion Data; Oakland, CA, September.

Song, J., Ellingwood, B., 1999; "Seismic Reliability of Special Moment Steel Frames with Welded Connections: II"; *Journal of Structural Engineering, ASCE*; Vol. 125, No. 4. April.

Stahl, B., Aune, S., Gebara, J., Cornell, C.A., 1998; "Acceptance Criteria for Offshore Platforms". Proceedings of the 17th International Conference on Offshore Mechanics and Arctic Engineering (OMAE '98). Lisbon, Portugal. July.

UBC, 1997; "Structural Engineering Design Provisions", Uniform Building Code, Vol. 2; International Conference of Building Officials.

U.S. Department of Energy (DOE), 1994; "Natural Phenomena Hazards Design and Evaluation Criteria for DOE Facilities"; DOE-STD-1020-94, Washington, D.C.

Vanmarcke, E.H., 1976, "Structural Response to Earthquakes", Chapter 8 in *Seismic Risk and Engineering Decisions*, C. Lomnitz and E. Rosenblueth, editors, Elsevier Publishing Co., Amsterdam, 287-337.

Wang, C. H.; Wen, Y. K., 1998; "Reliability and Redundancy of Pre-Northridge Low-Rise Steel Buildings under Seismic Excitation". Structural Research Series No. 624, Department of Civil and Environmental Engineering, University of Illinois at Urbana-Champaign, November.

Yeh, C.H.; Wen, Y.K., 1989; "Modeling of Nonstationary Earthquake Ground Motion and Bi-axial and Torsional Response of Inelastic Structures"; SRSS 546, Department of Civil Engineering., University of Illinois at Urbana-Champaign.